



TESIS DOCTORAL

**SÍNTESIS Y CARACTERIZACIÓN DE
NUEVOS QUIMIOTERÁPICOS DERIVADOS
DE PIRAZOL Y HETEROCICLOS S,N:
EFECTOS SOBRE LA APOPTOSIS EN
LÍNEAS CELULARES TUMORALES**

Elena Fernández Delgado

Biología molecular y celular, Biomedicina y Biotecnología por la Universidad de
Extremadura

Conformidad de los directores:

José Antonio Pariente Llanos

Javier Espino Palma

Emilio Viñuelas Zahínos

Esta tesis cuenta con la autorización del director y codirectores de la misma y de la Comisión Académica del programa. Dichas autorizaciones constan en el Servicio de la Escuela Internacional de Doctorado de la Universidad de Extremadura.

2023



UNIVERSIDAD DE EXTREMADURA

FACULTAD DE CIENCIAS

DEPARTAMENTO DE FISIOLÓGÍA

JOSÉ ANTONIO PARIENTE LLANOS, Catedrático del Departamento de Fisiología de la Facultad de Ciencias de la Universidad de Extremadura, JAVIER ESPINO PALMA, Profesor contratado doctor del Departamento de Fisiología de la Facultad de Ciencias de la Universidad de Extremadura y EMILIO VIÑUELAS ZAHÍNOS, Profesor Titular del Departamento de Química Orgánica Inorgánica de la Facultad de Ciencias de la Universidad de Extremadura,

INFORMAN:

Que la presente Tesis Doctoral, presentada por Dña. Elena Fernández Delgado, con el título: **SÍNTESIS Y CARACTERIZACIÓN DE NUEVOS QUIMIOTERÁPICOS DERIVADOS DE PIRAZOL Y HETEROCICLOS S,N: EFECTOS SOBRE LA APOPTOSIS EN LÍNEAS CELULARES TUMORALES**, ha sido realizada bajo nuestra dirección en el Departamento de Fisiología y en el Departamento de Química Orgánica e Inorgánica de la Universidad de Extremadura, y entendiendo que se encuentra finalizada y que reúne los requisitos de originalidad, autorizan su presentación para ser juzgada ante el tribunal correspondiente.

Y para que conste a los efectos oportunos, firman la presente conjuntamente en Badajoz, a 18 de septiembre de 2023.

José Antonio Pariente Llanos

Javier Espino Palma

Emilio Viñuelas Zahínos

La realización de esta Tesis Doctoral se ha llevado a cabo gracias al apoyo económico de las siguientes entidades:

- Ayudas para la financiación de contratos predoctorales para formación de doctores en los centros públicos de I+D pertenecientes al Sistema Extremeño de Ciencia, Tecnología e Innovación. (PD18020).
- Proyectos de Investigación en los Centros Públicos de I+D+i de la Comunidad Autónoma de Extremadura (IB18013).
- Ayudas para la realización de actividades de investigación y desarrollo tecnológico, de divulgación y de transferencia de conocimiento por los Grupos de Investigación de Extremadura (GR18040, GR18062, GR21042, GR21075).

JUNTA DE EXTREMADURA

Consejería de Economía, Ciencia y Agenda Digital



Fondo Social Europeo

Una manera de hacer Europa

Unión Europea

Scientific production resulting from this PhD thesis:

1. Articles:

Fernández-Delgado, E.; Estirado, S.; Espino, J.; Viñuelas-Zahínos, E.; Luna-Giles, F.; Rodríguez Moratinos, A.B.; Pariente, J.A. Influence of ligand lipophilicity in Pt(II) complexes on their antiproliferative and apoptotic activities in tumour cell lines". *J. Inorg. Biochem.* **2022**, *227*, 111688.

Fernández-Delgado, E.; Estirado, S.; Rodríguez, A.B.; Luna-Giles, F.; Viñuelas-Zahínos, E.; Espino, J.; Pariente, J.A. Cytotoxic effects of new palladium(II) complexes with thiazine or thiazoline derivative ligands in tumor cell lines. *Pharmaceutics* **2023**, *15*, 696.

Fernández-Delgado, E.; Estirado, S.; Rodríguez, A.B.; Viñuelas-Zahínos, E.; Luna-Giles, F.; Espino, J.; Pariente, J.A. Synthesis, characterization, crystal structures and cytotoxic activity of Pt(II) complexes with N,N-donor ligands in tumor cell lines. *Polyhedron* **2023**. Under review.

2. Lectures and oral communications:

Fernández-Delgado, E.; Estirado, S.; Luna-Giles, F.; Rodríguez Moratinos, A.B.; Pariente, J.A.; Espino, J.; Viñuelas-Zahínos, E. Comparison between proapoptotic effects of Pt(II) and Pd(II) complexes with thiazoline or thiazine-based ligands in tumour cell lines. XL Congress of the Spanish Society of Physiological Science. Badajoz, Spain. 19th-22nd September **2022**. Oral presentation No. O2-05

Fernández-Delgado, E.; Estirado, S.; Luna-Giles, F.; Rodríguez, A.B.; Pariente, J.A.; Espino, J.; Viñuelas-Zahínos, E. Proapoptotic effects of new analogs of Cisplatin with Thiazoline- or thiazine- based ligands and Pt(II) or Pd(II) as metal centers. I Jornadas de jóvenes investigadores en fisiología. Madrid, Spain. 28th October **2022**.

3. Work presented in congresses:

Viñuelas-Zahínos, E.; Luna-Giles, F.; Romero, S.; Fernández-Delgado, E.; Espino, J.; Estirado, S.; Espino, J.; Rodríguez Moratinos, A.B.; Pariente, J.A.; Bernalte-García A.; Barros-García, F.J. Estudio de la viabilidad y la actividad apoptótica de un complejo de Pt(II) frente a la línea celular HL-60. III Congreso Luso-Extremadureño de ciencias e tecnología. Évora, Portugal. 25th -26th November **2019**.

Fernández-Delgado, E.; Estirado, S.; Espino, J.; Viñuelas-Zahínos, E.; Luna-Giles, F.; Rodríguez Moratinos, A.B.; Pariente, J.A. Antiproliferative and proapoptotic effects of Pt(II) complexes in tumour cell lines. 43 Congreso de la Sociedad Española de Bioquímica y Biología Molecular. Barcelona, Spain. 19th-22nd July **2021**. Abstract No. 0480-P.

Fernández-Delgado, E.; Estirado, S.; Viñuelas-Zahínos, E.; Luna-Giles, F.; Pariente, J.A.; Rodríguez Moratinos, A.B.; Espino, J. New synthesis chemotherapeutic agents and melatonin as coadjuvant: Antitumoral potential. 7th International Electronic Conference on Medicinal Chemistry. Online. 1-30th November **2021**.

4. Science divulgation

Fernández-Delgado, E. Las detectives del cáncer. Jornadas de divulgación científica “Conócelas”. Badajoz, Spain. 8th February **2021**.

Fernández-Delgado, E. I Edición del Concurso de Divulgación #HiloTesis. Online. April-May **2021**.

Fernández-Delgado, E. La joven extremeña que “siembra” nuevos quimioterápicos contra el cáncer. Article in the newspaper “periódico Extremadura”. 16th May **2021**.

Fernández-Delgado, E. El poder de los anillos. V Jornadas Doctorales de la Universidad de Extremadura. Badajoz, Spain. 5th November **2021**.

Fernández-Delgado, E. II Edición del Concurso de Divulgación #HiloTesis. Online. April-May **2022**.

Fernández-Delgado, E. El poder de los anillos. IX Jornadas Doctorales G-9. Bilbao, Spain. 18-20th May **2022**.

Fernández-Delgado, E. Put a ring on it!. VI Jornadas Doctorales de la Universidad de Extremadura. Cáceres, Spain. 4th November **2022**.

Fernández-Delgado, E. Las detectives del cáncer. Jornadas de divulgación científica “Conócelas”. Badajoz, Spain. 8th February **2023**.

Fernández-Delgado, E. Put a ring on it!. X Jornadas Doctorales G-9. Oviedo, Spain. 31st May to 2nd June **2023**.

5. Awards:

First ranked in the regional phase of “I Edición del Concurso de Divulgación #HiloTesis”. April-May **2021**.

First award to the best poster in science branch in “V Jornadas Doctorales de la Universidad de Extremadura”. Badajoz, Spain. 5th November **2021**.

First award to the best poster in science branch in “IX Jornadas Doctorales G-9”. Bilbao, Spain. 18-20th May **2022**.

First award to the best oral communication in “XL Congress of the Spanish Society of Physiological Science”. Badajoz, Spain. 19th-22nd September **2022**.

First award to the best oral communication in “I Jornadas de jóvenes investigadores en fisiología”. Madrid, Spain. 28th October **2022**.

Second award to the best poster in science branch in “VI Jornadas Doctorales de la Universidad de Extremadura”. Cáceres, Spain. 4th November **2022**.

“Fundación Merck Salud-ASEICA a las Vocaciones Científicas” award for the presentation carried out in “Jornadas de divulgación científica Conócelas”. Madrid, Spain. 1st Juni **2023**.

Second award to the best poster in science branch in “X Jornadas Doctorales G-9”. Oviedo, Spain. 31st May-2nd June **2023**.

AGRADECIMIENTOS

Cuando comencé esta aventura dio la casualidad de que leí una frase que me ha acompañado todo este tiempo y que creo que refleja perfectamente lo que han supuesto estos años de trabajo. La frase dice así: “Y una vez que la tormenta termine no recordarás cómo lo lograste, cómo sobreviviste. Ni siquiera estarás seguro de si la tormenta ha terminado realmente. Pero una cosa sí es segura, cuando salgas de esa tormenta no serás la misma persona que entró en ella. De eso se trata esta tormenta.” Mi tormenta ha estado llena de altibajos, de alegrías, de frustración, de orgullo y de superación. Definitivamente, no soy la misma persona que entró en ella, y espero que al menos en algunos aspectos sea una persona mejor. Atravesar la tormenta no ha sido fácil, pero todos los que me habéis ayudado a remar la habéis hecho mucho más llevadera.

Como no podría ser de otra forma, me gustaría empezar agradeciendo a los tres tutores de esta tesis, los Doctores José Antonio Parientes, Javier Espino y Emilio Viñuelas, por su guía y apoyo durante estos años, y por no dejar que me diera por vencida en el camino. En especial a Javi, por transmitir siempre esa calma tan característica (y tan necesaria) y cuidarme como un hermano mayor.

A los integrantes de los Departamentos de Fisiología Animal y Química Orgánica e Inorgánica por acogerme tan bien desde el inicio. A Paco Luna por ser como un tutor más y a Ana Moratinos por creer siempre en mí y cuidarme tanto. Sin ti ni esta tesis ni la estancia hubiesen sido posibles. A Samuel, Patricia y Esther por darle color hasta a los días más grises, a María por meternos en los líos más divertidos y a Elena por estar siempre pendiente de que no nos falte de nada. Gracias también a Lourdes, Marta, Sergio, Rafa, Lierni y Yolanda por sus consejos.

Al servicio de apoyo a la investigación de la Universidad de Extremadura (SAIUEx), en especial a Alberto Álvarez, Esther Pérez y Pablo Muñoz, no solo por las mediciones sino por el excelente trato y la comprensión.

Ich möchte mich bei Professor Linden von der Universität Ulm und allen Kollegen seines Teams bedanken. Danke, dass Sie mich aufgenommen und in die Welt der

Nanopartikeln eingeführt haben. Besonderer Dank gilt dem zukünftigen Doktor Draphoen für sein Wissen, seine Hilfe und seine Geduld. Der beste Labor-Kollege, den ich je haben konnte.

A Elena, Fátima, Aroa, Javi, Carmen y Vicente por alegraros siempre por los éxitos, aunque sea desde la distancia. A Álvaro, por el apoyo incondicional, los consejos y las risas. Sé que siempre puedo contar contigo.

A Candi, por ayudarme a reencontrarme conmigo y enseñarme a ver la luz cuando parece que no la hay. Nunca tendré palabras de agradecimiento suficientes.

A Carlos, por la paciencia y el esfuerzo para que esto funcione. Por intentar entender qué hago con mis celulitas y por quererme siempre tanto.

A mi familia, en especial a mis padres y a mi hermano. Gracias por cuidarme, apoyarme y aguantarme durante toda esta andadura. Os tenéis el cielo ganado.

A mí, por no rendirme nunca y para que cuando lea esto en el futuro recuerde que soy capaz de hacer mucho más de lo que a veces creo.

Gracias.

ABBREVIATIONS

AIF: Apoptosis-Inducing Factor

AnnexinV-FITC: Annexin V conjugated with fluorescein isothiocyanate

APTES: (3-Aminopropyl)triethoxysilane

ATP: Adenosine triphosphate

AuNPs: Gold Nanoparticles

BH: Bcl-2 Homology

BP: Band-Pass

CAD: Caspase-Activated DNase

CARD: Caspase Recruitment Domain

CisPt: Cisplatin

CTAB: Cetyltrimethylammonium Bromide

DCFH-DA: 2',7'-dichlorodihydrofluorescein diacetate

DD: Death Domain

DED: Death Effector Domain

DISC: Death-Inducing Signaling Complex

DMEM: Dulbecco's modified Eagle's medium

DMF: Dimethylformamide

DMON: Dendritic Mesoporous Organosilica Nanoparticles

DMPzTn: 2-(3,5-dimethyl-1-pyrazolyl)-2-thiazoline

DMPzTz: 2-(3,5-dimethyl-1-pyrazolyl)-1,3-thiazine

DMSO: Dimethyl sulfoxide

DNA: Desoxyribonucleic acid

DOX: Doxorubicin

DPhPzTn: 2-(3,5-diphenyl-1-pyrazolyl)-2-thiazoline

DPhPzTz: 2-(3,5-diphenyl-1-pyrazolyl)-1,3-thiazine

DR: Death Receptors

DTT: Dithiothreitol

EDTA: Ethylenediaminetetraacetic acid

ER: Endoplasmic Reticulum

FA: Folic acid

FADD: Fas-Associated protein with Death Domain

FBS: Fetal Bovine Serum

FDA: Food and Drug Administration

HCPT: 10-hydroxycamptothecin

HEPES: 4-(2-hydroxyethyl)-1-piperazineethanesulfonic acid

IAP: Inhibitors of Apoptosis Proteins

ICP-MS: Inductively Coupled Plasma Mass Spectrometry

LNPs: Lipid Nanoparticles

MAPK: Mitogen-Activated Protein Kinase

MSNs: Mesoporous Silica Nanoparticles

MTS: 3-(4,5-dimethylthiazol-2-yl)-5-(3-carboxymethoxyphenyl)-2-(4-sulfophenyl)-2H-tetrazolium

MTT: 3-(4,5-dimethylthiazol-2-yl)-2,5-diphenyl tetrazolium bromide

NCDD: Nomenclature Committee on Cell Death

NLDFT: Non-local Density Functional Theory

NMSC: Non-melanoma Skin Cancer

NPs: Nanoparticles

NSCLC: Non-small Cell Lung Cancer

PBS: Phosphate Buffered Saline

PdDMPzTn: Dichloro-(2-(3,5-dimethyl-1-pyrazolyl)-2-thiazoline)-palladium(II)

PdDMPzTz: Dichloro-(2-(3,5-dimethyl-1-pyrazolyl)-1,3-thiazine)-palladium(II)

PdDPhPzTn: Dichloro-(2-(3,5-diphenyl-1-pyrazolyl)-2-thiazoline)-palladium(II)

PdDPhPzTz: Dichloro-(2-(3,5-diphenyl-1-pyrazolyl)-1,3-thiazine)-palladium(II)

PdPzTn: Dichloro-(2-(1-pyrazolyl)-2-thiazoline)-palladium(II)

PdPzTz: Dichloro-(2-(1-pyrazolyl)-1,3-thiazine)-palladium(II)

PI: Propidium Iodide

PtDMPzTn: Dichloro-(2-(3,5-dimethyl-1-pyrazolyl)-2-thiazoline)-platinum(II)

PtDMPzTz: Dichloro-(2-(3,5-dimethyl-1-pyrazolyl)-1,3-thiazine)-platinum(II)

PtDPhPzTn: Dichloro-(2-(3,5-diphenyl-1-pyrazolyl)-2-thiazoline)-platinum(II)

PtDPhPzTz: Dichloro-(2-(3,5-diphenyl-1-pyrazolyl)-1,3-thiazine)-platinum(II)

PtPzTn: Dichloro-(2-(1-pyrazolyl)-2-thiazoline)-platinum(II)

PtPzTz: Dichloro-(2-(1-pyrazolyl)-1,3-thiazine)-platinum(II)

PzTn: 2-(1-pyrazolyl)-2-thiazoline

PzTz: 2-(1-pyrazolyl)-1,3-thiazine

RA: Rheumatoid Arthritis

RIP: Receptor-Interacting Protein

RIPA: Radioimmunoprecipitation assay

Rpm: Revolutions per minute

RPMI: Roswell Park Memorial Institute

ROS: Reactive Oxygen Species

SD: Standard Deviation

SDS: Sodium Dodecyl Sulphate

TA: Trimethylammonium

TBE: Tris-borate-EDTA

TEM: Transmission Electron Microscopy

TGA: Thermogravimetric analysis

TMOS: Tetramethyl orthosilicate

TNF: Tumor Necrosis Factor

TRADD: TNF Receptor-Associated protein with Death Domain

WHO: World Health Organization

INDEX

RESUMEN	3
ABSTRACT	5
1. INTRODUCTION	9
1.1. CANCER	9
1.2. CELL DEATH.....	11
1.2.1. Apoptosis.....	12
1.2.1.a. Caspases.	14
1.2.1.b. Apoptosis pathways.....	15
• Extrinsic pathway.....	16
• Intrinsic pathway.....	17
1.2.1.c. Bcl-2 proteins	17
1.3. CHEMOTERAPEUTIC AGENTS	19
1.3.1. Classic chemotherapeutic agents.....	19
1.3.2. Other Pt-based chemotherapeutic agents	21
1.3.3. Chemotherapeutic agents with transition metals.....	22
1.3.3.a. Palladium.....	23
1.3.4. Chemotherapeutic agents with bioactive ligands	25
1.3.4.a. S,N and N,N-heterocycles. Structure and applications.....	25
• Pyrazole.....	26
• Thiazoline.....	27
• Thiazine.....	29
1.3.4.b Ligands employed	31
1.4. NANOPARTICLES	33
1.4.1. Nanoparticles as drug carriers	33
1.4.2. Mesoporous silica nanoparticles	35
2. JUSTIFICATION AND OBJECTIVES	41
3. MATERIALS AND METHODS	45
3.1. REAGENTS.....	45
3.1.1. Chemical reagents	45
3.1.2. Cell lines and culture media	46
3.1.3. Other reagents	46
3.2. LIGANDS SYNTHESIS	47
3.3. LIGANDS CHARACTERIZATION	49

3.4. SOLID PHASE SYNTHESIS FROM M(II)/LIGAND SYSTEM.....	49
3.4.1. Pt(II)/ligand system synthesis	49
3.4.1.a. Precursor <i>cis</i> -[PtCl ₂ (DMSO) ₂] synthesis.....	49
3.4.1.b. Pt(II)/ligand system synthesis	49
3.4.2. Pd(II)/ligand system synthesis.....	51
3.5. SOLID PHASE CHARACTERIZATION FROM M(II)/LIGAND SYSTEM....	52
3.5.1. Elemental analysis.....	52
3.5.2. Crystal structures.....	52
3.5.3. Infrared spectroscopy	54
3.5.4. ¹ H Nuclear magnetic resonance spectroscopy.....	54
3.6. EXPERIMENTAL DESIGN FOR BIOLOGICAL TESTING	54
3.6.1. Cell line culture	54
3.6.2. Cell treatment	54
3.6.3. Cell viability testing	55
3.6.4. Apoptosis determination.....	55
3.6.5. Reactive oxygen species determination	55
3.6.6. Inductively coupled plasma mass spectrometry accumulation	56
3.6.7. Intercalation assay	56
3.6.8. Statistical analysis	57
3.7. EXPERIMENTAL DESIGN OF NANOPARTICLES	57
3.7.1. Synthesis of nanoparticles.....	57
3.7.1.a. Synthesis of mesoporous silica nanoparticles	57
3.7.1.b. Amino functionalization of MSN.....	58
• ATTO-647N NSH ester functionalization of MSN-NH ₂	58
3.7.1.c Carboxy functionalization of MSN	59
3.7.2. Encapsulation of complexes in MSN-NH ₂ -ATTO	59
3.7.3. Characterization of nanoparticles	59
3.7.3.a. Physisorption measurements	59
3.7.3.b. Transmission Electron Microscopy	60
3.7.3.c. Thermogravimetric analysis	60
3.7.3.d. Z-potential	60
3.7.4. Biological testing.....	61
3.7.4.a. Cellular internalization and distribution	61
3.7.4.b. Apoptosis determination.....	61
3.7.4.c. Cellular uptake.....	61
3.7.4.d. Release analysis.....	62
4. RESULTS	65

4.1. ANALOGS OF CISPLATIN WITH PLATINUM AS METAL CENTER	65
4.1.1. Characterization from Pt(II)/Ligand systems	65
4.1.1.a. Elemental analysis	65
4.1.1.b. Crystal structures	65
4.1.1.c. Infrared spectroscopy	70
4.1.1.d. ¹ H Nuclear magnetic resonance spectroscopy	73
4.1.2. Biological testing from Pt(II)/Ligand system	78
4.1.2.a. Cell viability	78
4.1.2.b. Cellular uptake	80
4.1.2.c. Apoptosis determination	81
4.1.2.d. Reactive oxygen species determination	82
4.1.2.e. Intercalation assay	82
4.2. ANALOGS OF CISPLATIN WITH PALLADIUM AS METAL CENTER	83
4.2.1. Characterization from Pd(II)/Ligand systems	83
4.2.1.a. Elemental analysis	83
4.2.1.b. Crystal structures	84
4.2.1.c. Infrared spectroscopy	90
4.2.1.d. ¹ H Nuclear magnetic resonance spectroscopy	94
4.2.2. Biological testing from Pd(II)/Ligand system	98
4.2.2.a. Cell viability	98
4.2.2.b. Cellular uptake	101
4.2.2.c. Apoptosis determination	101
4.3. SYNTHESIS AND ENCAPSULATION OF COMPLEXES IN MESOPOROUS SILICA NANOPARTICLES	102
4.3.1. Characterization of mesoporous silica nanoparticles	102
4.3.1.a. Physisorption measurements	103
4.3.1.b. Transmission Electron Microscopy	104
4.3.1.c. Z-potential	105
4.3.2. Encapsulation of complexes in mesoporous silica nanoparticles	106
4.3.2.a. Thermogravimetric analysis	106
4.3.2.b. Z-potential	108
4.3.3. Biological testing of encapsulated complexes	109
4.3.3.a. Cellular internalization and distribution	109
4.3.3.b. Apoptosis determination	110
4.3.3.c. Cellular uptake	113
4.3.3.d. Release analysis	114
5. DISCUSSION	119

6. CONCLUSIONS.....	129
7. BIBLIOGRAPHY	133
8. APPENDIX	167

RESUMEN/ABSTRACT

RESUMEN

Dado el aumento de la incidencia del cáncer y las limitaciones y efectos secundarios de los tratamientos usados en la actualidad, en la presente tesis doctoral se han sintetizado y caracterizado 12 compuestos de coordinación que contienen heterociclos S,N y N,N en su estructura en combinación con platino(II) o paladio(II) como centros metálicos. La difracción de rayos X de monocristal, el análisis elemental, la espectroscopía infrarroja y la resonancia magnética nuclear de protón confirmaron la estructura y la estabilidad en disolución de dichos compuestos.

Respecto a la actividad biológica, se demostró que los compuestos presentaban actividad citotóxica en las tres líneas estudiadas (HeLa, HL-60 y U-937), siendo las células leucémicas las más sensibles. Entre los compuestos, se comprobó que el Pt(II) fue mucho más efectivo que el Pd(II) como centro metálico. Aunque los tiempos de incubación más largos (48 y 72 h) mejoraron la citotoxicidad de los compuestos de Pd(II) en HeLa, estos seguían sin alcanzar la eficacia de los compuestos con Pt(II). Tanto para los compuestos de Pt(II) como para los de Pd(II) se encontró la misma tendencia, corroborando que la presencia del anillo de pirazol en el ligando tiene un efecto moderado sobre la citotoxicidad, mientras que esta se ve mejorada por la incorporación de anillos fenilo y disminuida por la presencia de grupos metilos en el anillo de pirazol. Además, los compuestos con anillo fenilo fueron los más efectivos independientemente del centro metálico, lo cual indica que la actividad biológica de estos compuestos puede estar influenciada por la incorporación de anillos aromáticos a su estructura. Los complejos PtDPhPzTn y PtDPhPzTz mostraron los mejores resultados, teniendo una IC₅₀ menor que la del cisplatino (CisPt) en las tres líneas celulares. Estos compuestos también mostraron efectos pro-apoptóticos, una fuerte acumulación del metal e inducción de la producción de especies reactivas de oxígeno en células HeLa. Sin embargo, estos compuestos no presentaron capacidad intercalante con el ADN. También se demostró que los ligandos libres no afectaban de forma significativa la viabilidad, lo cual indica que la coordinación con el centro metálico es indispensable para que se produzca el efecto citotóxico.

Por otro lado, se logró con éxito la encapsulación de 6 de los compuestos sintetizados en nanopartículas mesoporosas de sílice (MSN), como pudo comprobarse mediante análisis termogravimétrico. Además, se confirmó que las partículas entraban en las células HeLa y se distribuían en el núcleo, aparato de Golgi, membrana plasmática y mitocondria. La encapsulación en MSN-NH₂ de los compuestos menos efectivos PtPzTn

y PtPzTz mejoró el transporte a las células y su citotoxicidad en HeLa, mostrando una mayor liberación y acumulación de estos compuestos que las nanopartículas de PtDPhPzTn y PtDPhPzTz. Así, PtPzTn encapsulado redujo notablemente la población de células vivas más de un 50% a una concentración mucho menor que la IC₅₀ del compuesto libre. Por otro lado, en el caso de PtPzTz, el descenso de la población de células vivas fue menor, pero la reducción de la concentración efectiva de compuesto fue mayor de tres veces. Estos datos confirmaron la efectividad de este tipo de nanopartículas como sistemas de transporte y administración de fármacos para algunos de nuestros complejos.

ABSTRACT

Due to the increasing incidence of cancer and the limitations and side effects produced by the treatments used nowadays, in the present PhD thesis 12 coordination complexes with S,N and N,N heterocycles in their structure, in combination with platinum(II) or palladium(II) as metallic centers have been synthesized and characterized. X-ray diffraction, elemental analysis, IR spectroscopy, and ^1H NMR spectroscopy confirmed the structure and stability in solution of the complexes.

Respect to their biological activity, it was demonstrated that the complexes presented cytotoxic effect in the three cell lines studied (HeLa, HL-60 and U-937), being the most sensitive cells the leukemic ones. Among the complexes, it was checked that Pt(II) was far more effective as metal center than Pd(II). Although longer incubation times (48 and 72 h) improved the cytotoxicity of the Pd(II) complexes in HeLa cells, they still did not reach the efficacy of Pt(II) complexes. For both Pt(II) and Pd(II) complexes the same trend was found, corroborating that the presence of the pyrazole ring on the ligand has a moderate effect on cytotoxicity, while this effect seems to be enhanced by the incorporation of phenyl rings and diminished by the presence of methyl groups in the pyrazole ring. In addition, complexes with phenyl substitutions were the most effective regardless the metal center, which indicate that the biological activity of these complexes could be influenced by the incorporation of aromatic groups into their structure. PtDPhPzTn and PtDPhPzTz displayed the best effects, having lower IC_{50} values than cisplatin (CisPt) in the three cell lines. These complexes also showed proapoptotic effects, strong metal accumulation and reactive oxygen species (ROS) induction in HeLa cells. Nevertheless, these complexes did not present DNA intercalating capacity. It was also demonstrated that none of the free ligands produced significant effects in cell viability, which indicates that their coordination to the metal center is indispensable to produce the cytotoxic effect.

On the other hand, the encapsulation of 6 of the synthesized complexes in mesoporous silica nanoparticles (MSNs) was successfully achieved, as ascertained by thermogravimetric analysis. Likewise, it was confirmed that the particles entered in HeLa cells and were distributed in the nucleus, Golgi, plasma membrane and mitochondria. The encapsulation of the less effective drugs PtPzTn and PtPzTz in MSN-NH₂ improved their transport to the cells and their cytotoxicity in HeLa cells, showing stronger release of the complexes from the particles and higher accumulation in cells than their counterparts

PtDPhPzTn and PtDPhPzTz. It was obtained a reduction of the population of live cells by more than 50% at a concentration of encapsulated PtPzTn that was far below the IC₅₀ of the free drug. Besides, encapsulated PtPzTz produced a smaller decrease in the population of live cells, but the reduction of the concentration of PtPzTz was greater than three times. This data confirmed the effectiveness of this kind of particles as drug delivery systems for some of our complexes.

1. INTRODUCTION

1. INTRODUCTION

1.1. CANCER

Cancer is a group of diseases characterized by the uncontrolled growing and propagation of abnormal cells. It can be caused by external factors such as tobacco, infectious organisms, and a poor healthy diet, and by internal factors like genetic mutations, hormones, and immune systems affections. The period between the exposition to the factor and the development of a detectable cancer can be longer than ten years [1].

There exists a mechanism in the body to eliminate aberrant and/or aged cells. When this mechanism fails, the abnormal cells divide uncontrollably, leading to the generation of a tumor. The common hallmarks of cancer cells are included in Figure 1.1, involving evasion of growth suppressors, tissue invasion and metastasis, replicative immortality, and death resistance, among others [2].

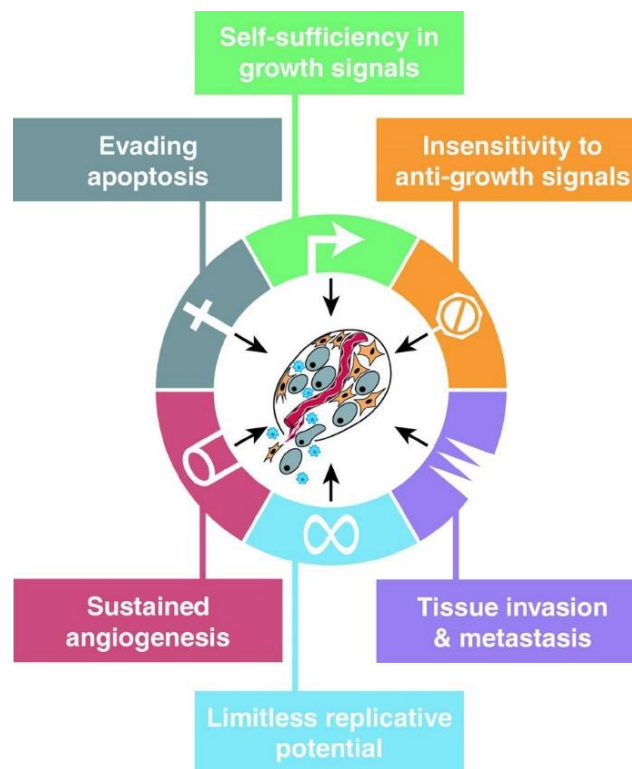


Figure 1.1. Acquired capabilities of cancer [2].

Many cancer types exist since it can develop and grow in any part of the body. In fact, the different forms of cancer are named according to the body part where they were initiated. However, there are two main categories established: hematological cancers, which are produced from blood cells (leukemia, lymphoma, and multiple myeloma), and

solid tumors, which are developed in any organ, tissue, or body part (e.g., breast, prostate, lung, colorectal). The different types can have many differences in the way they grow, respond to the treatment or spread to other body parts different from the ones where they initiated (metastasis) [3].

According to the World Health Organization (WHO), cancer is the main reason of death around the world, reaching approximately 10 million deaths (one out of six registered patients) in 2020 [4]. Moreover, it is expected to have an increase in the number of new diagnosed cases from 19.3 M in 2020 to 30.2 M in 2040 (numbers that exclude the non-melanoma skin cancers (NMSC)) and an increase in the mortality worldwide from 9.96 M in 2020 to 16.3 M in 2040.

The numbers of cancer in Spain is a report made by the Spanish Medical Oncology Society that includes the incidence, mortality, survival, and prevalence of cancer in Spain. The most frequent cancer diagnosed in Spain in 2023 will be colon and rectum (42,721 new cases), breast (35,001), lung (31,282), prostate (29,002) and bladder (21,694) [5]. Considering the data separately by sexes, prostate is the most diagnosed in men, while breast is the most diagnosed in women, being colon and rectum the second in both groups. These data are quite coincident with the most prevalent cancers worldwide, as can be seen in Figure 1.2 [6]. It can be also observed that some cancers, such as lung, stomach, and liver, have a higher rate of mortality respect to the number of cases diagnosed (Figure 1.2).

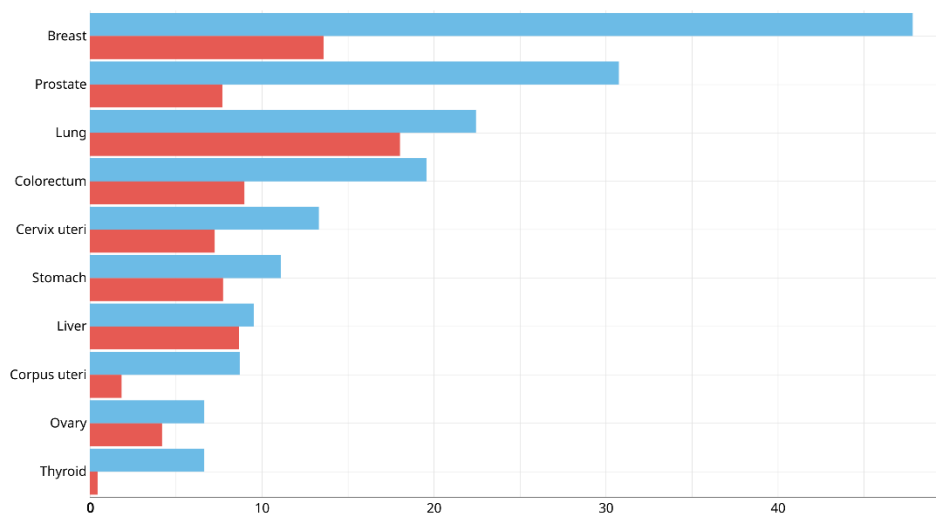


Figure 1.2. Estimated age-standardized incidence (blue) and mortality (red) rates in the world in 2020 including both sexes and all ages (excluding NMSC) [6].

Nevertheless, it is important to take into account that the figures could be influenced by the coronavirus pandemic of 2019 (COVID-19) due to the reduction to medical assistance and the restrictions. This could have led to a delay in the diagnosis and treatment of the patients that could have caused a drop in the incidence in the short term, followed by an upturn of the disease on the advance phase and mortality [7].

Nowadays there are different methods to treat cancer, being one of the main procedures used the chemotherapy, both alone or in combination with surgery and radiotherapy. Drugs employed to that purpose generally induce apoptosis, not only in cancer cells but also in non-tumor cells.

1.2. CELL DEATH

To achieve a proper physiological growth and development, cell death is an essential biological process. This event consists in ceasing biological functions of the cell, either as a result of a natural process of replacement of old cells for new ones, or because of localized injuries or diseases.

There are three classical forms of cell death: apoptosis, necrosis, and autophagy, which present different morphological characteristics (Figure 1.3). Nevertheless, the understanding of cell death has grown in the last decades, starting to realize that the molecular mechanisms of different types of cell death are distinct but also overlapping. Although the previously mentioned simplified classification of cell death is still widely used, the Nomenclature Committee on Cell Death (NCCD) has recently made an updated review of the pathways involved in programmed cell death [8].

However, in this work it will only be briefly described the classical forms of cell death, making a most extensive description of apoptosis in subsequent sections. Thus, apoptosis is a caspase-mediated form of programmed cell death. Among its characteristics, it can be found cytoplasmic shrinkage, chromatin condensation (pyknosis), nuclear fragmentation (karyorrhexis), and membrane blebbing with formation of small vesicles known as apoptotic bodies. These vesicles are eliminated by phagocytes and degraded within lysosomes, without causing inflammatory response. Another non-inflammatory cell death process is autophagy, which is based on an extensive cytoplasmic vacuolization. The vesicles formed, known as autophagosomes, fuse with lysosomes and promote the degradation of autophagosomal content. This process is considered a cellular 'recycling factory' that mediates damage control by removing non-functional molecules

and organelles, which can ultimately lead to cell death [9]. On the other hand, necrosis is classically considered unregulated and caused by nonspecific stress triggers. Unlike apoptosis, the expansion of cellular organelles, rupture of the plasma membrane and release of intracellular content, produce an inflammatory response [10,11]. However, some studies have found programmed forms of necrosis (necroptosis), which have changed the perception about it [12].

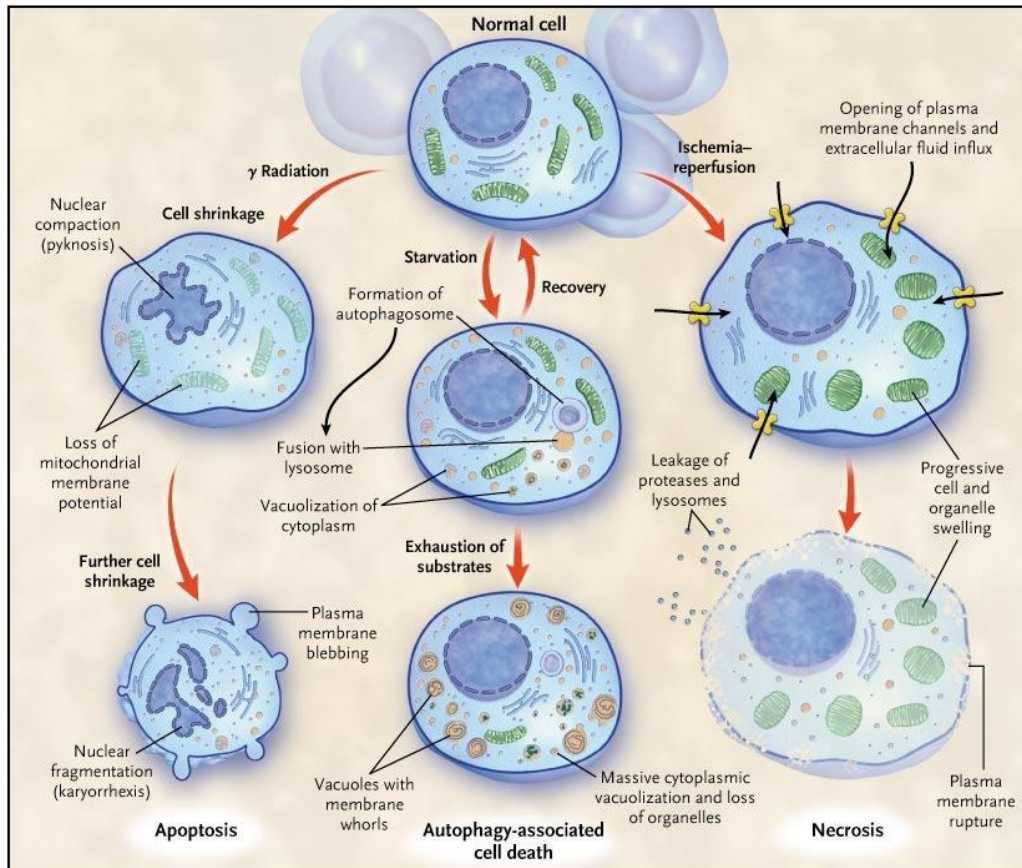


Figure 1.3. Models of cell death: Apoptosis, autophagy, and necrosis [13].

1.2.1. Apoptosis

Throughout history, physiological cell death has been known by many names. Firstly, it was defined as degeneration, mortification, and necrosis by Virchow in 1858 when studying the macroscopic parameters of cell death process. Then, microscopic observations in 1879 introduced the term *Karyorrhexis* and *Karyolysis*, referring to the disintegration of the nucleus. A decade later, Arnheim proposes *piknosis* and margination of chromatin, being followed by Fleming and their *chromatolysis*, term latter used by Gräper in 1914. Nevertheless, the widely known term apoptosis was introduced in the

biological terminology by J.F.R Kerr, A.H Wyllie and R. Currie in 1972 [14]. However, this term was suggested by James Cormack, professor of the Greek department of the University of Aberdeen. This word was used in Greece to describe the “dropping off” or “falling off” of petals from flowers or leaves from trees.

This process is typical from pluricellular organisms in which damaged cells are self-destroyed without an inflammatory response or harmful to the surrounding cells. It is considered a physiological process of cell death that is initiated by developmental or environmental stimuli that initiates a genetic program that controls, designs and initiates a series of events that lead to the ordered destruction of the cell. This is a process that requires energy in form of adenosine triphosphate (ATP) and afford the elimination of the apoptotic cell without modifying the physiology of the tissue [15].

Apoptosis is a highly regulated process due to the reception, integration and amplification of extra- and intra-cellular signals and is essential to maintain a homeostatic equilibrium between the number of new and damaged cells. A deregulation of this equilibrium can lead to different diseases. Thus, an uncontrolled proliferation of cells can derive in cancer, while an excessive level of cell death can lead to Alzheimer’s, Parkinson’s or rheumatoid arthritis [16–18].

Apoptosis can be divided into biochemically and morphologically distinct phases [19,20]. In the first one, pro-apoptotic stimuli trigger activation of the central molecular machinery of apoptosis, which is called the “initiation phase”. In this phase, mitochondria are essential, due to the production of multiprotein complexes which liberates intramitochondrial content such as cytochrome c, hormones from caspase family and other triggers of apoptosis. In the second phase, known as “effector phase”, the molecular executioner machinery becomes fully activated, producing the condensation of the chromatin and the induction of apoptotic changes in nuclei by cytosolic extracts [19,20]. Only after this, in the “degradation phase”, the hallmarks of apoptosis do become evident, which include morphologic changes and DNA fragmentation.

Respect to the morphological characteristics of apoptosis, the following features are highlighted (Figure 1.4) [21,22]:

- Intracellular density increases and the endoplasmic reticulum (ER) dilates and forms vesicles which fuse to the plasmatic membrane and release their content to the extracellular medium.
- Increases of calcium concentration on the cytoplasm.

- Translocation of glycan groups to the cellular surface, acting as signals to phagocytes and preventing from inflammation.
- Alteration of cytoskeleton conformation, activation of proteases and altering the intracellular transport of growth factors and proteins.
- Synthesis of proteins necessary to cell death routes.
- Condensation and fragmentation of chromatin and DNA by endogenous endonucleases in fragments called oligonucleosomes (nucleic acid fragments of about 180-200 bp integer multiples).

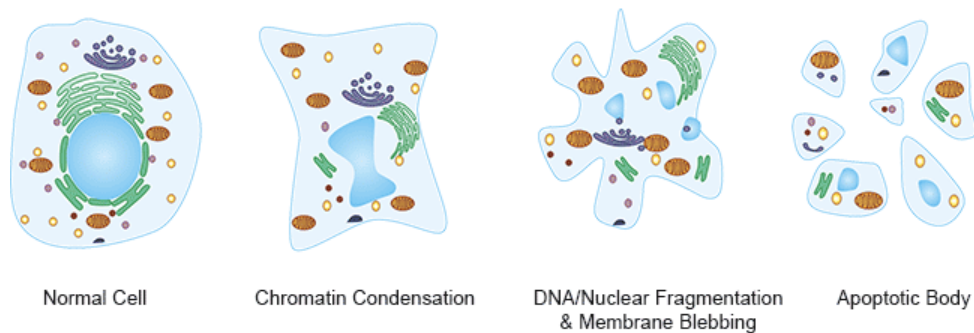


Figure 1.4. Morphological changes during apoptosis [22].

1.2.1.a. Caspases.

Caspases are cysteine proteases that cleave their substrate proteins specifically behind an aspartate residue [23]. Thus, their name is a contraction of **C**ysteine-dependent **A**Spartate-specific prote**A**SES. They are the main components of the apoptosis mechanism, are formed constitutively and are normally present as inactive proenzymes. For the induction of full enzymatic activity, they require cleavage at specific internal aspartate residues (Asp), which separate large and small subunits from each other (Figure 1.5) [23]. Caspases are mainly present in the cytosol, although they can be also found on the nucleus and the mitochondria.

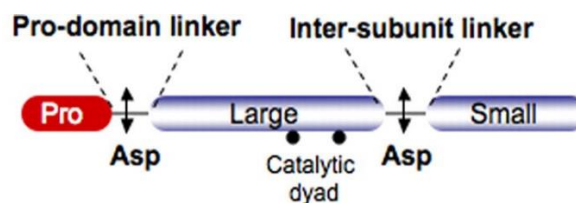


Figure 1.5. Caspase structure. A prodomain precedes the catalytic domain, composed of two covalently linked subunits. Sites for (auto)proteolysis at Asp residues are indicated [24].

In mammals, 14 proteins form the caspase family, although only eleven of them are expressed in humans: from caspase-1 to caspase-10 and caspase-14, which is only expressed in keratinocytes [25]. In addition, caspases are divided in three different groups according to their function (excluding caspases-14) (Table 1.1). Thus, it can be found initiator caspases, effector caspases or caspases implicated in inflammation [26].

Table 1.1. Classification of human caspases by function.

<i>Function</i>	<i>Mammalian caspases</i>
Apoptotic initiator caspases	-2, -8, -9, -10
Apoptotic effector caspases	-3, -6, -7
Inflammatory initiator caspases	-1, -4, -5, -11, -12
Keratinocyte differentiation effector caspases	-14

Initiator caspases (-2, -8, -9 and -10) have N-terminal prodomains and similar structural domains, i.e., DED (Death Effector Domain) or CARD (Caspase Recruitment Domain), and are activated via proteolysis. On the other hand, effector caspases (-3, -6 and -7) have prodomains of 20-30 amino acids eliminated by proteolysis, without structural domains.

Studies on substrate specificity, prodomain structure and biological function [23,27–30] have revealed that caspases are activated during apoptosis in a self-amplifying cascade. Activation of the upstream caspases, such as caspases -2, -8, -9 and -10, by pro-apoptotic signals leads to proteolytic activation of the downstream or effector caspases (-3, -6 and -7). The effector caspases cleave a set of vital proteins and thus initiate and execute the apoptotic degradation phase including DNA degradation and the typical morphologic features [31].

1.2.1.b. Apoptosis pathways

There are two main signaling pathways to activate apoptosis. The first one implicates the activation of members of the TNF (Tumor Necrosis Factor) receptor family [32], and it is known as extrinsic or death receptors pathway. The other one, called intrinsic or mitochondrial pathway, is induced by cellular stress like DNA damage, ER stress, viral infection, oncogene expression, UV radiation, etc. [33]. It can be described an additional pathway called perforin or granzyme pathway, that involves T-cell mediated cytotoxicity and perforin-granzyme killing of the cell [34]. All pathways activate initiator

caspsases and converge in effector caspsases activation. A schematic representation of the three pathways is included in Figure 1.6. In the next subsections a more detailed description of extrinsic and intrinsic pathways can be found.

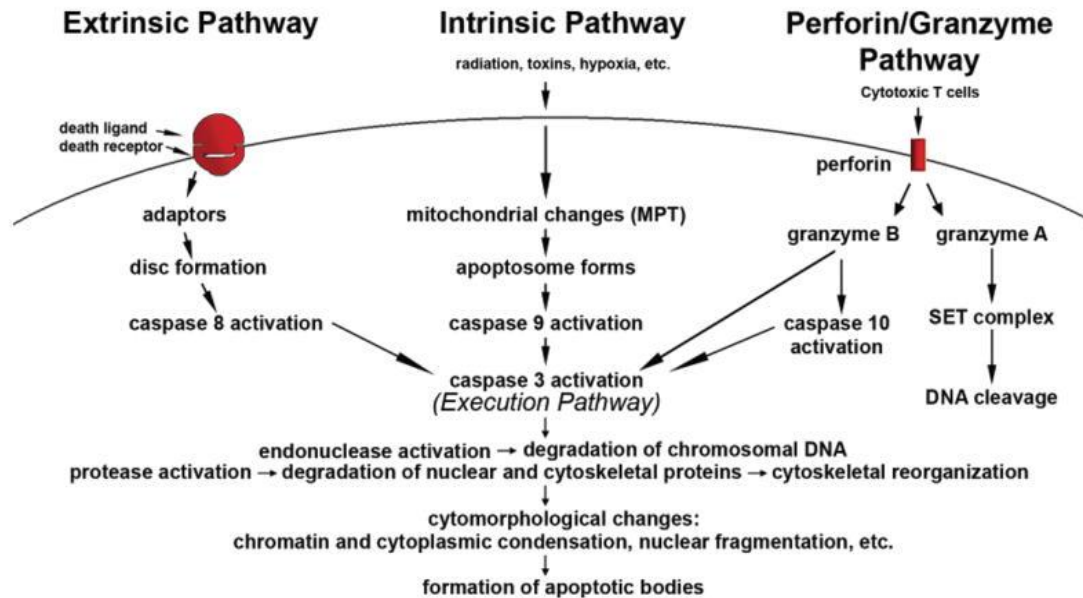


Figure 1.6. Schematic representation of apoptotic pathways [34].

- **Extrinsic pathway**

As previously indicated, this pathway involves death receptors from TNF superfamily [35], which have a cytoplasmic domain of about 80 amino acids called the “death domain” (DD). To be able to transmit the death signal from the cell surface to the intracellular environment, this domain is essential. Thus, this pathway is activated when extracellular ligands interact with the extracellular domain of the “death receptors” (DR) (transmembrane receptors) as it occurs with FasL/FasR, TNF- α /TNFR1 or Apo3L/DR3 [34,36–38].

A conformational change in DR is produced by the ligand joining, leading to the recruitment and binding of adaptor proteins through their DD. For example, FasL/FasR bind the adapter protein FADD (Fas-associated protein with death domain) and TNFL/TNFR bind TRADD (TNF receptor-associated protein with death domain) [34,37]. The joining of TRADD produces the recruitment of FADD and RIP (Receptor-interacting protein), and the later association of FADD with procaspase-8. At this point, a death-inducing signaling complex (DISC) is formed, which activates procaspase-8 so

that its prodomain stays at DISC, while active caspase-8 dissociates from DISC and initiates the caspase cascade of apoptosis execution phase [38].

- **Intrinsic pathway**

Intrinsic or mitochondrial pathway is triggered by non-receptor-mediated stimuli, involving extra and intracellular stresses. This entails intracellular signals that may act in a positive (radiation, hypoxia, free radical, viral infections, etc.) or negative (absence of growth factors, hormones, and cytokines) manner [34,39,40].

Changes produced by the stimuli are mainly focused on the mitochondria, resulting in the loss of membrane potential, mitochondrial membrane permeability, and liberation of pro-apoptotic proteins to the cytosol [41]. These proteins belong to two main groups:

- First group: cytochrome *c*, Smac/DIABLO, and serine protease HtrA2/Omi. Cytochrome *c* in combination with Apaf-1 and procaspase-9, form the apoptosome, a multi-protein complex which triggers caspase-9 activation and subsequent caspase-3 cascade [36,42]. On the other hand, Smac/DIABLO and HtrA2/Omi induce apoptosis via inhibiting IAP (inhibitors of apoptosis proteins) activity [43,44].
- Second group: AIF (apoptosis-inducing factor), CAD (Caspase-Activated DNase) and endonuclease G. Basically, these proteins cause DNA fragmentation and chromatin condensation [45,46].

The regulation of these apoptotic mitochondrial events take place through the Bcl-2 family proteins, which are described in the next subsection [47].

1.2.1.c. Bcl-2 proteins

The Bcl-2 family is formed by a group of proteins, which share sequence homology within conserved α -helical regions known as Bcl-2 homology (BH) domains and are closely involved in the mitochondrial membrane permeability. These proteins can be either pro-apoptotic, favoring the permeabilization of the mitochondrial membrane and later inducing apoptosis, or anti-apoptotic, maintaining the membrane integrity and avoiding the programmed cell death [34].

As can be seen in Figure 1.7, all anti-apoptotic members and some pro-apoptotic ones, such as BAX and BAK, are ‘multi-domain’ proteins that contain 3–4 BH domains. On the other hand, a single BH domain (BH3) is found in pro-apoptotic ‘BH3-only’ molecules. Several Bcl-2 proteins, not only have a BH domain but also a transmembrane domain, being able to localize to subcellular membranes, including outer mitochondrial membrane and the ER. As for the proteins that do not have this transmembrane domain, they can join the mitochondria establishing interactions with other proteins [48].

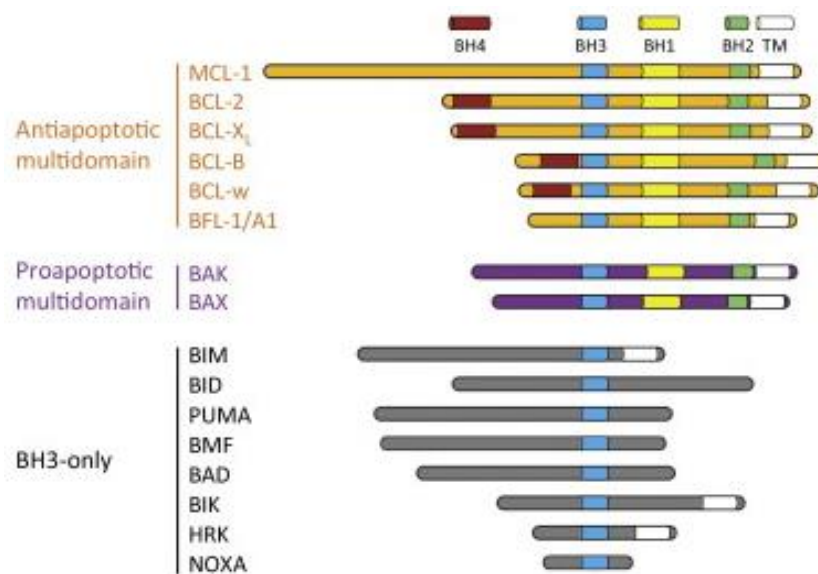


Figure 1.7. Classification of the proteins from Bcl-2 family [48].

Activation of BAX and BAK plays an important role in the intrinsic pathway through the permeabilization of the outer mitochondrial membrane, which causes the release of cytochrome *c* into the cytoplasm and later form the apoptosome and initiate the cascade of caspases, as already described [49,50]. However, these proteins can be inhibited by anti-apoptotic Bcl-2 family members, being apoptosis only initiated when anti-apoptotic proteins are bound to BH3-only proteins [51]. In the case of BH3-only proteins, their activity is initiated as a response to developmental and stress stimuli [52]. For example, PUMA and NOXA are critical for DNA damage-induced apoptosis [53], while Bid, which has a lipid transfer activity between mitochondria and other intracellular membranes, translocate to mitochondria to also ease the release of cytochrome *c* to the cytosol [54].

1.3. CHEMOTHERAPEUTIC AGENTS

Chemotherapy is one of the most extensive ways to treat a wide variety of cancers. It is based on the use of drugs to destroy cancer cells, preventing them from growing and dividing. This treatment usually consists of a systemic medication, which means that the drug travel through the bloodstream and reaches all parts of the body. For that reason, it can also damage healthy cells, causing numerous side effects such as hair loss, nausea, nephrotoxicity, neurotoxicity, etc. [55,56]. Moreover, cancer cells can acquire resistance to treatment, preventing the drugs from performing their effect [57].

1.3.1. Classic chemotherapeutic agents

One of the mainly used chemotherapeutic agents is *cis*-diamminedichloroplatinum(II) or cisplatin (CisPt), which presents a yellow color and a square-planar geometry (Figure 1.8) [58]. This drug was first synthesized by the Italian chemist M. Peyrone in 1844, although its structure was elucidated in 1893 when Alfred Werner studied it [59]. However, it was not until 1965 when Rosenberg and coworkers discovered their inhibitory effect of the cellular division of the bacterium *Escherichia coli* [60]. That was the hint to employ this compound to avoid the growth of cancer cells.

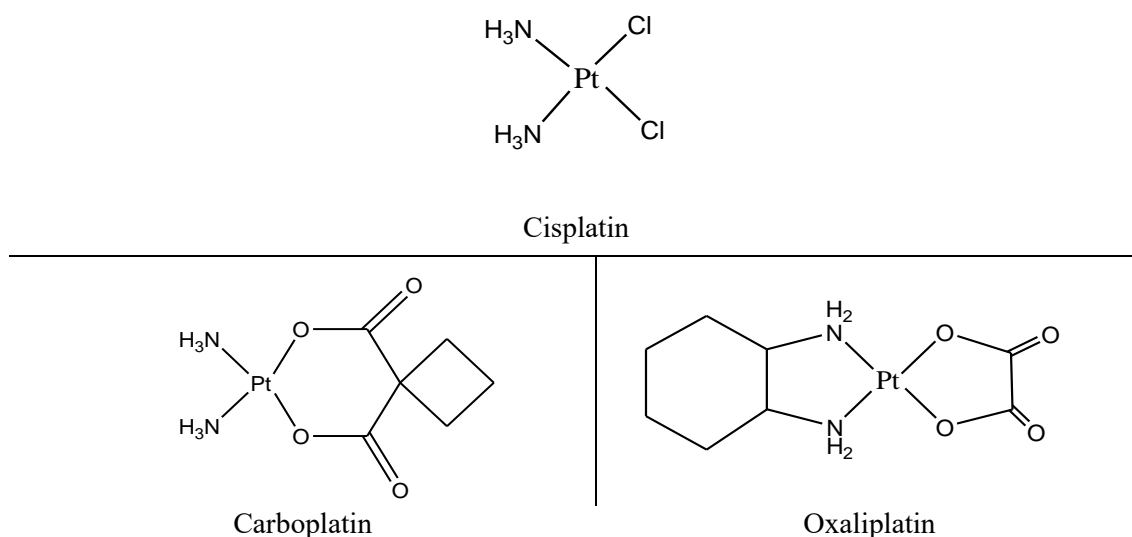


Figure 1.8. Cisplatin, carboplatin and oxaliplatin structures.

One of the first uses of CisPt in clinical trials was for the treatment of testicle cancer, where it led to a 70-90% of survival rate. In addition, since its approval by FDA (Food and Drug Administration) in 1978, it was also demonstrated to be quite effective

against solid tumors like head and neck, ovary, bladder, stomach, breast, lung, and prostate cancer. It can be also used in the treatment of neuroblastoma (adrenal glands, neck, chest, or spinal cord), sarcoma (bones or muscle), multiple myeloma (bone marrow), mesothelioma (tissue that cover lungs and other organs), melanoma (skin) and lymphoma (lymphatic system) [61–63]. Furthermore, it could be administrated alone or in combination with other agents like antimetabolites (methotrexate), topoisomerase II inhibitors (doxorubicin, mitomycin and bleomycin), taxol (paclitaxel) or vinca alkaloids (vinorelbine). Nevertheless, CisPt has also its limitations due to acquired or intrinsic resistance of cells to the drug [64].

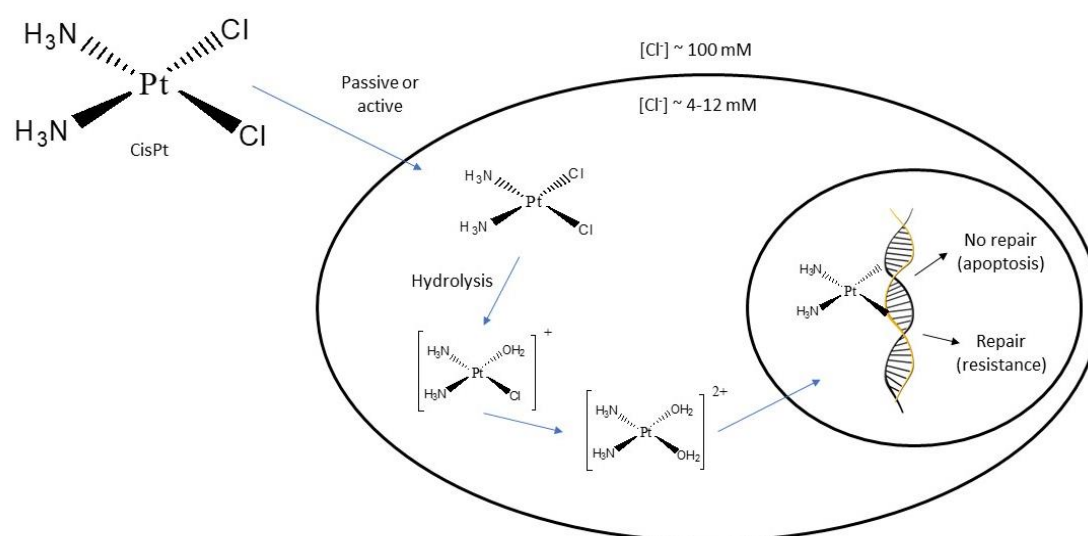


Figure 1.9. Mechanism of action of cisplatin (CisPt).

Respect to the action mechanism of CisPt (Figure 1.9), it forms adducts with DNA through an initial substitution of the chloride ligands by water and the subsequent formation of a platinum-DNA linkage [59]. This produces the constraint of DNA replication, which grants the cytotoxic effect, primarily in tumor cell, and eventually leads to apoptosis [65,66]. Nonetheless, CisPt has also its drawbacks, not only due to the previously mentioned acquired or intrinsic resistance, but also because of severe side effects such as nausea and vomits, anemia, and neuro and nephrotoxicity that also affect healthy cells [55–57,64,67].

In order to avoid or diminish the weaknesses of CisPt, over the last 40 years, 23 other platinum-based drugs have entered clinical trials. Among those, only carboplatin and oxaliplatin (Figure 1.8) have gained international marketing approval, and another three (nedaplatin, lobaplatin and heptaplatin) were approved only in regions of the Asiatic

continent [67–70] (Figure 1.10). Though these drugs present reduced neuro and nephrotoxicity in comparison to CisPt, they also have side effects, including thrombocytopenia [69–72].

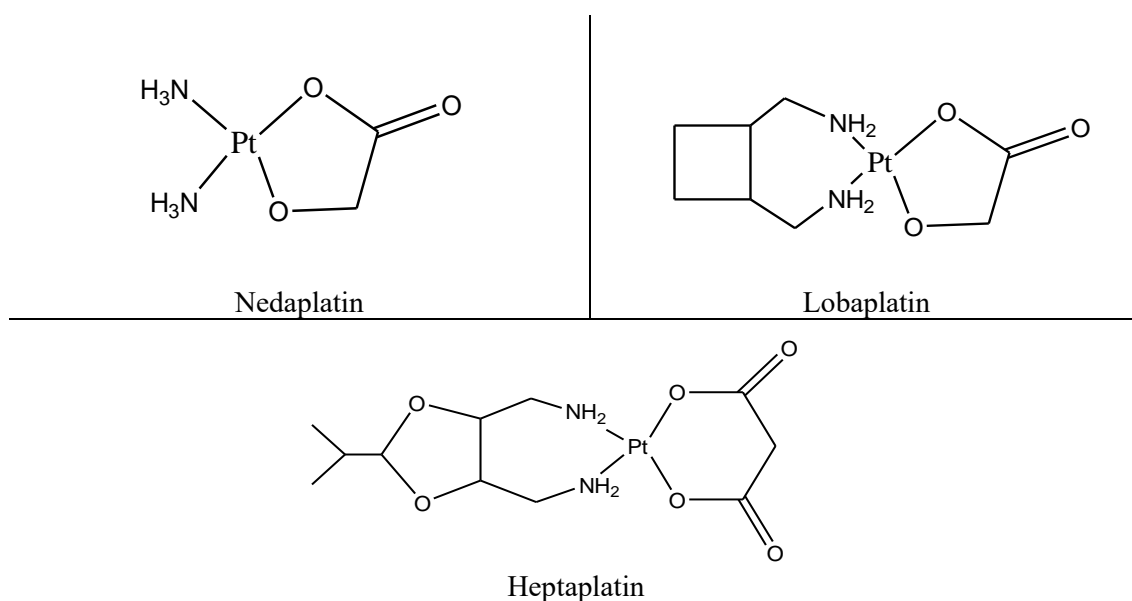


Figure 1.10. Nedaplatin, lobaplatin and heptaplatin structures.

1.3.2. Other Pt-based chemotherapeutic agents

Apart from the previously seen classical chemotherapeutic agents, other complexes with Pt(II) as metallic center have been developed, and several of them have even entered clinical trials. Among them, it could be mentioned BBR 3464, a triplatinum complex which showed cytotoxic properties at concentrations 10 times lower than CisPt in both *in vitro* and *in vivo* studies. Some Phase II studies demonstrated its efficiency against non-small cell lung carcinomas (NSCLC) and ovarian tumors in advanced stages, but also a lack of activity against gastric tumors and small cell lung cancer [73,74]. On the other hand, results from another Phase II study related with pancreatic cancer have not yet been made public [75].

Satraplatin was the first orally active platinum agent reported and showed greater antitumor efficacy *in vivo* relative to CisPt and carboplatin. Several Phase II studies have shown palliation in 46% of patients with metastatic NSCLC, 38% of response in patients with small-cell lung cancer and squamous cell head and neck cancer and clinically beneficial or partial rates of response in patients with relapsed ovarian cancer and advanced/recurrent squamous cancer of the cervix [76]. Currently, a Phase I clinical trial is ongoing regarding the efficacy of satraplatin on prostate cancer without metastases [75].

On the other hand, picoplatin (AMD473 or ZD0473) has shown effectiveness against some types of ovarian cancer, mesothelioma, small cell lung cancer and NSCLC in preclinical studies. In several Phase II trials it was observed some response in patients with small cell lung cancer, activity and benefits in terms of survival rate on ovarian tumors, and inhibition of the progression of the disease for approximately 50% of patients with mesothelioma and metastatic breast cancer [77–79]. Nevertheless, only one Phase III study was undertaken targeting small cell lung cancer, with promising results for patients with rapid disease progression [69].

Finally, it can be mentioned some complexes of Pt(IV) such as ormaplatin (NSC 363812), which has displayed *in vitro* and *in vivo* activity against some CisPt-resistant cancers, has been involved in six Phase I clinical trials, but no Phase II trials have been planned so far due to its neurotoxicity. On the other hand, iproplatin (JM9 or CHIP) is one of the most clinically studied platinum agents not approved for marketing. It undertook 38 clinical trials from Phase I to III. Phase II trials were run in patients with a wide range of cancer types, and Phase III were only studied in patients with ovarian cancer and with metastatic epidermoid carcinoma of the head and neck [80,81], but the results were not better than CisPt or carboplatin and no further trials were carried out.

1.3.3. Chemotherapeutic agents with transition metals

In the last decades, the search for new chemotherapeutics has been focused not only on the next generation of platinum-based complexes, but also on the study of other transition metals [76,82–84]. The exploration for alternative metal centers has been increasingly considered, especially the ones sharing physical and chemical properties with platinum. The use of a specific central metal ion can powerfully impact on biological activity since each metal shows distinctive physicochemical features, including redox ability, binding preferences with ligands and targeted molecules, and ligand-exchange kinetics. With all that in mind, over the last few decades a wide variety of transition metals have been used to synthesize new complexes with anticancer properties, such as ruthenium, copper, rhodium, palladium, osmium, iridium, etc. [82,85–87]. Nevertheless, many candidate drugs belonging to this class have been extensively evaluated in preclinical models *in vitro* and *in vivo*, but only a few have achieved different stages of clinical studies [88,89].

Based on the literature, the advancement in Ru-based anticancer agents is remarkable [90–96], although none of them are used in the clinic yet [91,97]. Nonetheless, well known species such as NAMI-A, KP1019, and NKP1339 are currently undergoing clinical trials, opening new approaches in cancer treatment [98]. On the other hand, promising results in preclinical studies were obtained with organoiridium(III) complexes, which exhibited higher cytotoxicity against several human cancer cells (e.g., breast, colon, prostate, melanoma, and leukemia) compared to CisPt [99]. Ir(III)-based complexes have also shown interesting results via mitochondria-targeted anticancer activity [100,101] and autophagy-regulating activities [102]. Respect to Au(I)-containing molecules, auranofin and aurothiomalate were able to inhibit cancer cell growth in both *in vitro* and *in vivo* models [103,104] and are being studied in clinical trials. For that reason, hundreds of analogs of auranofin were synthesized and tested in preclinical screenings, some of them showing higher activity than CisPt *in vitro* [103,105]. In addition, other complexes based on Au(III) with chelating ligands have showed bioactivity in both *in vitro* and *in vivo* models [106,107]. Considering complexes with Cu as metallic center, Casiopeinas are a group of copper-based chemical compounds with cytotoxic, genotoxic, antiproliferative and antineoplastic activity, demonstrated *in vitro* and *in vivo*. Among them, Casiopeina III was tested in a phase I clinical trial with acute myeloid leukemia and colon cancer patients, while Casiopeina II-gly (CasII-gly) was tested on cervical cancer patients. Unfortunately, a current phase I trial to test toxicity of CasII-gly in humans has shown a high cardiotoxic effect, which will probably lead to stop the clinical trials [76].

Extensive and updated information of other complexes with a wide variety of metal centers approved by FDA, in clinical trials or in preclinical studies, could be found in the review of Singh and co-workers, which includes more than 200 complexes with Ru, Pt, Fe, Rh, Au, Cu, Re, V, Zn, Ir, Ti, Co, Ga, Mo and Ag as metallic centers [88].

1.3.3.a. Palladium

Palladium (Pd) is under focus as the central coordinator metal in prospective anticancer complexes. The main interest of this metal is the similarity in its oxidative +2 state (the most common one) with Pt(II) in terms of both electronic structure and coordination chemistry [73,108]. The first potential anticancer Pd-based drugs were synthesized and tested in the 1980s. However, it was checked that the rapid hydrolysis of

these complexes drives to a lack of antitumoral activity [73]. In fact, Pd-based complexes exchange their ligands much faster than the analogous Pt-based complexes, leading to both instability in biological environment and failure to achieve drug targets [109]. For that reason, to improve stability in physiological conditions, researchers have envisioned Pd(II)-based complexes where metal ion is bound to strong coordination ligands and/or non-labile moieties [110,111]. Thus, Pd(II)-based stabilized complexes showed good anticancer activity and reduced toxicity to normal tissues in preclinical studies compared with Pt(II)-based congeners [112,113].

In the last decade, many original Pd-based complexes has been proposed as an alternative to Pt-based complexes in preclinical studies against many types of cancer cells. However, only a few derivatives have reached the clinic to date [109,114].

Based on the structural characteristics of these complexes, Scattolin and co-workers have classified Pd-based complexes into mono- and polynuclear. As it can be deduced, the first ones present only one Pd(II) atom in their core, while the second ones exhibit more palladium atoms (generally two) in their structure [109]. Among them, there are some derivatives that have higher activity than platinum derivatives in preclinical models of breast cancer [115] and some others have displayed anticancer effects in leukemic models [116]. In fact, some binuclear Pd-based complexes are undergoing preclinical evaluation [109,114,117,118].

Finally, despite the quantity of compounds that have been synthesized and developed for preclinical experimentation, only one Pd-based drug is currently being used in the clinic. Padeliporfin or TOOKAD (Figure 1.11) was commercialized in 2017 as the first Pd(II)-based compound used in the clinic, demonstrating hitherto to be a safe and well-tolerated photodynamic agent [119,120]. In addition, this drug is also under study for the treatment of some kidney neoplasms [121].

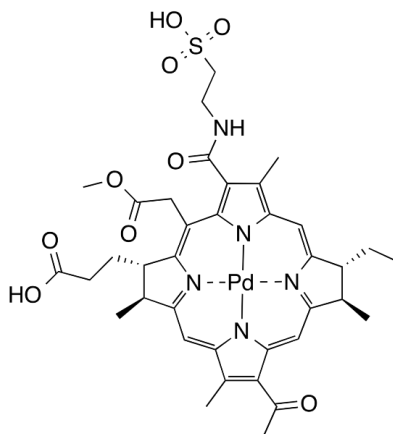


Figure 1.11. Padeliporfin or TOOKAD structure.

1.3.4. Chemotherapeutic agents with bioactive ligands

One of the most often employed approaches for developing new drugs is the coordination of bioactive ligands to transition metals, inasmuch as it could improve biological activity [122,123]. On that note, heterocycles have been extensively used as part of a wide variety of pharmaceutical drugs with multiple applications (antibacterial, antifungal, antimycobacterial, genotoxic, antimalarial, analgesic, antiinflammatory, antidepressant, antitumoral, etc. [124]). In fact, more than 85% of all biologically active chemical entities contain a heterocycle. Among them, it can be easily found the presence of five- or six-membered rings with one or various atoms of nitrogen, sulfur, and oxygen. This increasing use of heterocycles, both from natural or synthetic origin, can be explained by its usefulness to modify different characteristics of drugs such as lipophilicity, solubility, polarity, etc. [125]. Besides, their properties have been especially associated to the lone pair of electrons provided by these atoms, which allows the coordination to the metallic center [126].

For many years, nitrogen heterocycles and nitrogen-sulfur heterocycles have gained particular attention of pharmaceutical industry due to their structural variety and biological importance [127]. Actually, more than 60 drugs with nitrogen-containing heterocycles and anticancer properties have been approved by FDA. Among these heterocycles, it can be mentioned pyrimidine, quinolone, carbazole, pyridine, imidazole, benzimidazole, triazole, β -lactam, pyrazole, quinazoline, etc. [128]. On the other hand, nitrogen-sulfur heterocycles have also shown potential therapeutic interest especially with thiazole, thiazine, pyrimidine, benzothiazines, pyrazolylbenzothiazines, etc. [127].

For all that, the potential benefits of donor ligands containing S,N and N,N-heterocycles are undeniable, being selected for the structures of the synthesized complexes presented in this PhD thesis.

1.3.4.a. S,N and N,N-heterocycles. Structure and applications.

S,N- and N,N-heterocycles have been proven to have influence on complexes used for pharmacological applications. Some heterocycles bearing donor atoms such as pyrazole [129,130], thiazoline [131] and thiazine [132,133] meet these requirements. For that reason, in the next sections it will be described the different cycles conforming the structure of the ligands used in the present work, just like their properties and applications.

- **Pyrazole**

Pyrazole is an aromatic heterocycle of five members (Figure 1.12), which belongs to the 1,2-azol family, containing two nitrogen atoms in adjacent positions. From a chemical point of view, the two nitrogen atoms are not equivalent, being the nitrogen in position 1 an azole type, and the other one an azine type. The first one gives a couple of non-bonding electrons to the aromatic ring forming an N-H bond with a relatively acidic proton. On the other hand, the adjacent nitrogen on position 2 has the couple of electrons out of the aromatic system. This allows pyrazole to behave both as base and nucleophilic.

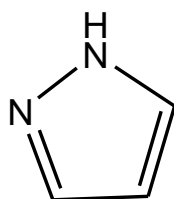


Figure 1.12. Pyrazole structure.

Although just a few natural products contain a pyrazole ring in their structures, most of their synthetic analogs have pharmacological applications. The most extensive use of these complexes are as antimicrobials, analgesics, antipyretics, and anti-inflammatories [134–136].

For example, some pyrazole derivatives, like sulfaphenazole and sulfazamet, and some diarylpyrazoles have been reported to have antimicrobial activity [137,138]. On the other hand, some drugs as the one known as Celecoxib act as potent analgesic and anti-inflammatory agents [139]. Nonetheless, the most extensively known pyrazole derivative group is probably 5-pyrazolone group, which are used as analgesic, antipyretic and anti-inflammatory agents [134,140,141], like aspirin (1-phenyl-2,3-dimethyl-5-pyrazolone), one of the first synthetic compounds used in medicine. In addition, this group of complexes has also been described to have cytostatic and cytotoxic effect when coordinated with Pt(II) and Pd(II) [142]. Other pyrazole derivatives have been demonstrated to have antitumoral effects as it happens with 3,5-diaryl-1H-pyrazoles [143] and 3-(3,4-dimethylphenyl)-5-(4-methoxyphenyl)-4,5-dihydropyrazole-1-carbotiamide [144] (Figure 1.13).

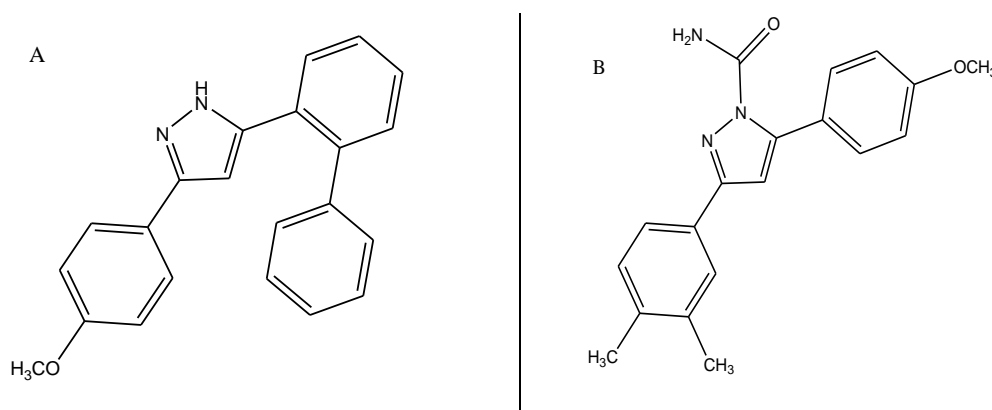


Figure 1.13. Structures of 3,5-diaryl-1H-pyrazoles (A) and 3-(3,4-dimethylphenyl)-5-(4-methoxyphenyl)-4,5-dihydropyrazole-1-carbotiamide (B).

In addition, in the last decades numerous Pt(II) complexes with pyrazole rings and cytotoxic activity have been synthesized. Among them, it can be found the complexes presented in Figure 1.14 [145]. Furthermore, 1-(2-dimethylaminoethyl)-1H-pyrazole derivatives with Pt(II) and Pd(II) as metal center have shown moderate antimalarial properties and remarkable cytotoxicity against several tumor cell lines [146]. Other Pt(II) complexes with alkylpyrazole [147] and substituted pyrazole ligands have also shown strong cytotoxic effect [148].

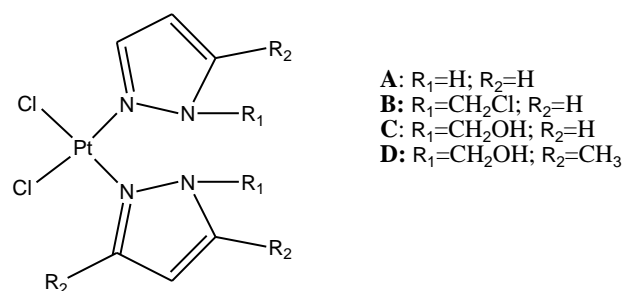


Figure 1.14. Structure of *cis*-[bis(pyrazole)]dichloroplatinum(II) (A), *cis*-[bis(*N*-chloromethylpyrazole)]dichloroplatinum(II) (B), *cis*-[bis(*N*-hydroxymethyl-pyrazole)]dichloroplatinum(II) (C), and *cis*-[bis(*N*-hydroxymethyl-3,5-dimethylpyrazole)]dichloroplatinum(II) (D).

In the next sections, the ligands used in this PhD thesis would be presented, being part of their structures a pyrazole ring with or without extra substituents in 3,5-disposition.

• Thiazoline

Thiazolines are a group of heterocycles which contain an atom of nitrogen and another of sulfur in their structure and derive from thiazole. Taking in consideration the position of these atoms, thiazolines can be classified as shown in Figure 1.15.

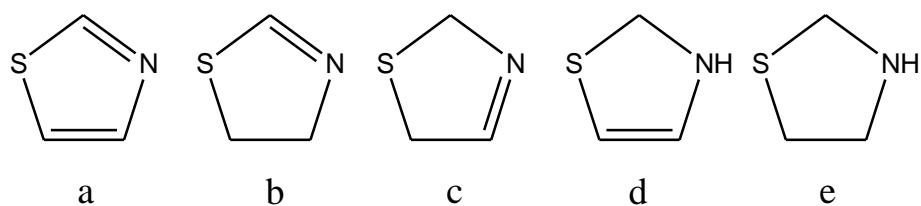


Figure 1.15. a) thiazole, b) 2-thiazoline, c) 3-thiazoline, d) 4-thiazoline, e) thiazolidine.

Respect to the conformation of the ring, some infrared and Raman spectroscopic studies of 2-thiazoline and some 2-alkyl derivatives indicate that the ring is almost plane [149], while the same studies in the thiazolidine ring indicate that the ring has a half-chair conformation [150].

Due to the biological activity shown by several natural substances derived from thiazolines, numerous similar complexes have been synthesized and have demonstrated its usefulness in the medical and pharmacological field. In fact, 2-thiazoline rings and cancer have a long relationship. From some natural products like Tantazol B, synthetic derivatives that inhibit the cellular growing of pancreatic, prostate and colon cancer have been developed [131]. Parallely, Curacin A and synthetic derivatives were also studied as cancer cell toxins and were checked to also produce growth inhibition in cancer cell lines [151]. On the other hand, there are also other synthetic derivatives containing the 2-thiazoline and/or thiazolidine ring that have antitumoral activity. That way, thiazolidine-4-carboxylic acid and chlorhydrate of 2-amino-2-thiazoline (Figure 1.16) can revert the carcinogenic process of cells [152,153].

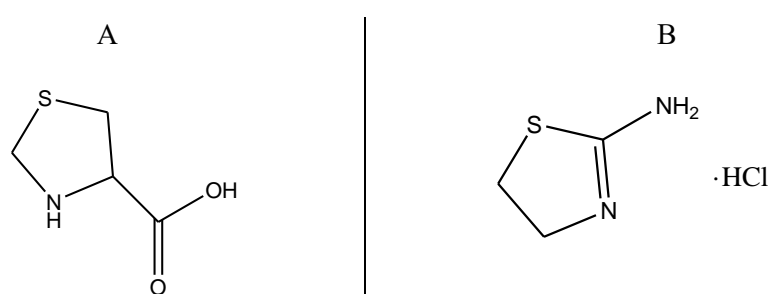


Figure 1.16. Structure of thiazolidine-4-carboxylic acid (A) and chlorhydrate 2-amino-2-thiazoline structure (B).

The antitumoral effect of these rings has been also observed in coordination complexes with different thiazoline derivatives and various metals like Pt(II) [154], Cu(II) [155,156], Ag or Au [157]. In fact, the *Coordination Chemistry Research group* of University of Extremadura has also synthesized and tested the cytotoxic effects of Pt(II) and Pd(II) complexes with thiazoline containing ligands like (2-(3,4-

dichlorophenyl)imine-N-(2-thiazolin-2-yl)thiazolidine) (TdTn) (Figure 1.17) [158] and 2-(2-pyridyl)imine-N-(2-thiazolin-2-yl)thiazolidine (PyTT) [116] with promising results.

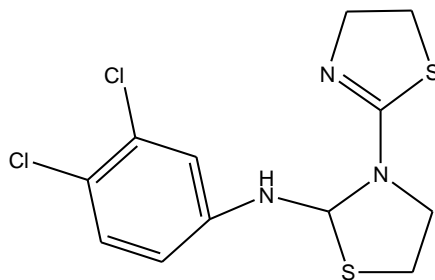


Figure 1.17. Structure of (2-(3,4-dichlorophenyl)imine-N-(2-thiazolin-2-yl)thiazolidine) (TdTn).

• Thiazine

Thiazines are six-membered heterocycles containing a sulfur and a nitrogen atom in their structure. A wide number of isomeric structures are possible due to the relative position of the two mentioned heteroatoms and the oxidation grade. Although the classification shown in Figure 1.18 is not clearly delimited because of some tautomeric equilibrium, it indicates the basic structures of the thiazine family. Some thiazines are widely known and others are rare and appear only as intermediate products [159].

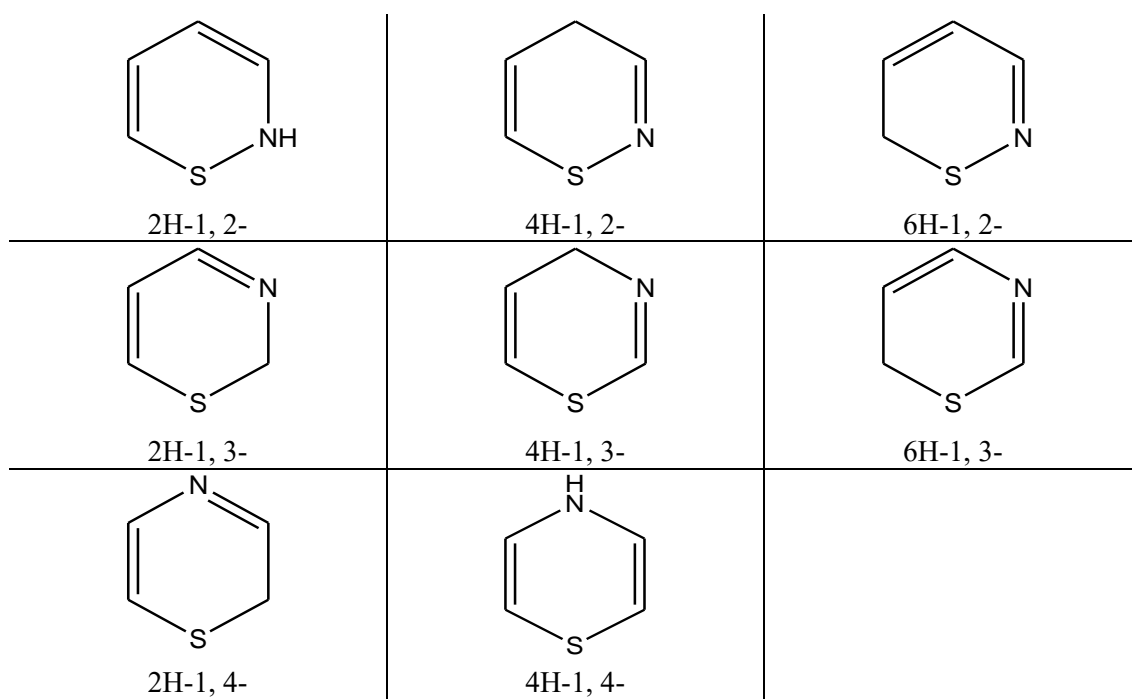


Figure 1.18. Structure of thiazines.

Among thiazines, some derivatives have shown cytotoxic activity. For example, N-(5,6-dihydro-4H-1,3-thiazin-2-yl)benzamide bromohydrate (Figure 1.19) has a strong cytotoxic activity on leukemia cells without being toxic for healthy lymphocytes [160].

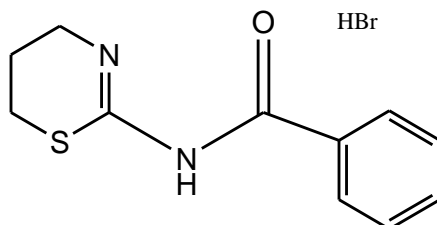


Figure 1.19. Structure of N-(5,6-dihydro-4H-1,3-thiazin-2-yl)benzamide bromohydrate derivative.

In the last decade, some quinonaftothiazines with cytotoxic activity against glioblastoma, melanoma and epithelial tumor cells have been synthesized. Among these, two have better results even than CisPt (Figure 1.20.) [161,162].

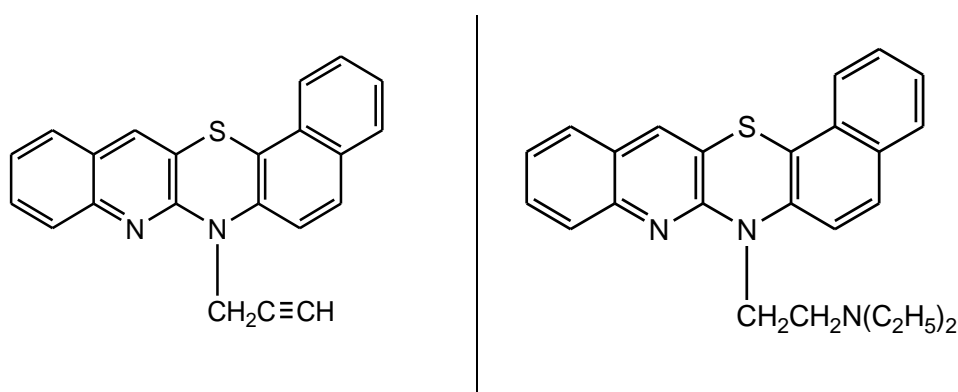


Figure 1.20. Structure of quinonaftothiazines with stronger cytotoxicity than CisPt.

On the other hand, several studies carried out with benzothiazines have also shown promising results due to their cytotoxic activity on different tumor cell lines [163–169]. In the same way, some research done with phenothiazines also revealed antitumoral properties [170–174].

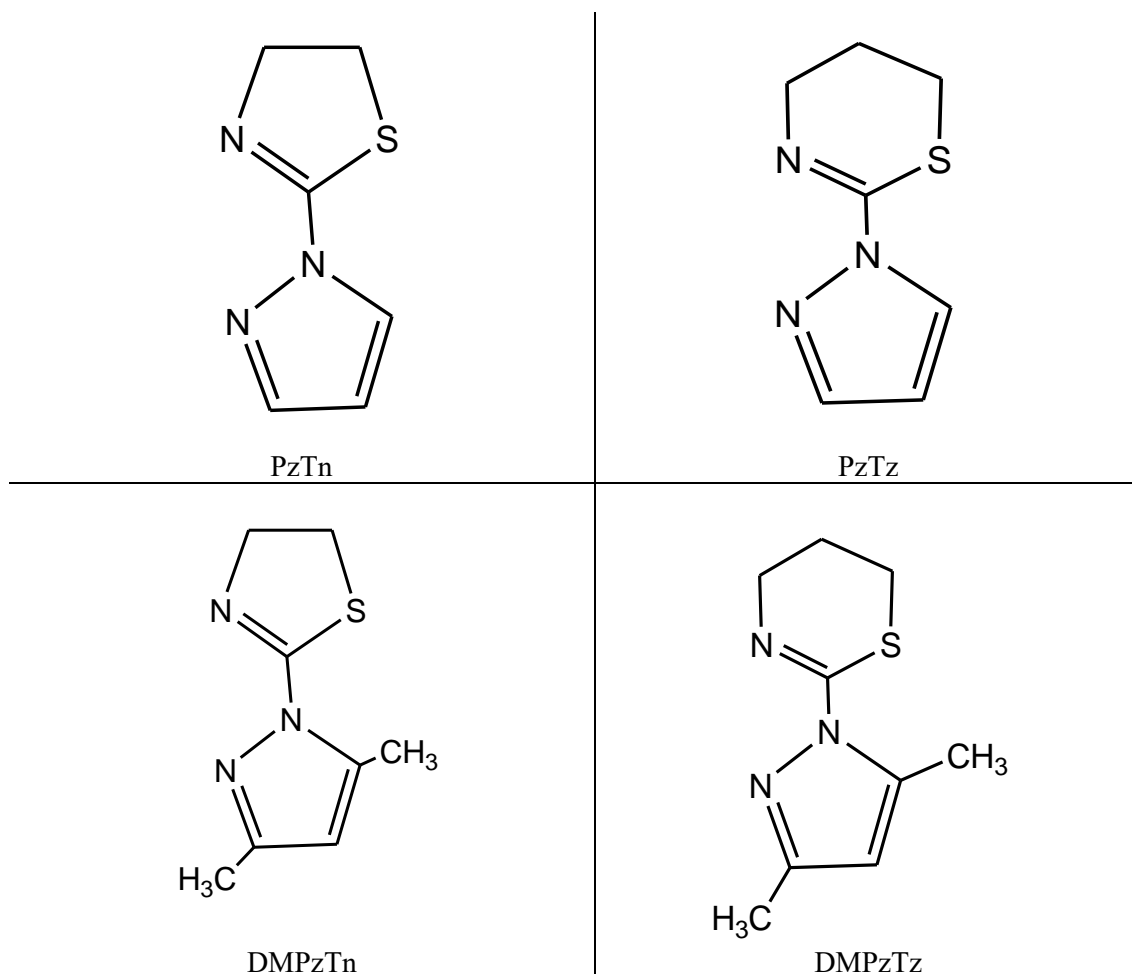
With respect to complexes with coordination between Pt(II) and 1,3-thiazines or derivatives, there is not a large amount in the literature. Nevertheless, one of these belongs to the *Coordination Chemistry Research group* of University of Extremadura. In this case, it was synthesized and tested the cytotoxic effects of Pt(II) and Pd(II) complexes with the ligand (2-(2-pyridyl)iminotetrahydro-1,3-thiazine) (PyTz), showing a moderate cytotoxicity in four tumor cell lines [175].

1.3.4.b Ligands employed

As previously mentioned, S,N and N,N-heterocycles are excellent precursors to synthesize a wide variety of coordination complexes. For that reason, the *Coordination Chemistry Research group* of the Organic and Inorganic Department of the University of Extremadura has been working on new ligands containing those kinds of heterocycles for more than a decade. In the present work, the ligands used for the synthesis of new potential chemotherapeutic agents were:

- 2-(1-pyrazolyl)-2-thiazoline (PzTn)
- 2-(1-pyrazolyl)-1,3-thiazine (PzTz)
- 2-(3,5-dimethyl-1-pyrazolyl)-2-thiazoline (DMPzTn)
- 2-(3,5-dimethyl-1-pyrazolyl)-1,3-thiazine (DMPzTz)
- 2-(3,5-diphenyl-1-pyrazolyl)-2-thiazoline (DPhPzTn)
- 2-(3,5-diphenyl-1-pyrazolyl)-1,3-thiazine (DPhPzTz)

In Figure 1.21, it can be observed the structure of these six ligands.



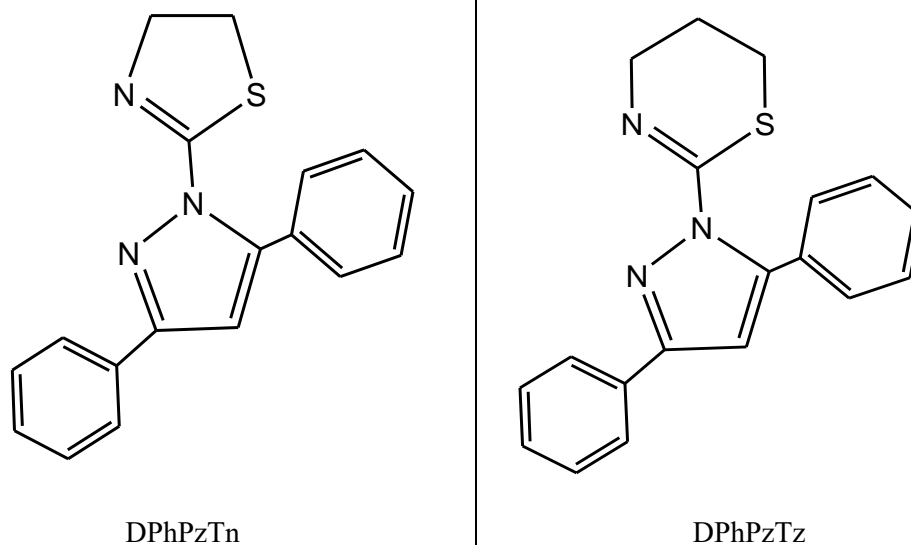


Figure 1.21. Structure of PzTn, PzTz, DMPzTn, DMPzTz, DPhPzTn and DPhPzTz.

The behavior of the ligands is going to be determined by the presence of donor atoms in the S,N-heterocycles. In fact, the joining to the metallic ions is produced through the iminic nitrogen and the nitrogen of the 2-thiazoline or 1,3-thiazine rings, acting as bidentate and forming a five-membered chelate ring, which gives an additional stabilization due to the chelate effect. A scheme of the coordination produced between the metal ion and the ligands can be seen in Figure 1.22. This way of joining is supported by previously synthesized complexes with these ligands. All the six ligands have been coordinated to Cu(II) and Cd(II) [176–183], while almost all ligands (except for DPhPzTn) were also coordinated to Co(II) and Zn(II) [176–178,184]. On the other hand, the three ligands with thiazine ring and PzTn have been coordinated to Ni(II) [178,185], while only PzTn and PzTz have been previously coordinated with Pt(II) [186]. Nevertheless, the potential cytotoxic effect on tumor cell lines of any of these complexes has been previously tested.

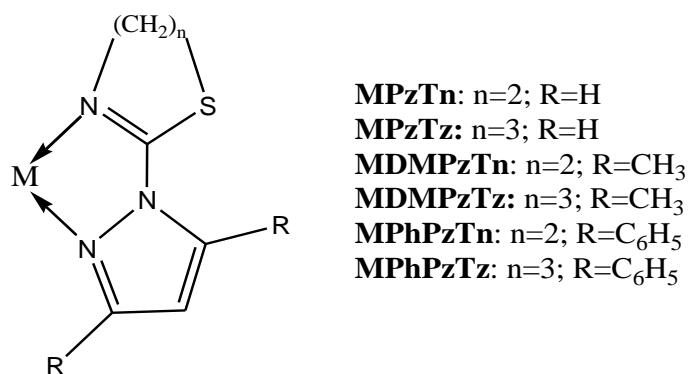


Figure 1.22. Scheme of metal ion coordination to the ligands.

1.4. NANOPARTICLES

Last decades have been characterized for an increased interest and development in nanotechnology field. Nanoparticles (NPs), particles with 1 to 100 nm dimension, exhibit a wide variety of properties according to its size and surface functionalities.

One of their advantages is their small size and large surface area, which has led to numerous applications in diverse fields such as electronics, cosmetics, food science and medicine [187]. Respect to the medical field, NPs have been used as drug carriers with applications both in diagnosis and therapy. This alternative to direct administration of traditional drugs, which have usually shown a considerable amount of undesirable and harmful side effects to healthy organs, has awakened scientific interest in the last decades. Nevertheless, their clinical usage is affected by their physical and chemical characteristics, drug loading and release efficiency, as well as low or no toxicity [188].

1.4.1. Nanoparticles as drug carriers

As it was previously mentioned, one of the most relevant fields of application for nanoparticles is medicine. Their relevance as nanocarriers is correlated with their advantages in comparison to free drug delivery. Among them, it could be stood out the enhanced biodistribution, improvement of bioavailability and drug solubility, decrease of toxicity and prevention of multi-drug resistance [189]. In addition, NPs increase drug stability, preventing the degradation of the encapsulated cargo, and allow a large volume of drugs encapsulation without any chemical reaction [190].

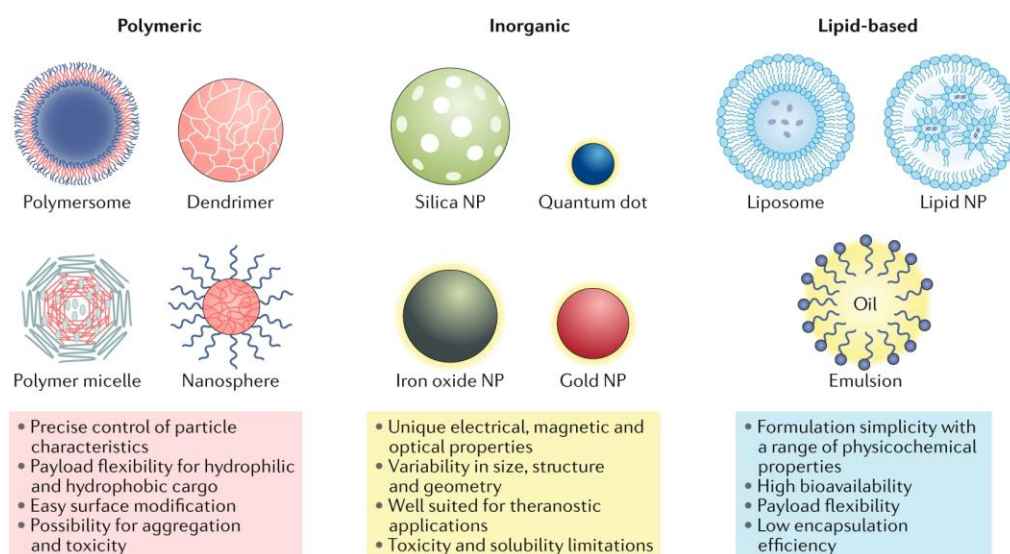


Figure 1.23. Classes and physicochemical characteristics of nanoparticles [189].

Nanocarriers can be divided in different groups with particular properties (Figure 1.23) [189]. Next, the main groups of nanocarriers are described:

- **Lipid-based NPs:** These particles are typically spherical platforms with at least one lipid bilayer surrounding no less than one internal aqueous compartment. Among their advantages can be highlighted its biocompatibility, formulation simplicity and high bioavailability. That is the reason why they are the most common class of FDA-approved nanomedicines [191]. As for the subsets existing, there are liposomes (they can form unilamellar and multilamellar vesicular structures), which can deliver hydrophilic, hydrophobic, and lipophilic drugs [192,193], and lipid nanoparticles (LNPs), which are widely used for nucleic acids delivery [194] but with limitations due to low drug loading and biodistribution [191].
- **Polymeric NPs:** This group presents a precise control and good delivery due to its compatibility and simple formulation parameters. Drugs can be encapsulated in a wide range of ways including within the NP core, chemical conjugation, entrapped in the matrix or bound to the surface [195,196]. The modulation of some characteristics like composition, surface charge or release kinetics allow that they can be precisely controlled. The most common forms of these particles are nanocapsules and nanospheres, having within these two categories a differentiation by shape in polymersomes (artificial vesicles, with membranes made using amphiphilic block copolymers, specially recommended for deliver in the cytosol [197]), micelles (nanospheres with a hydrophilic core and a hydrophobic coating, used for drug delivery in clinical trials [198]) and dendrimers (hyperbranched polymers with complex three-dimensional architectures, specially used for nucleic acids and small molecules delivery [199]). Although they present advantages such as biocompatibility, water solubility or storage stability, the drawbacks include risk of particle aggregation and toxicity.
- **Inorganic NPs:** This group includes gold, iron and silica for drug delivery and imaging application. This group presents some interesting properties including a variety of sizes and geometries, and unique physical, electrical, magnetic, and optical properties. The most extensively known nanocarriers of this group involves gold NPs (AuNPs) used in numerous forms [200], iron oxide, making the majority of FDA-approved inorganic nanomedicines [201], mesoporous

silica nanoparticles (MSNs), successfully used for gene and drug delivery [202], and quantum dots, used mainly for imaging application [203]. Most of them have good stability and biocompatibility. On the other hand, their main limitations are low solubility and toxicity.

Above all this, one of the most important uses of nanoparticles application is in the treatment of cancer, which is known as nano-oncology. Taking into account its small size and improved delivery of the drug, both by active or passive targeting, it can diminish the off-target distribution of the drug and their associated side effects [204–206]. As it is described in next section, MSNs have shown promising properties as carriers for numerous anticancer drugs, which is the reason why they have been selected for the encapsulation of the new complexes presented in this PhD thesis.

1.4.2. Mesoporous silica nanoparticles

These inorganic NPs have been in the spotlight as potential drug delivery agents in the last years. This is due to its numerous characteristics such as high drug loading capacity, variability in particle size, ease to modify their surface, relatively undemanding synthesis process and biosafety status since they are “generally regarded as safe” (GRAS) by FDA [204,207]. In addition, it has been seen that they can act as vehicles of not only drugs, but also genes, proteins and antigens, mitigating the progress of diseases, inflammatory responses, and cancer [208].

The application of MSNs as carriers can be classified in two groups: sustained and controlled drug-release [209]. The latter respond to one or more stimuli which can be either external (pH, temperature, redox capacity, etc.) or internal (UV light, magnetic field, etc.). As examples of controlled release, the conjugation of doxorubicin with poly-L-lysine-coated MSNs allowed a successful and controlled drug release mediated by pH [210], while MSN attached with chitosan granted a doxorubicin release in response to colonic enzymes, achieving a great internalization of the drug in tumor cells [211].

Moreover, the delivery capability of these materials is strongly influenced by their decoration with functional groups of both the external surface and pores. In the review of Farjadian and coworkers it could be found a table with applications of different types of MSN materials for anti-cancer drug delivery with both sustained and controlled release [208].

Among the application of MSNs in medicine, one of the main ones is the encapsulation of hydrophobic drugs, which supposes a drawback for many treatments. In fact, around 40% of small-molecule drugs in pharmaceutical companies have low water solubility, which hinders their administration through some routes even completely prevents it [212]. Numerous studies have proposed MSNs as solution to this problem in drug development due to the improvement of solubility and greater distribution *in vitro*. For example, their conjugation with umbelliferone was studied in human breast cancer cells (MCF-7), being more effective in the reduction of tumor volume and mass than the free drug [213]. The encapsulation of camptothecin into the pores of MSNs led to growth inhibition and cell death of three pancreatic cancer cell lines (PANC-1, Capan-1, and AsPc-1), a colon cancer-cell line (SW480), and a stomach cancer-cell line (MKN45) [214]. The improvement of drug delivery of anthelmintics [215] and telmisartan [216] has also been studied. The enhancement of cytotoxic effect of several commercial drugs respect to the effect of the free drug has been also checked for quercetin in MCF-7 [217], with an improvement of cell uptake and toxicity, paclitaxel in HepG2 (hepatocellular carcinoma) [218] and MCF-7 [219], vorinostat in HCT116 (colon cancer cell line) [220], oxaliplatin [221] and ursolic acid in HepG2 [222], CisPt(IV) in HeLa with the formation of DNA-adducts [223], resveratrol in A375 and MNT-1 (melanoma cell lines), with a high loading percentage (93%) and pH-dependent [224], and in AGS and HGC-27 (mouse gastric cancer cells) *in vitro* and *in vivo* with proliferation and migration inhibition [225], and combinatory delivery of CisPt and doxorubicin in HeLa and A357 (melanoma cell line) [226], among other studies.

Related to the cellular uptake route of these particles, it seems to involve membrane wrapping in a process called endocytosis [227]. This appears to be the main route for MSNs internalization by eukaryotic cells and consists in comprising the particle, formation of an early endosome or membrane-bound vesicle, forming a lysosome and sorting them for different purposes (Figure 1.24) [208,228]. Taking in account the size of the particles, it can be differentiated between phagocytosis (micro-sized particles) and pinocytosis (fluids and particles through clathrin-coated vesicles). Although the particles enter the cells, the process is only considered successful after avoiding the degradation in endosomal/lysosomal vesicles and release of the cargo into the cytoplasm.

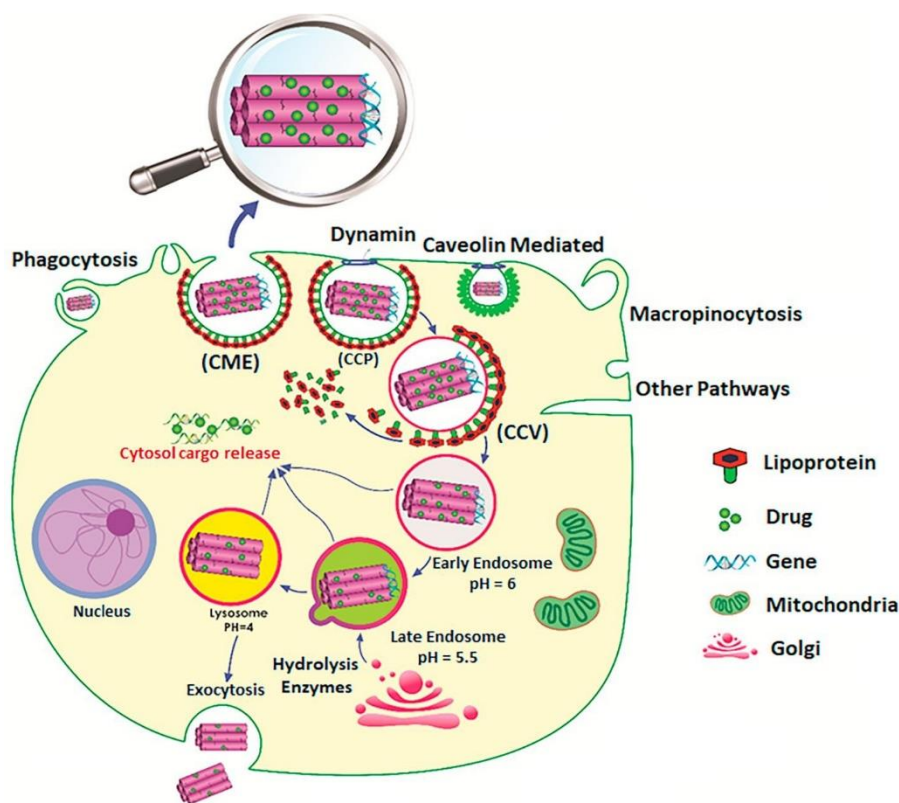


Figure 1.24. Routes of cellular uptake of nanoparticles [208].

The application of these particles in the medical field has raised the concerns about their possible toxicity [229]. Considering amorphous silica particles, they are degradable over time into ortho-silicic acid $\text{Si}(\text{OH})_4$, which is nontoxic and water soluble, being excreted via urine [230,231]. In fact, MSNs can be completely degraded over a month in simulated body fluid [230,232,233], in cells [234], and in the body [235,236], while it is not so easy to degrade under physiological conditions, reason why FDA give them the GRAS consideration [237,238].

Numerous groups have investigated and evaluated the cytotoxicity, genotoxicity and blood and tissue compatibility of these particles with varying results. It seems that the biosafety of particles can be influenced by particle size, surface properties (charge and functionalities), morphology and structure, and pore size [208]. In addition, choosing an adequate *in vitro* cell viability assay for cytotoxicity analysis is fundamental for getting reliable results. The concentration, treatment period and cell type studied may also influence the results. For example, a negligible genotoxic effect has been found in colon cancer cells (HT-29), while a significant effect in embryonic kidney cells after overnight exposure to MSNs was detected [239,240]. Nevertheless, in normal and cancer cell lines, such as HeLa, MCF-41, or A549, MSNs are regarded as safe [241,242].

2. JUSTIFICATION AND OBJECTIVES

2. JUSTIFICATION AND OBJECTIVES

According to the numbers presented by the WHO, cancer is the major cause of death worldwide and mournfully the perspective is that the figures continue growing in the next decades [4]. It is also true that the mortality ratio has been reduced due to the rapid evolution of therapies. Nevertheless, these treatments are not completely effective and have numerous side effects.

Among the main treatments used for cancer, chemotherapy is one of the most extensively studied to destroy cancer cells. However, although several drugs with relevant applications in cancer therapies such as CisPt have been developed [62,63,68,243], over the last 40 years only 23 other platinum-based drugs have entered clinical trials. Among them, only five gained marketing approval: carboplatin and oxaliplatin (internationally); and nedaplatin, lobaplatin and heptaplatin (only regionally in the Asiatic continent) [67–70]. Moreover, all of them present different types of side effects, from neurotoxicity to thrombocytopenia, including nausea and vomiting.

In order to improve the effectivity of new chemotherapeutic agents and reduce their drawbacks, the substitution of the metallic center for another transition metal and the modification of the structure via incorporation of ligands on the non-labile site are two extensively used strategies. Although numerous metals have been studied as alternatives to Pt(II) as metal center (e.g., Ru, Au, Ir, Os, etc.) [82], Pd(II) could be an interesting option to replace platinum due to their similarities both in electronic structure and coordination geometry [73,108]. As for the incorporation of ligands in their structure, it has been demonstrated that the presence of heterocycles bearing donor atoms has influenced their pharmacological applications. For example, heterocycles such as pyrazole [129,130], thiazine [132,133] and thiazoline [131] meet these requirements.

On the other hand, the use of nanoparticles as drug carriers seems to be a promising way to deliver the medications faster and in a more selective way. In addition, they present other advantages such as drug stability, prevention of the degradation of the encapsulated cargo, and large volume of drugs encapsulation [190]. Moreover, a high number of small-molecule drugs have low water solubility and the use of nanoparticles could solve this issue [212]. Among all the nanoparticles types existing, MSNs are being amply studied for drugs, genes, proteins, and antigens delivery [208] due to its numerous features such as high drug loading capacity, ease to modify surface, relatively

undemanding synthesis process and biosafety status since they are considered GRAS by FDA [204,207].

For all the previously exposed, the main objective of this PhD thesis was to synthesize and characterize several analogs of cisplatin, both using platinum and palladium as metal centers, to study their potential cytotoxic and pro-apoptotic effect on tumor cell lines. For that aim, three tumor cell lines were used, being one derived from solid tumors and two from non-solid tumors. These cell lines were human epithelial cervix carcinoma (HeLa), human histiocytic lymphoma (U-937) and human promyelocytic leukemia (HL-60) cells. The general objective described can be itemized in the following specific objectives:

1. Synthesize and characterize CisPt analogs with Pt(II) and Pd(II) as metal centers and N,N and N,S-bidentate donor ligands.
2. Evaluate the effect of CisPt and the new chemotherapeutic agents synthesized on cell viability and apoptosis in the indicated tumor cell lines.
3. Establish structure-biological activity relationships that could help in future designs of more effective drugs against cancer.
4. Synthesize, characterize, and encapsulate several of the CisPt analogs synthesized on MSNs to improve the delivery inside the tumor cells.

3. MATERIALS AND METHODS

3. MATERIALS AND METHODS

In this chapter, it will be detailed both the synthesis of the organic ligands and the metal complexes studied in this PhD thesis, as well as the different characterization techniques and the biological tests performed. For that purpose, the material and equipment available in both the *Department of Organic and Inorganic Chemistry* and the *Department of Physiology* of the University of Extremadura, and in the *Servicios de Apoyo a la Investigación* (Core Facilities) from University of Extremadura, University of Santiago de Compostela and University of Oviedo were used and will be detailed next. In addition, for the synthesis, functionalization, and characterization of nanoparticles used in this work, reagents and equipment of the *Institute of Inorganic Chemistry II* of Ulm University (Germany) were used.

3.1. REAGENTS

To the consecution of the experimental work of this PhD thesis, the reagents listed in the following sections were used.

3.1.1. Chemical reagents

- Acetone (Scharlau S.L., Barcelona, Spain)
- Acetonitrile (Scharlau S.L., Barcelona, Spain)
- Chloroform (Scharlau S.L., Barcelona, Spain)
- Cyclohexane (Scharlau S.L., Barcelona, Spain)
- Dichloromethane (Scharlau S.L., Barcelona, Spain)
- Diethyl ether (Scharlau S.L., Barcelona, Spain)
- Dimethyl sulfoxide (DMSO) (Panreac Química S.A., Barcelona, Spain)
- Dimethyl sulfoxide-d₆ (DMSO-d₆) (Panreac Química S.A., Barcelona, Spain)
- Ethanol 96% (Scharlau S.L., Barcelona, Spain)
- Ethyl acetate (Scharlau S.L., Barcelona, Spain)
- Methanol (Scharlau S.L., Barcelona, España)
- N,N-dimethylformamide (DMF) (Scharlau S.L., Barcelona, Spain)
- N,N-dimethylformamide-d₇ (DMF-d₇) (ABCR, Karlsruhe, Germany)
- Petroleum ether (Scharlau S.L., Barcelona, Spain)
- Potassium iodide (Panreac Química S.A., Barcelona, Spain)

- Potassium tetrachloroplatinate (II) (ABCR, Karlsruhe, Germany)
- Pyrazole (Sigma Aldrich S.A, Madrid, Spain)
- Sodium carbonate (ABCR, Karlsruhe, Germany)
- Sodium hydride (Sigma Aldrich S.A, Madrid, Spain)
- Sodium sulphate anhydrous (Scharlau S.L., Barcelona, Spain)
- Sodium tetrachloropalladate (II) (ABCR, Karlsruhe, Germany)
- Toluene (Panreac Química S.A., Barcelona, Spain)
- 2-chloroethyl isothiocyanate (ABCR, Karlsruhe, Germany)
- 3-chloropropyl isothiocyanate (ABCR, Karlsruhe, Germany)
- 3,5-dimethylpyrazole (Sigma Aldrich S.A, Madrid, Spain)
- 3,5-diphenylpyrazole (ABCR, Karlsruhe, Germany)

3.1.2. Cell lines and culture media

Cells lines selected to perform the biological testing were purchased from the European Collection of Authenticated Cell Cultures (ECACC) (Dorset, UK.):

HeLa: Human epithelial cervix carcinoma cell line (No. 93021013),

U-937: Human histiocytic lymphoma cell line (No. 85011440)

HL-60: Human promyelocytic leukemia cell line (No. 88120805)

And the cultured media used were:

DMEM: Dulbecco's modified Eagle's medium (Gibco)

RPMI-1640: Roswell Park Memorial Institute-1640 (HyClone)

The conditions used are described in subsequent sections.

3.1.3. Other reagents

- AnnexinV-FITC/PI (Annexin V conjugated with fluorescein isothiocyanate/Propidium iodide) (eBioscience Dx, Barcelona, Spain)
- Binding buffer (eBioscience Dx, Barcelona, Spain)
- Butanol (Panreac Química S.L.U., Barcelona, Spain)
- Cisplatin (Sigma Aldrich S.A, Madrid, Spain)
- DCFH-DA (2',7'-dichlorodihydrofluorescein diacetate) (Life Technologies, Barcelona, Spain)

- DTT (Dithiothreitol) (Sigma Aldrich S.A, Madrid, Spain)
- EDTA (Ethylenediaminetetraacetic acid) (Sigma Aldrich S.A, Madrid, Spain)
- FBS (Fetal bovine serum) (Gibco, Life technologies, Barcelona, Spain)
- Glycerol (Sigma Aldrich S.A, Madrid, Spain)
- Hoechst 33258 (Life technologies, Barcelona, Spain)
- L- glutamine (Lonza Ibérica S.A.U., Barcelona, Spain)
- MTS (3-(4,5-dimethylthiazol-2-yl)-5-(3-carboxymethoxyphenyl)-2-(4-sulfophenyl)-2H-tetrazolium) (Promega Corporation, Madrid, Spain)
- NaCl (Panreac Química S.L.U., Barcelona, Spain)
- Nitric acid (Honeywell Fluka, Madrid, Spain)
- PBS (Phosphate buffered saline) (Gibco, Life technologies, Barcelona, Spain)
- SDS (Sodium dodecyl sulphate) (Sigma Aldrich S.A., Madrid, Spain)
- Sodium chloride (Panreac, Castellar del Vallés, Barcelona, Spain)
- Sodium deoxycholate (Sigma Aldrich S.A, Madrid, Spain)
- Streptomycin/Penicillin (Lonza Ibérica S.A.U., Barcelona, Spain)
- TBE (Tris-borate-EDTA) (Life technologies, Barcelona, Spain)
- Topoisomerase I (Inspiralis, Norwich, UK)
- TrisCl (Sigma Aldrich S.A, Madrid, Spain)
- Triton-X100 (Sigma Aldrich S.A, Madrid, Spain)
- Trypan-blue (Sigma Aldrich S.A, Madrid, Spain)
- Trypsin (Lonza Ibérica S.A.U., Barcelona, Spain)

3.2. LIGANDS SYNTHESIS

In this work, six ligands with S,N- and N,N-heterocycles have been synthesized. All six ligands had been previously studied and published for the *Coordination Chemistry Research group* from the University of Extremadura [176,179,184].

A summary of the main steps followed for the synthesis of the ligands is next included. The corresponding quantity of pyrazole, 3,5-dimethylpyrazole or 3,5-diphenylpyrazole was solved in toluene and mixed during 3 h at room temperature with the corresponding amount of NaH 60% (Table 3.1). Then, 1 mL (10 mmol) of 2-chloroethyl isothiocyanate in the case of PzTn, DMPzTn and DPhPzTn or 3-chloropropyl isothiocyanate for PzTz, DMPzTz and DPhPzTz was added, and the mixture was maintained under reflux and agitation during 24 h.

After that time, the reaction mixture was concentrated in a R-3000 rotary evaporator (BUCHI) once the addition of 5 mL of methanol was made. The next step was adding water to the residue and extracting the organic phase with chloroform. Afterwards, the solution obtained, previously dried with sodium sulphate, was evaporated again with the rotary evaporator. The product was purified via flash chromatography using diethyl ether-petroleum ether 1:1 v/v as eluent for PzTn and PzTz and dichloromethane-diethyl ether 20:1 v/v for the rest of the ligands. The chromatography phases containing the purified ligand were crystallized in the same mixture that was used as eluent. All the amounts of reagents used and the yields obtained are shown in Table 3.1.

Table 3.1. Reagents amounts and yields.

Ligand	Pyrazole	3,5-dimethylpyrazole	3,5-diphenylpyrazole	NaH 60%	Yield
PzTn	0.695 g 10 mmol			0.400 g 17 mmol	42.3 %
PzTz	0.695 10 mmol			0.600 25 mmol	32.5 %
DMPzTn		0.971 10 mmol		0.400 17 mmol	41.7 %
DMPzTz		0.971 10 mmol		0.400 17 mmol	43.9 %
DPhPzTn			2.200 10 mmol	0.600 25 mmol	30.6 %
DPhPzTz			2.200 10 mmol	0.600 25 mmol	36.5 %

A possible mechanism for the synthesis of the ligands would be the previous reaction between pyrazole and NaH to generate a pyrazolate, being followed by a nucleophilic attack of the anion to the carbon atom of the thiocarbonyl of the isothiocyanate group. Finally, the last step could be an intramolecular substitution by the attack of the sulfur atom to the carbon joined to the chlorine (Figure 3.1).

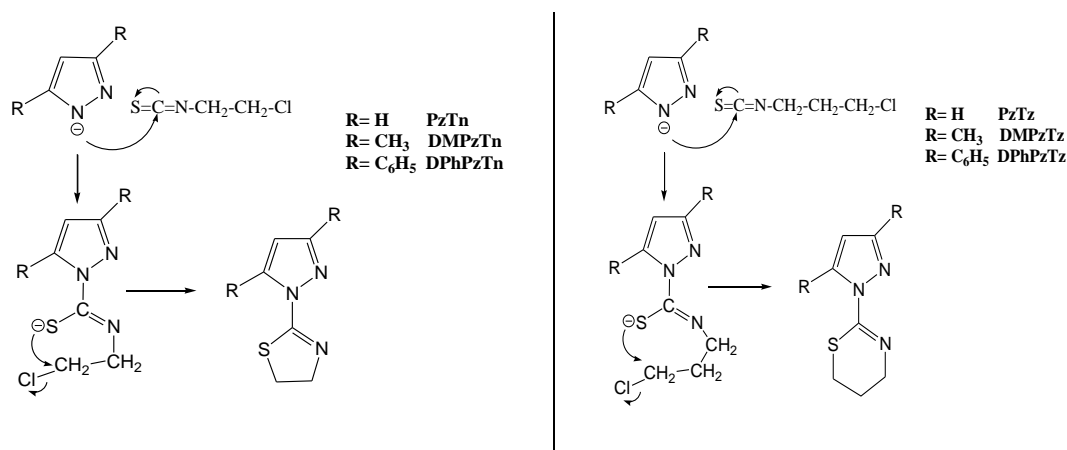


Figure 3.1. Possible mechanism for the synthesis of the ligands.

3.3. LIGANDS CHARACTERIZATION

To confirm the successful synthesis of the ligands mentioned in the previous section, both ^1H NMR and IR measurements were made. The spectra and data obtained are included in section 8. Appendix (Figures A1-A6 and Tables A1-A2). Further spectroscopic data of these ligands can be found in [176,179,184].

3.4. SOLID PHASE SYNTHESIS FROM M(II)/LIGAND SYSTEM

3.4.1. Pt(II)/ligand system synthesis

3.4.1.a. Precursor *cis*-[PtCl₂(DMSO)₂] synthesis

The synthesis of precursor *cis*-[PtCl₂(DMSO)₂] (Figure 3.2) was made through *Price and cols.* method [244]. The experimental procedure started with the solution of K₂[PtCl₄] (1.25 g, 3 mmol) in distilled water (10 mL). After that, DMSO was added dropwise (0.7 mL, 9 mmol), forming immediately a yellow powder. The mixture was maintained under agitation during 1h, being filtered and washed with distilled water and cold diethyl ether afterwards.

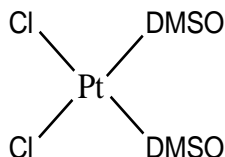


Figure 3.2. *Cis*-[PtCl₂(DMSO)₂] structure.

3.4.1.b. Pt(II)/ligand system synthesis

For the synthesis of solid phases of Pt(II) complexes, the precursor *cis*-[PtCl₂(DMSO)₂] was dissolved in the less amount possible of hot ethanol. From an addition funnel, a solution of the corresponding ligand in ethanol was added, being the stoichiometry metal-ligand 1:1. The mixture was maintained under reflux and agitation during 24 h. A yellow powder was formed during that time, being then filtered, and washed with distilled water and cold diethyl ether. The solid phases were crystallized, obtaining monocrystals with enough size and quality to be studied by X-ray diffraction. In Table 3.2 it could be found the formula and nomenclature used for the synthesized complexes, which will be named as indicated from now on. A scheme of the reaction of

the synthesis for PtCl₂/Ligand solid phases is shown in Figure 3.3 and the solubility of the different complexes at room temperature is depicted in Table 3.3. The solvents used to crystallize the complexes are indicated in Table 3.3 with yellow-colored cells. For further information on PtPzTn and PtPzTz, it can be consulted the Final Master Thesis of Felipe de la Cruz Martínez [186], who previously synthesized these two complexes.

Table 3.2. Formula and nomenclature of Pt(II) complexes.

Formula	Nomenclature
[PtCl ₂ (PzTn)]	PtPzTn
[PtCl ₂ (PzTz)]	PtPzTz
[PtCl ₂ (DMPzTn)]	PtDMPzTn
[PtCl ₂ (DMPzTz)]	PtDMPzTz
[PtCl ₂ (DPhPzTn)]	PtDPhPzTn
[PtCl ₂ (DPhPzTz)]	PtDPhPzTz

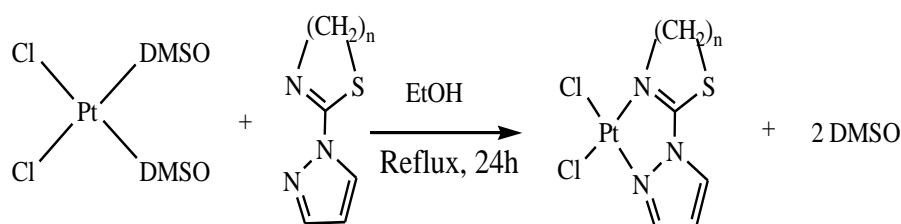


Figure 3.3. Reaction scheme for PtCl₂/Ligands solid phase.

Table 3.3. Solubility of PtDMPzTn, PtDMPzTz, PtDPhPzTn and PtDPhPzTz.

	<i>PtDMPzTn</i>	<i>PtDMPzTz</i>	<i>PtDPhPzTn</i>	<i>PtDPhPzTz</i>
<i>Diethyl ether</i>	I	I	I	PS
<i>Dichloromethane</i>	SS	SS	S	S
<i>Acetone</i>	SS	SS	S	PS
<i>Chloroform</i>	SS	SS	S	S
<i>Methanol</i>	SS	SS	I	I
<i>Ethyl acetate</i>	SS	SS	PS	I
<i>Ethanol</i>	SS	SS	I	I
<i>Cyclohexane</i>	I	I	I	I
<i>Acetonitrile</i>	SS	SS	S	PS
<i>Water</i>	I	I	I	I
<i>Toluene</i>	I	I	PS	I
<i>DMF</i>	SS	SS	S	S
<i>DMSO</i>	SS	SS	S	S

S: soluble; PS: partially soluble; SS: slightly soluble; I: insoluble

3.4.2. Pd(II)/ligand system synthesis

For the synthesis of solid phases of Pd(II) complexes, the salt $\text{Na}_2[\text{PdCl}_4] \cdot \text{H}_2\text{O}$ was dissolved in the less amount possible of ethanol. From an addition funnel, a solution of the corresponding ligand in ethanol was added, being the stoichiometry metal-ligand 1:1. The mixture was maintained under agitation during 24 h. An orange powder was formed during that time, being then filtered and washed with distilled water and cold diethyl ether. The solid phases were crystallized, obtaining monocrystals with enough size and quality to be studied by X-ray diffraction. In Table 3.4 it could be found the formula and nomenclature used for the synthesized complexes, which will be named as indicated from now on. A scheme of the reaction of the synthesis for $\text{PdCl}_2/\text{Ligand}$ solid phases is shown in Figure 3.4 and the solubility of the different complexes at room temperature is displayed in Table 3.5. The solvents used to crystallize the complexes are indicated in Table 3.5 with yellow-colored cells.

Table 3.4. Formula and nomenclature of Pd(II) complexes.

Formula	Nomenclature
$[\text{PdCl}_2(\text{PzTn})]$	PdPzTn
$[\text{PdCl}_2(\text{PzTz})]$	PdPzTz
$[\text{PdCl}_2(\text{DMPzTn})]$	PdDMPzTn
$[\text{PdCl}_2(\text{DMPzTz})]$	PdDMPzTz
$[\text{PdCl}_2(\text{DPhPzTn})]$	PdDPhPzTn
$[\text{PdCl}_2(\text{DPhPzTz})]$	PdDPhPzTz

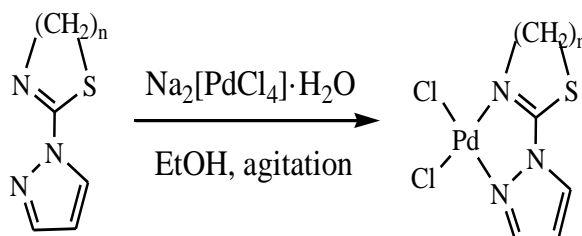


Figure 3.4. Reaction scheme for $\text{PdCl}_2/\text{Ligands}$ solid phase.

Table 3.5. Solubility of PdPzTn, PdPzTz PdDMPzTn, PdDMPzTz, PdDPhPzTn and PdDPhPzTz.

	<i>PdPzTn</i>	<i>PdPzTz</i>	<i>PdDMPzTn</i>	<i>PdDMPzTz</i>	<i>PdDPhPzTn</i>	<i>PdDPhPzTz</i>
<i>Diethyl ether</i>	I	I	I	I	S	S
<i>Dichloromethane</i>	PS	PS	SS	SS	PS	PS
<i>Acetone</i>	PS	PS	SS	SS	PS	PS
<i>Chloroform</i>	PS	PS	SS	SS	S	S
<i>Methanol</i>	PS	PS	SS	SS	PS	PS
<i>Ethyl acetate</i>			SS	I	PS	PS
<i>Ethanol</i>	I	I	SS	SS	PS	PS
<i>Cyclohexane</i>			I	I	I	I
<i>Acetonitrile</i>	S	PS	SS	SS	S	S
<i>Water</i>	I	I	I	I	I	I
<i>Toluene</i>			I	I	PS	PS
<i>DMF</i>	S	S	PS	SS	S	S
<i>DMSO</i>	S	S	PS	SS	S	S

S: soluble; PS: partially soluble; SS: slightly soluble; I: insoluble

3.5. SOLID PHASE CHARACTERIZATION FROM M(II)/LIGAND SYSTEM

The characterization of solid phases was made through different techniques, which would be indicated in the next subsections.

3.5.1. Elemental analysis

The content of C, H, N and S of the solid phases was determined with a Leco CHNS-932 microanalyzer.

3.5.2. Crystal structures

X-ray single-crystal diffraction measurements were performed using a Bruker Kappa APEXII CCD diffractometer (PtPzTn and PtPzTz) or a Bruker D8 VENTURE PHOTON III-14 diffractometer (PtDMPzTn, PtDMPzTz, PtDPhPzTn, PtDPhPzTz, PdPzTn, PdPzTz, PdDMPzTn, PdDMPzTz, PdDPhPzTn and PdDPhPzTz), both using graphite monochromated Mo-K α radiation ($\lambda = 0.71073 \text{ \AA}$) and the ω scan technique at 100 K. All data were corrected for Lorentz and polarization effects, while absorption corrections were performed by means of SADABS [245] program. The structures were

solved by direct methods and subsequent Fourier differences, except for PtDMPzTz for which Patterson method was used, in both cases using the SHELXS-14 [246] program and refined by full-matrix least-squares on F2 with SHELXL-18 [247], included in WINGX [248] package, assuming anisotropic displacement parameters for non-hydrogen atoms. Hydrogen atoms were placed at calculated positions and refined using a riding model.

In case of PtDMPzTn, the crystals available were all twinned and were refined as a 2-component perfect twin. A twin integration was made combining both domains in one hk15 data file. The asymmetric unit comprises thus two crystallographically different molecules of [PtCl₂(DMPzTn)]. There are minor differences in bond lengths as well as bond and torsion angles. EADP constraint instruction was applied for C1A, C2A and N3A atoms in PtDMPzTn and for N3 in PtDMPzTz.

Crystallographic data has been deposited at the CCDC (Cambridge Crystallographic Data Center; copies of the data can be obtained, e-mail: deposit@ccdc.cam.ac.uk or www: <http://www.ccdc.cam.ac.uk/structures/>). In Table 3.6, it can be found the CCDC numbers assigned to the complexes. The graphic representation of the molecular structures was made with the applications Mercury [249] and POV-Ray [250] for Windows.

Table 3.6. CCDC numbers of the different complexes.

<i>Complex</i>	<i>CCDC number</i>
<i>PtPzTn</i>	2086351
<i>PtPzTz</i>	2086353
<i>PtDMPzTn</i>	2260597
<i>PtDMPzTz</i>	2260598
<i>PtDPhPzTn</i>	2086352
<i>PtDPhPzTz</i>	2086354
<i>PdPzTn</i>	2224537
<i>PdPzTz</i>	2224538
<i>PdDMPzTn</i>	2224539
<i>PdDMPzTz</i>	2224540
<i>PdDPhPzTn</i>	2224541
<i>PdDPhPzTz</i>	2224542

3.5.3. Infrared spectroscopy

IR spectra were recorded on a Perkin-Elmer 100 FTIR spectrophotometer from KBr pellets in the 4000–400 cm^{-1} range.

3.5.4. ^1H Nuclear magnetic resonance spectroscopy

^1H NMR spectra were obtained with a Bruker Avance III 500 instrument at 500 MHz in DMF- d_7 for Pt(II) complexes and for PdDPhPzTn and PdDPhPzTz, and with a Bruker AV300 instrument at 300 MHz for PdPzTn and PdPzTz also in DMF- d_7 and for PdDMPzTn in DMSO- d_6 . ^1H NMR data could not be obtained for PtDMPzTn, PtDMPzTz and PdDMPzTz due to its low solubility. ^1H NMR signals were referenced to residual proton resonances in deuterated solvents.

3.6. EXPERIMENTAL DESIGN FOR BIOLOGICAL TESTING

3.6.1. Cell line culture

Cells were cultured in DMEM (HeLa) or RPMI-1640 (U-937 and HL-60) medium, which were supplemented with 2 mM L-glutamine, 10% heat-inactivated FBS, 100 U/mL penicillin, and 10 $\mu\text{g}/\text{mL}$ streptomycin. Cells were usually plated at a density of 7×10^5 cells/mL (HeLa) or 3×10^5 cells/mL (HL-60 and U-937) into 25 cm^2 culture flasks (TPP) and were kept under a humidified atmosphere containing 95% air and 5% CO_2 at 37 $^\circ\text{C}$ (ICO105 incubator, Memmert). Their viability was routinely tested by the Trypan-blue exclusion method.

3.6.2. Cell treatment

In order to test the different complexes and ligands synthesized, it was necessary to prepare solutions of those complexes in solvents in which they had enough solubility. For that reason, solutions of 5 mM of complexes were prepared in DMF, except for complexes with methyl substituents which were prepared in DMSO. For these last ones, suspensions were obtained due to the low solubility of these four complexes.

Treatments used covered from 1 to 100 μM and CisPt was included as positive control for Pt(II) complexes. To consider the solvent effect, a control with DMF or DMSO was used (vehicle), being the final concentrations of these solvents lower than 0.5% (v/v).

3.6.3. Cell viability testing

The cytotoxic effects of the different compounds were evaluated on the three cell lines selected by means of the CellTiter 96 AQueous One Solution Cell Proliferation Assay, which is based on the reduction of MTS. Cells were seeded in 96-well plates at a density of 8×10^3 cells/well (HeLa), 1.5×10^4 cells/well (U-937) or 2.5×10^4 cells/well (HL-60) and regularly treated during 24 h. In addition, 48 and 72h incubation times were also used for the testing of some complexes (PdPzTn, PdPzTz, PdDPhPzTn and PdDPhPzTz) in HeLa cells. After treatment, assays were performed by adding 10 μ L of the CellTiter 96 AQueous One Solution Reagent directly to culture wells, incubating for 15 min (HeLa), 1 h (U-937) or 2 h (HL-60) at 37 °C. Then, the absorbances were recorded on a microplate reader (Infinite M200; Tecan) at a test wavelength of 490 nm and a reference wavelength of 650 nm to subtract background. All analyses were run in triplicate. The cell viability was calculated as percentage of control values (untreated samples).

3.6.4. Apoptosis determination

Induction of apoptosis was determined using an annexin V-FITC apoptosis detection kit (BD Biosciences), as reported elsewhere [251]. Briefly, stimulated or resting HeLa cells were harvested by trypsinization (2×10^5 cells/mL), washed twice with PBS, and centrifuged at $500 \times g$ for 5 min; then the supernatant was discarded, and the pellet was resuspended in 200 μ L of binding buffer containing 5 μ L of annexin V-FITC. Cells were incubated for 10 min at room temperature, washed twice, and finally resuspended in 200 μ L of binding buffer containing 2 μ L of PI. Double-stained cells were immediately analyzed by a MACS-Quant X flow cytometer (Miltenyi Biotech). Annexin V-FITC was excited with 488 nm laser and its fluorescence was acquired through 525/50 nm band-pass (BP) filter, while PI was excited with 488 nm laser and its fluorescence was acquired through 585/40 nm BP filter. Ten thousand events/cells were analyzed per condition. Each sample was tested eight times in independent experiments.

3.6.5. Reactive oxygen species determination

HeLa cells were seeded in 6-well plates at a density of 2×10^5 cells/well. After treating cultures for 4 h, assays were performed by incubating cells (30 min, 37 °C) with

0.4 μM DCFH-DA, which allows to determine intracellular ROS production. Flow cytometry analysis was performed using a MACSQuant Analyzer 10 flow cytometer (Miltenyi Biotec). DCF was excited with 488 nm laser and its fluorescence was acquired through 525/50 nm BP filter. Analysis of ROS production was restricted to live cells that were detected by using the vital dye Hoechst 33258 (10 $\mu\text{g}/\text{mL}$), which was excited with 405 nm laser and its fluorescence acquired through 450/50 nm BP filter. Ten thousand events/cells were analyzed per condition. Each sample was tested four times in independent experiments. Data were presented as percentage of DCF stained cells.

3.6.6. Inductively coupled plasma mass spectrometry accumulation

To quantify the metal accumulation inside the cells, HeLa cells were seeded in 100 mm Petri dishes at a density of 2×10^6 cells. After 24 h, cells were treated with IC_{50} of the complexes for 4 h. Then, cells were trypsinized, washed twice with PBS, and centrifuged at $500 \times g$ for 5 min. Finally, the supernatant was discarded, and the cell pellet was resuspended in 1 mL of Radioimmunoprecipitation assay (RIPA) buffer (150 mM NaCl, 50 mM Tris-Cl pH 7.4, 1% Triton-X100, 0.5% sodium deoxycholate, and 0.1% SDS). Afterwards, the different samples were digested with 65% HNO_3 at room temperature and analyzed by inductively coupled plasma mass spectrometry (ICP-MS 7900, Agilent Technologies, Madrid, Spain).

3.6.7. Intercalation assay

DNA intercalation was assessed by examining the ability of the compounds to unwind supercoiled DNA or displace topoisomerase I from the DNA groove. To do so, DNA unwinding assay kit (Inspiralis) was used following manufacturer's instructions. Briefly, 0.5 μg of DNA (supercoiled or relaxed pBR322) were added to 15 μL of $2\times$ assay buffer (50 mM Tris-HCl (pH 7.9), 1 mM EDTA, 1 mM DTT, 20% (v/v) glycerol, 50 mM NaCl) and then incubated with the compounds or the vehicle (negative control) for 5 min at room temperature. Afterwards, 2 μL of $1\times$ dilution buffer (50 mM Tris-HCl (pH 7.9), 1 mM EDTA, 1 mM DTT, 50% (v/v) glycerol, 500 mM NaCl) and 2 μL of wheat germ Topoisomerase I were added to initiate unwinding and samples were incubated at 37°C for further 30 min. Reactions were terminated by addition of 20 μL of water and 50 μL of butanol. Reactions were separated on 1% (w/v) agarose gel in $1\times$ TBE buffer and gel was

run at 80 V for approximately 4 h, stained with ethidium bromide, and visualized with a gel documentation system (ChemiDoc XRS+ System, Bio-Rad).

3.6.8. Statistical analysis

Data were presented as mean \pm standard deviation (SD). To compare the different treatments, statistical significance was calculated by one-way analysis of variance (ANOVA) followed by Tukey's test or Dunnett's test, as indicated in figure legends. IC₅₀ values obtained from the dose-response curve of each compound were calculated by fitting the curve to the data using nonlinear regression to generate a four-parameter sigmoid dose-response equation. $P < 0.05$ was considered to indicate a statistically significant difference. The statistics software used was GraphPad Prism 7.04 (GraphPad Software, San Diego, CA, USA) for Windows.

3.7. EXPERIMENTAL DESIGN OF NANOPARTICLES

3.7.1. Synthesis of nanoparticles

For the synthesis of MSN and further functionalization and characterization, the preestablished protocols of the group I was working with during my short internship in Germany (*Institute of Inorganic Chemistry II*, Ulm, Germany) were followed. The reagents and equipment necessary for that process were provided by the hosting lab. In addition, dendritic mesoporous organosilica nanoparticles (DMON) were also supplied by the hosting lab.

3.7.1.a. Synthesis of mesoporous silica nanoparticles

For the synthesis of MSN, 14 g of cetyltrimethylammonium bromide (CTAB) were mixed at 300 rpm during 45 min with 1280 g of methanol and 1920 g of MilliQ water. Then, the speed was up to 550 rpm while adding 4.8 mL of tetramethyl orthosilicate (TMOS) and left under agitation during 15 min. After that time, 9.12 mL of NaOH 1 M were added and stirred. After 1 h of agitation, the speed was down to 300 rpm to stir overnight.

The mixture was added to a beaker with 1 L of acetone and was agitated at 700 rpm for 15 min. Then, it was necessary to leave the solution to precipitate. Once the supernatant was clear, it was removed until half liter was left. The rest was centrifuged in

bottles at 10 °C and 10000 rpm for 10 min. Once the supernatant was carefully removed by decantation, MilliQ water was added to wash the particles. This process implicates to sonicate the particles in water for 10 min and centrifugate again at the same conditions as the previous one. The process was repeated twice with water and twice with ethanol. Then, the particles were dried overnight in the oven at 60 °C. Finally, the particles were grinded with a quartz mortar and retained in a ceramic plate, which was kept in the oven during 16-18 h at 550 °C reached gradually (1 K/min) to calcinate the particles. Last step was to dry them on vacuum overnight at 100 °C.

3.7.1.b. Amino functionalization of MSN

For the amino functionalization of the previously synthesized MSN, 403 mg of them were weighted and mixed with 80 mL of toluene dehydrated. After 30 min of ultrasound, 242 µL of (3-aminopropyl)triethoxysilane (APTES) previously dissolved in 7 mL of toluene were added. The mixture was kept in the oven at 85 °C under agitation at 300 rpm overnight. Then, the mix was centrifuged at 10000 rpm and 10 °C for 10 min. The supernatant was removed and replaced with toluene and a little amount of water and sonicated for 10 min before centrifuged again. Then, the particles were washed twice with MilliQ water and twice with ethanol like it was done for the MSN synthesis. After the washing steps, the particles were dried at 60 °C at the vacuum during 24 h, and then grinded and kept on a vial.

- **ATTO-647N NSH ester functionalization of MSN-NH₂**

For the fluorescent functionalization of the previously synthesized MSN-NH₂, ATTO-S47N NSH ester was selected due to its strong absorption, high photostability, and high fluorescence quantum yield. For the synthesis of MSN-NH₂-ATTO, 100 mg of MSN-NH₂ particles were mixed with 10 mL of 7.2 pH HEPES 25% (4-(2-hydroxyethyl)-1-piperazineethanesulfonic acid) and dispersed in Covaris S220 (Covaris Ltd, Brighton, United Kingdom) for 10 min. Then, 100 µL of ATTO dye were added and incubated during 1 h in the dark under rotation. After a centrifugation at 6000 rpm for 10 min, the sample was dispersed in absolute ethanol during 10 min in Covaris and then centrifuged at 6000 rpm during 10 min. This process was repeated two times. Finally, the particles were dried at 60 °C at the vacuum overnight. During this process the MSN-NH₂ particles

turn from a whitish to an intense blue color, which indicates that the MSN-NH₂-ATTO particles have been achieved.

3.7.1.c Carboxy functionalization of MSN

For the carboxy functionalization of the previously synthesized MSN, 404 mg of them were weighted and mixed with 100 mL of 7.2 pH HEPES 25%. After 6 min of dispersion in Covaris S220 (Covaris Ltd, Brighton, United Kingdom), the sample was mixed manually. Then, 910 µL of carboxyethyl silanetriol in aqueous solutions was added and kept under movement in a rotary wheel for three hours. After a centrifugation at 10 °C and 10000 rpm for 10 min, the particles were washed with MilliQ water and twice with ethanol like was done for the MSN synthesis. After the washing steps, the particles were dried at 60 °C at the vacuum during 24 h, and the grinded and kept on a vial.

3.7.2. Encapsulation of complexes in MSN-NH₂-ATTO

For the encapsulation of PtPzTn, PtPzTz, PtDPhPzTn, PtDPhPzTz, PdDPhPzTn and PdDPhPzTz in the MSN-NH₂-ATTO previously synthesized and characterized, 50 mg of particles were dispersed in 5 mL of cyclohexane for 1 min. Then, 5 mL of a solution of the corresponding complex (10 mg in 5 mL of dichloromethane) were added. After an incubation of 3 h in a rotary wheel in the dark, particles were centrifuged at 6000 rpm during 30 min. Then, particles were washed with diethyl ether, firstly dispersed for 10 min and then centrifuged for 15 min. Finally, particles with a blue color were obtained and dried in a vacuum at room temperature overnight.

3.7.3. Characterization of nanoparticles

The characterization of synthesized and functionalized nanoparticles was made through different techniques, which would be indicated in the next subsections.

3.7.3.a. Physisorption measurements

Physisorption or physical gas adsorption using BET (Brunauer, Emmett and Teller) and NLDFIT (non-local density functional theory) is used to obtain the specific surface area, pore size distribution and pore volume of adsorbents. Adsorption and

desorption isotherms were obtained using nitrogen as an adsorptive at cryogenic conditions.

Once the synthesized particles were heated and vacuumed, nitrogen sorption measurements were conducted on a Quadrasorb⁻¹ (Quantachrome Instruments, Germany) at $-196\text{ }^{\circ}\text{C}$. The specific surface areas were determined using the BET method, pore diameters were determined using the equilibrium NLDFT kernel (silica, cylindrical pores) in a relative pressure range of 0–0.9.

3.7.3.b. Transmission Electron Microscopy

Transmission Electron Microscopy (TEM) is a technique that uses an electron beam to image a nanoparticle sample. For sample preparation, a pint of a spatula of the nanoparticles sample was solved in 500 μL of ethanol. A drop of the solution was deposited in a carbon-supported grid for further observation once the sample was dried. A Jeol 1200 (Jeol, Germany) TEM using a HT voltage of 120 kV and a beam current of 65 μA was used. Grey-scale images of the electron diffraction patterns were obtained via fast Fourier transformation (FFT) using the FFT plug-in of ImageJ version 1.52n.

3.7.3.c. Thermogravimetric analysis

Thermogravimetric analysis (TGA) provides information about physical phenomena of samples, such as phase transitions, adsorption and desorption as well as chemisorption, thermal decomposition, and solid-gas reactions. This is produced through the changes of the mass of sample over time with increasing temperature.

Once the adsorption of complexes was done, and after drying the samples in the vacuum at room temperature overnight, the particles were measured on a TG209 F1 Libra (Netzsch, Germany) at a heating rate of $10\text{ }^{\circ}\text{C min}^{-1}$ in nitrogen/oxygen (70%/30%) atmosphere.

3.7.3.d. Z-potential

Zeta-potential is a determination of the effective electric charge on the nanoparticle's surface. When nanoparticles have a net surface charge, this is screened by the concentration of ions of opposite charge near the nanoparticle surface.

Zeta-potentials were measured three times with a Zetasizer NanoZS Zen3600 (Malvern Panalytical, Germany) in aqueous HEPES buffer (25 mM, pH 7.2) using a particle concentration of 0.1 mg mL^{-1} .

3.7.4. Biological testing

To perform the biological testing described next, HeLa cell line was selected. In addition, solutions of 1 mg/mL particles in DMEM were made as mother solutions for these experiments. Both the remaining particles and solutions were kept in a $-80 \text{ }^{\circ}\text{C}$ ultrafreezer.

3.7.4.a. Cellular internalization and distribution

Cellular internalization and distribution were studied via confocal microscopy. To do that, HeLa cells were seeded in μ -Slide 8 well ibiTreat chambered coverslips (Ibidi, Martinsried, Germany) at a density of 1.5×10^4 cells. After 24 h, cells were treated with $10 \text{ }\mu\text{g/mL}$ of MSN-NH₂-ATTO-PtPzTn or MSN-NH₂-ATTO-PtDPhPzTz during 24 h. Then, MSN-challenged cells were counterstained with DAPI (nuclear staining), MitoTracker Green FM (mitochondria staining) and/or BODIPY FL C₅-sphingomyelin (Golgi/plasma membrane staining) to study the subcellular distribution of the nanoparticles. Finally, the samples were imaged with a spectral multiphoton confocal microscope (FV1000, Olympus). Fluorescence analysis was done using the FV10 software (Olympus).

3.7.4.b. Apoptosis determination

Apoptosis induction was analyzed as previously described in the section 3.6.4. *Apoptosis determination*. This time, the density of HeLa cells was 6×10^4 cells/mL and the concentration of nanoparticles was $200 \text{ }\mu\text{g/mL}$. The rest of the process was performed as described previously, except for the substitution of the $2 \text{ }\mu\text{L}$ of PI for $2 \text{ }\mu\text{L}$ Hoechst 33258, due to the interaction of PI with the ATTO dye.

3.7.4.c. Cellular uptake

It was studied as previously described in the section 3.6.6. *Inductively coupled plasma mass spectrometry accumulation*. This time, HeLa cells were seeded in 100 mm

Petri dishes at a density of 5×10^6 cells. After 24 h, cells were treated with 100 $\mu\text{g/mL}$ of the loaded nanoparticles for 4 h. The rest of the process was performed exactly as described before.

3.7.4.d. Release analysis

A metal leaching study was performed to determine the concentration of Pt or Pd species in simulated body fluid (pH 7.4 PBS buffer). For that, 200 μg of the loaded nanoparticles were suspended in 1 mL of PBS buffer and incubated at 37 °C in an orbital shaker incubator (Optic ivymen system, Comecta) under rotation during 4 and 24 h. Then, the samples were centrifuged at 14000 rpm and room temperature. The supernatant was conserved and analyzed by ICP-MS to determine the quantity of Pt or Pd leached during the incubation. Experiments were run in duplicate.

4. RESULTS

4. RESULTS

4.1. ANALOGS OF CISPLATIN WITH PLATINUM AS METAL CENTER

As it was previously described in section 3. *Materials and methods*, six complexes have been synthesized with platinum as metallic center. In this section, the results obtained from the characterization techniques used and the biological testing performed are exposed and analyzed. It is important to mention that elemental analysis, X-ray diffraction and IR analysis are not included for PtPzTn and PtPzTz since they were formerly described in the Final Master Thesis of Felipe de la Cruz Martínez [186], as previously mentioned.

4.1.1. Characterization from Pt(II)/Ligand systems

4.1.1.a. Elemental analysis

Elemental analysis for the solid phases of Pt(II) complexes are shown in Table 4.1, where it can be also seen the calculated values from the empiric formula. A good concordance between data could be observed.

Table 4.1. Elemental analysis data for Pt(II) complexes.

		%C	%H	%N	%S	<i>Empiric formula</i>
<i>PtDMPzTn</i>	Experimental	23.61	2.85	8.83	7.20	C ₈ H ₁₁ Cl ₂ PtN ₃ S
	Calculated	23.43	2.85	9.12	6.95	
<i>PtDMPzTz</i>	Experimental	21.57	2.51	9.22	7.19	C ₉ H ₁₃ Cl ₂ PtN ₃ S
	Calculated	21.48	2.48	9.40	7.17	
<i>PtDPhPzTn</i>	Experimental	37.78	2.57	7.45	5.45	C ₁₈ H ₁₅ Cl ₂ PtN ₃ S
	Calculated	37.84	2.65	7.35	5.61	
<i>PtDPhPzTz</i>	Experimental	38.32	2.89	7.38	5.15	C ₁₉ H ₁₇ Cl ₂ PtN ₃ S
	Calculated	38.97	2.93	7.18	5.48	

4.1.1.b. Crystal structures

As it was previously mentioned, monocrystals suitable for X-ray diffraction analysis were obtained for PtDMPzTn, PtDMPzTz, PtDPhPzTn and PtDPhPzTz. In Table 4.2, it can be found the main information of the examined crystals, the data collection and refinement details.

Table 4.2. Crystal information, data collection and refinement details for PtDMPzTn, PtDMPzTz, PtDPhPzTn and PtDPhPzTz.

	<i>PtDMPzTn</i>	<i>PtDMPzTz</i>	<i>PtDPhPzTn</i>	<i>PtDPhPzTz</i>
<i>Crystal shape</i>	Needle	Plate	Plate	Prism
<i>Colour</i>	Yellow	Yellow	Orange	Orange
<i>Size (mm)</i>	0.07×0.03×0.02	0.06×0.04×0.02	0.17×0.16×0.06	0.18×0.13×0.06
<i>Chemical formula</i>	C ₈ H ₁₁ Cl ₂ N ₃ PtS	C ₉ H ₁₃ Cl ₂ N ₃ PtS	C ₁₈ H ₁₅ Cl ₂ N ₃ PtS	C ₁₉ H ₁₇ Cl ₂ N ₃ PtS·C ₂ H ₃ N
<i>Formula weight</i>	447.25	461.27	571.38	626.46
<i>Crystal system</i>	Monoclinic	Orthorhombic	Triclinic	Triclinic
<i>Space group</i>	P 2 ₁ /c	P b c a	P $\bar{1}$	P $\bar{1}$
<i>Unit cell dimensions</i>				
<i>a (Å)</i>	17.9683(9)	7.4526(3)	9.3943(7)	9.5617(7)
<i>b (Å)</i>	7.3231(4)	17.5917(7)	9.6599(8)	11.1072(9)
<i>c (Å)</i>	17.3899(8)	18.3353(8)	11.7278(10)	11.4558(9)
<i>α (°)</i>	90	90	68.234(3)	66.525(3)
<i>β (°)</i>	91.123(2)	90	76.018(3)	77.155(3)
<i>γ (°)</i>	90	90	64.339(3)	74.355(3)
<i>Cell volume (Å³)</i>	2287.8(2)	2404.22(17)	886.73(13)	1065.48(15)
<i>Z</i>	8	8	2	2
<i>D_{calc} (g cm⁻³)</i>	2.597	2.549	2.140	1.953
<i>μ (mm⁻¹)</i>	12.884	12.265	8.337	6.949
<i>F(000)</i>	1664	1728	544	604
<i>θ range</i>	2.583-26.494	2.315-28.279	2.417-30.504	2.231-30.506
<i>Index ranges</i>	-22≤h≤22, 0≤k≤9, 0≤l≤21	-9≤h≤9, -23≤k≤23, -24≤l≤24	-13≤h≤13, -13≤k≤13,-16≤l≤16	-13≤h≤13, -15≤k≤15,-16≤l≤16
<i>Temperature</i>	100	100	100	100
<i>Independent Reflections</i>	8082	2979	5421	6502
<i>Observed reflections</i>	6475	2228	5195	6256
<i>No. of refined parameters</i>	253	141	226	263
<i>R [F>4.0 σ(F)]</i>	0.0597	0.0290	0.0153	0.0123
<i>wR [F>4.0 σ(F)]</i>	0.14	0.0520	0.037	0.036
<i>GOF</i>	1.051	1.027	1.057	0.974
<i>ρ_{max}, ρ_{min} (e Å⁻³)</i>	4.442, -3.043	1.090, -1.209	0.992, -1.601	0.518, -0.688

The metal complexes showed crystal structures that consist of monomeric units of $[\text{PtCl}_2\text{L}]$ ($\text{L} = \text{DMPzTn}$, DMPzTz and DPhPzTn) or $[\text{PtCl}_2\text{L}] \cdot \text{C}_2\text{H}_3\text{N}$ ($\text{L} = \text{DPhPzTz}$), as can be observed in the molecular structures presented in Figure 4.1. In the case of PtDMPzTn , there were two types of independent molecules in the unit cell. The coordinated geometry around Pt(II) for the complexes was slightly distorted square-planar with the dihedral angles between Cl(1)-Pt-Cl(2) and N(1)-Pt-N(3) being lower than 7° . Data corresponding to dihedral angles can be found in Table 4.3. The Pt(II) ion was joined to two chlorines in *cis* disposition and a ligand molecule, which acted as bidentate and formed a chelate ring of five members. The ligand was coordinated to platinum through the nitrogen of pyrazole cycle and the nitrogen of 2-thiazoline ring for complexes PtDMPzTn and PtDPhPzTn , and through the nitrogen of 1,3-thiazine ring for complexes PtDMPzTz and PtDPhPzTz . The selected interatomic distances and angles are listed in Table 4.4.

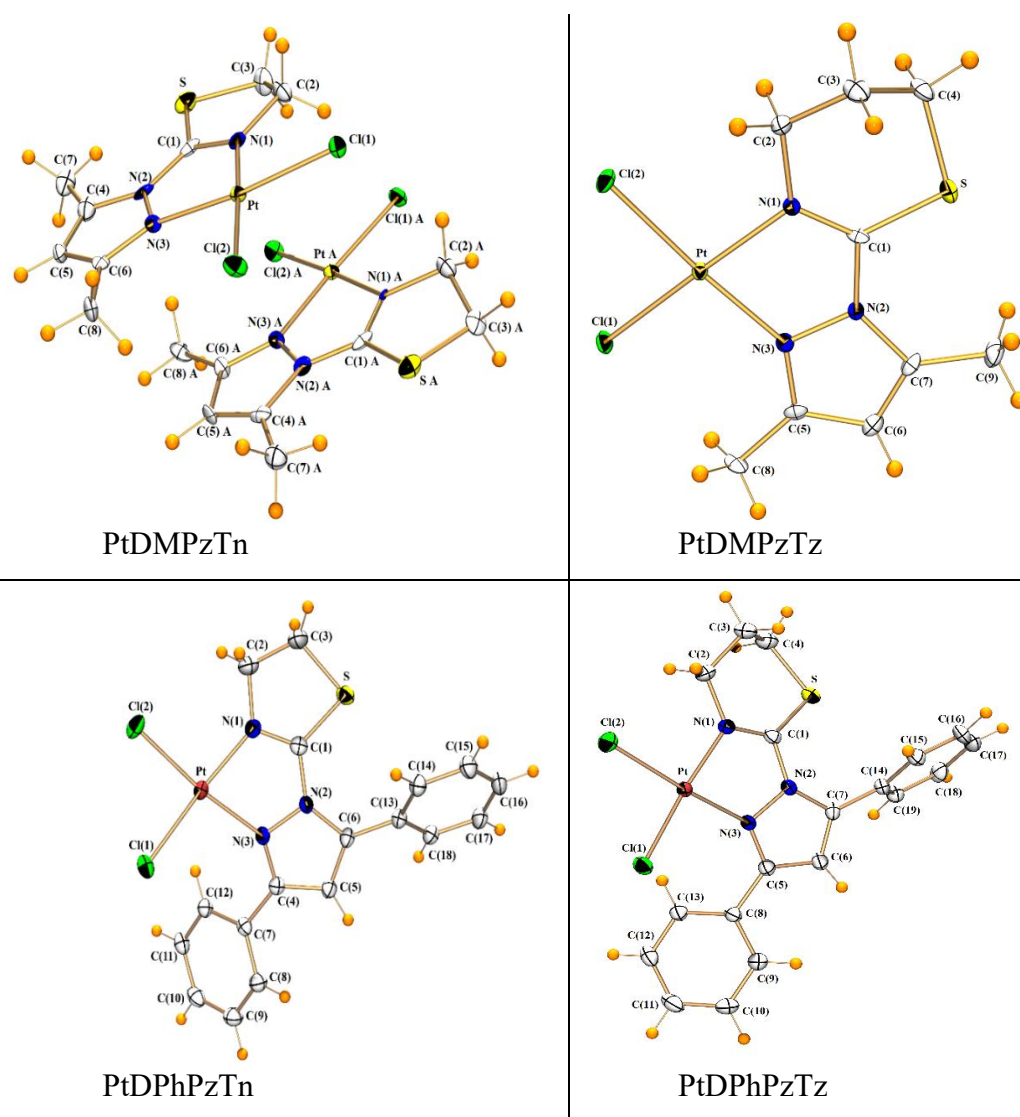


Figure 4.1. Crystal structure of PtDMPzTn , PtDMPzTz , PtDPhPzTn and PtDPhPzTz .

Table 4.3. Dihedral angles (°) between the planes Cl(1)-Pt-Cl(2) and N(1)-Pt-N(3) in Pt(II) complexes and torsion angles (°) for Pt(II) complexes and their respective ligands.

	<i>Dihedral angle between Cl(1)-Pt-Cl(2) and N(1)-Pt-N(3)</i>	<i>Torsion angle S-C(1)-N(2)-N(3)</i>
<i>PtDMPzTn</i>	2.27 / 2.72	-178.95 / -176.82
<i>DMPzTn</i>		-
<i>PtDMPzTz</i>	4.44	-173.7(4)
<i>DMPzTz</i>		-
<i>PtDPhPzTn</i>	4.66	-163.8(1)
<i>DPhPzTn</i>		0.6 (2)
<i>PtDPhPzTz</i>	6.18	-159.1(1)
<i>DPhPzTz</i>		-50.7(2)

*DMPzTn and DMPzTz are oils, so X-ray diffraction data are not available.

Table 4.4. Selected bond distances (Å) and angles (°) for Pt(II) complexes.

	<i>PtDMPzTn</i>	<i>PtDMPzTz</i>	<i>PtDPhPzTn</i>	<i>PtDPhPzTz</i>
<i>Pt-Cl(1)</i>	2.287(4)	2.296(1)	2.299(1)	2.294(1)
<i>PtA-Cl(1)A</i>	2.303(4)			
<i>Pt-Cl(2)</i>	2.299(3)	2.298(1)	2.290(1)	2.298(1)
<i>PtA-Cl(2)A</i>	2.288(3)			
<i>Pt-N(1)</i>	1.984(14)	2.022(4)	1.995(2)	2.018(1)
<i>PtA-N(1)A</i>	1.992(13)			
<i>Pt-N(3)</i>	2.022(11)	2.003(4)	2.019(2)	2.006(1)
<i>PtA-N(3)A</i>	2.024(11)			
<i>Cl(1)-Pt-Cl(2)</i>	89.3(1)	87.5(1)	89.56(2)	88.25(2)
<i>Cl(2)A-PtA-Cl(1)A</i>	87.9(1)			
<i>N(1)-Pt-Cl(1)</i>	176.9(3)	175.4(1)	174.50(5)	174.84(4)
<i>N(1)A-PtA-Cl(1)A</i>	177.6(3)			
<i>N(1)-Pt-Cl(2)</i>	93.6(3)	95.3(1)	93.84(5)	95.09(4)
<i>N(1)A-PtA-Cl(2)A</i>	94.2(3)			
<i>N(1)-Pt-N(3)</i>	79.6(5)	79.8(2)	78.84(7)	79.49(5)
<i>N(1)A-PtA-N(3)A</i>	78.9(5)			
<i>N(3)-Pt-Cl(1)</i>	97.6(4)	97.5(1)	97.85(5)	97.46(4)
<i>N(3)A-PtA-Cl(1)A</i>	99.1(4)			
<i>N(3)-Pt-Cl(2)</i>	172.8(4)	174.7(1)	172.54(5)	173.03(4)
<i>N(3)A-PtA-Cl(2)A</i>	172.8(4)			

Pt-Cl bond lengths were similar for the four examined complexes and slightly longer than Pt-N bond lengths, as can be seen in Table 4.4. Furthermore, after an exhaustive research on Cambridge Structural Database (CSD, version v5.44, Jun 2023) [252], it was checked that all the Pt-Cl distances were in the same order as the mean

values for squared-planar *cis*-complexes with a Cl₂N₂ coordination environment around Pt(II) [2.299(17) Å for 665 Pt(II) complexes]. This was also true for Pt-N_{pyrazole} bond distances, which were similar to the mean value calculated for squared-planar complexes with Pt(II) in a Cl₂N₂ coordination environment [2.007(24) Å for 34 Pt(II) complexes] in CSD [252], especially for complexes with thiazoline rings, being slightly larger in the case of complexes with thiazine rings. As for the Pt-N_{thiazoline} bond distance, it was a bit shorter than the average values calculated for this type of bonds in CSD [252]: 2.106(38) Å for 5 Pt(II) complexes; occurring the same way for Pt-N_{thiazine} bond distance, which was also a little shorter than the mean value calculated in CSD [252]: 2.082(31) Å for 11 Pt(II) complexes.

Regarding the arrangement of the organic ligands in the Pt(II) complexes, the thiazoline and thiazine rings rotated around C(1)-N(2) bond so that the N(1) and N(3) atoms were on the same side in order to coordinate simultaneously to Pt(II) ions. To prove this, the values of the corresponding torsion angles of the complexes and their free ligands are shown in Table 4.3.

Respect to the interactions produced in these complexes, both PdDMPzTn and PdDMPzTz showed π - π stacking interactions between pyrazole rings, and PtDPhPzTn displayed parallel displaced aromatic interactions between phenyl rings. The values and a representation of these interactions could be found in Figure 4.2 and Table 4.5.

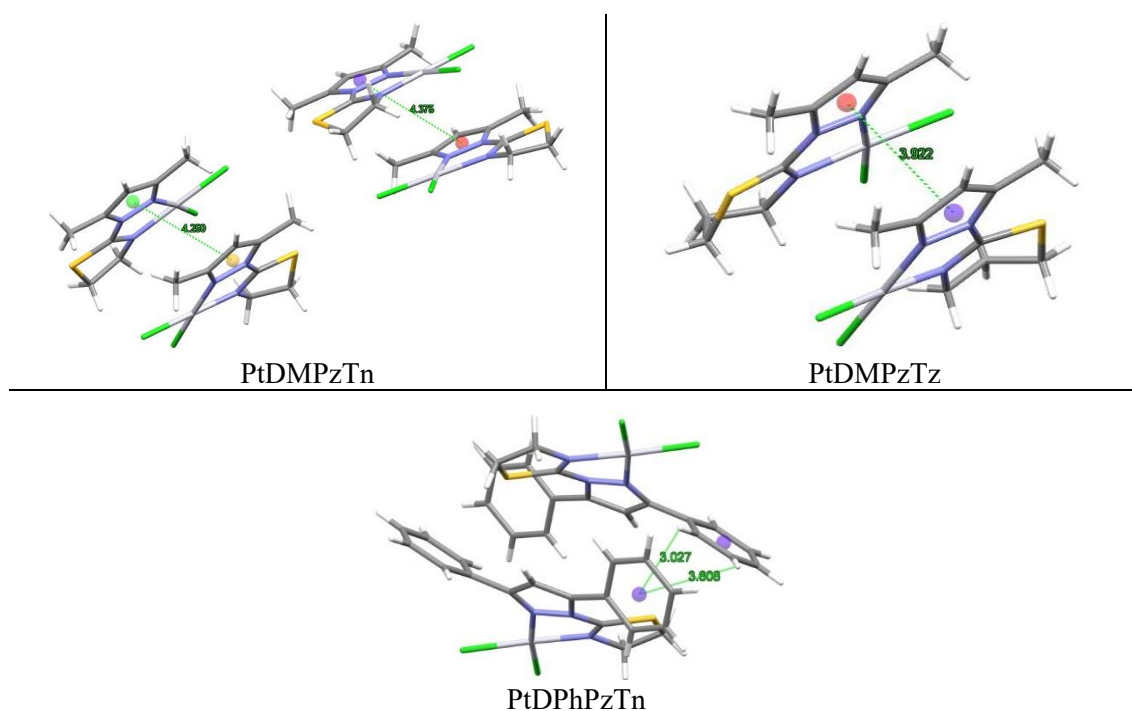


Figure 4.2. Aromatic interactions in PtDMPzTn, PtDMPzTz and PdDPhPzTn.

Table 4.5. Aromatic interactions in PtDMPzTn, PtDMPzTz and PtDPhPzTn.

	<i>Type of interaction</i>	<i>ANG</i>	<i>DC</i>	<i>DZ</i>	<i>DZ'</i>	<i>DS</i>	<i>ANGS</i>
<i>PtDMPzTn</i>	π - π stacking (pyrazole rings)	1.82	4.375	3.447	3.407	3.268	86.57
		1.82	4.250	3.431	3.509	3.465	80.66
<i>PtDMPzTz</i>	π - π stacking (pyrazole rings)	0.83	3.922	3.526	3.508	3.827	76.72
<i>PtDPhPzTn</i>	T type (phenyl rings)	64.39	5.203	4.511	1.099	3.222	138.03

4.1.1.c. Infrared spectroscopy

The coordination of a metallic ion to a ligand produces the formation of metal-ligand bonds and variation in the energy of the free ligand bonds. These changes due to the metal-ligand bonds generate the displacement of the ligand bands due to the coordination. A comparison between the IR spectra of the free ligand and its corresponding complex could provide information about what ligand atoms are implicated in the metal coordination, which allow to confirm the structure of the complexes.

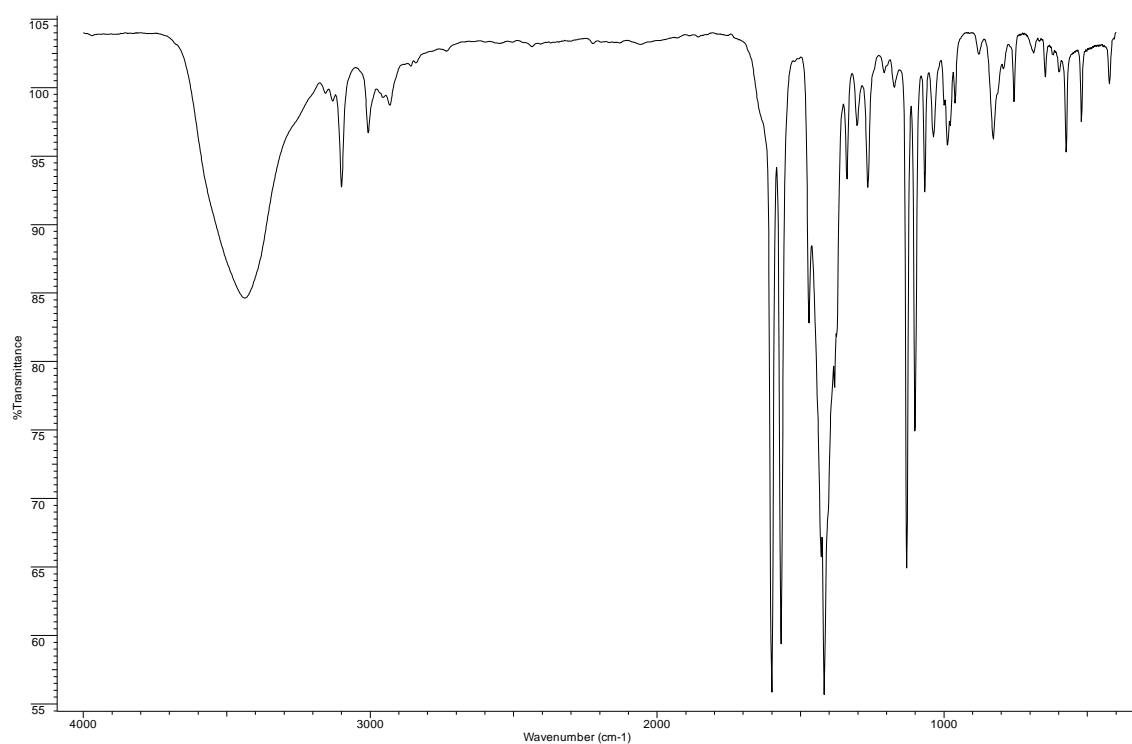
For that reason, a comparison of the most relevant signals corresponding to the pyrazole, thiazine and thiazoline ring vibrations of the free ligands [176,179,184] and their complexes can be found in Table 4.6 and Table 4.7. Additionally, the IR spectra in 4000-400 cm^{-1} region of PtDMPzTn, PtDMPzTz, PtDPhPzTn and PtDPhPzTz can be observed in Figure 4.3-Figure 4.6.

Table 4.6. IR spectral assignments (cm^{-1}) for PzTn, PtPzTn, DMPzTn, PtDMPzTn, DPhPzTn and PtDPhPzTn.

	<i>PzTn</i>	<i>PtPzTn</i>	<i>DMPzTn</i>	<i>PtDMPzTn</i>	<i>DPhPzTn</i>	<i>PtDPhPzTn</i>
$W_1[\nu(C=N)]$	1641	1596	1635	1600	1639	1587
<i>Pyrazole ring vibrations</i>	1514	1518	1574	1568	1560	1555
	1382	1413	1410	1417	1408	1412
	1350	1359	1387	1381	1319	1319
	991	1004	970	977	1000	998

Table 4.7. IR spectral assignments (cm^{-1}) for PzTz, PtPzTz, DMPzTz, PtDMPzTz, DPhPzTz and PtDPhPzTz.

	<i>PzTz</i>	<i>PtPzTz</i>	<i>DMPzTz</i>	<i>PtDMPzTz</i>	<i>DPhPzTz</i>	<i>PtDPhPzTz</i>
$\Psi_1[\nu(\text{C}=\text{N})]$	1635	1606	1639	1592	1639	1606
<i>Pyrazole ring vibrations</i>	1510	1527	1566	1562	1548	1556
	1419	1437	1411	1405	1406	1404
	1386	1416	1375	1387	1303	1314
	1327	1373	1315	1346		
	995	1003	981	995	998	1006

**Figure 4.3.** IR spectrum of $\text{PtCl}_2(\text{DMPzTn})$ in $4000\text{-}400\text{ cm}^{-1}$ region.

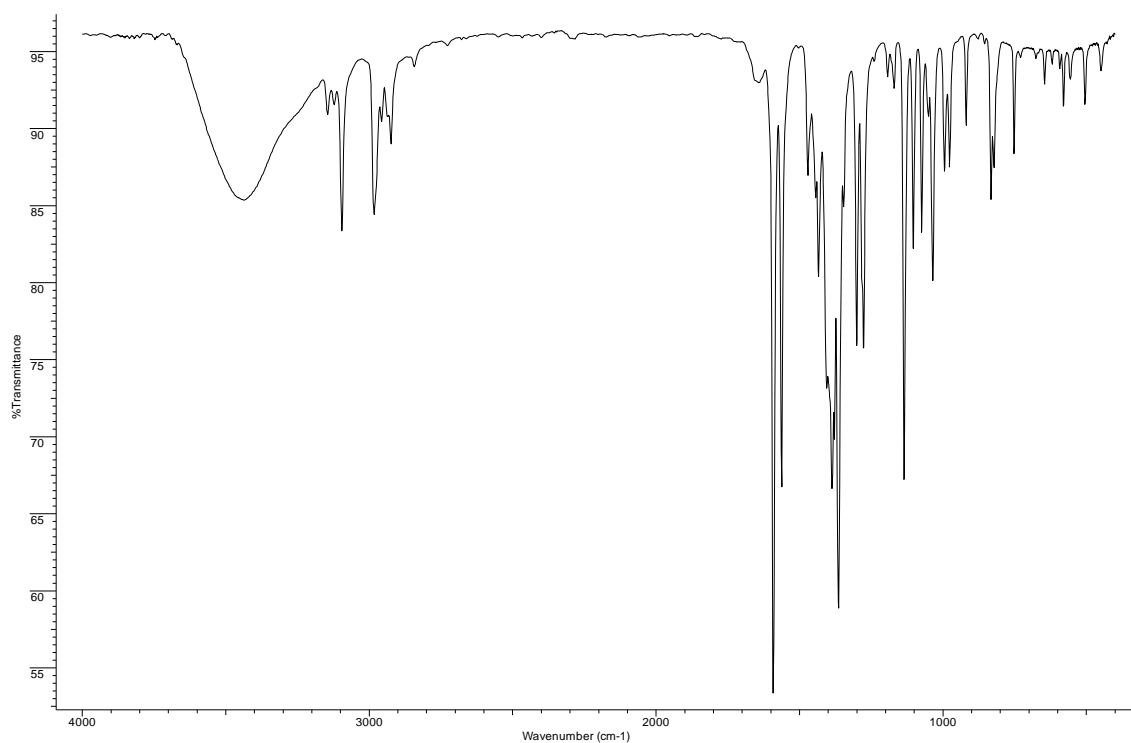


Figure 4.4. IR spectrum of PtCl₂(DMPzTz) in 4000-400 cm⁻¹ region.

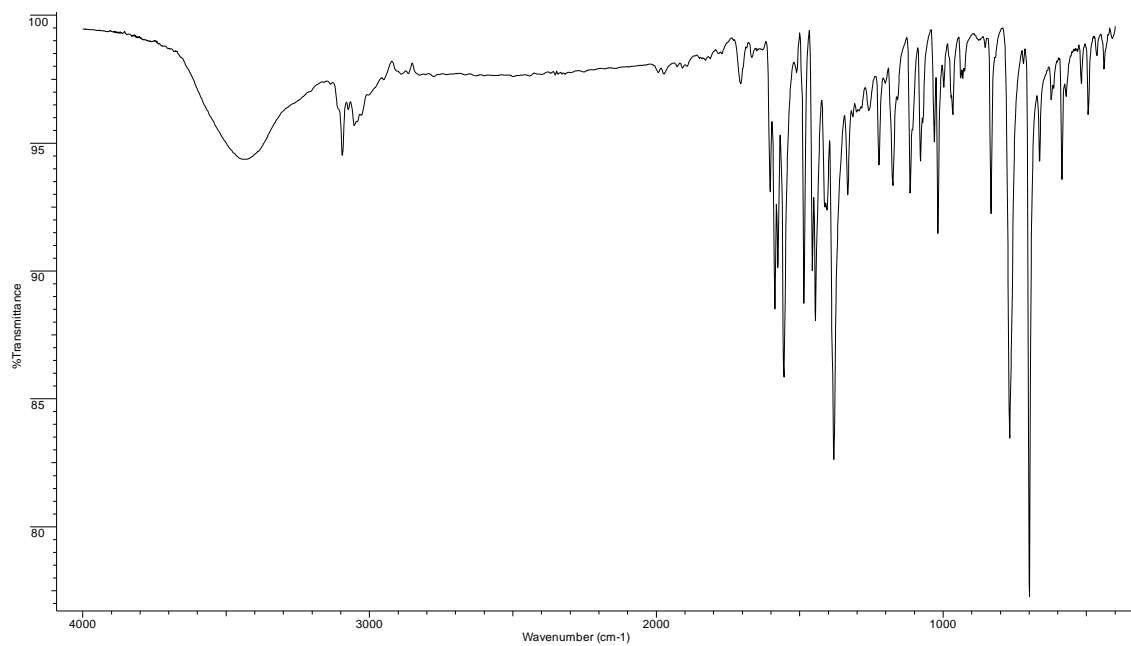


Figure 4.5. IR spectrum of PtCl₂(DPhPzTn) in 4000-400 cm⁻¹ region.

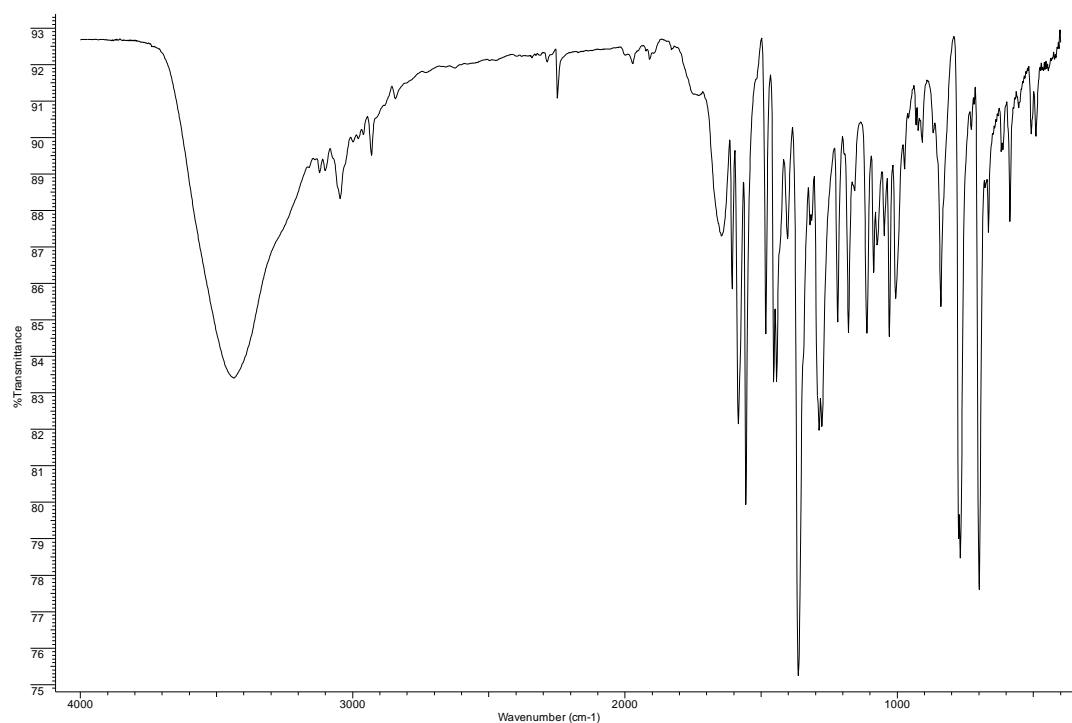


Figure 4.6. IR spectrum of PtCl₂(DPhPzTz) in 4000-400 cm⁻¹ region.

The IR spectra of all Pt(II) complexes showed that $\nu(\text{C}=\text{N})$ vibration from thiazine and thiazoline rings are shifted to a lower wavenumber in the complexes compared to their respective ligands. It has been found that the tension vibration of the C=N band can be shifted to lower frequencies when it is part of a chelate ring due to an increase in conjugation therein. This occurs because of back-coordination in the metal to ligand direction, which counteracts the loss of electron density on the donor nitrogen atom in the C=N bond.

On the other hand, the stretching vibrations from pyrazole ring vibrations for PtPzTn and PtPzTz were shifted to higher wavenumbers than their respective ligands, while for PtDPhPzTn and PtDPhPzTz this occurred to a lesser extent probably due to some electron transfer by inductive effect of the phenyl rings to the pyrazole ring. In the case of PtDMPzTn and PtDMPzTz, they did not show a well-defined pattern, which can be explained by the presence of the methyl substituents. These frequency shifts in the IR spectra of the platinum complexes confirmed their coordination to the metal ion through the nitrogen atoms of both heterocycles [179,184].

4.1.1.d. ¹H Nuclear magnetic resonance spectroscopy

The ¹H NMR spectral data of Pt(II) complexes in deuterated DMF can be seen in Figures 4.7-4.10. The position and assignation of the signals can be found in Table 4.8

and Table 4.9, both for the complexes and for the ligands, in order to clearly identify de displacements between them, which confirmed de coordination of the metal ion to the ligand.

As it was indicated previously, the data for PtDMPzTn and PtDMPzTz could not be obtained due to their low solubility.

Table 4.8. ^1H NMR spectral data for PzTn, PtPzTn, DPhPzTn and PtDPhPzTn in DMF- d_7 solvent.

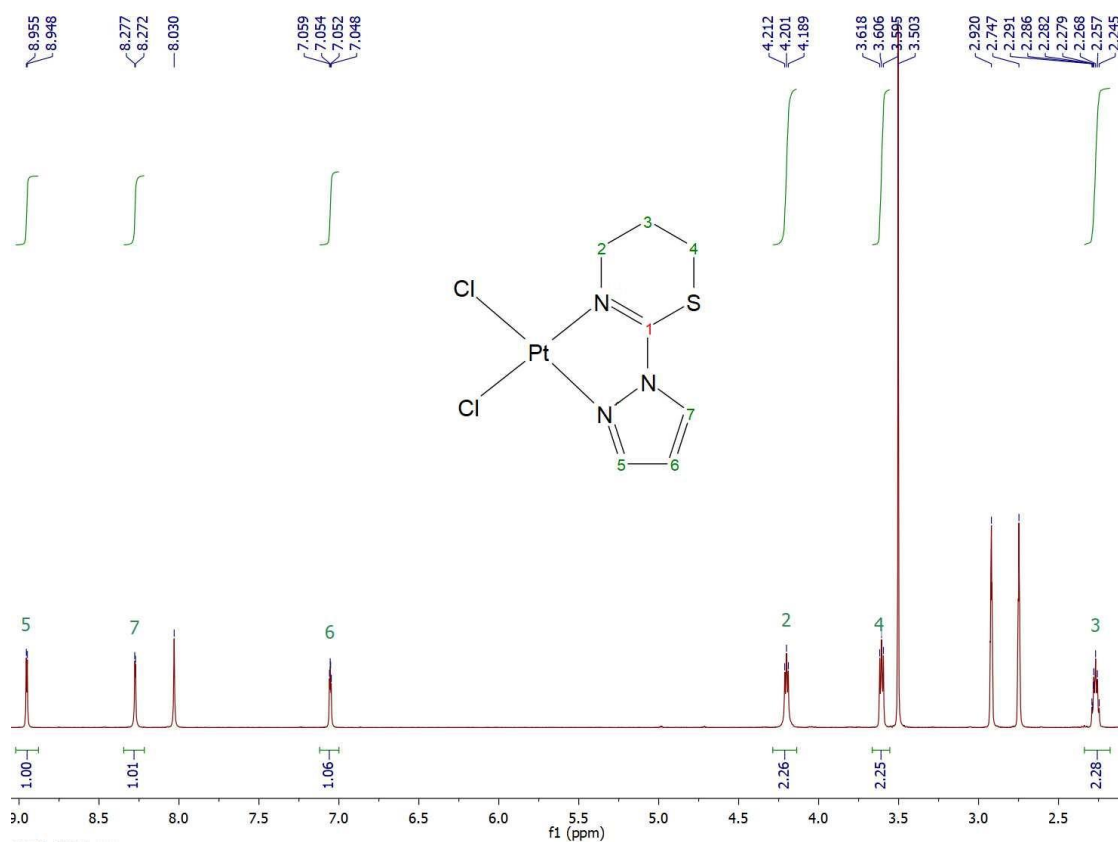
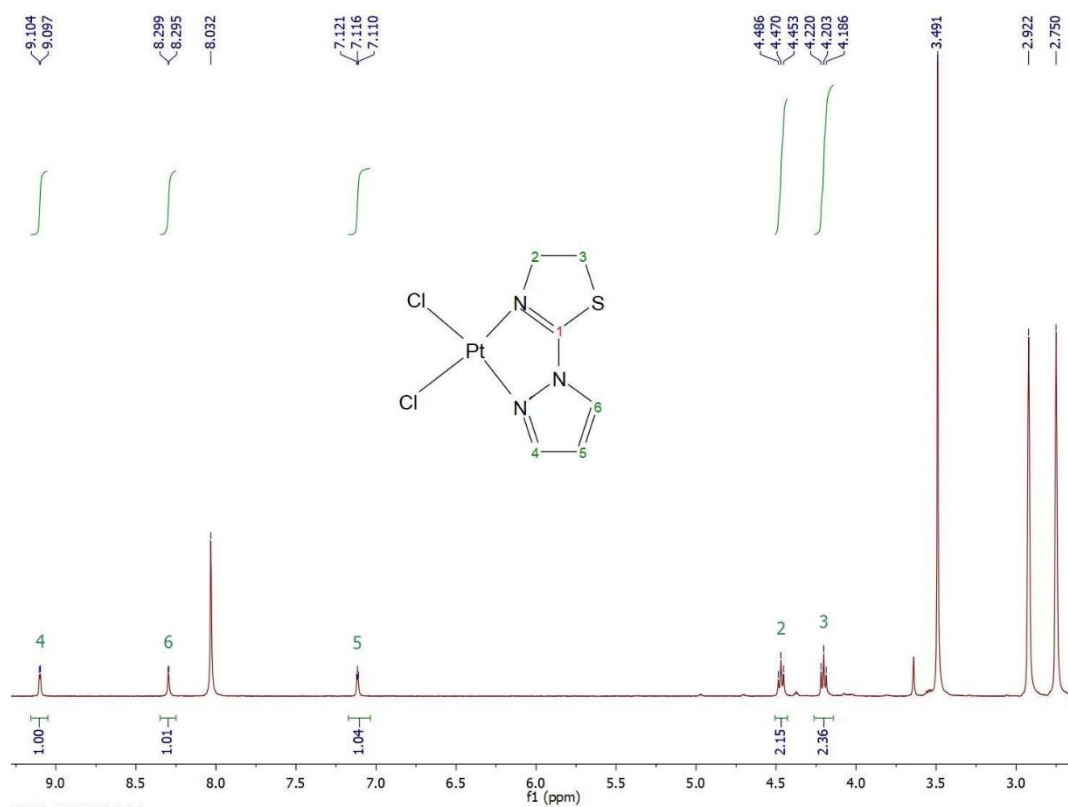
	<i>N-CH₂</i>	<i>S-CH₂</i>	<i>H(4)</i>	<i>H(5)</i>	<i>H(6)</i>	<i>H(8-18)</i>
<i>PzTn</i>	4.34	3.58	8.40	6.60	7.81	-
<i>PtPzTn</i>	4.47	4.20	9.08	7.11	8.29	-
<i>DPhPzTn</i>	4.19	3.51	-	7.20	-	7.46-8.08
<i>PtDPhPzTn</i>	4.42	3.87	-	7.19	-	7.49-7.86

Table 4.9. ^1H NMR spectral data for PzTz, PtPzTz and DPhPzTz, PtDPhPzTz in DMF- d_7 solvent.

	<i>N-CH₂</i>	<i>H₂(3)</i>	<i>S-CH₂</i>	<i>H(5)</i>	<i>H(6)</i>	<i>H(7)</i>	<i>H(9-19)</i>
<i>PzTz</i>	3.83	1.92	3.21	8.33	6.50	7.69	-
<i>PtPzTz</i>	4.20	2.27	3.61	8.95	7.05	8.27	-
<i>DPhPzTz</i>	3.65	1.91	3.31	-	7.16	-	7.47-8.01
<i>PtDPhPzTz</i>	4.25	2.31	3.30	-	7.12	-	7.48-7.85

The results of the ^1H NMR spectral data comparison for the four ligands and its complexes showed in Table 4.8 and Table 4.9 denoted that signals are shifted to downfield respect to free ligands. These differences indicate that, in the complexes, the organic ligand was coordinated to metal ion in DMF solution. Thus, the highest value of shifts for the $\text{CH}_2\text{-N}_{\text{thiazine}}$ signal in PtDPhPzTz respect to free ligand was in accordance with the fact that the coordination in this complex took place through the nitrogen atom of the thiazine ring to the metal ion. However, for the other platinum complexes, apart from the displacement of the hydrogen signals belonging to the methylene groups attached to the nitrogen atom of the S,N heterocycles, a displacement of the hydrogen signals corresponding to the methylene groups attached to the sulfur atom was observed. This can be explained by the loss of electron density in the sulfur atom due to the increase of the double bond character of the carbon-sulfur linkage because of the extension of conjugation in the chelate ring to the sulfur atom. These electronic redistributions in the heterocyclic rings as a result of coordination were in agreement with the length increase of the C(1)-N(1) bonds and the length decrease of the C(1)-N(2) and C(1)-S bonds in the complexes with respect to non-coordinated ligands.

These findings of NMR spectroscopy in DMF solution suggested that the platinum complexes remained intact in solution. Additionally, the complexes were kept in solution for 21 days before being measured by NMR again (data not included), showing the high stability of these complexes in the DMF medium.



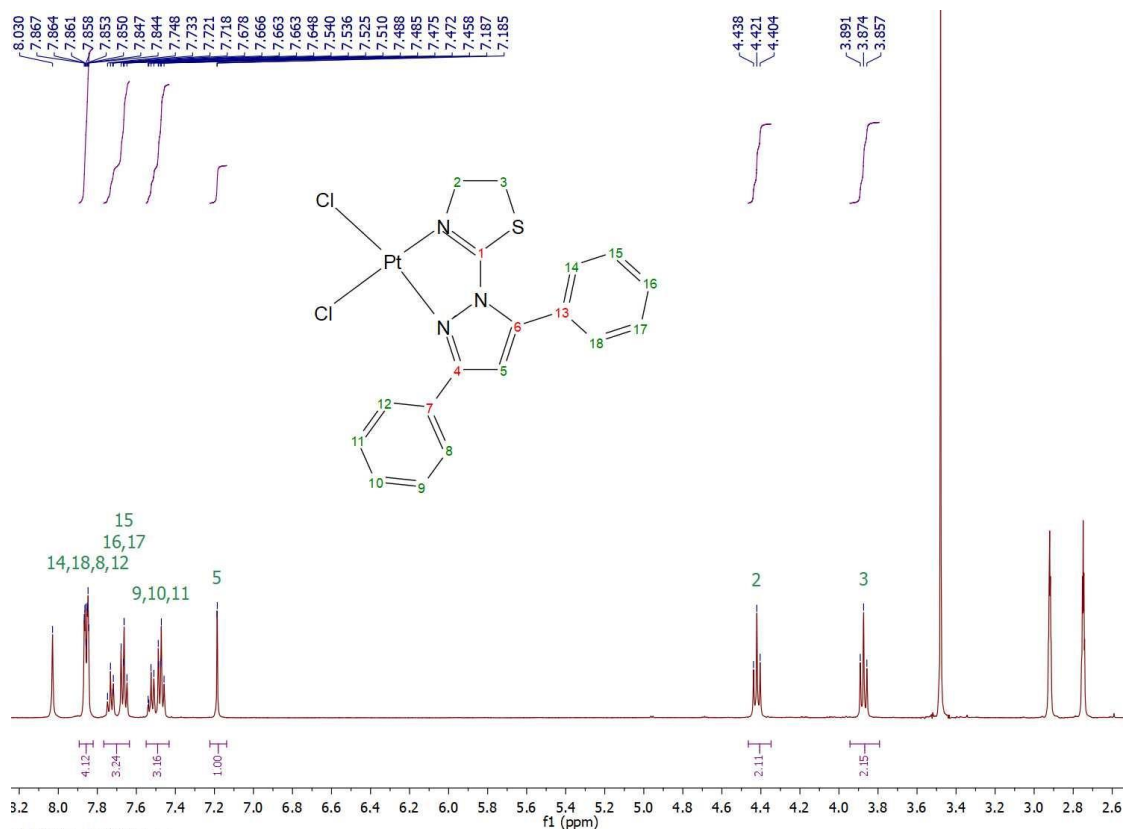


Figure 4.9. ^1H NMR spectrum of $\text{PtCl}_2(\text{DPhPzTn})$ in DMF-d_7 .

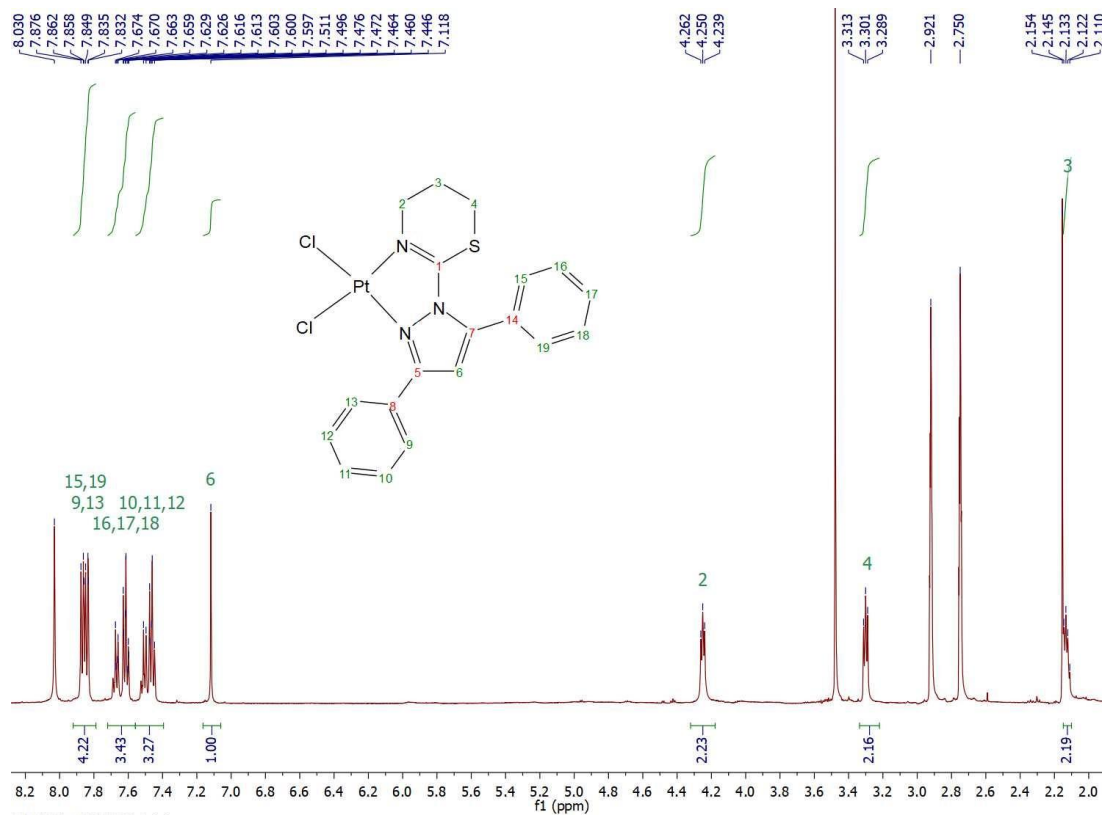


Figure 4.10. ^1H NMR spectrum of $\text{PtCl}_2(\text{DPhPzTz})$ in DMF-d_7 .

4.1.2. Biological testing from Pt(II)/Ligand system

4.1.2.a. Cell viability

The cytotoxic potential of all the synthesized Pt(II) complexes was assessed against three selected human tumor cell lines (HL-60, U-937, and HeLa), which were challenged with increasing concentrations (0-100 μM) of the compounds and CisPt for 24 h. As can be observed in Figure 4.11 and Table 4.10, data obtained showed that Pt(II) compounds had a potent cytotoxicity towards leukemic cell lines HL-60 and U-937, among which PtDPhPzTn and PtDPhPzTz displayed higher antiproliferation effects compared to CisPt in both leukemic cell lines. In fact, PtDPhPzTn and PtDPhPzTz were tested in concentrations from 0-10 μM in the two lines mentioned due to its high cytotoxicity. Particularly, the cytotoxic effect of PtDPhPzTn and PtDPhPzTz with IC_{50} values of $3.23 \pm 0.34 \mu\text{M}$ and $2.75 \pm 0.29 \mu\text{M}$, respectively, was two-fold lower than that of cisplatin in U-937 cells. A similar trend was found in HL-60, with PtDPhPzTn and PtDPhPzTz depicting the highest cytotoxic effect. Furthermore, PtPzTn and PtPzTz were able to significantly reduce the cell viability of the leukemic cells HL-60 and U-937 at moderately higher concentrations. On the other hand, PtDMPzTn and PtDMPzTz showed moderate cytotoxicity on non-solid tumor HL-60 and U-937 cell lines, presenting lower IC_{50} values for PtDMPzTn in both cases. However, in HeLa cells, neither PtPzTn, PtPzTz, PtDMPzTn nor PtDMPzTz exhibited cytotoxic potential (IC_{50} values $>100 \mu\text{M}$), while PtDPhPzTn and PtDPhPzTz showed a cell killing ability comparable to that of CisPt (IC_{50} values were $12.15 \pm 0.89 \mu\text{M}$ and $14.09 \pm 1.17 \mu\text{M}$, respectively). Likewise, none of the free ligands produced significant effects in cell viability of U-937 and HL-60 cells, whereas DPhPzTn and DPhPzTz only affected cell viability of HeLa cells at the highest dose, i.e., 100 μM (Figure A.7 and Table A.3). These findings indicated that HL-60 and U-937 leukemic cells were more sensitive than HeLa cells to all six Pt(II) complexes. Therefore, given that HeLa were the most resistant cells to the different compounds and the remarkable differences observed in this cell line between PtDPhPzTz and PtDPhPzTn and their analogs without phenyl groups, the subsequent experiments were carried out in such cellular model derived from a solid tumor.

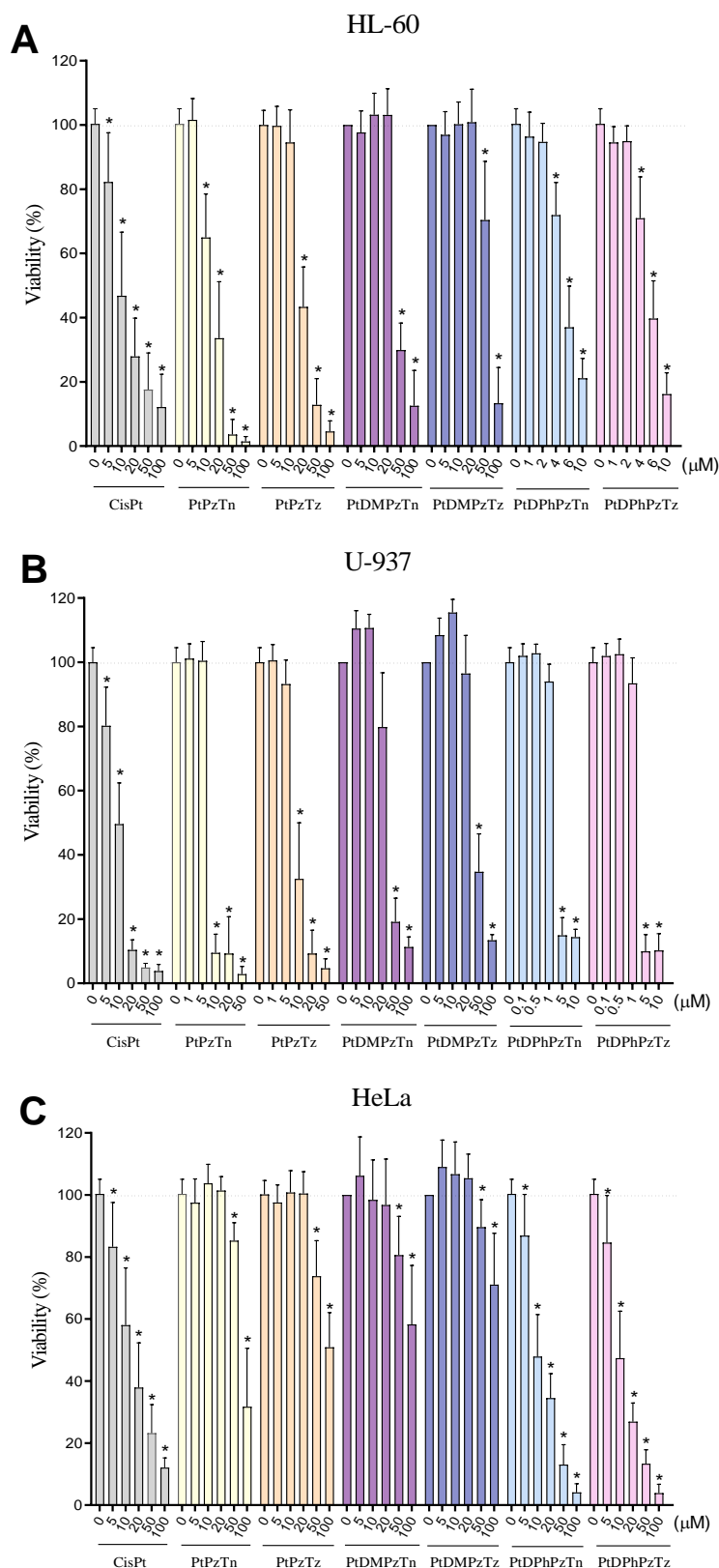


Figure 4.11. Cytotoxic effect of Pt(II) complexes. HL-60 (A), U-937 (B) and HeLa (C) cell lines were challenged with concentrations from 0-100 μM of cisplatin (CisPt), the six Pt(II) complexes, namely PtPzTn, PtPzTn, PtDMPzTn, PtDMPzTz, PtDPhPzTn and PtDPhPzTz, or the vehicle (DMF or DMSO) for 24 h. Values are presented as means \pm SD ($n = 6$) and depicted as percentage over untreated samples. * $P < 0.05$ vs. control (0.5% DMF or DMSO). (Dunnett's test).

Table 4.10. Cytotoxic effect of PtPzTn, PtPzTz, PtDMPzTn, PtDMPzTz, PtDPhPzTn and PtDPhPzTz and their respective ligands towards selected tumor cell lines.

	<i>HeLa</i>	<i>HL-60</i>	<i>U-937</i>
<i>CisPt</i>	16.08 ± 1.01 ^a	11.32 ± 1.04 ^b	7.89 ± 0.54 ^b
<i>PtPzTn</i>	140.20 ± 24.31 ^b	15.02 ± 1.41 ^c	6.48 ± 0.81 ^c
<i>PtPzTz</i>	142.20 ± 14.26 ^b	23.93 ± 2.49 ^d	8.09 ± 0.83 ^b
<i>PtDMPzTn</i>	119.8 ± 8.38 ^c	42.83 ± 1.75 ^e	32.59 ± 1.17 ^d
<i>PtDMPzTz</i>	144.7 ± 14.25 ^b	62.32 ± 1.87 ^f	43.04 ± 1.36 ^e
<i>PtDPhPzTn</i>	12.15 ± 0.89 ^a	6.05 ± 0.47 ^a	3.23 ± 0.34 ^a
<i>PtDPhPzTz</i>	14.09 ± 1.17 ^a	5.79 ± 0.45 ^a	2.75 ± 0.29 ^a

For a given cell line, a different lowercase letter indicates statistically significant ($P < 0.05$) changes (Tukey's test). Data are presented as $IC_{50} \pm SD$ (μM).

4.1.2.b. Cellular uptake

In order to verify the Pt(II) accumulation into HeLa cells, ICP-MS measurements were done. For that, the complexes with the best cytotoxic effects were selected. Therefore, the tumor cells were incubated with the IC_{50} of PtPzTn, PtPzTz, PtDPhPzTn, PtDPhPzTz and CisPt during 4h. As it can be seen in Figure 4.12, an accumulation of the metal ion was produced after incubation with the four compounds. Additionally, it was observed that complexes with phenyl substituents accumulated into cells much more efficiently than CisPt (10-fold higher in both cases). The higher accumulation and lower IC_{50} values of these complexes might indicate that the presence of aromatic groups in the ligands improved their cellular uptake. This could be related with a presumable higher lipophilicity of PtDPhPzTn and PtDPhPzTz.

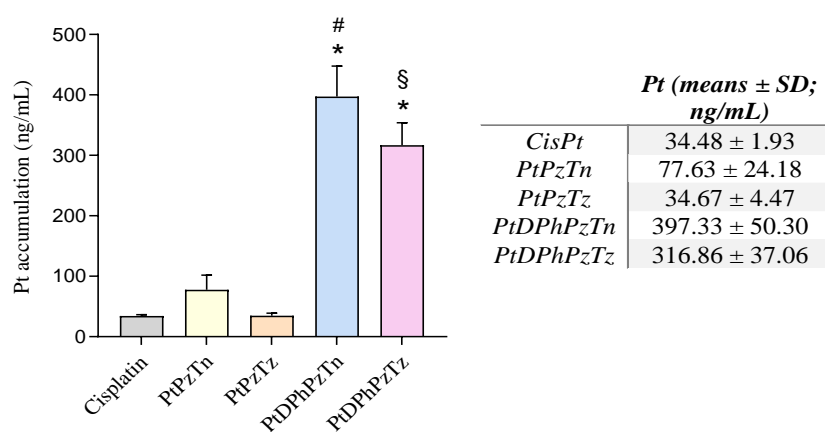


Figure 4.12. Platinum accumulation in HeLa cells. Cells were treated with 16.08 μM of cisplatin (CisPt), 12.15 μM of PtDPhPzTn, 140.20 μM of PtPzTn, 14.09 μM of PtDPhPzTz or 142.20 μM of PtPzTz for 4 h, and then samples were digested with 65% HNO_3 and subsequently analyzed by ICP-MS. Pt concentrations were given in ng/mL. Values represent means \pm SD of 3 independent experiments. [#] $P < 0.05$ compared to cisplatin values. ^{*} $P < 0.05$ compared to PtPzTn values. [§] $P < 0.05$ compared to PtPzTz values. (Tukey's test).

4.1.2.c. Apoptosis determination

Once it was checked the higher cytotoxic effect and stronger accumulation of the complexes with phenyl rings, these two complexes were selected for the rest of the experiments (apoptosis determination, ROS production and intercalation assay). To test whether the reduction in cell viability was associated with induction of apoptosis, the redistribution of phosphatidylserine in the presence of PI was analyzed. The treatment of HeLa cells with IC₅₀ of the complexes with phenyl rings, their respective ligands and CisPt during 24 h produced significant changes in the percentage of cell populations (Figure 4.13). Particularly, it could be observed a significant decrease of live cells for CisPt and the two complexes respect to the control, as well as significant differences between the complexes and their corresponding ligands. Although no significance was found for early and late apoptotic cells neither for CisPt nor the complexes or their respective ligands, it can be noticed an increase of late apoptotic cells of all of them respect to the control levels, especially for CisPt and the two complexes. On the other hand, a significant increase of secondary necrotic cells for CisPt and the two complexes was produced respect to the control, being also significant when comparing the effect of the complexes with that of CisPt. Significant differences between the secondary necrosis induced by the complexes and their corresponding ligands were also observed. These results suggested that the major type of cell death prompted by PtDPhPzTn and PtDPhPzTz was apoptosis.

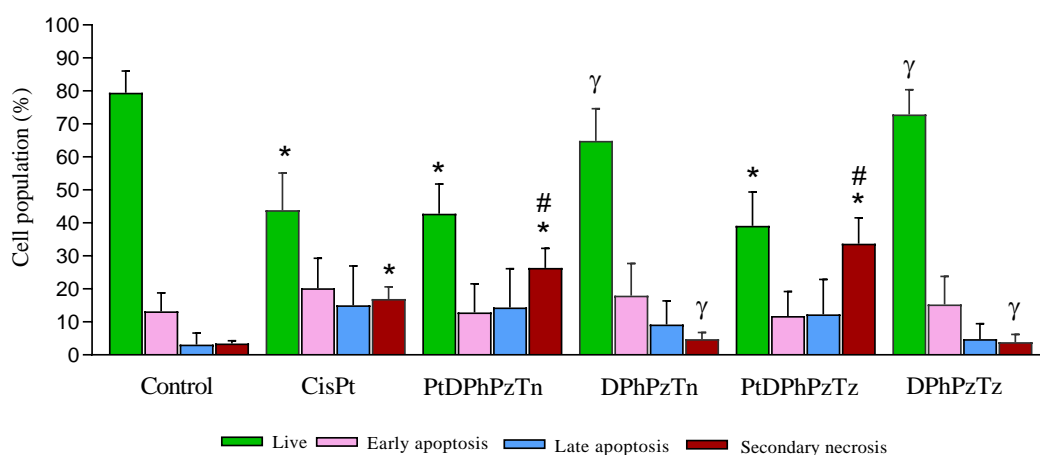


Figure 4.13. Flow cytometry results including live cells, early and late apoptosis, and secondary necrosis caused by platinum complexes. HeLa cells were challenged with 16.08 μ M cisplatin (CisPt), 12.15 μ M PtDPhPzTn, 12.15 μ M DPhPzTn, 14.09 μ M PtDPhPzTz, 14.09 μ M DPhPzTz or the vehicle (0.5% DMF) during 24 h. Histograms show percentages of cell population detected by flow cytometry. Values are presented as means \pm SD of four independent experiments. * P < 0.05 compared to control values; # P < 0.05 compared to the corresponding CisPt value; ^γ P < 0.05 comparing each complex with its respective ligand (Tukey's test).

4.1.2.d. Reactive oxygen species determination

On the other hand, the Pt(II) complexes PtDPhPzTn and PtDPhPzTz were checked to cause a dramatic increase of intracellular ROS production (35.7 ± 6.1 and $31.6 \pm 4.5\%$ DCF positive cells for PtDPhPzTn and PtDPhPzTz, respectively; Figure 4.14) that ultimately led to apoptotic cell death. Surprisingly, the free ligands *per se* also produced a significant increase in the intracellular production of ROS (Figure 4.14), which was not correlated either with increases in the percentage of apoptotic cells (Figure 4.13) or with modifications of cell viability (Figure A.7). This effect of the free ligands on ROS production may be due to nonspecific effects inherent to the nature of the molecules, or to possible interferences with the fluorescent probe used for the determination of ROS.

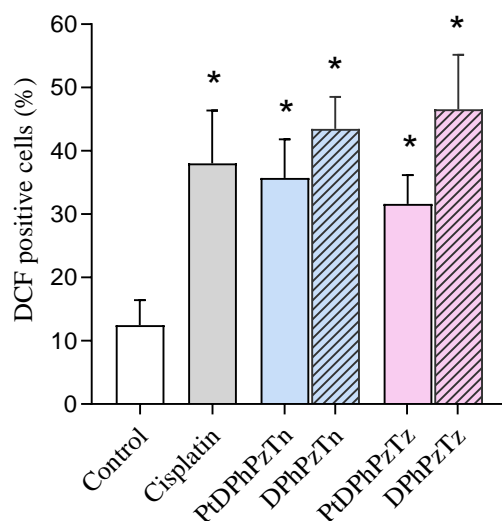


Figure 4.14. Reactive oxygen species (ROS) production triggered by Pt(II) complexes. HeLa cells were challenged with $16.08 \mu\text{M}$ cisplatin, $12.15 \mu\text{M}$ PtDPhPzTn, $12.15 \mu\text{M}$ DPhPzTn, $14.09 \mu\text{M}$ PtDPhPzTz, $14.09 \mu\text{M}$ DPhPzTz, or the vehicle (DMF, control) for 4 h, and the production of intracellular ROS was determined by flow cytometry by means of DCFH. Histograms show percentages of DCF positive cells. Values are presented as means \pm SD of four independent experiments. * $P < 0.05$ compared to control values. (Tukey's test).

4.1.2.e. Intercalation assay

Once it was performed the intercalation assay, it could be affirmed that, unlike cisplatin, apoptosis induction by both PtDPhPzTn and PtDPhPzTz was independent of their DNA intercalating capacity. This was demonstrated by the inability of both complexes to either unwind the supercoiled DNA or displace topoisomerase I from the groove, which would produce DNA mobility shifts (Figure 4.15).

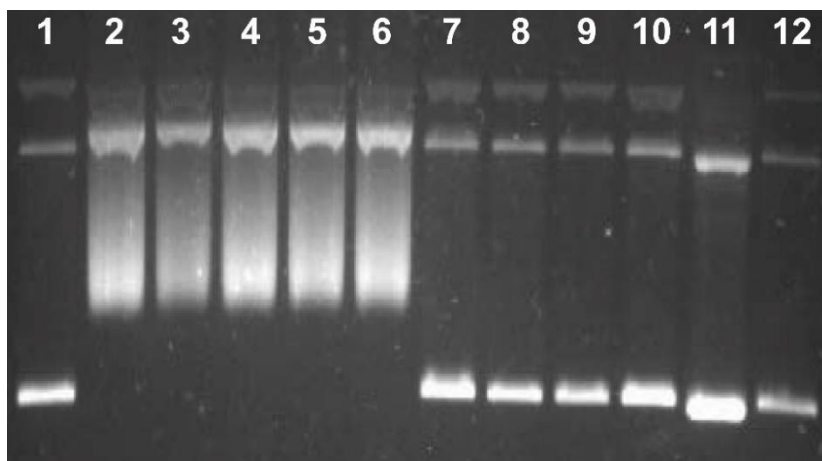


Figure 4.15. The Pt(II) complexes lack DNA intercalating capacity. DNA intercalation was assessed by means of a DNA unwinding assay kit, as explained in *Section 3. Materials and methods*. Lane 1: supercoiled pBR322 + wheat germ Topoisomerase I; lane 2: supercoiled pBR322; lane 3: supercoiled pBR322 + 14.09 μM PtDPhPzTz; lane 4: supercoiled pBR322 + 12.15 μM PtDPhPzTn; lane 5: supercoiled pBR322 + 14.09 μM DPhPzTz; lane 6: supercoiled pBR322 + 12.15 μM DPhPzTn; lane 7: supercoiled pBR322 + wheat germ Topoisomerase I + 14.09 μM PtDPhPzTz; lane 8: supercoiled pBR322 + wheat germ Topoisomerase I + 12.15 μM PtDPhPzTn; lane 9: supercoiled pBR322 + wheat germ Topoisomerase I + 14.09 μM DPhPzTz; lane 10: supercoiled pBR322 + wheat germ Topoisomerase I + 12.15 μM DPhPzTn; lane 11: relaxed pBR322; lane 12: relaxed pBR322 + wheat germ Topoisomerase I. If a given compound was an intercalating agent, it would unwind the supercoiled DNA or displace topoisomerase I from the groove, thus producing DNA mobility shifts which is not the case for any of the tested compounds.

4.2. ANALOGS OF CISPLATIN WITH PALLADIUM AS METAL CENTER

As for the Pt(II) complexes, another six metallodrugs were synthesized with palladium as metallic center as it was previously described in section 3. *Materials and methods*. In this section, the results obtained from the characterization techniques used and the biological testing performed are exposed and analyzed.

4.2.1. Characterization from Pd(II)/Ligand systems

4.2.1.a. Elemental analysis

Elemental analysis for the solid phases of Pd(II) complexes are shown in Table 4.11, where it can be also seen the calculated values from the empiric formula. A good concordance between data could be appreciated.

Table 4.11. Elemental analysis data for Pd(II) complexes.

		%C	%H	%N	%S	<i>Empiric formula</i>
<i>PdPzTn</i>	Experimental	21.73	2.08	12.53	9.39	C ₆ H ₇ Cl ₂ PdN ₃ S
	Calculated	21.80	2.14	12.72	9.70	
<i>PdPzTz</i>	Experimental	24.52	2.65	12.10	9.28	C ₇ H ₉ Cl ₂ PdN ₃ S
	Calculated	24.39	2.64	12.20	9.30	
<i>PdDMPzTn</i>	Experimental	26.83	3.08	11.34	9.24	C ₈ H ₁₁ Cl ₂ PdN ₃ S
	Calculated	26.79	3.10	11.73	8.94	
<i>PdDMPzTz</i>	Experimental	28.85	3.57	11.17	8.71	C ₉ H ₁₃ Cl ₂ PdN ₃ S
	Calculated	29.03	3.52	11.29	8.60	
<i>PdDPhPzTn</i>	Experimental	44.59	3.02	8.76	6.67	C ₁₈ H ₁₅ Cl ₂ PdN ₃ S
	Calculated	44.78	3.14	8.71	6.64	
<i>PdDPhPzTz</i>	Experimental	45.90	3.41	8.92	6.24	C ₁₉ H ₁₇ Cl ₂ PdN ₃ S
	Calculated	45.93	3.46	8.47	6.45	

4.2.1.b. Crystal structures

As it was previously mentioned, monocrystals suitable for X-ray diffraction analysis were obtained for all Pd(II) complexes synthesized. In Table 4.12 and Table 4.13, it can be found the main information of the examined crystals, the data collection and refinement details.

The metal complexes showed crystal structures that consist of monomeric units of [PdCl₂L] (L= PzTn, PzTz, DMPzTn, DMPzTz, DPhPzTn) or [PdCl₂L]·C₂H₃N (L= DPhPzTz), as can be observed in the molecular structures presented in Figure 4.16. The coordinated geometry around Pd(II) for the complexes was slightly distorted square-planar with the dihedral angles between Cl(1)-Pd-Cl(2) and N(1)-Pd-N(3) being lower than 8°, except for PdPzTn whose geometry was square-planar with a dihedral angle of 0°. Data corresponding to dihedral angles can be found in Table 4.14. The Pd(II) ion was joined to two chlorines in *cis* disposition and a ligand molecule, which acted as bidentate and formed a chelate ring of five members. The ligand was coordinated to palladium through the nitrogen of pyrazole cycle and the nitrogen of 2-thiazoline ring for complexes PdPzTn, PdDMPzTn and PdDPhPzTn, and through the nitrogen of 1,3-thiazine ring for complexes PdPzTz, PdDMPzTz and PdDPhPzTz. The selected interatomic distances and angles are listed in Table 4.15.

Table 4.12. Crystal information, data collection and refinement details for PdPzTn, PdPzTz, PdDMPzTn and PdDMPzTz.

	<i>PdPzTn</i>	<i>PdPzTz</i>	<i>PdDMPzTn</i>	<i>PdDMPzTz</i>
<i>Crystal shape</i>	Needle	Plate	Needle	Needle
<i>Colour</i>	Yellow	Orange	Yellow	Yellow
<i>Size (mm)</i>	0.16x0.05x0.03	0.19x0.18x0.06	0.25x0.02x0.02	0.24x0.03x0.02
<i>Chemical formula</i>	C ₆ H ₇ Cl ₂ N ₃ PdS	C ₇ H ₉ Cl ₂ N ₃ PdS	C ₈ H ₁₁ Cl ₂ N ₃ PdS	C ₉ H ₁₃ Cl ₂ N ₃ PdS
<i>Formula weight</i>	330.51	344.53	358.56	372.58
<i>Crystal system</i>	Monoclinic	Monoclinic	Monoclinic	Orthorhombic
<i>Space group</i>	C 2/m	P 2 ₁ /n	P 2 ₁ /c	P b c a
<i>Unit cell dimensions</i>				
<i>a (Å)</i>	16.317(3)	8.9806(5)	17.9491(18)	7.4256(4)
<i>b (Å)</i>	6.7035(10)	7.3615(4)	7.2963(7)	17.6074(12)
<i>c (Å)</i>	8.7925(14)	16.2772(10)	17.5523(15)	18.3241(13)
<i>α (°)</i>	90	90	90	90
<i>β (°)</i>	95.489(9)	101.738(2)	91.305(3)	90
<i>γ (°)</i>	90	90	90	90
<i>Cell volume (Å³)</i>	957.3(3)	1053.59(10)	2298(14)	2395.8(3)
<i>Z</i>	4	4	8	8
<i>D_{calc} (g cm⁻³)</i>	2.293	2.172	2.073	2.066
<i>μ (mm⁻¹)</i>	2.666	2.427	2.23	2.143
<i>F(000)</i>	640	672	1408	1472
<i>θ range</i>	2.327-30.494	2.407-30.529	2.27-28.439	2.313-26.369
<i>Index ranges</i>	-23 ≤ h ≤ 23, -9 ≤ k ≤ 9, -12 ≤ l ≤ 12	-12 ≤ h ≤ 12, -10 ≤ k ≤ 10, -23 ≤ l ≤ 23	-24 ≤ h ≤ 23, -0 ≤ k ≤ 9, -0 ≤ l ≤ 23	-9 ≤ h ≤ 9, -22 ≤ k ≤ 22, -22 ≤ l ≤ 22
<i>Temperature</i>	100	101	100	100
<i>Independent reflections</i>	1579	3228	10104	2448
<i>Observed reflections</i>	1506	3106	7828	2112
<i>No. of refined parameters</i>	79	127	272	147
<i>R [F > 4.0 σ(F)]</i>	0.0243	0.0161	0.059	0.0335
<i>wR [F > 4.0 σ(F)]</i>	0.0643	0.0503	0.1311	0.0786
<i>GOF</i>	0.875	1.057	1.06	1.087
<i>ρ_{max}, ρ_{min} (e Å⁻³)</i>	1.777, -1.155	0.413, -0.772	1.325, -1.441	0.671, -0.781

Table 4.13. Crystal information, data collection and refinement details for PdDPhPzTn and PdDPhPzTz.

	<i>PdDPhPzTn</i>	<i>PdDPhPzTz</i>
<i>Crystal shape</i>	Prism	Prism
<i>Colour</i>	Orange	Orange
<i>Size (mm)</i>	0.12x0.11x0.08	0.13x0.12x0.11
<i>Chemical formula</i>	C ₁₈ H ₁₅ Cl ₂ N ₃ PdS	C ₁₉ H ₁₇ Cl ₂ N ₃ PdS·C ₂ H ₃ N
<i>Formula weight</i>	482.69	537.77
<i>Crystal system</i>	Triclinic	Triclinic
<i>Space group</i>	P $\bar{1}$	P $\bar{1}$
<i>Unit cell dimensions</i>		
<i>a (Å)</i>	9.5024(6)	9.498(3)
<i>b (Å)</i>	9.7838(6)	11.092(4)
<i>c (Å)</i>	11.4434(7)	11.502(4)
<i>α (°)</i>	76.448(3)	66.569(13)
<i>β (°)</i>	71.639(3)	77.150(13)
<i>γ (°)</i>	62.954(3)	74.427(13)
<i>Cell volume (Å³)</i>	894.07(10)	1061.9(6)
<i>Z</i>	2	2
<i>D_{calc} (g cm⁻³)</i>	1.793	1.682
<i>μ (mm⁻¹)</i>	1.459	1.239
<i>F(000)</i>	480	540
<i>θ range</i>	2.479-36.316	2.245-36.316
<i>Index ranges</i>	-15≤h≤15,-16≤k≤16,-19≤l≤19	-15≤h≤15,-18≤k≤18,-19≤l≤19
<i>Temperature</i>	100	100
<i>Independent reflections</i>	8668	10285
<i>Observed reflections</i>	6943	8316
<i>No. of refined parameters</i>	226	163
<i>R [F>4.0 σ(F)]</i>	0.0349	0.034
<i>wR [F>4.0 σ(F)]</i>	0.0742	0.0797
<i>GOF</i>	1.028	0.987
<i>ρ_{max}, ρ_{min} (e Å⁻³)</i>	0.673, -1.689	0.735, -1.415

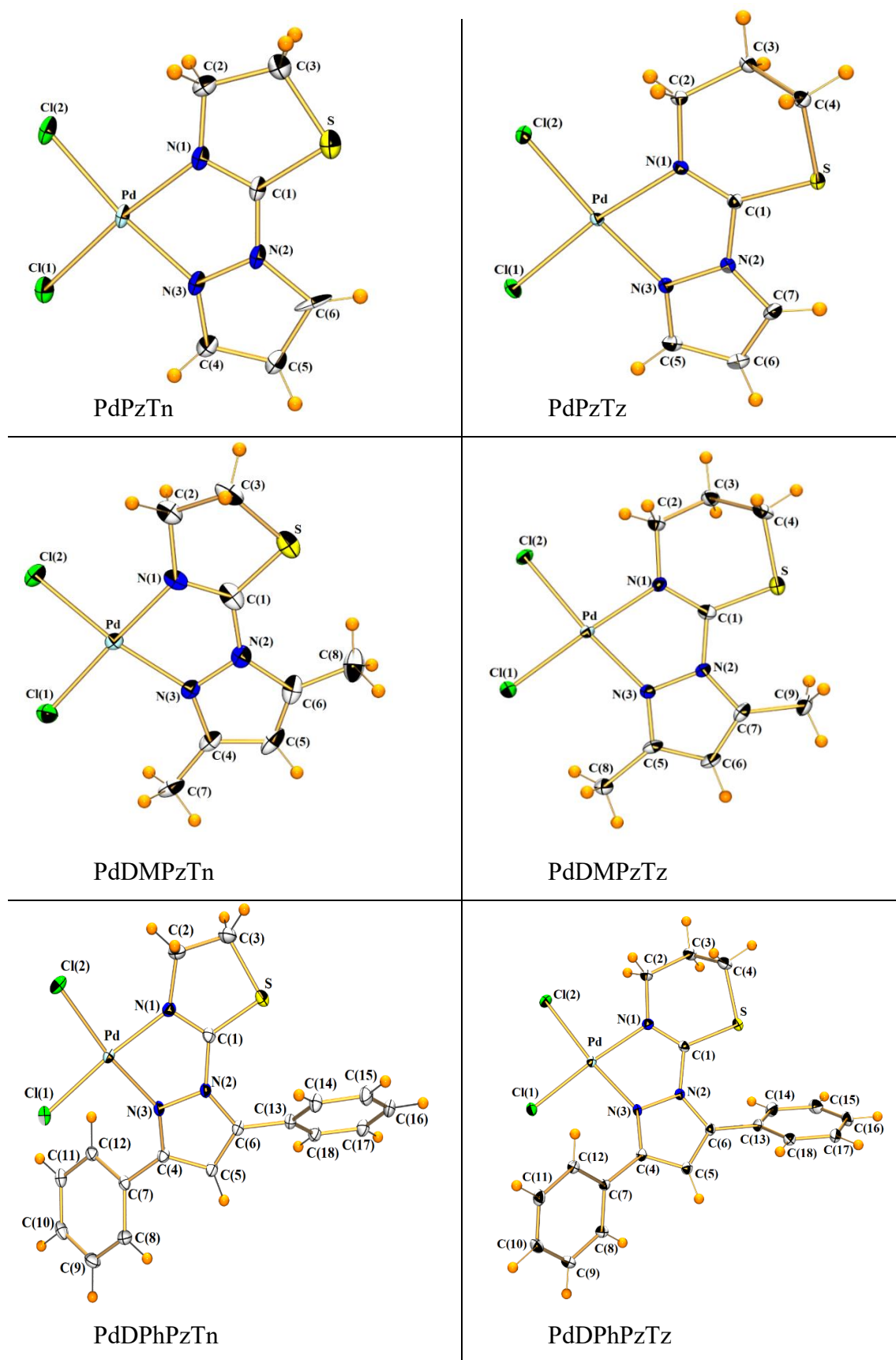


Figure 4.16. Crystal structure of PdPzTn, PdPzTz, PdDMPzTn, PdDMPzTz, PdDPhPzTn and PdDPhPzTz.

Table 4.14. Dihedral angles (°) between the planes Cl(1)-Pt-Cl(2) and N(1)-Pt-N(3) in Pd(II) complexes and torsion angles (°) for Pd(II) complexes and their respective ligands.

	Dihedral angle between Cl(1)-Pd-Cl(2) and N(1)-Pd-N(3)	Torsion angle S-C(1)-N(2)-N(3)
<i>PdPzTn</i>	0.0	-180.0
<i>PzTn</i>		-4.7(2)
<i>PdPzTz</i>	4.13	174.9(1)
<i>PzTz</i>		-17.9(2)
<i>PdDMPzTn</i>	2.61	179.3(6)
<i>DMPzTn</i>		-
<i>PdDMPzTz</i>	4.65	173.1(2)
<i>DMPzTz</i>		-
<i>PdDPhPzTn</i>	5.68	-164.8(1)
<i>DPhPzTn</i>		0.6(2)
<i>PdDPhPzTz</i>	7.69	158.7(1)
<i>DPhPzTz</i>		-50.7(2)

*DMPzTn and DMPzTz are oils, so X-ray diffraction data are not available.

Table 4.15. Selected bond distances (Å) and angles (°) for Pd(II) complexes.

	<i>PdPzTn</i>	<i>PdPzTz</i>	<i>PdDMPzTn</i>	<i>PdDMPzTz</i>	<i>PdDPhPzTn</i>	<i>PdDPhPzTz</i>
<i>Pd-Cl(1)</i>	2.278(1)	2.292(0)	2.280(2)	2.289(1)	2.283(1)	2.291(1)
<i>Pd-Cl(2)</i>	2.299(1)	2.294(0)	2.304(2)	2.285(1)	2.285(1)	2.283(1)
<i>Pd-N(1)</i>	2.008(3)	2.030(1)	1.999(7)	2.025(3)	2.005(2)	2.031(2)
<i>Pd-N(3)</i>	2.009(3)	1.996(1)	2.036(6)	2.007(3)	2.036(1)	2.026(2)
<i>Cl(1)-Pd-Cl(2)</i>	92.76(4)	92.41(1)	88.73(8)	88.21(4)	90.53 (2)	89.08(3)
<i>N(1)-Pd-Cl(1)</i>	93.43(9)	95.14(4)	93.3(2)	94.90(9)	93.45(4)	94.78(5)
<i>N(1)-Pd-Cl(2)</i>	173.82(8)	171.42(4)	177.30(19)	175.03(9)	174.03(4)	174.06(4)
<i>N(1)-Pd-N(3)</i>	79.60(2)	79.81(5)	79.2(3)	79.87(3)	78.89(6)	79.40(6)
<i>N(3)-Pd-Cl(1)</i>	172.93(9)	174.84(3)	172.3(2)	174.23(9)	171.67(4)	171.79(4)
<i>N(3)-Pd-Cl(2)</i>	94.31(9)	92.55(3)	98.8(2)	97.26(9)	97.37(4)	97.19(5)

In Table 4.15, it can be observed that the Pd-Cl bond lengths were similar in all complexes and longer than the Pd-N bond lengths. After checking the data obtained from the CSD (version v5.44, Jun 2023) [252], it can be affirmed that all the Pd-Cl distances were in the same order as the mean values for squared-planar *cis*-complexes with a Cl₂N₂ coordination environment around Pd(II) [2.295(19) Å for 973 Pd(II) complexes]. Same asseveration can be done for Pd-N_{pyrazole} bond distances, which were similar to the mean value calculated for squared-planar complexes with Pd(II) in a Cl₂N₂ coordination environment [2.031(19) Å for 109 Pd(II) complexes] in CSD [252]. As for the Pd-N_{thiazoline} bond distances, they were slightly shorter than the average values calculated for this type of bonds in CSD [252]: 2.037(59) Å for 14 Pd(II) complexes; unlike Pd-N_{thiazine} bond distances, which were slightly larger than the only complex found in CSD: 2.016 Å [175].

With respect to the arrangement of the organic ligands in the Pd(II) complexes, it can be observed that the thiazoline and thiazine rings were rotated around the C(1)-N(2) bond so that the N(1) and N(3) atoms simultaneously coordinated to the Pd(II) ion. This can be confirmed by the data corresponding to the torsion angles of the complexes and the free ligands showed in Table 4.14. Moreover, the crystal structures were stabilized by the parallel displaced aromatic interactions between phenyl rings in both PdDPhPzTn and PdDPhPzTz complexes and between pyrazole rings in PdPzTz. On the other hand, π - π stacking interactions were produced in both PdDMPzTn and PdDMPzTz complexes. A representation of these interactions can be found in Figure 4.17 and the specific values in Table 4.16.

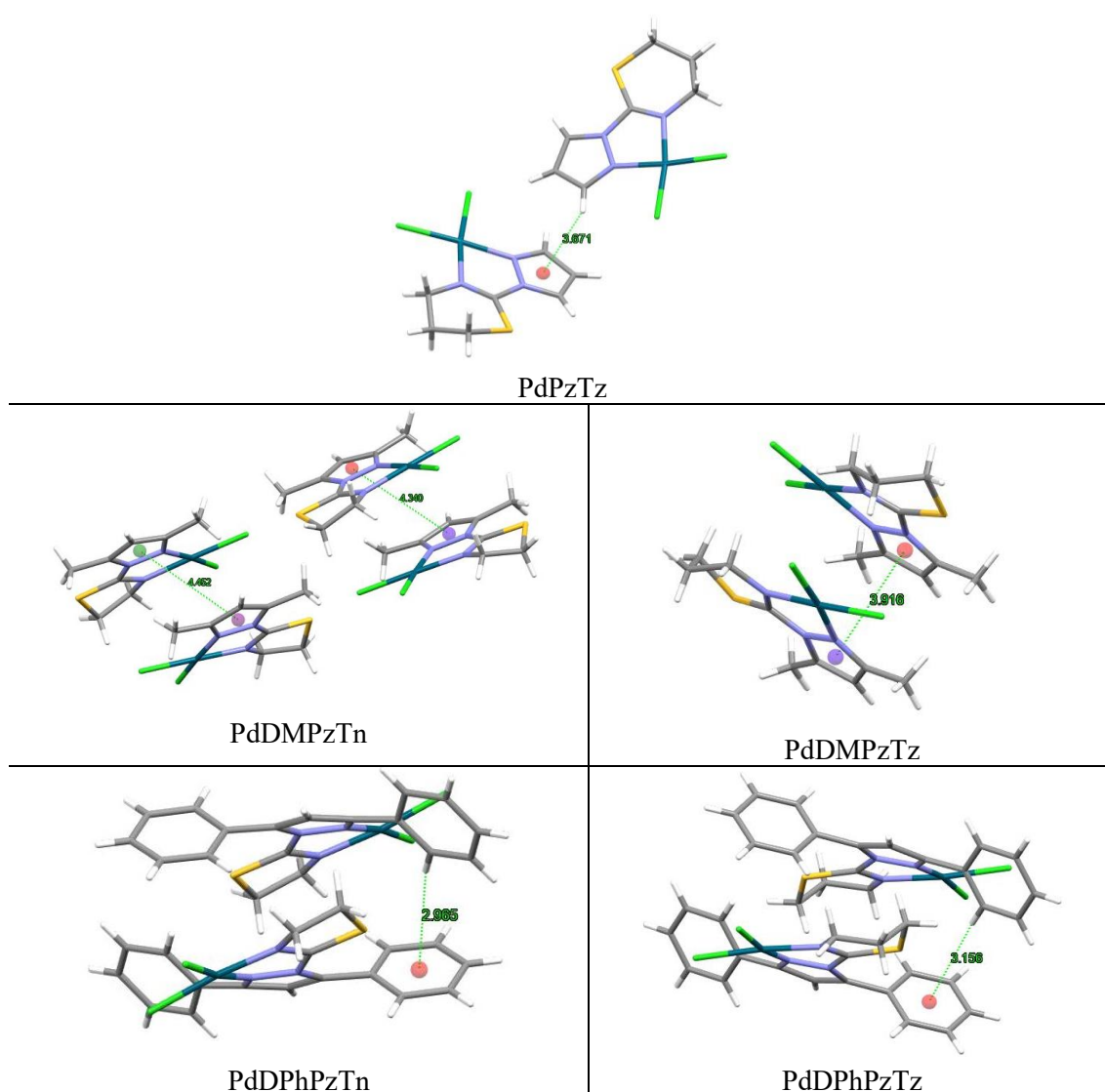


Figure 4.17. Aromatic interactions in PdPzTz, PdDMPzTn, PdDMPzTz, PdDPhPzTn and PdDPhPzTz.

Table 4.16. Aromatic interactions in PdPzTz, PdDMPzTn, PdDMPzTz, PdDPhPzTn and PdDPhPzTz.

	<i>Type of interaction</i>	<i>ANG</i>	<i>DC</i>	<i>DZ</i>	<i>DS</i>	<i>ANGS</i>
<i>PdPzTz</i>	C··H (pyrazole rings)	0	4.887	4.454	4.446	113.10
<i>PdDMPzTn</i>	π - π stacking (pyrazole rings)	1.54	4.340	3.371	4.391	74.67
		1.54	4.452	3.432	4.628	71.87
<i>PdDMPzTz</i>	π - π stacking (pyrazole rings)	1.28	3.916	3.494	3.813	76.80
<i>PdDPhPzTn</i>	T type (phenyl rings)	75.72	4.956	4.908	2.965	137.86
<i>PdDPhPzTz</i>	T type (phenyl rings)	88.08	5.327	5.182	3.156	150.96

4.2.1.c. Infrared spectroscopy

A comparison of the most relevant signals corresponding to the pyrazole, thiazine and thiazoline ring vibrations of the free ligands [176,179,184] and the complexes can be found in Table 4.17 and Table 4.18. Additionally, the IR spectra in 4000-400 cm⁻¹ region of PdPzTn, PdPzTz, PdDMPzTn, PdDMPzTz, PdDPhPzTn and PdDPhPzTz can be observed in Figure 4.18-Figure 4.23.

Table 4.17. IR spectral assignments (cm⁻¹) for PzTn, PdPzTn, DMPzTn, PdDMPzTn, DPhPzTn and PdDPhPzTn.

	<i>PzTn</i>	<i>PdPzTn</i>	<i>DMPzTn</i>	<i>PdDMPzTn</i>	<i>DPhPzTn</i>	<i>PdDPhPzTn</i>
$W_1[\nu(C=N)]$	1641	1608	1635	1601	1639	1587
<i>Pyrazole ring vibrations</i>	1514	1532	1574	1571	1560	1556
	1382	1413	1410	1413	1408	1411
	1350	1371	1387	1397	1319	1314
				1378		
	991	1001	970	973	1000	996

Table 4.18. IR spectral assignments (cm⁻¹) for PzTz, PdPzTz, DMPzTz, PdDMPzTz, DPhPzTz and PdDPhPzTz.

	<i>PzTz</i>	<i>PdPzTz</i>	<i>DMPzTz</i>	<i>PdDMPzTz</i>	<i>DPhPzTz</i>	<i>PdDPhPzTz</i>
$\Psi_1[\nu(C=N)]$	1635	1596	1639	1592	1639	1606
<i>Pyrazole ring vibrations</i>	1510	1524	1566	1564	1548	1556
	1419	1441	1411	1404	1406	1404
	1386	1413	1375	1382		
	1327	1358	1315	1341	1303	1313
	995	1003	981	991	998	1000

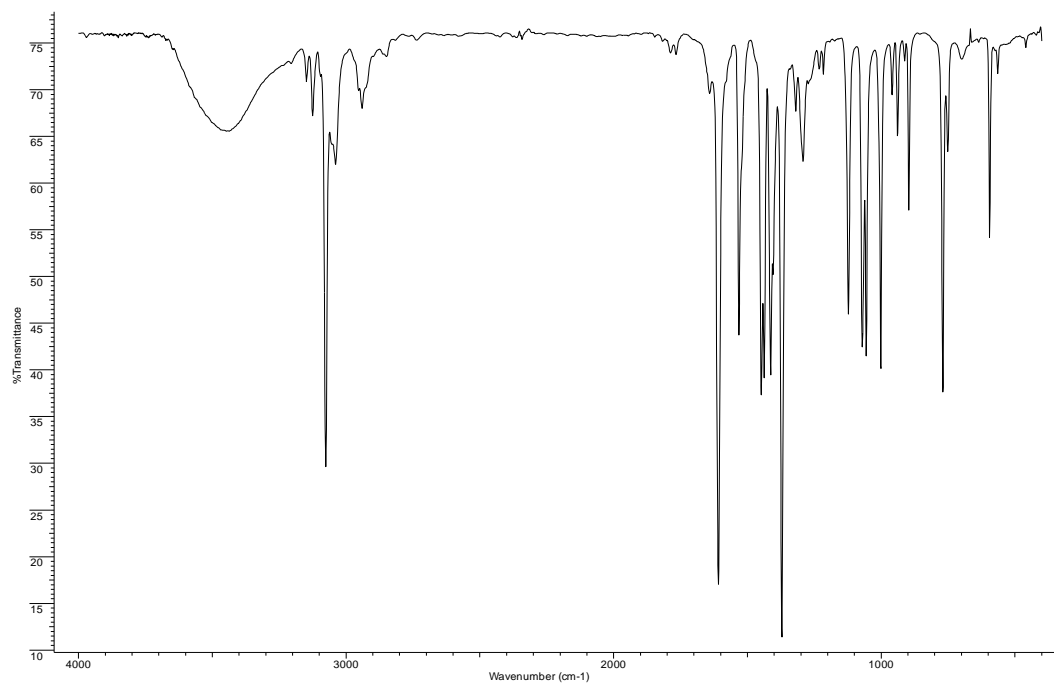


Figure 4.18. IR spectrum of PdCl₂(PzTn) in 4000-400 cm⁻¹ region.

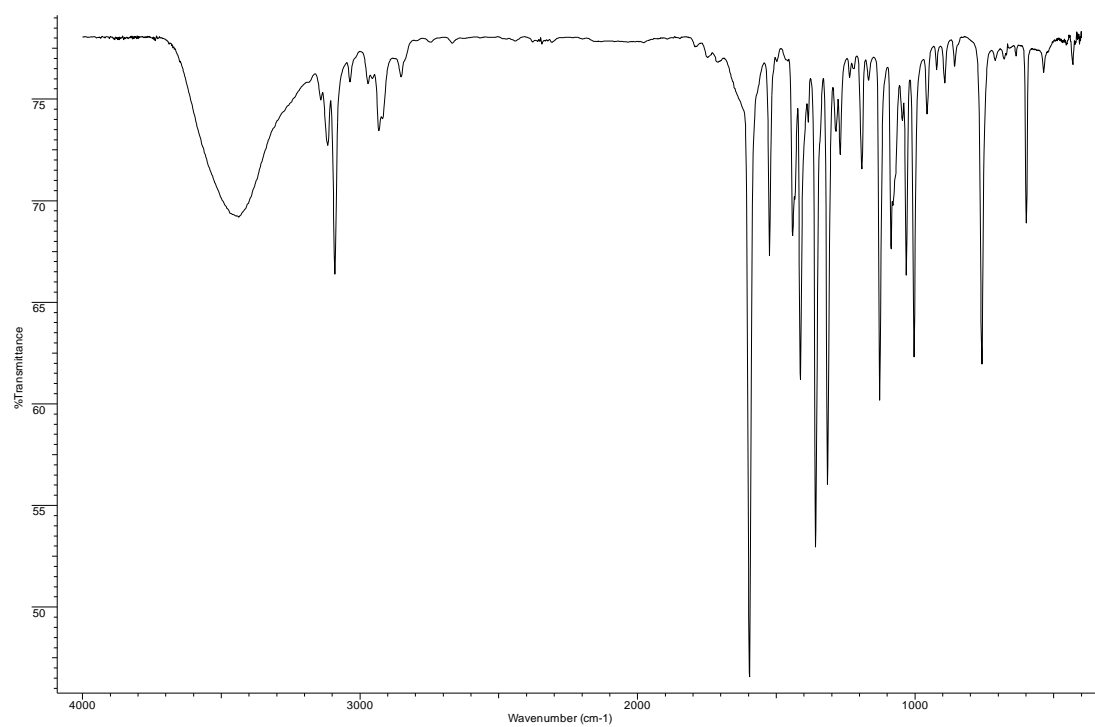


Figure 4.19. IR spectrum of PdCl₂(PzTz) in 4000-400 cm⁻¹ region.

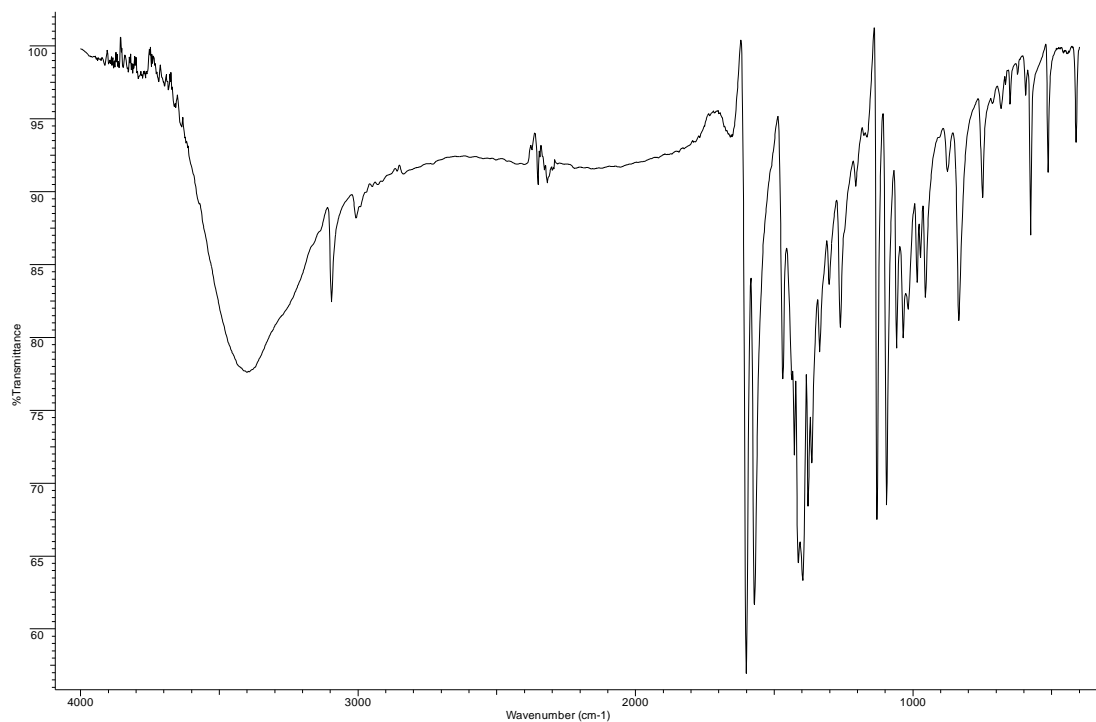


Figure 4.20. IR spectrum of PdCl₂(DMPzTn) in 4000-400 cm⁻¹ region.

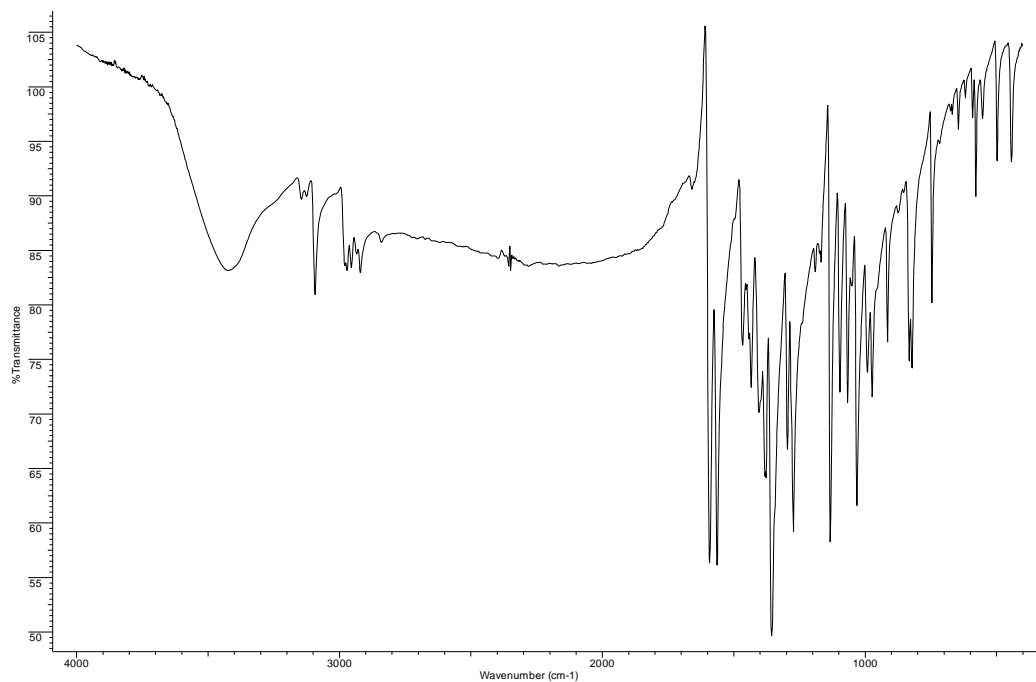


Figure 4.21. IR spectrum of PdCl₂(DMPzTz) in 4000-400 cm⁻¹ region.

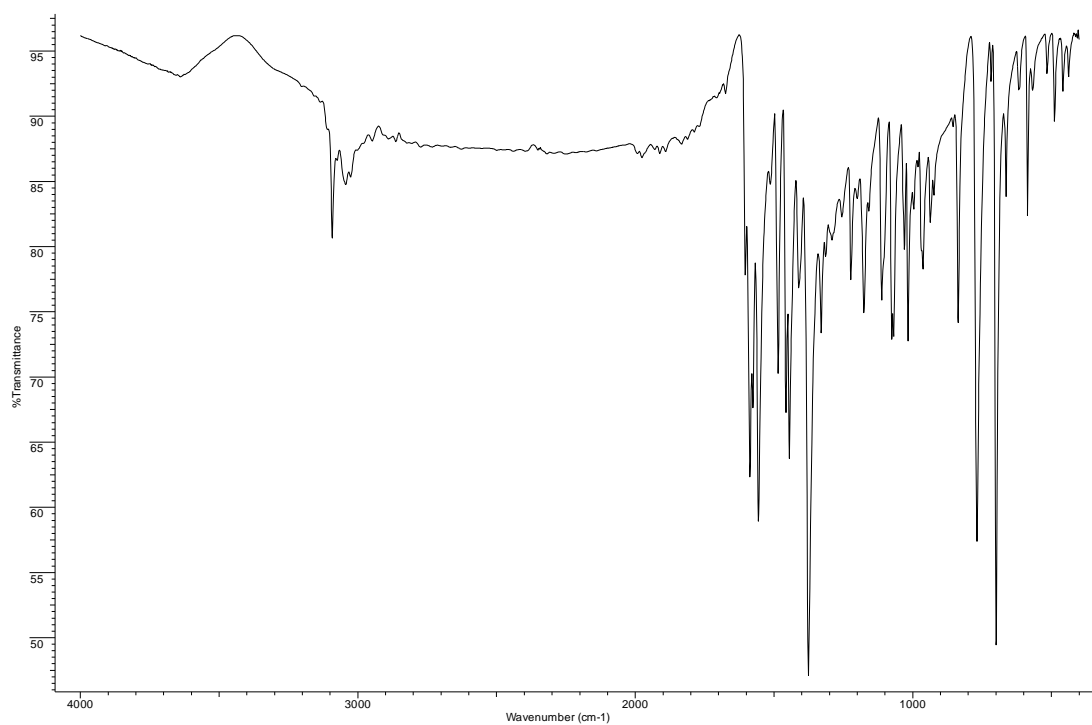


Figure 4.22. IR spectrum of PdCl₂(DPhPzTn) in 4000-400 cm⁻¹ region.

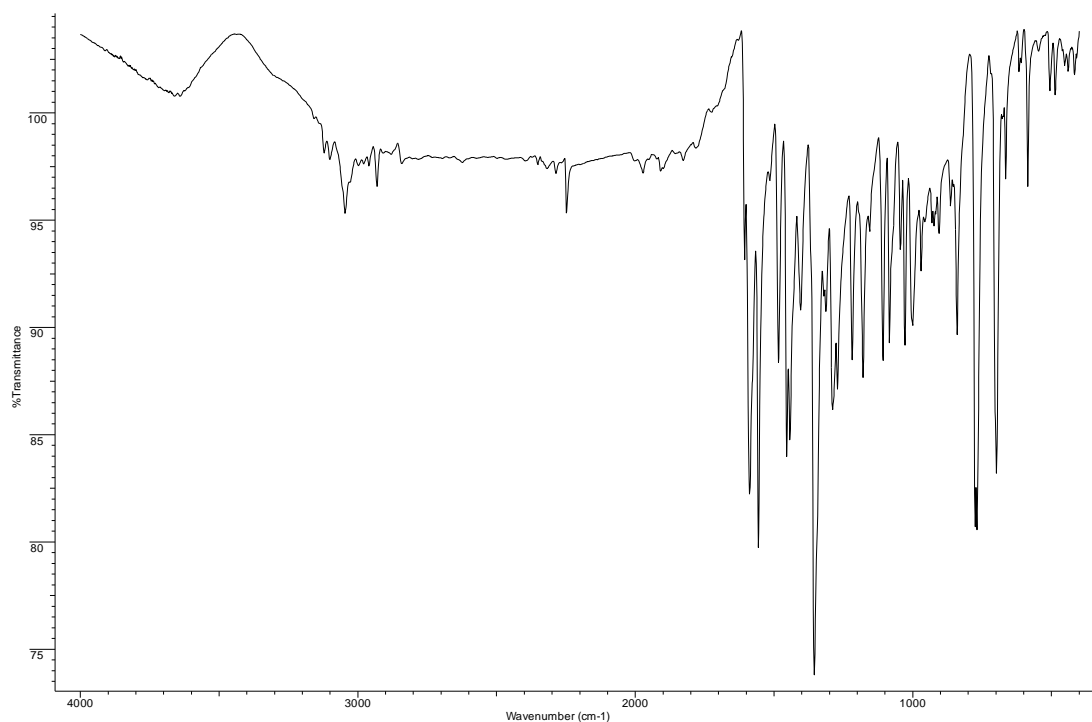


Figure 4.23. IR spectrum of PdCl₂(DPhPzTz) in 4000-400 cm⁻¹ region.

The IR spectra of Pd(II) complexes showed that the bands attributable to $\nu_1[\nu(\text{C}=\text{N})]$ vibration in thiazoline and $\Psi_1[\nu(\text{C}=\text{N})]$ vibration in thiazine suffered a shift to lower wavenumber in the complexes with respect to their respective ligands, as it was

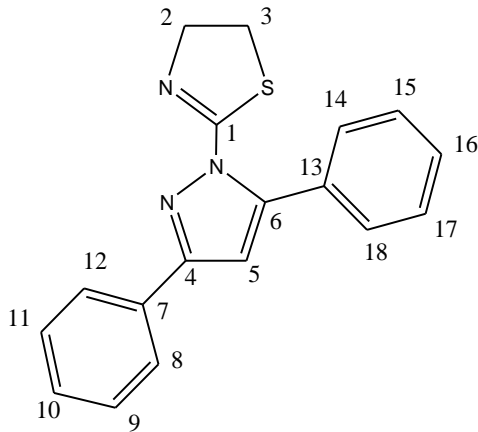
seen for Pt(II) complexes. It has been described that the reason for this displacement could be related to the presence of the C–N bond as part of a chelate ring where the back-coordination from the metal to the ligand compensates for the loss of electron density on the nitrogen atom. In addition, the bands assigned to pyrazole ring vibrations were shifted to higher wavenumber for PdPzTn and PdPzTz, not showing such well-defined patterns for the other four complexes, which can be explained by the presence of the substituents. Therefore, the palladium coordination to both heterocycles through the nitrogen atoms was confirmed for these frequency shifts in the IR spectra [179,184].

4.2.1.d. ¹H Nuclear magnetic resonance spectroscopy

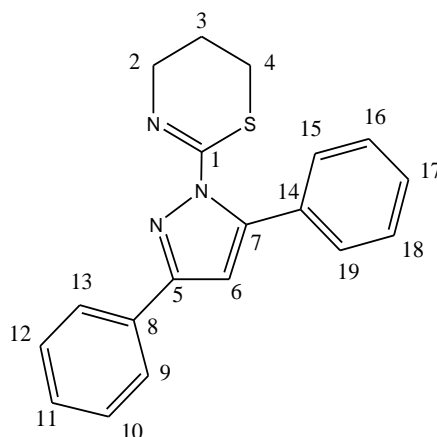
The ¹H NMR spectral data of Pd(II) complexes in DMF-d₇, except for DMPzTn and PdDMPzTn which were done in DMSO-d₆, can be seen in Figures 4.24-4.28. The position and assignation of the signals can be found in Table 4.19 and Table 4.20 for both the complexes and the ligands in order to clearly identify the displacements between them, which confirmed the coordination of the metal ion to the ligand.

As it was indicated previously, the data for PdDMPzTz could not be obtained due to their low solubility.

Table 4.19. ¹H NMR spectral data for PzTn, PdPzTn, DPhPzTn and PdDPhPzTn complexes in DMF-d₇ solvent and for DMPzTn and PdDMPzTn in DMSO-d₆.

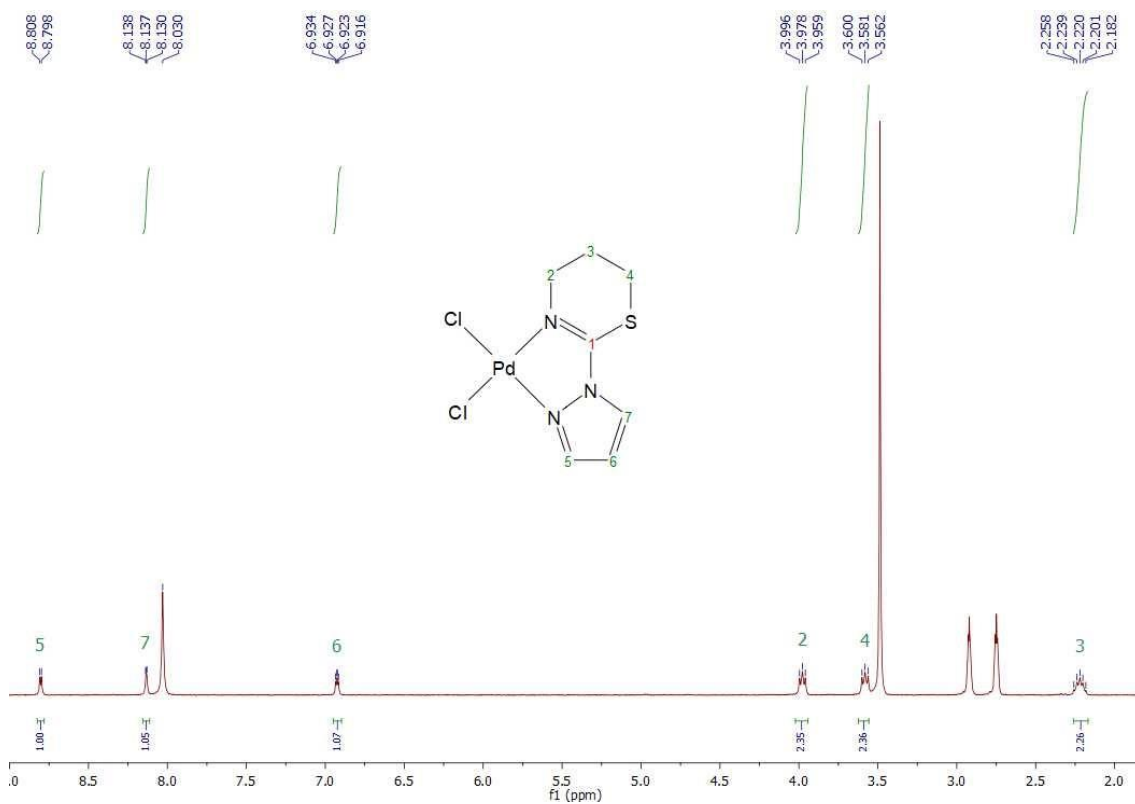
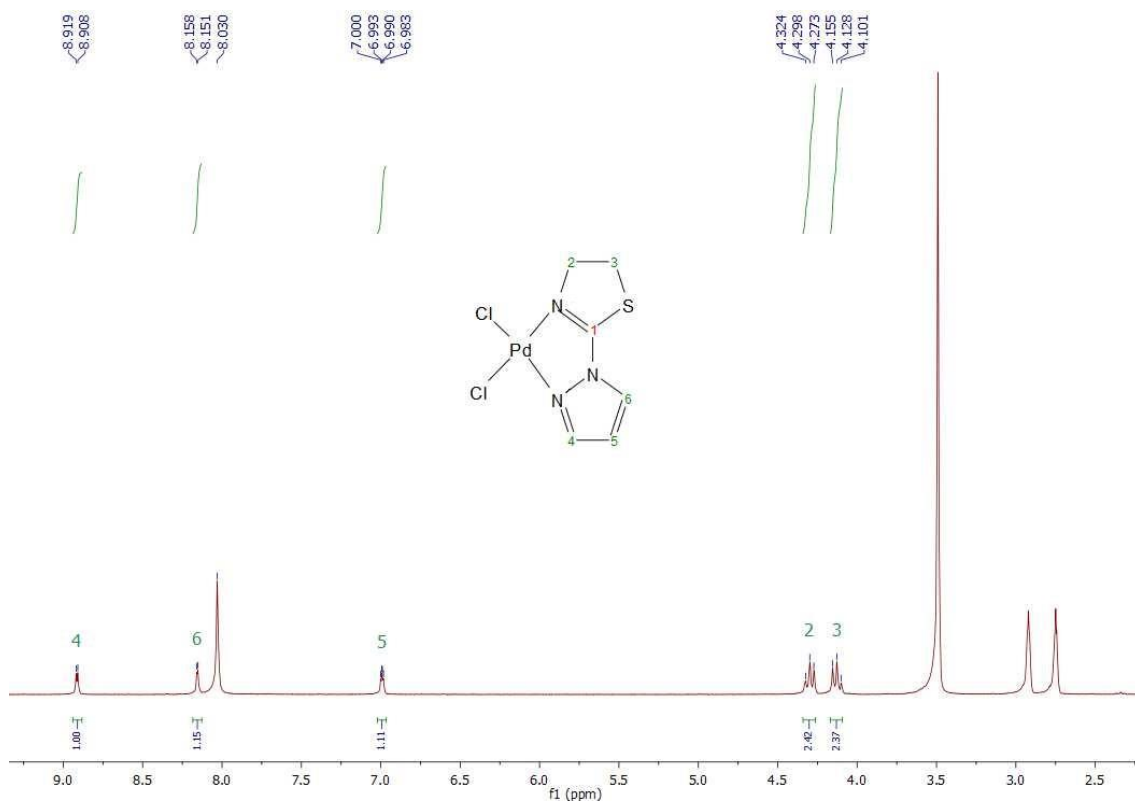


	<i>N</i> -CH ₂	<i>S</i> -CH ₂	<i>H</i> (4)	<i>H</i> (5)	<i>H</i> (6)	CH ₃	<i>H</i> (8-18)
<i>PzTn</i>	4.34	3.58	8.40	6.60	7.81	-	-
<i>PdPzTn</i>	4.30	4.13	8.91	6.99	8.15	-	-
<i>DMPzTn</i>	4.27	3.35	-	6.12	-	2.13 ; 2.46	-
<i>PdDMPzTn</i>	4.22	3.98	-	6.60	-	2.63 , 2.65	-
<i>DPhPzTn</i>	4.19	3.51	-	7.20	-	-	7.46-8.08
<i>PdDPhPzTn</i>	4.22	3.78	-	7.12	-	-	7.47-7.84

Table 4.20. ^1H NMR spectral data for PzTz, PdPzTz, DPhPzTz and PdDPhPzTz complexes in DMF- d_7 .

	<i>N-CH₂</i>	<i>H₂(3)</i>	<i>S-CH₂</i>	<i>H(5)</i>	<i>H(6)</i>	<i>H(7)</i>	<i>H(9-19)</i>
<i>PzTz</i>	3.83	1.92	3.21	8.33	6.50	7.69	-
<i>PdPzTz</i>	3.98	2.22	3.58	8.81	6.92	8.14	-
<i>DPhPzTz</i>	3.65	1.91	3.31	-	7.16	-	7.47-8.01
<i>PdDPhPzTz</i>	4.02	2.09	3.28	-	7.07	-	7.47-7.86

The results presented in Tables 4.19 and Table 4.20 indicated that ^1H NMR signals of thiazine and thiazoline of all complexes were in general shifted to higher frequencies respect to their free ligands. This also occurred for pyrazole ring signals of PdPzTn, PdPzTz and PdDMPzTn, while the signals of complexes with phenyl substituents were slightly shifted to lower frequencies probably due to the presence of aromatic groups, which helps with the redistribution of electronic density loss [253,254]. Therefore, it can be concluded that the ligands were coordinated to palladium in DMF solution for PdPzTn, PdPzTz, PdDPhPzTn and PdDPhPzTz and in DMSO solution for PdDMPzTn. To confirm the stability of the complexes in solution, they were kept in DMF or DMSO for 21 days. After that time, the ^1H NMR was measured again (data not included), remaining intact, thus showing the high stability of the complexes in solution conditions.



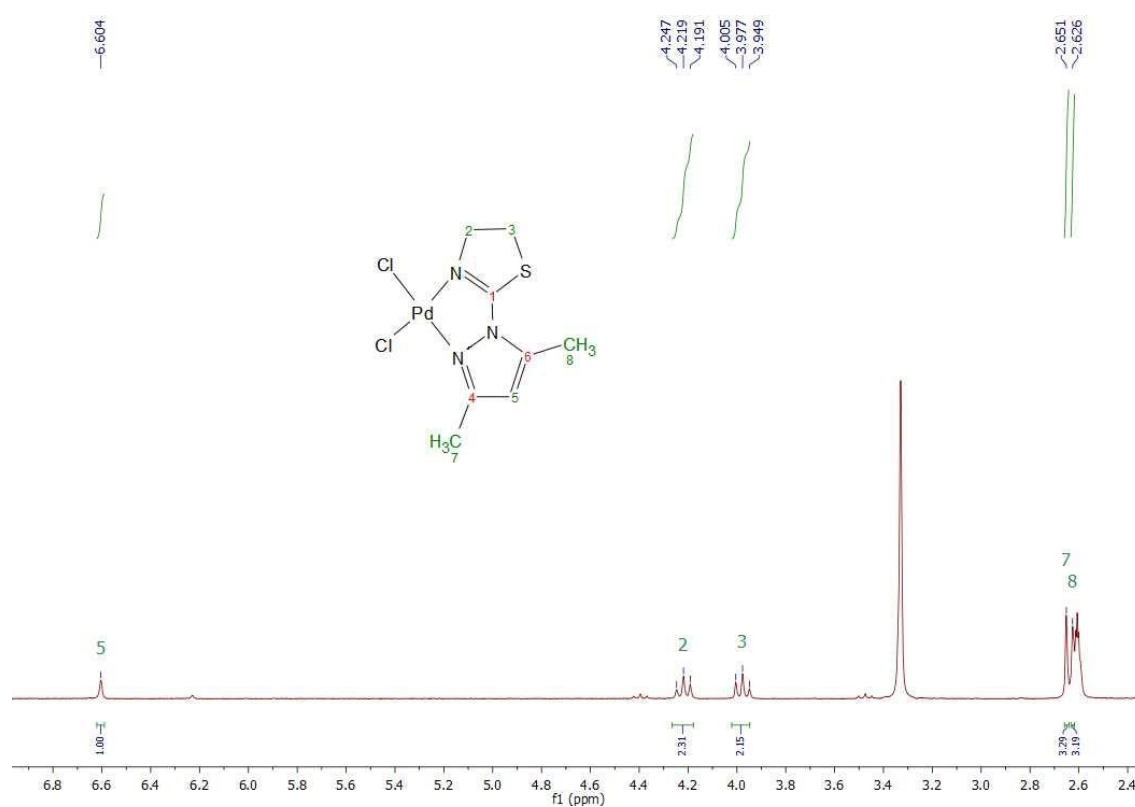


Figure 4.26. ^1H NMR spectrum of $\text{PdCl}_2(\text{DMPzTn})$ in DMSO-d_6 .

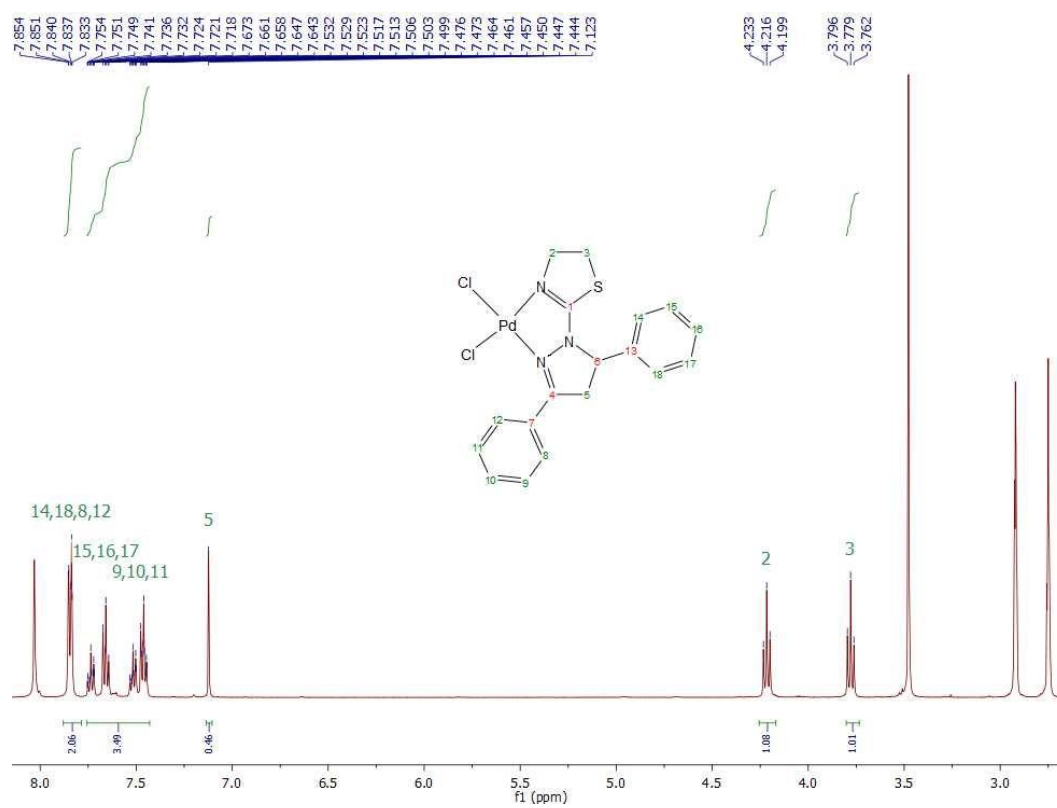


Figure 4.27. ^1H NMR spectrum of $\text{PdCl}_2(\text{DPhPzTn})$ in DMF-d_7 .

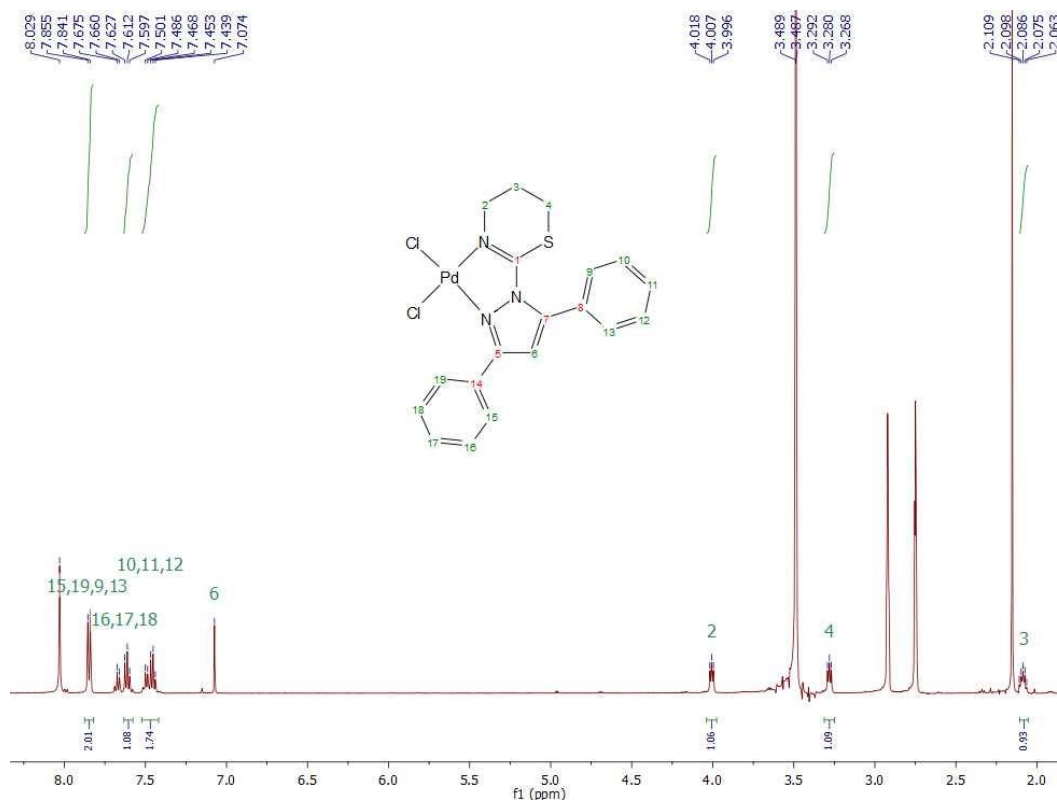


Figure 4.28. ¹H NMR spectrum of PdCl₂(DPhPzTz) in DMF-d₇.

4.2.2. Biological testing from Pd(II)/Ligand system

4.2.2.a. Cell viability

In this section, the viability results of the Pd(II) complexes can be found. In order to verify the cytotoxicity of the compounds, Pd(II) complexes were tested at concentrations from 1 to 100 μ M on HL-60, U-937 and HeLa tumor cell lines for 24 h. As can be observed in Figure 4.29 and Table 4.21, data obtained showed that PdPzTn, PdPzTz, PdDPhPzTn and PdDPhPzTz had a moderate cytotoxic effect towards all the three cell lines studied. On the contrary, PdDMPzTn and PdDMPzTz, did not show cytotoxic effects until high concentrations (IC₅₀ values >100 μ M). Moreover, complexes with the presence of ligands with phenyl groups (PdDPhPzTn, PdDPhPzTz) showed lower IC₅₀ values than the analogs without extra substituents, improving the cytotoxicity of the compounds. The IC₅₀ values found for these two complexes were between $46.39 \pm 3.99 \mu$ M and $62.74 \pm 6.45 \mu$ M in the three cell lines, not existing strong differences between the complexes or the cell lines.

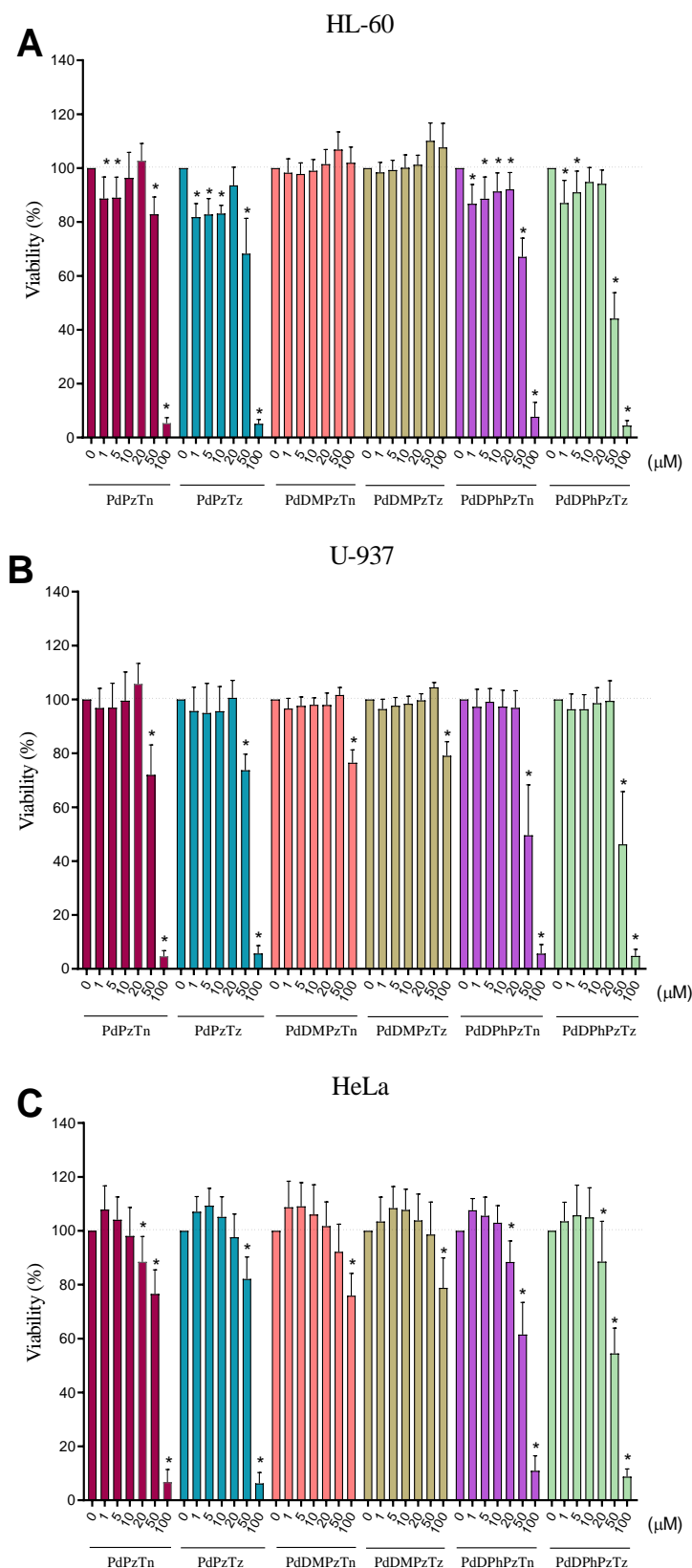


Figure 4.29. Cytotoxic effect of Pd(II) complexes. HL-60 (A), U-937 (B) and HeLa (C) cell lines were challenged with 1, 5, 10, 20, 50 and 100 μM of the six Pd(II) complexes, namely PdPzTn, PdPzTn, PdDMPzTn, PdDMPzTz, PdDPhPzTn and PdDPhPzTz, or the vehicle (DMF or DMSO) for 24 h. Values are presented as means ± SD (n = 6) and depicted as percentage over untreated samples. * $P < 0.05$ vs. control (0.5% DMF or DMSO) (Dunnett's test).

Table 4.21. Cytotoxic effect of PdPzTn, PdPzTz, PdDMPzTn, PdDMPzTz, PdDPhPzTn and PdDPhPzTz towards selected tumor cell lines.

	<i>HeLa</i>	<i>HL-60</i>	<i>U-937</i>
<i>PdPzTn</i>	67.55 ± 7.27 ^a	71.81 ± 9.09 ^a	70.95 ± 8.73 ^a
<i>PdPzTz</i>	77.75 ± 9.68 ^a	54.50 ± 6.68 ^a	70.21 ± 7.67 ^a
<i>PdDMPzTn</i>	> 150 ^b	> 150 ^b	> 150 ^b
<i>PdDMPzTz</i>	> 150 ^c	> 150 ^b	> 150 ^c
<i>PdDPhPzTn</i>	62.74 ± 6.45 ^a	58.83 ± 4.94 ^a	53.43 ± 4.91 ^a
<i>PdDPhPzTz</i>	57.83 ± 6.45 ^a	46.39 ± 3.99 ^a	50.35 ± 4.82 ^a

For a given cell line, a different lowercase letter indicates statistically significant ($P < 0.05$) changes (Tukey's test). Data are presented as $IC_{50} \pm SD$ (μM).

As reported in previous publications, other palladium(II) complexes have been also studied on tumor cell lines, but in general with longer incubation times (48-72 h) [255–259]. To properly compare our findings with the literature, and due to the lower cytotoxic effects showed in comparison with Pt(II) complexes (see 4.1.2.a Cell viability), the cytotoxicity assay was also performed at 48 and 72 h in HeLa cells. The results obtained showed a reduction of the IC_{50} values of the complexes PdPzTn, PdPzTz, PdDPhPzTn and PdDPhPzTz, unlike PdDMPzTn and PdDMPzTz, which did not improve their effect along time (Table 4.22). The decrease in the IC_{50} values was around 10 μM for PdPzTn and PdPzTz after 48 h of treatment, and between 25-30 μM at 72 h. These results were even better for both complexes with phenyl groups, whose IC_{50} values decreased more than 25 μM at 48 h and between 30-40 μM at 72 h. Therefore, the best results obtained were those of PdDPhPzTn and PdDPhPzTz after 72 h of treatment, with IC_{50} values of $23.28 \pm 2.44 \mu M$ and $27.98 \pm 3.33 \mu M$, respectively. It could be concluded that, in general, longer incubation times improved the cytotoxic effect of most of our Pd(II) complexes.

Table 4.22. Cytotoxicity ($IC_{50} \pm SD$, μM) of the different Pd(II) complexes in HeLa cells treated for 48 and 72h.

	<i>48 h</i>	<i>72 h</i>
<i>PdPzTn</i>	58.22 ± 9.66 ^a	44.17 ± 6.33 ^a
<i>PdPzTz</i>	66.01 ± 11.43 ^a	46.59 ± 6.55 ^a
<i>PdDMPzTn</i>	>150 ^b	>150 ^b
<i>PdDMPzTz</i>	>150 ^c	>150 ^c
<i>PdDPhPzTn</i>	34.85 ± 4.00 ^a	23.28 ± 2.44 ^a
<i>PdDPhPzTz</i>	32.09 ± 4.23 ^a	27.98 ± 3.33 ^a

Within each column, values followed by a diverse lowercase letter are significantly different ($P < 0.05$; Tukey's test).

4.2.2.b. Cellular uptake

In order to verify the Pd(II) accumulation into HeLa cells, ICP-MS measurements were done. For that, the complexes with the best cytotoxic effects were selected. Thus, the tumor cells were incubated with the IC_{50} of PdPzTn, PdPzTz, PdDPhPzTn and PdDPhPzTz during 4 h. As it can be seen in Figure 4.30, accumulation of the metal ion was produced after incubation with the four compounds. However, PdDPhPzTn and PdDPhPzTz showed a more efficient accumulation into cells than their analogs, although any significant difference was found. Even so, the higher accumulation and lower IC_{50} values of the two complexes with phenyl rings might indicate that the presence of aromatic groups in the ligands improved their cellular uptake. This could be related with a presumable higher lipophilicity for PdDPhPzTn and PdDPhPzTz since they showed the same trend as that found for platinum(II) complexes with the same ligands (see 4.1.2.a *Cell viability*).

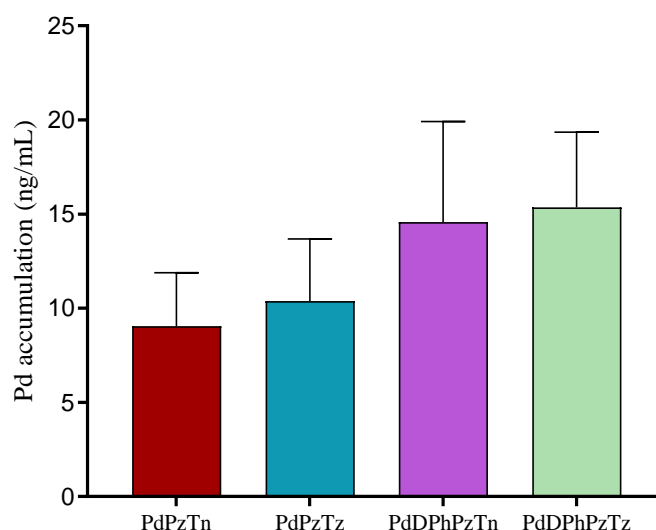


Figure 4.30. Palladium accumulation in HeLa cells. Cells were treated with 67.55 μ M of PdPzTn, 77.75 μ M of PdPzTz, 62.74 μ M of PdDPhPzTn or 57.83 μ M of PdDPhPzTz for 4 h, and then samples were digested with 65% HNO_3 and subsequently analyzed by ICP-MS. Pd concentrations were given in ng/mL. Values represent means \pm SD of 4 independent experiments.

4.2.2.c. Apoptosis determination

Finally, based on the higher accumulation of Pd(II) checked in the previous section and in order to verify whether the reduction in cell viability showed by PdDPhPzTn and PdDPhPzTz was mediated by apoptosis, flow cytometry experiments using annexin V-FITC and PI were carried out. The treatment of HeLa cells with IC_{50} of the complexes

with phenyl rings during 24 h produced significant changes in the percentage of cell populations, particularly in the case of live cells (decrease) and late apoptotic and secondary necrotic cells (increase) for both complexes, in comparison with vehicle-treated and control cells (Figure 4.31). These results suggested that the major type of cell death prompted by PdDPhPzTn and PdDPhPzTz was apoptosis.

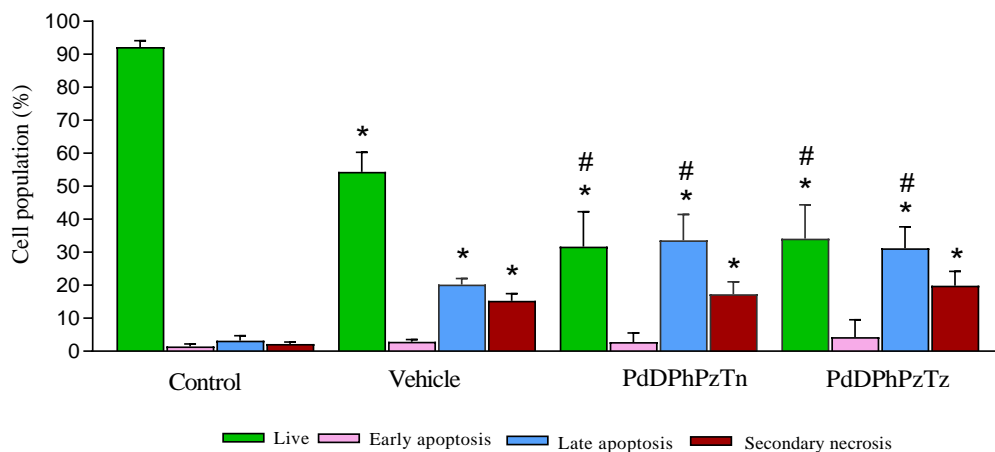


Figure 4.31. Flow cytometry results including live cells, early and late apoptosis, and secondary necrosis caused by palladium complexes on HeLa cells. IC₅₀ of PdDPhPzTn (57.83 μ M), PdDPhPzTz (62.74 μ M), 1.5% DMF (vehicle) or 0.5% DMF (control) were tested on HeLa cells for 24 h. Histograms show percentages of cell population detected by flow cytometry. Values are presented as means \pm SD of four independent experiments. * $P < 0.05$ compared to its corresponding control value. # $P < 0.05$ compared to its corresponding vehicle value (Tukey's test).

4.3. SYNTHESIS AND ENCAPSULATION OF COMPLEXES IN MESOPOROUS SILICA NANOPARTICLES

As it was previously described in section 3. *Materials and methods*, MSNs have been synthesized, functionalized, and characterized to use them as nanocarriers. Once this was done, six complexes were encapsulated in the MSNs. In this section, the results obtained from the characterization techniques used and the biological testing performed are included.

4.3.1. Characterization of mesoporous silica nanoparticles

Firstly, MSN-NH₂ and MSN-COOH particles were characterized via gas adsorption, TEM and Z-potential, whose results are included in the next subsections.

4.3.1.a. Physisorption measurements

Gas adsorption employing BET and DFT methods were used to obtain specific surface area, pore size distribution and pore volume of adsorbents of the amino- and carboxy-functionalized MSNs. During this process, controlled increments of the adsorptive (nitrogen) are applied to the solid from low to high relative pressures. After each increment, the volume of adsorbed gas is measured till reaching the saturation pressure, which is equivalent to the pressure of the atmosphere ($p/p_0 = 1$). An isotherm, which shows the volume uptake versus the relative pressure, is obtained (Figure 4.32). The low-pressure region relates to monolayer adsorption, and it is used to define the surface area by the BET method, while the high-pressure region corresponds to multilayer adsorption. The isotherm also allows for the calculation of pore volume and pore size via simulation with a DFT kernel (Figure 4.32 and Table 4.23).

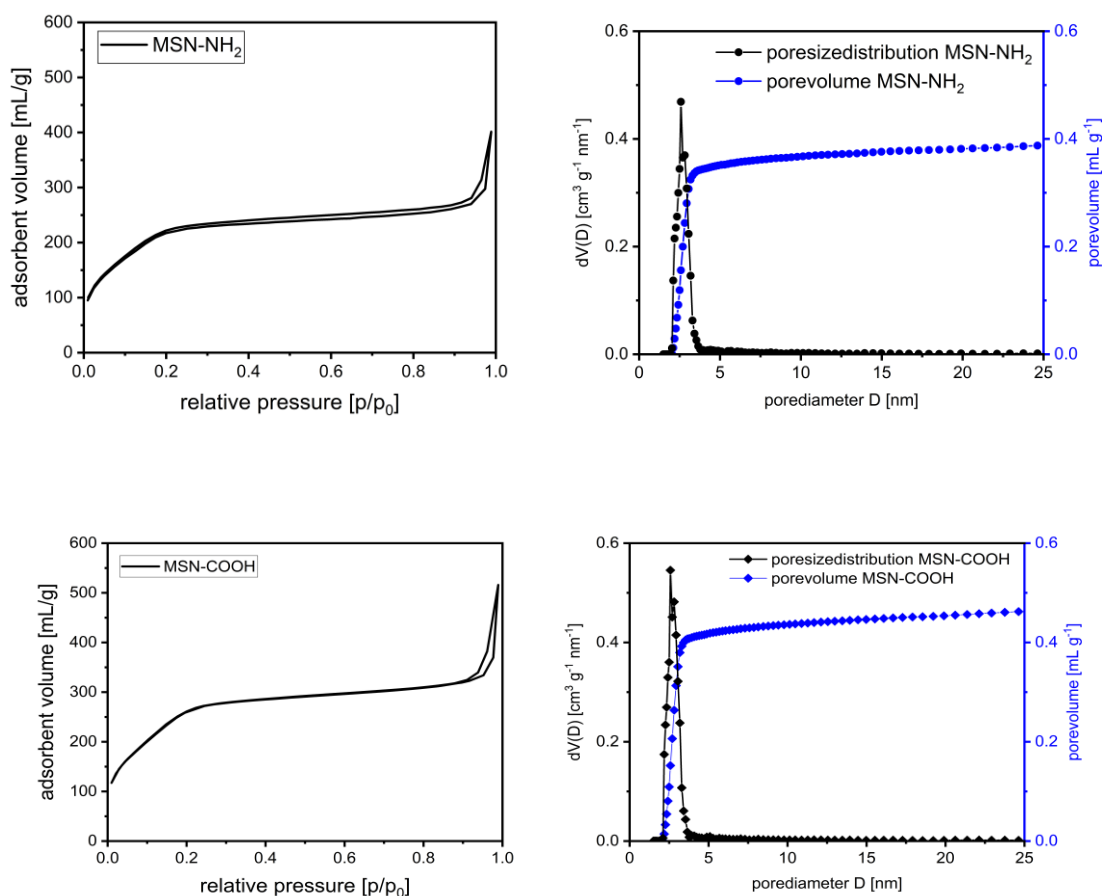


Figure 4.32. Nitrogen sorption isotherms of MSN-NH₂ and MSN-COOH (left), and the corresponding DFT-calculated pore-size distribution (right).

The isotherms obtained were clearly type IV isotherms (Figure 4.32). This type of isotherm appears when capillary condensation occurs. Gases condense in the tiny capillary pores of the solid at pressures below the saturation pressure of the gas. The different parameters obtained with BET method and DFT calculation are included in Table 4.23.

Table 4.23. N₂ adsorption/desorption parameters of MSN, MSN-COOH and MSN-NH₂.

	<i>BET surface area (m²/g)</i>	<i>Pore volume (cm³/g)</i>	<i>Mean pore diameter (nm)</i>
<i>MSN</i>	1288	0.696	3.2
<i>MSN-COOH</i>	1004	0.464	2.6
<i>MSN-NH₂</i>	848	0.394	2.6

As can be observed, when comparing pure MSN with the functionalized ones a reduction of the surface area and a loss of pore volume were produced, being sharper for amino than for carboxy functionalized particles. On the other hand, a reduction on pore diameter was also seen, being identical for both MSN-NH₂ and MSN-COOH.

4.3.1.b. Transmission Electron Microscopy

As for the morphology, it could be observed that both MSN-NH₂ and MSN-COOH particles were monodisperse and spherical, and that the mesopores of the particles could be clearly identified (Figure 4.33). Respect to the size distribution of particles, the Software ZEISS ZEN was used, being concluded that the size distribution was quite homogeneous, with an average diameter of 168 ± 24 nm (14% standard-deviation) and 138 ± 25 nm (18% standard-deviation) for MSN-NH₂ and MSN-COOH, respectively.

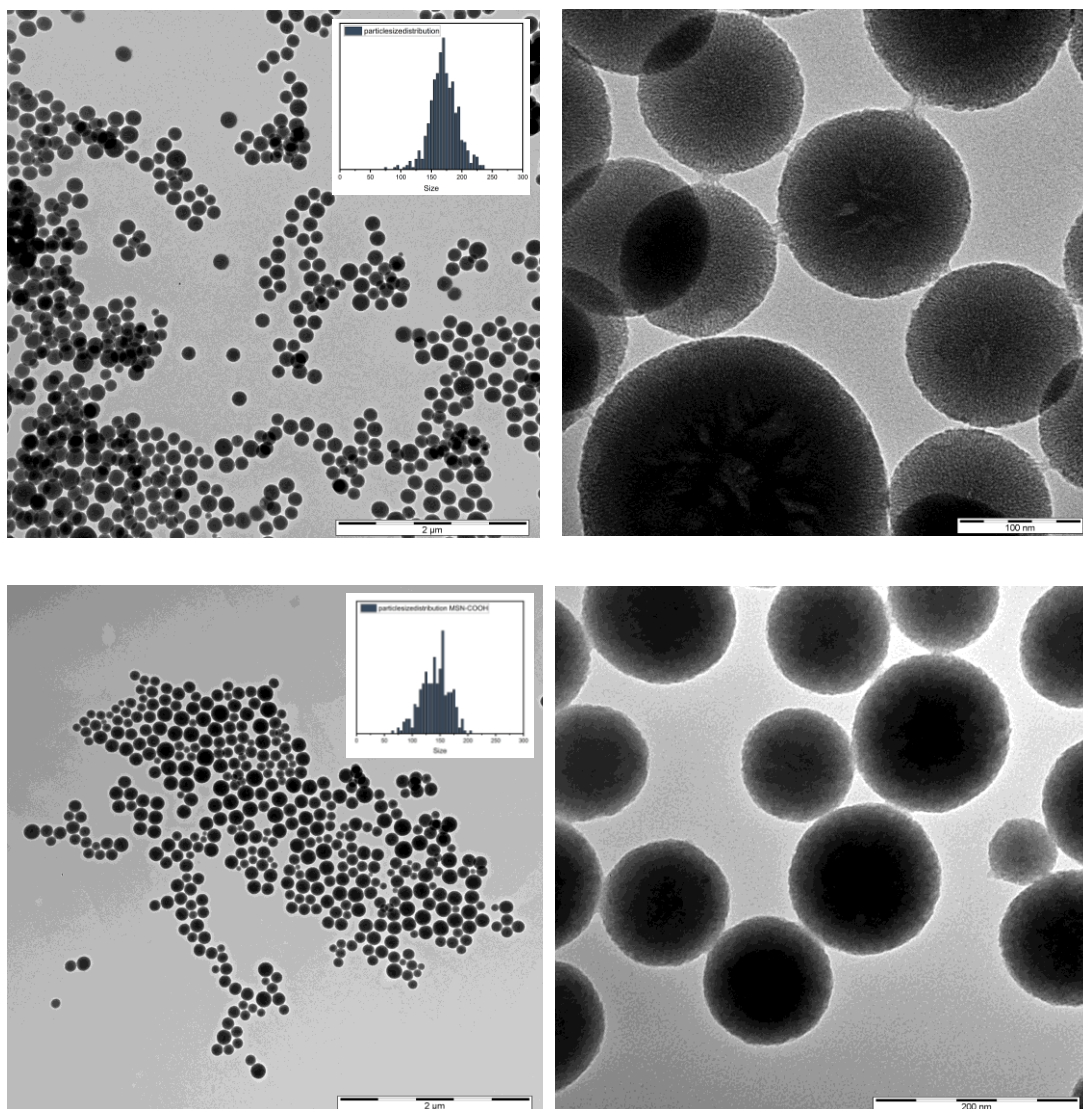


Figure 4.33. TEM-images of the MSN-NH₂ with a 25k and a 250k resolution (top left and top right, respectively) and MSN-COOH with a 25k and a 250k resolution (bottom left and bottom right, respectively), and particle size distribution (insets).

4.3.1.c. Z-potential

The corresponding Z-potentials of MSN-NH₂ and MSN-COOH were also measured, obtaining values of 13.0 ± 0.5 mV and -37.1 ± 8.52 mV respectively. Both values are slightly lower compared with some results found on the literature, such as the work of He and coworkers [260] with a value for MSN-NH₂ of 22.78 ± 0.32 mV, and the work of Gou and coworkers [261] with a value -30.4 ± 2.2 mV for MSN-COOH. Nevertheless, the values remain normal as the positive value correlate with the presence of amino groups and the negative one with the presence of carboxy groups.

4.3.2. Encapsulation of complexes in mesoporous silica nanoparticles

The encapsulation process was made as described in section 3. *Materials and methods*, but before trying for all complexes, it was made an initial test using one complex (i.e., PtDPhPzTz) and different types of particles. A thermogravimetric assay was made to check the adsorption of PtDPhPzTz into MSN, MSN-NH₂, MSN-COOH and DMON. As can be observed in Figure 4.34, the compound was adsorbed in all particles, obtaining the best loading results for MSN-NH₂, where the loading was more than two times higher than in the rest of particles tested. For that reason, amino-functionalized MSN were selected for the rest of the experiments.

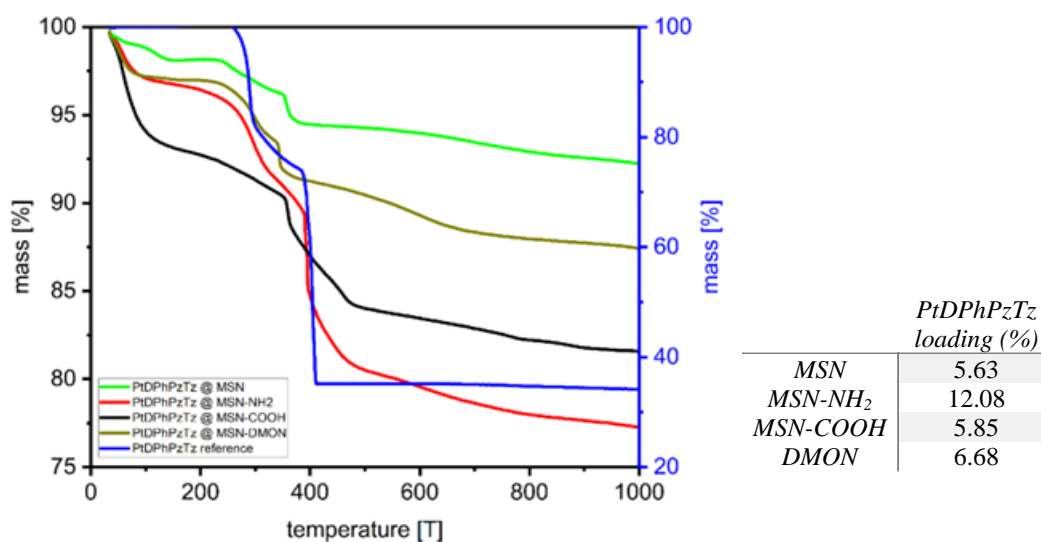


Figure 4.34. TGA data of PtDPhPzTz alone and encapsulated in MSN, MSN-NH₂, MSN-COOH and DMON nanoparticles and loading percentages in the different types of nanoparticles.

4.3.2.a. Thermogravimetric analysis

Once MSN-NH₂ were selected and after their functionalization with ATTO dye, the loading of all complexes was made with these particles. To check the adsorption of the compounds, TGA was performed as can be seen in Figure 4.35. Each loaded particle is compared to the compound alone and to non-loaded particles, which were treated with the same solvent as the loaded particles, as a reference. A comparison of TGA data of all loaded particles respect to the non-loaded ones is shown in Figure 4.36.

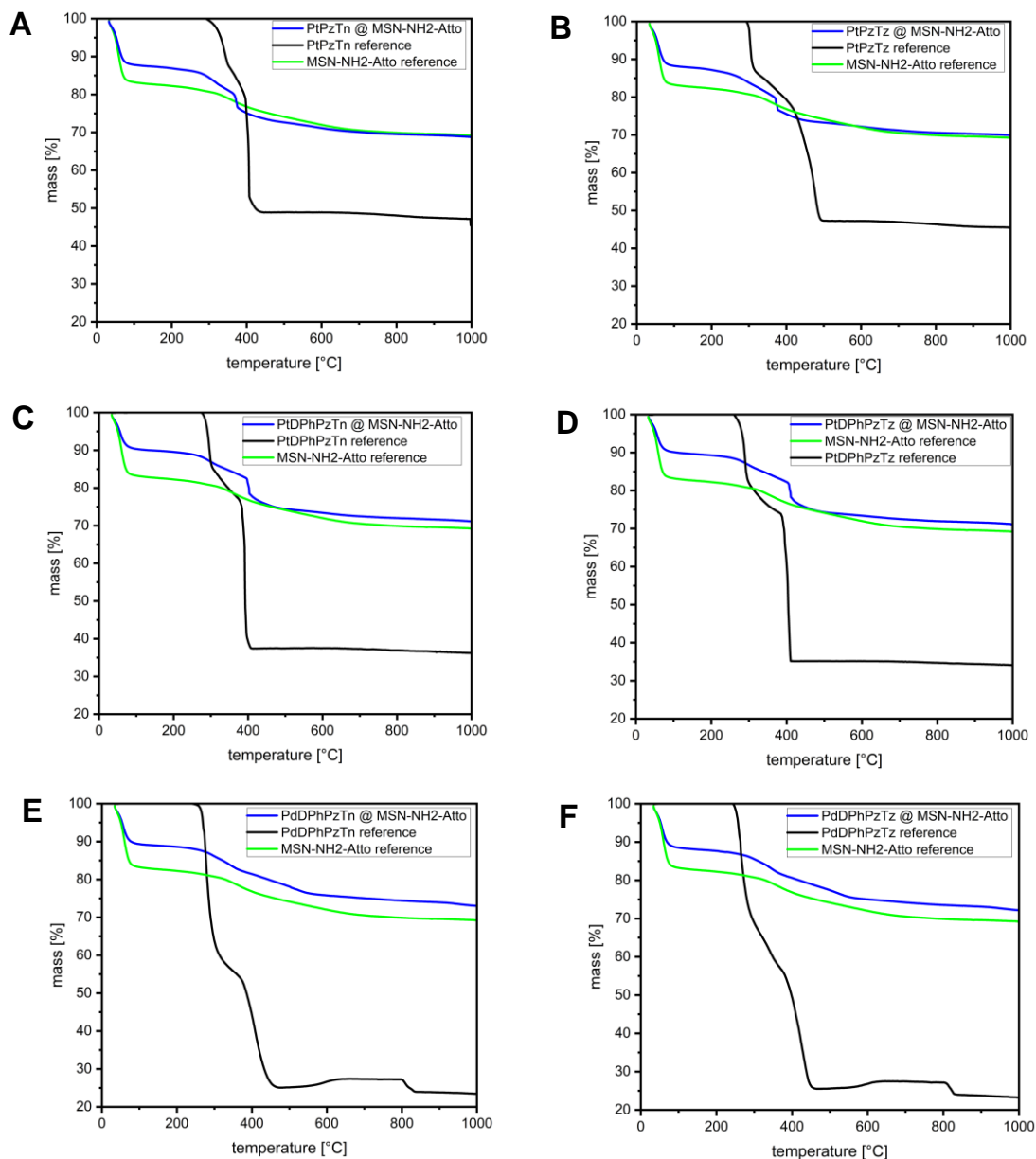


Figure 4.35. TGA data of MSN-NH₂-ATTO-PtPzTn (A), MSN-NH₂-ATTO-PtPzTz (B), MSN-NH₂-ATTO-PtDPhPzTn (C), MSN-NH₂-ATTO-PtDPhPzTz (D), MSN-NH₂-ATTO-PdDPhPzTn (E) and MSN-NH₂-ATTO-PdDPhPzTz (F) in comparison with non-loaded particles (MSN-NH₂-ATTO) and the compounds alone.

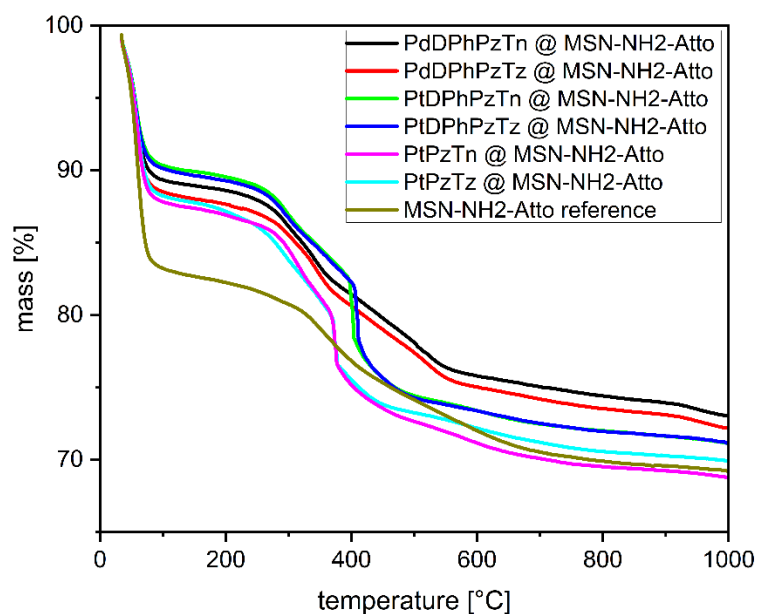


Figure 4.36. TGA data comparison of all encapsulated complexes in MSN-NH₂-ATTO and non-loaded particles.

With the data obtained from TGA, loading percentage of each compound in the particles could be calculated (Table 4.24). The highest loading percentages were found for Pt(II) complexes, particularly for PtDPhPzTz and PtPzTn, being followed by PtDPhPzTn and PtPzTz. On the other hand, Pd(II) complexes did not show a strong loading, reaching only a 3%, which is three or four times lower than that found for Pt(II) complexes.

Table 4.24. Loading percentage of all complexes in MSN-NH₂-ATTO particles.

<i>MSN-NH₂-ATTO-</i>	<i>Compound loading (%)</i>
<i>PtPzTn</i>	10.89
<i>PtPzTz</i>	9.16
<i>PtDPhPzTn</i>	9.70
<i>PtDPhPzTz</i>	12.61
<i>PdDPhPzTn</i>	3.28
<i>PdDPhPzTz</i>	3.12

4.3.2.b. Z-potential

The corresponding Z-potentials of loaded and non-loaded particles were measured in 7.2 pH HEPES buffer, and the values are included in Table 4.25.

As it can be observed, there was a clear trend for the Pt(II) complexes with thiazine rings, which were more negative than the Pt(II) complexes with thiazoline rings. Nevertheless, this observation was not consistent throughout all the complexes as the Pd(II) ones exhibited a positive value for PdDPhPzTz and a negative value for PdDPhPzTn.

Table 4.25. Z-potential of all complexes in MSN-NH₂-ATTO particles and non-loaded particles in 7.2 pH HEPES buffer.

<i>MSN-NH₂-ATTO-</i>	<i>Z-potential</i>
<i>Reference</i>	-3.0 ± 0.5
<i>PtPzTn</i>	8.52 ± 0.5
<i>PtPzTz</i>	-11.2 ± 0.5
<i>PtDPhPzTn</i>	3.8 ± 0.2
<i>PtDPhPzTz</i>	-5.3 ± 0.3
<i>PdDPhPzTn</i>	-4.3 ± 0.2
<i>PdDPhPzTz</i>	1.9 ± 0.1

4.3.3. Biological testing of encapsulated complexes

In the next subsections, the release, accumulation, distribution and proapoptotic ability of the synthesized nanoparticles are analyzed.

4.3.3.a. Cellular internalization and distribution

Firstly, HeLa cells treated with 10 µg/mL of loaded particles were imaged by confocal microscopy. The cells were incubated with two of the loaded particles (MSN-NH₂-ATTO-PtPzTn and MSN-NH₂-ATTO-PtDPhPzTz) in order to observe if the particles entered the cells and their subcellular distribution. To study the subcellular distribution of MSNs, live cells were counterstained with nuclear, Golgi, plasma membrane and mitochondria markers. In Figure 4.37, it can be observed that the particles (red dots/aggregates) are clearly entering the cells. In addition, they seem to be distributed in different subcellular compartments, including nucleus, Golgi, plasma membrane and mitochondria.

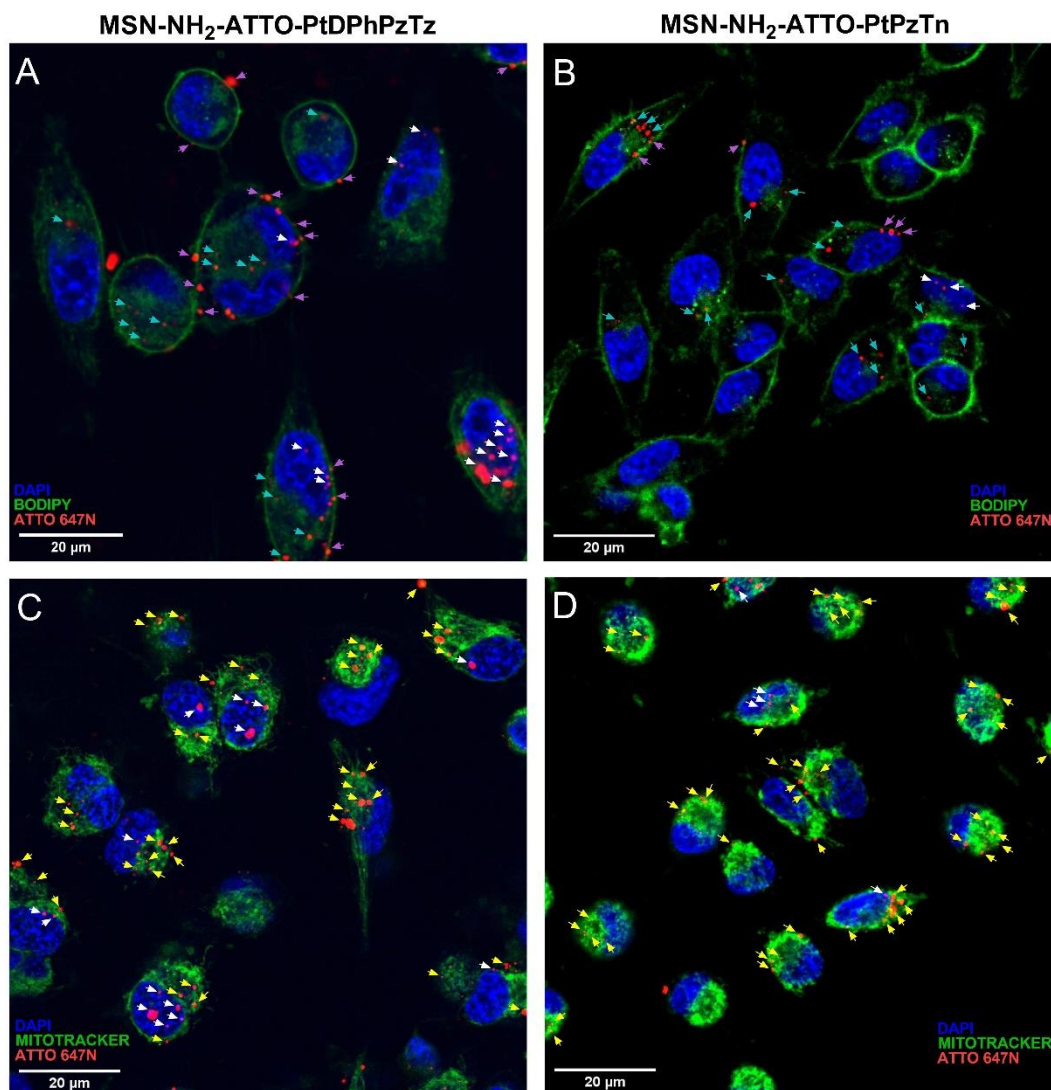


Figure 4.37. Subcellular localization of MSN-NH₂-ATTO loaded particles. HeLa cells were treated with 10 μg/mL of MSN-NH₂-ATTO-PtDPhPzTz (A and C) or MSN-NH₂-ATTO-PtPzTn (B and D). To localize different cellular compartments, HeLa cells were counterstained with DAPI (nucleus), BODIPY FL C₅-sphingomyelin (Golgi and plasma membrane), and/or MitoTracker Green FM (mitochondria), as indicated in each panel. Individual particles or clusters of particles are pointed by white arrows (nucleus), blue-light arrows (Golgi), purple arrows (plasma membrane) or yellow arrows (mitochondria).

4.3.3.b. Apoptosis determination

Once it was checked that the particles were entering the cell, their cytotoxic ability was tested. Initially, measurement via MTS method was performed, but data were not accurate (data not included). As indicated in the literature, this group of methods tends to overestimate the results when used with nanoparticles [262,263]. For that reason, apoptosis was analyzed by flow cytometry using annexin V-FITC and Hoechst 33258. The treatment of HeLa cells with 200 μg/mL of the loaded particles during 24 h produced

significant changes in the percentage of cell populations for MSN-NH₂-ATTO-PtPzTn and MSN-NH₂-ATTO-PtPzTz. Particularly, a decrease in live cells and an increase in late apoptotic cells for both systems were observed. In the case of MSN-NH₂-ATTO-PtPzTn, the differences were significant in comparison with both the untreated and the non-loaded particle samples, and for MSN-NH₂-ATTO-PtPzTz the differences were only significant respect to the untreated sample (Figure 4.38 and Table 4.26). For the rest of loaded particles (those with complexes containing phenyl rings), the apoptotic effect was similar among them and only slightly higher than the one showed by non-loaded particles. However, the differences respect to non-loaded particles were non-significant, indicating that their main effect was produced by the silica material and not by the complexes themselves.

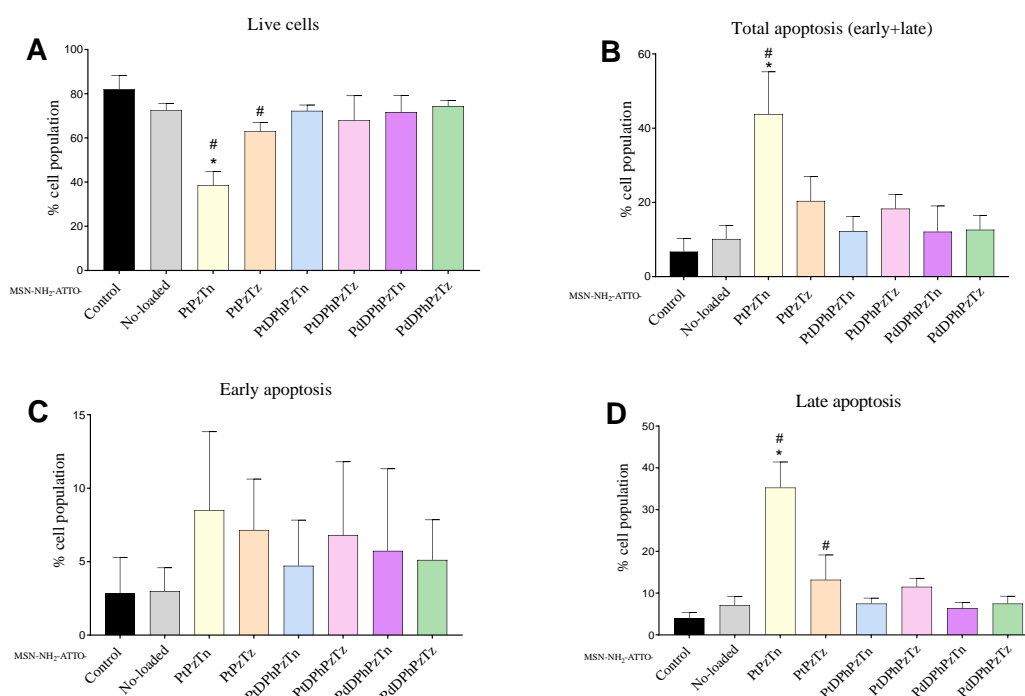


Figure 4.38. Flow cytometry results including live cells, early, late, and total apoptosis triggered by loaded and non-loaded particles. HeLa cells were challenged with 200 μ g/mL of the indicated particles for 24 h. Histograms show percentages of cell population detected by flow cytometry. Values are presented as means \pm SD of three independent experiments. * P < 0.05 compared to non-loaded particles. # P < 0.05 compared to control values (Dunnett's test).

Table 4.26. Flow cytometry values including live cells, early, late, and total apoptosis triggered by loaded and non-loaded particles.

<i>MSN-NH₂-ATTO-</i>	<i>Live cells</i>	<i>Total apoptosis</i>	<i>Early apoptosis</i>	<i>Late apoptosis</i>
<i>Control</i>	82.06 ± 6.20	6.76 ± 3.52	2.83 ± 2.44	3.93 ± 1.42
<i>Non-loaded</i>	72.49 ± 3.50	10.16 ± 3.66 * [#]	3.00 ± 1.58	7.16 ± 2.08 * [#]
<i>PtPzTn</i>	38.53 ± 6.29 * [#]	43.78 ± 11.39	8.49 ± 5.35	35.28 ± 6.12 [#]
<i>PtPzTz</i>	62.99 ± 3.99 [#]	20.39 ± 6.57	7.16 ± 3.46	13.23 ± 5.91
<i>PtDPhPzTn</i>	72.27 ± 2.61	12.24 ± 4.02	4.72 ± 3.11	7.52 ± 1.30
<i>PtDPhPzTz</i>	64.97 ± 11.11	18.13 ± 3.81	6.79 ± 5.01	11.54 ± 2.03
<i>PdDPhPzTn</i>	71.70 ± 7.44	12.13 ± 6.91	5.74 ± 5.58	6.39 ± 1.38
<i>PdDPhPzTn</i>	74.37 ± 2.64	12.64 ± 3.79	5.12 ± 2.73	7.52 ± 1.77

* $P < 0.05$ compared to non-loaded particles. [#] $P < 0.05$ compared to control values (Tukey's test).

To properly understand what these results implicate, relevant values corresponding to the free compound IC_{50} and the concentration of complexes in the particles used in the apoptosis experiment were collected in Table 4.27.

Table 4.27. Comparison of IC_{50} of free compounds and the compound concentration used in apoptosis experiments.

<i>MSN-NH₂-ATTO-</i>	<i>IC₅₀ free compound (μM)</i>	<i>Compound concentration in 200 μg particles (μM)</i>
<i>PtPzTn</i>	140.20	51.90
<i>PtPzTz</i>	142.20	42.31
<i>PtDPhPzTn</i>	12.15	33.98
<i>PtDPhPzTz</i>	14.09	43.08
<i>PdDPhPzTn</i>	62.74	13.57
<i>PdDPhPzTn</i>	57.83	12.54

Interestingly, the best results were observed for the two complexes with less cytotoxic effects as free drugs (i.e., PtPzTn and PtPzTz), while the effect of any of the complexes with phenyl rings was not improved. In fact, focusing the attention on PtPzTn, the encapsulation allowed the use of much less concentration of the complex to produce a similar effect. Thus, the IC_{50} of the free compound is nearly 150 μM , while the concentration of the compound encapsulated is 51.9 μM , the latter generating a decrease of more than 50% in the population of live cells compared to control cells. Therefore, a strong improvement in the effect of PtPzTn was achieved by encapsulating the complex in the MSN-NH₂ system, thus reducing almost three times the concentration of compound used. In the case of PtPzTz, the decrease in cell viability was smaller, but the reduction of the concentration of compound used was greater than three times. Nevertheless, part of the effect of PtPzTz was probably due to the silica itself.

On the other hand, the lack of effect of the complexes with phenyl rings could be related with some interactions of these complexes with the particles, which could difficult either their internalization in the cell or their liberation and further accumulation inside the cells, thereby preventing them to act. This might explain why such an increase on the concentration used for PtDPhPzTn and PtDPhPzTz had apparently no effect, or a similar one to the non-loaded particles. However, in the case of palladium complexes, the explanation could be related with the low loading achieved (around 3%) and the subsequent low quantity used in comparison to the free complexes. To identify if there was any difference in the accumulation and liberation of compounds, ICP-MS experiments were performed and included in the next subsections.

4.3.3.c. Cellular uptake

To verify the metal accumulation in HeLa cells, ICP-MS measurements were performed. For that, cells were treated with 100 $\mu\text{g/mL}$ of the loaded nanoparticles for 4 h. As can be observed in Figure 4.39, the strongest accumulation was produced for PtPzTn, which presented statistically significant differences with all complexes with phenyl rings, both with Pt(II) and Pd(II) as metal centers. This intense accumulation could be related with the higher cytotoxic effect displayed in the apoptosis assay. In fact, PtPzTz was also the second compound with higher accumulation and the second one with higher cytotoxic effect, while the complexes with phenyl groups were the ones with less accumulation and less cytotoxic effect. Thus, the accumulation seems to be in line with the cytotoxic effect of the complexes. To verify whether the complexes were being freed from the particles, a cell-free release experiment was also performed.

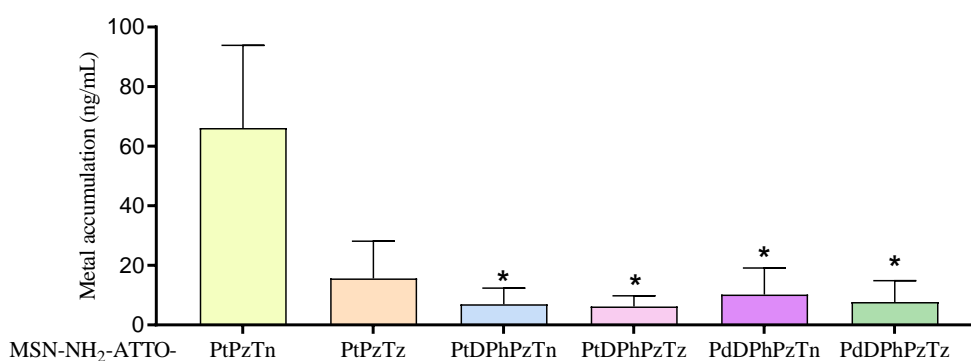


Figure 4.39. Platinum or palladium accumulation in HeLa cells. Cells were treated with 100 $\mu\text{g/mL}$ of loaded nanoparticles for 4 h, and then samples were digested with 65% HNO_3 and subsequently analyzed by ICP-MS. Pt(II) or Pd(II) concentrations were given in ng/mL. Values represent means \pm SD of 3 independent experiments. * $P < 0.05$ compared to MSN-NH₂-ATTO-PtPzTn (Dunnett's test).

4.3.3.d. Release analysis

To confirm whether the complexes were released from the particles, the amount of Pt(II) or Pd(II) leached after 4 and 24 h of incubation in pH 7.4 PBS buffer was measured by ICP-MS. After the incubation of 200 μg of the loaded nanoparticles in 1 mL of PBS buffer, the release results (Figure 4.40) indicated that a considerably strong release was produced for the complexes PtPzTn, PdDPhPzTn and PdDPhPzTz at 4 h, which was slightly lower for PtPzTz. In this sense, significant differences were found for PtPzTn respect to PtPzTz, PtDPhPzTn and PtDPhPzTz at 4 h of incubation. After 24 h, the leaching was vaguely increased for PtPzTn, PdDPhPzTn and PdDPhPzTz, showing a pronounced increase for PtPzTz, which even surpassed the amount released for the complexes with palladium. On the other hand, the complexes PtDPhPzTn and PtDPhPzTz showed practically no release neither after 4 h nor 24 h. Significant differences were found for PtPzTn and PtPzTz respect to the Pt(II) complexes with phenyl rings at 24 h. On the other hand, significant differences were observed for the Pt(II) complexes with phenyl rings respect to both Pd(II) complexes at short and long incubation times.

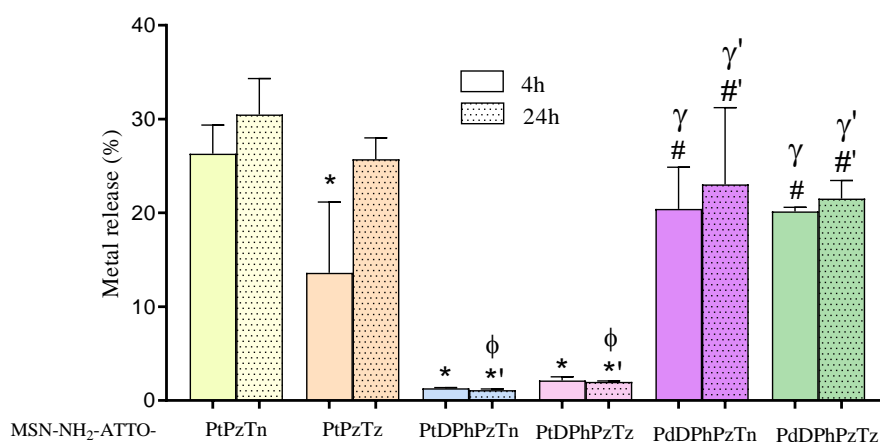


Figure 4.40. Platinum or palladium release. HeLa cells were treated with 200 μg of loaded nanoparticles in 1 mL of pH 7.4 PBS buffer for 4 h and 24 h. The samples were digested with 65% HNO_3 and subsequently analyzed by ICP-MS. Pt(II) or Pd(II) concentrations were given in percentage respect to the theoretically calculated maximum release. Values represent means \pm SD of 2 independent experiments. * $P < 0.05$ compared to MSN-NH₂-ATTO-PtPzTn (4 h); *' $P < 0.05$ compared to MSN-NH₂-ATTO-PtPzTn (24 h); # $P < 0.05$ compared to MSN-NH₂-ATTO-PtDPhPzTn (4 h); #' $P < 0.05$ compared to MSN-NH₂-ATTO-PtDPhPzTn (24 h); $\gamma P < 0.05$ compared to MSN-NH₂-ATTO-PtDPhPzTz (4 h); $\gamma' P < 0.05$ compared to MSN-NH₂-ATTO-PtDPhPzTz (24 h); $\phi P < 0.05$ compared to MSN-NH₂-ATTO-PtPzTz (24 h) (Tukey's test).

The highest release was achieved by PtPzTn at both 4 and 24 h, reaching 30% of release after the longest incubation time. These results seem to correlate with the

accumulation of metal in cells, which was also higher for PtPzTn and PtPzTz. Although it appears that there is also a high release for palladium complexes, their accumulation and cytotoxicity were quite low, which could be justified by the limited loading achieved for these two complexes. On the other hand, some interactions could be occurring between the particles and the complexes PtDPhPzTn and PtDPhPzTz preventing them from being released, which would explain the low accumulation on the cells and the lack of cytotoxic effect even with a high loading of these complexes.

5. DISCUSSION

5. DISCUSSION

Cancer is one of the main causes of death around the world and it is characterized by the uncontrolled growing and propagation of abnormal cells in any part of the body. Notwithstanding the advances on the understanding of this disease and the improvements achieved on treatments development, it is expected an increase in the number of new diagnosed cases and mortality rates worldwide for the next decades [5]. On the other hand, the methods used to treat cancer are not always effective and include many side effects. One of the principal ways to treat this illness is chemotherapy, which is based on the use of drugs to destroy cancer cells, preventing them from dividing and growing. Nevertheless, it can also damage healthy cells, causing nausea, neurotoxicity, etc., or even stop working due to acquired resistance of the tumor cells [264].

CisPt has been one of the most relevant chemotherapeutic agents used since its approval by the FDA in 1978. But, as previously mentioned, it also has some drawbacks that led to the synthesis of other analogs. For that reason, not only platinum but also different metals have been studied, as well as the incorporation of a wide variety of ligands in order to improve its antitumoral effects and avoid their side effects [55,57,67]. With all that in mind, in the present PhD thesis it has been synthesized and characterized 12 complexes with S,N and N,N-heterocycles in the ligand structure, in combination with platinum(II) or palladium(II) as metallic centers. The structure and stability of the synthesized complexes was checked via X-ray diffraction, elemental analysis, IR spectroscopy, and ^1H NMR spectroscopy. Based on those data, it could be affirmed that the structure of the complexes consists of monomeric units of $[\text{MCl}_2\text{L}]$ (L = bidentate ligand), being the coordinate geometry around the metal slightly distorted square-planar. In addition, it was confirmed that the ligands were coordinated to the metal through the nitrogen of pyrazole cycle and the nitrogen of 2-thiazoline ring or the nitrogen of 1,3-thiazine ring according with the compound. Moreover, it was checked that those agents that were soluble were stable in solution during at least 21 days.

The results achieved in this PhD thesis showed that the CisPt analogs synthesized presented cytotoxic effect in the three cell lines selected (HL-60, U-937 and HeLa). The most sensitive cells to these chemotherapeutic agents were the leukemic ones, as ascertained by the lower IC_{50} values obtained in comparison with HeLa cells.

When comparing with other *cis*-complexes with a Cl_2N_2 coordination environment around Pt(II) reported in the literature*, it could be found some complexes

* All complexes mentioned can be found in Table A.4, Table A.5 and Table A.6.

(1-4, 6, 8-15, Table A.4, and 1-9, Table A.6) displaying higher cytotoxicity than our most potent complexes (PtDPhPzTn and PtDPhPzTz) both in HeLa [265–268] and U-937 [269], but in general with quite different chemical structures and with larger incubation times (48 h-7 days). On the other hand, it could be affirmed that PtDPhPzTn and PtDPhPzTz showed stronger cytotoxicity than some other platinum(II) complexes at the same, or even at shorter, incubation times (24h) against HeLa (5, 7, 16-38, Table A.4) [266,270–276] and HL-60 (1-7, Table A.5) [270,271,277]. Moreover, PtPzTn, PtPzTz, PtDMPzTn and PtDMPzTz also had stronger cytotoxic effect in HeLa and HL-60 than some of these complexes (16-21, 23, 25 and 26, Table A.4 and 1-7, Table A.5) found in the literature [270–273,277] at the same or even at shorter incubation times. Nevertheless, it is important to highlight that some of the comparisons are not accurate because some authors measured cell proliferation by other methods different from MTS assay [265,272].

As it was already mentioned, the chemical structures of the complexes found in the literature are quite distinct from ours. Hence, to compare to closer structures, results from some complexes previously synthesized by the *Coordination Chemistry Research group* of University of Extremadura will be discussed. Among them, it can be stated that the complexes PtTdTz [278] and PtPyTz [175], both tested in HeLa cells, showed better results than our complexes with methyl or no substitutions, but lower cytotoxicity than PtDPhPzTn and PtDPhPzTz. Nevertheless, the complex PtTzTz presented a slightly lower IC₅₀ ($9.8 \pm 0.9 \mu\text{M}$) than our best complex (PtDPhPzTn) [279]. On the other hand, four of our Pt(II) complexes (PtPzTn, PtPzTz, PtDPhPzTn and PtDPhPzTz) performed better cytotoxic effect than PtPyTz in U-937 and HL-60, and PtTdTn in U-937 [175,280].

Respect to Pd(II) analogs, when comparing with other Pd(II) complexes reported in the literature, it could be also found some complexes displaying higher cytotoxicity than our most potent complexes (PdDPhPzTn and PdDPhPzTz) in HeLa cells (42, 44, 47 and 48, Table A.4) [272,281,282] at the same incubation times. Nonetheless, as happened with Pt(II) complexes, they had in general quite different chemical structures or even used different methods to measure cytotoxicity [272]. In contrast, our complexes improved some of the IC₅₀ values achieved with other palladium(II) compounds, thereby decreasing the concentration of some of them at the same incubation times. This happened for complexes PdDPhPzTn, PdDPhPzTz, PdPzTn and PdPzTz in HeLa (43, 45, 46, 49-51, 53 and 55, Table A.4) [259,272,282,283] and HL-60 (7, Table A.5) [277], while only PdDPhPzTn and PdDPhPzTz demonstrated lower IC₅₀ values than other Pd(II)

complexes in HeLa cells (52 and 54, Table A.4) [259,283]. Moreover, when comparing to closer structures, the Pd(II) complexes described in this PhD thesis were not able to improve the biological activity of complexes PdTdTn [280] in U-937, and PdTdTz and PdTzTz [278,279] in HeLa cells, although the effect of the latter compounds was apparently due to the ligands and not influenced by the metal center. In contrast, the complexes with phenyl or no substitutions improved the cytotoxic effect showed by PdPyTz in the three cell lines selected [175]. Additionally, it was also verified that longer incubation times (48 and 72 h) improved the cytotoxicity of the Pd(II) complexes in HeLa cells, unlike PdDMPzTn and PdDMPzTz, which did not enhance their effect with time. The greater decrease in the IC₅₀ values was around 30-40 μM at 72 h for PdDPhPzTn and PdDPhPzTz.

In general, data obtained demonstrated a higher sensitivity of leukemic cell lines in comparison to the solid-tumor cell line towards the chemotherapeutic agents tested, among which PtDPhPzTn and PtDPhPzTz displayed the best effects. In fact, lower IC₅₀ values were obtained for these two complexes compared to CisPt in the three cell lines, being almost two-fold lower in HL-60 and more than two-fold lower in U-937.

The results followed the same trend for Pt(II) and Pd(II) complexes, corroborating that the methyl substitution of pyrazole ring in the ligand is not as effective as the phenyl substitution or the absence of extra substituents. Besides, the methyl substitution did not improve the effect of the complex with either Pt(II) nor Pd(II) as metal center, except for a moderate effect of PtDMPzTn and PtDMPzTz in leukemic cell lines. It is undeniable that there is an influence of the substituents presented in the pyrazole ring, where complexes with phenyl substituents promoted strong cytotoxicity in all three cell lines, with both Pt(II) and Pd(II) as metallic centers in comparison to their analogs with the same metal. Thus, it was presumed that the biological activity of the CisPt analogs could be influenced by the incorporation of aromatic groups into their structure [284,285]. In fact, Segapelo and coworkers [266] also demonstrated that the aryl substitution of pyrazole ring in their Pt(II) complexes (6 and 8, Table A.4) improved their cytotoxicity in comparison with alkyl substitutions (5 and 7, Table A.4). Same conclusion was obtained by Zafar and coworkers [259], who also improved cytotoxicity with benzyl instead of methyl substitutions of their Pd(II) complexes (54 and 55, Table A.4), but in this case making the substitution on the pyridine ring. Moreover, in the case of Keter and coworkers [272], the methyl substitution of bis-pyrazoles remarkably worsened the cytotoxicity of their complexes (22, 23, 42 and 43, Table A.4), both with Pt(II) and Pd(II)

as metallic centers. On the other hand, when HeLa cells were incubated for 4 h with the IC_{50} of our Pt(II) and Pd(II) complexes with phenyl rings or no extra substituents, stronger accumulation was observed for complexes with phenyl substituents in comparison with their respective counterparts. Moreover, PtDPhPzTn and PtDPhPzTz accumulated into cells much more efficiently than CisPt (10-fold higher in both cases). This may indicate that the presence of aromatic groups in the ligands, which structurally confers enhanced lipophilicity to these complexes, improved their cellular uptake and accumulation.

Likewise, it was also demonstrated that none of the free ligands produced significant effects in cell viability of U-937 and HL-60 cells, whereas they only affected cell viability of HeLa cells at the highest dose, e.g., 100 μ M in the case of DPhPzTn and DPhPzTz. This indicates that the coordination to the metal center is indispensable to produce the cytotoxic effect. In addition, it was also clearly identified that the complexes with Pt(II) as metallic center have a greater cytotoxic effect than Pd(II) complexes. This could be related to the higher kinetic lability of Pd(II) complexes in comparison to Pt(II) ones [286]. This usually generates a rapid hydrolysis of palladium-ligand bonds, generally resulting in the formation of reactive species unable to reach the target biomolecules inside cancer cells [82,287].

Focusing on the phenyl substituted complexes, which were the most promising ones, it was also confirmed that the cell death produced in HeLa cells was mediated via apoptosis, as occurred with other complexes with similar structure [280]. The increase in the percentage of apoptotic cells was akin to that elicited by the IC_{50} of CisPt. On the other hand, although the apoptosis induction was similar to that of CisPt, it was checked that PtDPhPzTn and PtDPhPzTz did not produce DNA intercalation, unlike CisPt, which suggest that these complexes may act through a different mechanism. In fact, PtDPhPzTn and PtDPhPzTz also caused a dramatic increase of intracellular ROS production that ultimately led to apoptotic cell death. In this sense, previously described Pt(II)-based complexes were also shown to exert their cytotoxic effect through mechanisms distinct from cisplatin, including ROS-mediated apoptosis [288–290], mitochondrial dysfunction and ER stress response [290,291], and mitogen-activated protein kinase (MAPK) modulation [288]. Surprisingly, although the free ligands DPhPzTn and DPhPzTz did not significantly modify the percentage of apoptotic cells, they produced a significant increase in the intracellular production of ROS. This effect may be due to nonspecific effects inherent to the nature of the molecules, or to possible interferences with the fluorescent probe used for the determination of ROS.

On the other hand, encapsulation of drugs in nanoparticles has been an extensive approach used in recent years to improve their biological effects and some physicochemical properties such as solubility and transport [292,293]. Among nanoparticles, MSNs have been widely used to improve the delivery of hydrophobic and hydrophilic drugs both *in vitro* and *in vivo*. In addition, one of their advantages is their biosafety status since they are regarded as GRAS by FDA [294]. Among some studies with promising results for anticancer drug delivery with MSN, it can be mentioned that Tao and coworkers encapsulated CisPt and transplatin on two types of MSN (MCM-41 or SBA-15) achieving an enhanced cytotoxicity at 24h of incubation greater than that of the free drugs in lymphoid cells [295]. Similarly, Lin and coworkers also improved CisPt effect by encapsulating it on trimethylammonium (TA)-MSN-carboxylate, showing highly anti-proliferative effect through the induction of cell apoptosis in HT-29 cell line [296]. Nevertheless, the encapsulation of doxorubicin (DOX) in MSN-NH₂ only showed comparable results on A549 cell line when incubated during 72h [260], while other study on HeLa cells and MSNs as carriers improved the cytotoxicity of DOX alone [297]. On the other hand, the encapsulation of oxaliplatin in MSN-COOH reduced the IC₅₀ obtained for the free drug on HepG-2 cells and changed the internalization mechanism, as they were taken up via endocytosis instead of passive diffusion [221]. For all this, in the present PhD thesis MSNs were selected as drug delivery systems for several of the synthesized complexes. Furthermore, amino functionalization of MSNs was selected due to an enhanced loading of PtDPhPzTz in comparison with other particles (MSN, MSN-COOH and DMON). MSN-NH₂ were then synthesized and characterized via TEM, gas adsorption, and Z-potential. In addition, they were also functionalized with ATTO dye to make easier the studies on their subcellular localization. Finally, six (PtPzTn, PtPzTz, PtDPhPzTn, PtDPhPzTz, PdDPhPzTn and PdDPhPzTz) of our complexes were successfully encapsulated. The loading was checked via TGA, where it could be seen that the loading percentage was higher for Pt(II) complexes than for the Pd(II) ones. Afterwards, it was confirmed that the particles successfully entered in HeLa cells, as particles were imaged through confocal microscopy and seemed to be distributed in the nucleus, Golgi, plasma membrane and mitochondria. In addition, release of complexes from the particles and accumulation on HeLa cells were also checked by ICP-MS, showing that MSN-NH₂-ATTO-PtPzTn and MSN-NH₂-ATTO-PtPzTz had the stronger release and MSN-NH₂-ATTO-PtPzTn produced the higher metal accumulation on cells. This intense accumulation could be related with a higher apoptosis-inducing effect. In

fact, when encapsulated into MSN-NH₂-ATTO system, PtPzTn remarkably decreased the population of live cells by more than 50% at a concentration that was far below the IC₅₀ of the free drug (51.90 μM vs. 140.20 μM). In the case of MSN-NH₂-ATTO-PtPzTz, the decrease in population of live cells was smaller (~20 % vs. control), but the reduction of the concentration of PtPzTz was greater than three times (42.31 μM for encapsulated drug vs. 142.20 μM for free drug). Nevertheless, it cannot be ignored that a minor part of the effect was probably due to the silica itself and that the release of complexes from the synthesized MSNs was not completed after 24h (e.g., ~30 % and ~25 % release for PtPzTn and PtPzTz respectively). Therefore, the actual amount of readily bioavailable complex should be lower than the total amount concentration in the MSN-NH₂, making the encapsulated complexes more effective than it was considered. On the other hand, the lack of effect of the complexes with phenyl rings could be related with some interactions of this complexes with the particles, which could hinder their liberation and further accumulation in the cells, thereby preventing them to act. However, in the case of palladium-containing nanoparticles, the explanation could be related with the low loading achieved and subsequent low quantity used in comparison to the free complexes.

It is important to highlight that making a comparison of the results obtained with other complexes or nanoparticles in the literature is complex and not completely accurate. This is due to the lack of works with the exact same functionalization that was used in this PhD thesis and the wide range of coating options existing. In addition, as it was already mentioned, MTT (3-(4,5-dimethylthiazol-2-yl)-2,5-diphenyl tetrazolium bromide) assay and methods alike are not precise to study cell viability when treating cells with nanoparticles [262,263]. Nevertheless, many researchers still use this assay. Having said that, when comparing with the work of Gu and coworkers [298], where they encapsulated CisPt in carboxylic group modified MSNs (MSNs-C) with enhanced results in HeLa cells respect to free CisPt, MSN-NH₂-ATTO-PtPzTn was able to improve the IC₅₀ (55.7 μM) of particles of comparable size and at an equivalent incubation time. Similarly, Ren and coworkers [299] used MSN and amino functionalized MSN modified with folic acid (FA) to load 10-hydroxycamptothecin (HCPT) and checked their cytotoxicity by MTS assay on HeLa cells. Although both types of particles showed antitumor activity, their IC₅₀ (71.08 μM for MSN and 152.03 μM for MSN-FA) were also higher than the ones achieved by MSN-NH₂-ATTO-PtPzTn and MSN-NH₂-ATTO-PtPzTz. On the other hand, Cheralayikkal and coworkers [300] encapsulated 5-fluorouracil, another potent chemotherapeutic agent, in amine functionalized hollow

MSNs and then coated with a biocompatible polydopamine. The IC_{50} values obtained using MTT assay on HeLa cells were 20.3 and 31.3 $\mu\text{g/mL}$ for both loaded particles, which improved the value of the free drug (40.7 $\mu\text{g/mL}$), being also higher or very similar to the ones showed by MSN-NH₂-ATTO-PtPzTn and MSN-NH₂-ATTO-PtPzTz. Nevertheless, other works showed impressive results in this field and presented other ideas to improve the effectivity of the particles. For example, Racles and coworkers [301] remarkably reduced DOX concentrations from 50 $\mu\text{g/mL}$ to 1–2 $\mu\text{g/mL}$ when encapsulated in mesoporous and nonporous functionalized silica nanoparticles with methyl, thiol and glucose groups. On the other hand, Li and coworkers [226] demonstrated the utility of poly(acrylic acid) modified MSNs as carries for combined drugs such as CisPt and DOX on HeLa cells studying the cell viability with CCK-8 assays. The synergic effect achieved values of IC_{50} lower than 10 μM . Alternatively, MSNs with a carboxylic acid or amine surface group can be successfully decorated with long-chain hydrophilic polymer via an amide bond. This occurred in the work of Al-Nadaf and coworkers [302] who described the encapsulation and cytotoxicity of DOX-loaded/decorated MSNs further coupled with FA, both chemically bound or as a complex with carboxymethyl beta-cyclodextrin (CM-b-CD). The IC_{50} values obtained ranged between 0.07-0.015 mg/mL on HeLa cells.

On the other hand, with the encapsulation of PtPzTn and PtPzTz it was possible to improve the IC_{50} values of some of the complexes found in the literature in HeLa cells (5, 28-33, 36, 38 and 40, Table A.4), which was not possible when using the PtPzTn and PtPzTz as free drugs. Nevertheless, it was not feasible to improve the results obtained for the free complexes PtDPhPzTn and PtDPhPzTz, or the complexes 1-4, 6, 8-15 (Table A.4, incubation times from 48 h to 7 days) in HeLa cells. Nonetheless, the encapsulated PtPzTn and PtPzTz were able to improve the effect of all the six Pd(II) complexes presented in this PhD thesis.

To sum up, the results presented in this PhD thesis proved that the incorporation of aromatic groups to the ligands gave rise to an enhanced cellular uptake and accumulation of the metallodrugs, which resulted in increased biological activity for both Pt(II) and Pd(II) complexes. In fact, Pt(II) complexes PtDPhPzTn and PtDPhPzTz were far more effective in terms of cytotoxicity than their less lipophilic counterparts, especially in HeLa cells, even showing lower IC_{50} than CisPt itself. Altogether, our results suggest that modulating the lipophilicity of the ligands can help improve the cytotoxic

effect of the metal complexes. On the other hand, the encapsulation of the less effective drugs PtPzTn and PtPzTz in MSN-NH₂ improves their transport to the cells and their cytotoxicity towards HeLa cells, which confirms the effectiveness of this kind of particles as drugs delivery systems for some of the synthesized complexes.

6. CONCLUSIONS

6. CONCLUSIONS

From the results obtained in the present PhD thesis, in which it was intended to synthesize and characterize new Pt(II) and Pd(II) analogs of cisplatin with N,N- and N,S-heterocycles-bearing ligands, and to study their potential cytotoxic and pro-apoptotic effect on three tumor cell lines (HeLa, U-937 and HL-60), it can be concluded that:

1. The synthesis and characterization of twelve cisplatin analogs, six with Pt(II) and six with Pd(II) as metal centers and N,N- and N,S-bidentate ligands, were successfully achieved. The structures of these complexes were confirmed by X-ray diffraction, elemental analysis and IR spectroscopy. That way, it could be affirmed that the complexes' structure consists of monomeric units of $[MCl_2L]$ (L = bidentate ligand), being the coordinate geometry around the metal slightly distorted square-planar. In addition, it was verified that the ligands were coordinated to the metal through the nitrogen of pyrazole cycle and the nitrogen of 2-thiazoline ring or the nitrogen of 1,3-thiazine ring according with the compound. On the other hand, it was checked by 1H RMN that those metallodrugs that were soluble were stable in the selected solvents during at least 21 days.
2. The evaluation of the cytotoxicity effects of the twelve complexes showed a higher effect on leukemic cell lines (HL-60 and U-937) than in the solid tumor cell line HeLa for most complexes. In addition, an improvement of IC_{50} values of complexes with respect to CisPt itself was achieved by PtDPhPzTn and PtDPhPzTz in all the three tumor cell lines, and similar values were obtained for PtPzTn in both U-937 and HL-60 cells and for PtPzTz in U-937 cells. Furthermore, the cell death detected was mediated via apoptosis for the complexes with phenyl rings on HeLa cells. In fact, the total cell death produced by PtDPhPzTn and PtDPhPzTn was higher than that produced by CisPt even using lower concentrations than the commercial agent.
3. The results obtained from the different complexes showed that the presence of aromatic rings in the ligand improved the biological activity of these complexes. This tendency was maintained in both complexes with Pt(II) and

Pd(II) as metal centers. Likewise, the presence of methyl substituents did not improve the cytotoxic activity of the complexes. On the other hand, it was also checked that, for the complexes synthesized, Pt(II) was more effective as metallic center than Pd(II), except for PdPzTn and PdPzTz in HeLa cells, which showed lower IC₅₀ values than their Pt(II) counterparts. Having all that in mind, for future drug development, further investigations of complexes with Pt(II) and aromatic rings in their structure can lead to promising results.

4. The synthesis, characterization, and encapsulation of six of the synthesized complexes in MSNs were achieved successfully. In addition, it was accomplished an improvement of solubility of all complexes encapsulated and an upgrade of the cytotoxic effects of PtPzTn and PtPzTz in HeLa cells. This suggested that the use of MSNs as carriers of these type of complexes could be useful for the delivery of poorly soluble drugs for cancer treatment.

7. BIBLIOGRAPHY

7. BIBLIOGRAPHY

1. Sociedad Americana Contra El Cáncer. *Datos y Estadísticas Sobre El Cáncer Entre Los Hispanos/Latinos 2021-2023.* ; Atlanta, 2021;
2. Hanahan, D.; Weinberg, R.A. The Hallmarks of Cancer. *Cell* **2000**, *100*, 57–70, doi:10.1016/S0092-8674(00)81683-9.
3. American Cancer Society American Cancer Society Available online: <https://www.cancer.org/es/tratamiento/como-comprender-su-diagnostico/que-es-el-cancer.html> (accessed on 3 May 2023).
4. World Health Organization World Health Organization Available online: <https://www.who.int/es/news-room/fact-sheets/detail/cancer> (accessed on 27 March 2023).
5. Sociedad Española de Oncología Médica (SEOM) *Las Cifras Del Cancer En España*; 2023;
6. GLOBOCAN 2020 Global Cancer Observatory Available online: <https://gco.iarc.fr/today/home> (accessed on 4 May 2023).
7. Siegel, R.L.; Miller, K.D.; Fuchs, H.E.; Jemal, A. Cancer Statistics, 2022. *CA. Cancer J. Clin.* **2022**, *72*, 7–33, doi:10.3322/CAAC.21708.
8. Vitale, I.; Pietrocola, F.; Guilbaud, E.; Aaronson, S.A.; Abrams, J.M.; Adam, D.; Agostini, M.; Agostinis, P.; Alnemri, E.S.; Altucci, L.; et al. Apoptotic Cell Death in Disease—Current Understanding of the NCCD 2023. *Cell Death Differ.* **2023**, *30*, 1097–1154, doi:10.1038/s41418-023-01153-w.
9. Bialik, S.; Dasari, S.K.; Kimchi, A. Autophagy-Dependent Cell Death - Where, How and Why a Cell Eats Itself to Death. *J. Cell Sci.* **2018**, *131*, jcs215152, doi:10.1242/JCS.215152/56766.
10. Chen, Q.; Kang, J.; Fu, C. The Independence of and Associations among Apoptosis, Autophagy, and Necrosis. *Signal Transduct. Target. Ther.* **2018**, *3*, 1–11, doi:10.1038/s41392-018-0018-5.
11. Galluzzi, L.; Vitale, I.; Aaronson, S.A.; Abrams, J.M.; Adam, D.; Agostinis, P.; Alnemri, E.S.; Altucci, L.; Amelio, I.; Andrews, D.W.; et al. Molecular Mechanisms of Cell Death: Recommendations of the Nomenclature Committee on Cell Death 2018. *Cell Death Differ.* **2018**, *25*, 486–541, doi:10.1038/s41418-017-0012-4.
12. Hitomi, J.; Christofferson, D.E.; Ng, A.; Yao, J.; Degterev, A.; Xavier, R.J.; Yuan,

- J. Identification of a Molecular Signaling Network That Regulates a Cellular Necrotic Cell Death Pathway. *Cell* **2008**, *135*, 1311–1323, doi:10.1016/J.CELL.2008.10.044.
13. Hotchkiss, R.S.; Strasser, A.; McDunn, J.E.; Swanson, P.E. Cell Death. *N. Engl. J. Med.* **2009**, *361*, 1570–1583, doi:10.1056/NEJMRA0901217.
 14. Kerr, J.F.R.; Wyllie, A.H.; Curriett, A.R. Apoptosis: A Basic Biological Phenomenon with Wide-Ranging Implications in Tissue Kinetics. *Br. J. Cancer* **1972**, *26*, 239, doi:10.1038/bjc.1972.33.
 15. Strasser, A.; O'Connor, L.; Dixit, V.M. Apoptosis Signaling. *Annu. Rev. Biochem.* **2000**, *69*, 217–245, doi:doi.org/10.1146/annurev.biochem.69.1.217.
 16. Zakeri, Z.F.; Ahuja, H.S. Cell Death/Apoptosis: Normal, Chemically Induced, and Teratogenic Effect. *Mutat. Res. Mol. Mech. Mutagen.* **1997**, *396*, 149–161, doi:10.1016/S0027-5107(97)00181-4.
 17. Dragovich, T.; Rudin, C.M.; Thompson, C.B. Signal Transduction Pathways That Regulate Cell Survival and Cell Death. *Oncogene* **1999**, *17*, 3207–3213, doi:10.1038/sj.onc.1202587.
 18. D'Arcy, M.S. Cell Death: A Review of the Major Forms of Apoptosis, Necrosis and Autophagy. *Cell Biol. Int.* **2019**, *43*, 582–592, doi:10.1002/CBIN.11137.
 19. Lazebnik, Y.A.; Cole, S.; Cooke, C.A.; Nelson, W.G.; Earnshaw, W.C. Nuclear Events of Apoptosis in Vitro in Cell-Free Mitotic Extracts: A Model System for Analysis of the Active Phase of Apoptosis. *J. Cell Biol.* **1993**, *123*, 7–22, doi:10.1083/JCB.123.1.7.
 20. Solary, E.; Bertrand, R.; Kohn, K.W.; Pommier, Y. Differential Induction of Apoptosis in Undifferentiated and Differentiated HL-60 Cells by DNA Topoisomerase I and II Inhibitors. *Blood* **1993**, *81*, 1359–1368, doi:10.1182/BLOOD.V81.5.1359.1359.
 21. Jordán, J. *Apoptosis: Muerte Celular Programada Ámbito Farmacéutico*; 2003; Vol. 22;.
 22. Get an Overview of Apoptosis and Its Involved Genes- CUSABIO Available online: <https://www.cusabio.com/Cell-Biology/Apoptosis.html> (accessed on 17 May 2023).
 23. Thornberry, N.A.; Lazebnik, Y. Caspases: Enemies Within. *Science* **1998**, *281*, 1312–1316, doi:10.1126/SCIENCE.281.5381.1312.
 24. Pop, C.; Salvesen, G.S. Human Caspases: Activation, Specificity, and Regulation.

- J. Biol. Chem.* **2009**, *284*, 21777–21781, doi:10.1074/jbc.R800084200.
25. Pistritto, G.; Jost, M.; Srinivasula, S.M.; Baffa, R.; Poyet, J.L.; Kari, C.; Lazebnik, Y.; Rodeck, U.; Alnemri, E.S. Expression and Transcriptional Regulation of Caspase-14 in Simple and Complex Epithelia. *Cell Death Differ.* **2002**, *9*, 995–1006, doi:10.1038/sj.cdd.4401061.
 26. Degtarev, A.; Boyce, M.; Yuan, J. A Decade of Caspases. *Oncogene* **2003**, *22*, 8543–8567, doi:https://doi.org/10.1038/sj.onc.1207107.
 27. Martin, S.J.; Green, D.R. Protease Activation during Apoptosis: Death by a Thousand Cuts? *Cell* **1995**, *82*, 349–352, doi:10.1016/0092-8674(95)90422-0.
 28. Thornberry, N.A.; Rano, T.A.; Peterson, E.P.; Rasper, D.M.; Timkey, T.; Garcia-Calvo, M.; Houtzager, V.M.; Nordstrom, P.A.; Roy, S.; Vaillancourt, J.P.; et al. A Combinatorial Approach Defines Specificities of Members of the Caspase Family and Granzyme B: Functional Relationships Established for Key Mediators of Apoptosis. *J. Biol. Chem.* **1997**, *272*, 17907–17911, doi:10.1074/JBC.272.29.17907.
 29. Hirata, H.; Takahashi, A.; Kobayashi, S.; Yonehara, S.; Sawai, H.; Okazaki, T.; Yamamoto, K.; Sasada, M. Caspases Are Activated in a Branched Protease Cascade and Control Distinct Downstream Processes in Fas-Induced Apoptosis. *J. Exp. Med.* **1998**, *187*, 587, doi:10.1084/JEM.187.4.587.
 30. Slee, E.A.; Harte, M.T.; Kluck, R.M.; Wolf, B.B.; Casiano, C.A.; Newmeyer, D.D.; Wang, H.G.; Reed, J.C.; Nicholson, D.W.; Alnemri, E.S.; et al. Ordering the Cytochrome c-Initiated Caspase Cascade: Hierarchical Activation of Caspases-2, -3, -6, -7, -8, and -10 in a Caspase-9-Dependent Manner. *J. Cell Biol.* **1999**, *144*, 281, doi:10.1083/JCB.144.2.281.
 31. Saraste, A.; Pulkki, K. *Morphologic and Biochemical Hallmarks of Apoptosis*; 2000; Vol. 45;.
 32. Ashkenazi, A.; Dixit, V.M. Death Receptors: Signaling and Modulation. *Science*. **1998**, *281*, 1305–1308, doi:10.1126/SCIENCE.281.5381.1305.
 33. Green, D.R.; Reed, J.C. Mitochondria and Apoptosis. *Science*. **1998**, *281*, 1309–1312, doi:10.1126/SCIENCE.281.5381.1309.
 34. Elmore, S. Apoptosis: A Review of Programmed Cell Death. *Toxicol. Pathol.* **2007**, *35*, 495, doi:10.1080/01926230701320337.
 35. Locksley, R.M.; Killeen, N.; Lenardo, M.J. The TNF and TNF Receptor Superfamilies: Integrating Mammalian Biology. *Cell* **2001**, *104*, 487–501,

- doi:10.1016/S0092-8674(01)00237-9.
36. Jin, Z.; El-Deiry, W.S. Overview of Cell Death Signaling Pathways. *Cancer Biol. Ther.* **2005**, *4*, 147–171, doi:10.4161/CBT.4.2.1508.
 37. Guicciardi, M.E.; Gores, G.J. Life and Death by Death Receptors. *FASEB J.* **2009**, *23*, 1625–1637, doi:10.1096/FJ.08-111005.
 38. Jan, R.; Chaudhry, G. e. S. Understanding Apoptosis and Apoptotic Pathways Targeted Cancer Therapeutics. *Adv. Pharm. Bull.* **2019**, *9*, 205, doi:10.15171/APB.2019.024.
 39. Espino, J.; Bejarano, I.; Paredes, S.D.; Barriga, C.; Reiter, R.J.; Pariente, J.A.; Rodríguez, A.B. Melatonin Is Able to Delay Endoplasmic Reticulum Stress-Induced Apoptosis in Leukocytes from Elderly Humans. *Age (Omaha)*. **2011**, *33*, 497–507, doi:10.1007/S11357-010-9194-0.
 40. Espino, J.; Bejarano, I.; Paredes, S.D.; Barriga, C.; Rodríguez, A.B.; Pariente, J.A. Protective Effect of Melatonin against Human Leukocyte Apoptosis Induced by Intracellular Calcium Overload: Relation with Its Antioxidant Actions. *J. Pineal Res.* **2011**, *51*, 195–206, doi:10.1111/J.1600-079X.2011.00876.X.
 41. Saelens, X.; Festjens, N.; Vande Walle, L.; Van Gorp, M.; Van Loo, G.; Vandenabeele, P. Toxic Proteins Released from Mitochondria in Cell Death. *Oncogene* **2004**, *23*, 2861–2874, doi:10.1038/sj.onc.1207523.
 42. Yuan, S.; Akey, C.W. Apoptosome Structure, Assembly, and Procaspase Activation. *Structure* **2013**, *21*, 501–515, doi:10.1016/J.STR.2013.02.024.
 43. van Loo, G.; van Gorp, M.; Depuydt, B.; Srinivasula, S.M.; Rodriguez, I.; Alnemri, E.S.; Gevaert, K.; Vandekerckhove, J.; Declercq, W.; Vandenabeele, P. The Serine Protease Omi/HtrA2 Is Released from Mitochondria during Apoptosis. Omi Interacts with Caspase-Inhibitor XIAP and Induces Enhanced Caspase Activity. *Cell Death Differ.* **2002**, *9*, 20–26, doi:10.1038/SJ.CDD.4400970.
 44. Schimmer, A.D. Inhibitor of Apoptosis Proteins: Translating Basic Knowledge into Clinical Practice. *Cancer Res.* **2004**, *64*, 7183–7190, doi:10.1158/0008-5472.CAN-04-1918.
 45. Susin, S.A.; Daugas, E.; Ravagnan, L.; Samejima, K.; Zamzami, N.; Loeffler, M.; Costantini, P.; Ferri, K.F.; Irinopoulou, T.; Prévost, M.C.; et al. Two Distinct Pathways Leading to Nuclear Apoptosis. *J. Exp. Med.* **2000**, *192*, 571–579, doi:10.1084/JEM.192.4.571.
 46. Li, L.Y.; Luo, X.; Wang, X. Endonuclease G Is an Apoptotic DNase When

- Released from Mitochondria. *Nature* **2001**, *412*, 95–99, doi:10.1038/35083620.
47. Cory, S.; Adams, J.M. The Bcl2 Family: Regulators of the Cellular Life-or-Death Switch. *Nat. Rev. Cancer* **2002**, *2*, 647–656, doi:10.1038/nrc883.
48. Giménez-Cassina, A.; Danial, N.N. Regulation of Mitochondrial Nutrient and Energy Metabolism by BCL-2 Family Proteins. *Trends Endocrinol. Metab.* **2015**, *26*, 165–175, doi:10.1016/J.TEM.2015.02.004.
49. Strasser, A.; Vaux, D.L. Cell Death in the Origin and Treatment of Cancer. *Mol. Cell* **2020**, *78*, 1045–1054, doi:10.1016/J.MOLCEL.2020.05.014.
50. Espino, J.; Bejarano, I.; Redondo, P.C.; Rosado, J.A.; Barriga, C.; Reiter, R.J.; Pariente, J.A.; Rodríguez, A.B. Melatonin Reduces Apoptosis Induced by Calcium Signaling in Human Leukocytes: Evidence for the Involvement of Mitochondria and Bax Activation. *J. Membr. Biol.* **2010**, *233*, 105–118, doi:10.1007/S00232-010-9230-0.
51. Singh, R.; Letai, A.; Sarosiek, K. Regulation of Apoptosis in Health and Disease: The Balancing Act of BCL-2 Family Proteins. *Nat. Rev. Mol. Cell Biol.* **2019**, *20*, 175–193, doi:10.1038/s41580-018-0089-8.
52. Puthalakath, H.; Strasser, A. Keeping Killers on a Tight Leash: Transcriptional and Post-Translational Control of the pro-Apoptotic Activity of BH3-Only Proteins. *Cell Death Differ.* **2002**, *9*, 505–512, doi:10.1038/SJ.CDD.4400998.
53. Shibue, T.; Taniguchi, T. BH3-Only Proteins: Integrated Control Point of Apoptosis. *Int. J. Cancer* **2006**, *119*, 2036–2043, doi:10.1002/IJC.21751.
54. Esposti, M.D.; Erler, J.T.; Hickman, J.A.; Dive, C. Bid, a Widely Expressed Proapoptotic Protein of the Bcl-2 Family, Displays Lipid Transfer Activity. *Mol. Cell. Biol.* **2001**, *21*, 7268, doi:10.1128/MCB.21.21.7268-7276.2001.
55. Was, H.; Borkowska, A.; Bagues, A.; Tu, L.; Liu, J.Y.H.; Lu, Z.; Rudd, J.A.; Nurgali, K.; Abalo, R. Mechanisms of Chemotherapy-Induced Neurotoxicity. *Front. Pharmacol.* **2022**, *13*, 750507, doi:10.3389/fphar.2022.750507.
56. Barckhausen, C.; Roos, W.P.; Naumann, S.C.; Kaina, B. Malignant Melanoma Cells Acquire Resistance to DNA Interstrand Cross-Linking Chemotherapeutics by P53-Triggered Upregulation of DDB2/XPC-Mediated DNA Repair. *Oncogene* **2014**, *33*, 1964–1974, doi:10.1038/ONC.2013.141.
57. Shen, D.W.; Pouliot, L.M.; Hall, M.D.; Gottesman, M.M. Cisplatin Resistance: A Cellular Self-Defense Mechanism Resulting from Multiple Epigenetic and Genetic Changes. *Pharmacol. Rev.* **2012**, *64*, 706, doi:10.1124/PR.111.005637.

58. Kelland, L. The Resurgence of Platinum-Based Cancer Chemotherapy. *Nat. Rev. Cancer* **2007**, *7*, 573–584, doi:10.1038/NRC2167.
59. Dasari, S.; Bernard Tchounwou, P. Cisplatin in Cancer Therapy: Molecular Mechanisms of Action. *Eur. J. Pharmacol.* **2014**, *740*, 364–378, doi:10.1016/J.EJP HAR.2014.07.025.
60. Rosenberg, B.; Van Camp, L.; Krigas, T. Inhibition of Cell Division in Escherichia Coli by Electrolysis Products from a Platinum Electrode. *Nature* **1965**, *205*, 698–699, doi:10.1038/205698a0.
61. Discovery – Cisplatin and The Treatment of Testicular and Other Cancers - NCI Available online: <https://www.cancer.gov/research/progress/discovery/cisplatin> (accessed on 12 June 2023).
62. Lebwohl, D.; Canetta, R. Clinical Development of Platinum Complexes in Cancer Therapy: An Historical Perspective and an Update. *Eur. J. Cancer* **1998**, *34*, 1522–1534, doi:10.1016/S0959-8049(98)00224-X.
63. Desoize, B.; Madoulet, C. Particular Aspects of Platinum Compounds Used at Present in Cancer Treatment. *Crit. Rev. Oncol. Hematol.* **2002**, *42*, 317–325, doi:10.1016/S1040-8428(01)00219-0.
64. Kartalou, M.; Essigmann, J.M. Mechanisms of Resistance to Cisplatin. *Mutat. Res. - Fundam. Mol. Mech. Mutagen.* **2001**, *478*, 23–43, doi:10.1016/S0027-5107(01)00141-5.
65. Pariente, R.; Pariente, J.A.; Rodríguez, A.B.; Espino, J. Melatonin Sensitizes Human Cervical Cancer HeLa Cells to Cisplatin-Induced Cytotoxicity and Apoptosis: Effects on Oxidative Stress and DNA Fragmentation. *J. Pineal Res.* **2016**, *60*, 55–64, doi:10.1111/JPI.12288.
66. Pariente, R.; Bejarano, I.; Espino, J.; Rodríguez, A.B.; Pariente, J.A. Participation of MT3 Melatonin Receptors in the Synergistic Effect of Melatonin on Cytotoxic and Apoptotic Actions Evoked by Chemotherapeutics. *Cancer Chemother. Pharmacol.* **2017**, *80*, 985–998, doi:10.1007/S00280-017-3441-3.
67. Dilruba, S.; Kalayda, G. V. Platinum-Based Drugs: Past, Present and Future. *Cancer Chemother. Pharmacol.* **2016**, *77*, 1103–1124, doi:10.1007/S00280-016-2976-Z.
68. Wheate, N.J.; Walker, S.; Craig, G.E.; Oun, R. The Status of Platinum Anticancer Drugs in the Clinic and in Clinical Trials. *Dalton Trans.* **2010**, *39*, 8113–8127, doi:10.1039/C0DT00292E.

69. Monneret, C. Platinum Anticancer Drugs. From Serendipity to Rational Design. *Ann. Pharm. Fr.* **2011**, *69*, 286–295, doi:10.1016/J.PHARMA.2011.10.001.
70. Dabrowiak, J.C. *Metals in Medicine.*; John Wiley & Sons, Ed.; 2017;
71. Argyriou, A.A.; Polychronopoulos, P.; Iconomou, G.; Chroni, E.; Kalofonos, H.P. A Review on Oxaliplatin-Induced Peripheral Nerve Damage. *Cancer Treat. Rev.* **2008**, *34*, 368–377, doi:10.1016/J.CTRV.2008.01.003.
72. McWhinney, S.R.; Goldberg, R.M.; McLeod, H.L. Platinum Neurotoxicity Pharmacogenetics. *Mol. Cancer Ther.* **2009**, *8*, 10–16, doi:10.1158/1535-7163.MCT-08-0840.
73. Lazarević, T.; Rilak, A.; Bugarčić, Ž.D. Platinum, Palladium, Gold and Ruthenium Complexes as Anticancer Agents: Current Clinical Uses, Cytotoxicity Studies and Future Perspectives. *Eur. J. Med. Chem.* **2017**, *142*, 8–31, doi:10.1016/J.EJMECH.2017.04.007.
74. Hensing, T.A.; Hanna, N.H.; Gillenwater, H.H.; Gabriella Camboni, M.; Allievi, C.; Socinski, M.A. Phase II Study of BBR 3464 as Treatment in Patients with Sensitive or Refractory Small Cell Lung Cancer. *Anticancer. Drugs* **2006**, *17*, 697–704, doi:10.1097/01.CAD.0000215054.62942.7F.
75. U.S. National Institutes of Health. Clinical Trials Database, Clinicaltrials.Gov. Available Online Available online: <https://clinicaltrials.gov/> (accessed on 14 June 2023).
76. Lucaciu, R.L.; Hangan, A.C.; Sevastre, B.; Oprean, L.S. Metallo-Drugs in Cancer Therapy: Past, Present and Future. *Molecules* **2022**, *27*, 6485, doi:10.3390/MOLECULES27196485.
77. Treat, J.; Schiller, J.; Quoix, E.; Mauer, A.; Edelman, M.; Modiano, M.; Bonomi, P.; Ramlau, R.; Lemarie, E. ZD0473 Treatment in Lung Cancer: An Overview of the Clinical Trial Results. *Eur. J. Cancer* **2002**, *38*, S13–S18, doi:10.1016/S0959-8049(02)80016-8.
78. Gore, M.E.; Atkinson, R.J.; Thomas, H.; Cure, H.; Rischin, D.; Beale, P.; Bougnoux, P.; Dirix, L.; Smit, W.M. Results of ZD0473 in Platinum-Pretreated Ovarian Cancer: Analysis According to Platinum Free Interval. *Eur. J. Cancer* **2002**, *38*, S7–S12, doi:10.1016/S0959-8049(02)80014-4.
79. Gelmon, K.A.; Vandenberg, T.A.; Panasci, L.; Norris, B.; Crump, M.; Douglas, L.; Walsh, W.; Matthews, S.J.; Seymour, L.K. A Phase II Study of ZD0473 given as a Short Infusion Every 3 Weeks to Patients with Advanced or Metastatic Breast

- Cancer: A National Cancer Institute of Canada Clinical Trials Group Trial, IND 129. *Ann. Oncol. Off. J. Eur. Soc. Med. Oncol.* **2003**, *14*, 543–548, doi:10.1093/ANNONC/MDG171.
80. de Wit, R.; Tesselaar, M.; Kok, T.C.; Seynaeve, C.; Rodenburg, C.J.; Verweij, J.; Helle, P.A.; Stoter, G. Randomised Phase II Trial of Carboplatin and Iproplatin in Advanced Urothelial Cancer. *Eur. J. Cancer* **1991**, *27*, 1383–1385, doi:10.1016/0277-5379(91)90015-6.
81. Sessa, C.; Vermorken, J.; Renard, J.; Kaye, S.; Smith, D.; Ten Bokkel Huinink, W.; Cavalli, F.; Pinedo, H. Phase II Study of Iproplatin in Advanced Ovarian Carcinoma. *J. Clin. Oncol.* **1988**, *6*, 98–105, doi:10.1200/JCO.1988.6.1.98.
82. Ferraro, M.G.; Piccolo, M.; Misso, G.; Santamaria, R.; Irace, C. Bioactivity and Development of Small Non-Platinum Metal-Based Chemotherapeutics. *Pharmaceutics* **2022**, *14*, 954, doi:10.3390/pharmaceutics14050954.
83. Bai, L.; Gao, C.; Liu, Q.; Yu, C.; Zhang, Z.; Cai, L.; Yang, B.; Qian, Y.; Yang, J.; Liao, X. Research Progress in Modern Structure of Platinum Complexes. *Eur. J. Med. Chem.* **2017**, *140*, 349–382, doi:10.1016/J.EJMECH.2017.09.034.
84. Komeda, S.; Casini, A. Next-Generation Anticancer Metallodrugs. *Curr. Top. Med. Chem.* **2012**, *12*, 219–235, doi:10.2174/156802612799078964.
85. Chen, D.; Milacic, V.; Frezza, M.; Dou, Q. Metal Complexes, Their Cellular Targets and Potential for Cancer Therapy. *Curr. Pharm. Des.* **2009**, *15*, 777–791, doi:10.2174/138161209787582183.
86. Benjamin Garbutcheon-Singh, K.; P. Grant, M.; W. Harper, B.; M. Krause-Heuer, A.; Manohar, M.; Orkey, N.; R. Aldrich-Wright, J. Transition Metal Based Anticancer Drugs. *Curr. Top. Med. Chem.* **2011**, *11*, 521–542, doi:10.2174/156802611794785226.
87. Ott, I.; Gust, R. Non Platinum Metal Complexes as Anti-Cancer Drugs. *Arch. Pharm.* **2007**, *340*, 117–126, doi:10.1002/ARDP.200600151.
88. Kumar Singh, A.; Kumar, A.; Singh, H.; Sonawane, P.; Pathak, P.; Grishina, M.; Pal Yadav, J.; Verma, A.; Kumar, P. Metal Complexes in Cancer Treatment: Journey So Far. *Chem. Biodivers.* **2023**, *20*, e202300061, doi:10.1002/CBDV.202300061.
89. Liang, J.X.; Zhong, H.J.; Yang, G.; Vellaisamy, K.; Ma, D.L.; Leung, C.H. Recent Development of Transition Metal Complexes with in Vivo Antitumor Activity. *J. Inorg. Biochem.* **2017**, *177*, 276–286, doi:10.1016/J.JINORGBIO.2017.06.002.

90. Zeng, L.; Gupta, P.; Chen, Y.; Wang, E.; Ji, L.; Chao, H.; Chen, Z.S. The Development of Anticancer Ruthenium(II) Complexes: From Single Molecule Compounds to Nanomaterials. *Chem. Soc. Rev.* **2017**, *46*, 5771–5804, doi:10.1039/C7CS00195A.
91. Lee, S.Y.; Kim, C.Y.; Nam, T.G. Ruthenium Complexes as Anticancer Agents: A Brief History and Perspectives. *Drug Des. Devel. Ther.* **2020**, *14*, 5375, doi:10.2147/DDDT.S275007.
92. Riccardi, C.; Musumeci, D.; Trifuoggi, M.; Irace, C.; Paduano, L.; Montesarchio, D. Anticancer Ruthenium(III) Complexes and Ru(III)-Containing Nanoformulations: An Update on the Mechanism of Action and Biological Activity. *Pharmaceuticals* **2019**, *12*, 146, doi:10.3390/PH12040146.
93. Thota, S.; Rodrigues, D.A.; Crans, D.C.; Barreiro, E.J. Ru(II) Compounds: Next-Generation Anticancer Metallotherapeutics? *J. Med. Chem.* **2018**, *61*, 5805–5821, doi:10.1021/acs.jmedchem.7b01689.
94. Dragutan, I.; Dragutan, V.; Demonceau, A. Editorial of Special Issue Ruthenium Complex: The Expanding Chemistry of the Ruthenium Complexes. *Molecules* **2015**, *20*, 17244, doi:10.3390/MOLECULES200917244.
95. Levina, A.; Mitra, A.; Lay, P.A. Recent Developments in Ruthenium Anticancer Drugs. *Metallomics* **2009**, *1*, 458–470, doi:10.1039/B904071D.
96. Kostova, I. Ruthenium Complexes as Anticancer Agents. *Curr. Med. Chem.* **2006**, *13*, 1085–1107, doi:10.2174/092986706776360941.
97. Coverdale, J.P.C.; Laroiya-McCarron, T.; Romero-Canelón, I. Designing Ruthenium Anticancer Drugs: What Have We Learnt from the Key Drug Candidates? *Inorganics* **2019**, *7*, 31, doi:10.3390/INORGANICS7030031.
98. Alessio, E.; Messori, L. NAMI-A and KP1019/1339, Two Iconic Ruthenium Anticancer Drug Candidates Face-to-Face: A Case Story in Medicinal Inorganic Chemistry. *Molecules* **2019**, *24*, 1995, doi:10.3390/MOLECULES24101995.
99. Li, J.; Tian, M.; Tian, Z.; Zhang, S.; Yan, C.; Shao, C.; Liu, Z. Half-Sandwich Iridium(III) and Ruthenium(II) Complexes Containing P[^]P-Chelating Ligands: A New Class of Potent Anticancer Agents with Unusual Redox Features. *Inorg. Chem.* **2018**, *57*, 1705–1716, doi:10.1021/ACS.INORGCHEM.7B01959.
100. Li, Y.; Liu, B.; Xu, C.X.; He, L.; Wan, Y.C.; Ji, L.N.; Mao, Z.W. Mitochondria-Targeted Phosphorescent Cyclometalated Iridium(III) Complexes: Synthesis, Characterization, and Anticancer Properties. *J. Biol. Inorg. Chem.* **2020**, *25*, 597–

- 607, doi:10.1007/S00775-020-01783-2.
101. Ye, R.R.; Tan, C.P.; Ji, L.N.; Mao, Z.W. Coumarin-Appended Phosphorescent Cyclometalated Iridium(III) Complexes as Mitochondria-Targeted Theranostic Anticancer Agents. *Dalton Trans.* **2016**, *45*, 13042–13051, doi:10.1039/C6DT00601A.
 102. Liang, X.; Zhang, L.; Li, F.; Luan, S.; He, C.; Yin, L.; Yin, Z.; Zou, Y.; Yue, G.; Li, L.; et al. Autophagy-Regulating N-Heterocycles Derivatives as Potential Anticancer Agents. *Future Med. Chem.* **2020**, *12*, 223–242, doi:10.4155/FMC-2019-0294.
 103. Mirabelli, C.; Johnson, R.; Sung, C.; Faucette, L.; Muirhead, K.; Crooke, S. Evaluation of the in Vivo Antitumor Activity and in Vitro Cytotoxic Properties of Auranofin, a Coordinated Gold Compound, in Murine Tumor Models. *Cancer Res.* **1985**, *45*, 32–39.
 104. Zhang, X.; Selvaraju, K.; Saei, A.A.; D'Arcy, P.; Zubarev, R.A.; Arnér, E.S.; Linder, S. Repurposing of Auranofin: Thioredoxin Reductase Remains a Primary Target of the Drug. *Biochimie* **2019**, *162*, 46–54, doi:10.1016/J.BIOCHI.2019.03.015.
 105. Ott, I. On the Medicinal Chemistry of Gold Complexes as Anticancer Drugs. *Coord. Chem. Rev.* **2009**, *253*, 1670–1681, doi:10.1016/J.CCR.2009.02.019.
 106. Bertrand, B.; Williams, M.R.M.; Bochmann, M. Gold(III) Complexes for Antitumor Applications: An Overview. *Chemistry* **2018**, *24*, 11840–11851, doi:10.1002/CHEM.201800981.
 107. Zou, T.; Lum, C.T.; Lok, C.N.; Zhang, J.J.; Che, C.M. Chemical Biology of Anticancer Gold(III) and Gold(I) Complexes. *Chem. Soc. Rev.* **2015**, *44*, 8786–8801, doi:10.1039/C5CS00132C.
 108. Simpson, P. V.; Desai, N.M.; Casari, I.; Massi, M.; Falasca, M. Metal-Based Antitumor Compounds: Beyond Cisplatin. *Future Med. Chem.* **2019**, *11*, 119–135, doi:10.4155/FMC-2018-0248.
 109. Prince, S.; Mapolie, S.; Blanckenberg, A. Palladium-Based Anti-Cancer Therapeutics. *Encycl. Cancer* **2015**, 1–9, doi:10.1007/978-3-642-27841-9_7085-1.
 110. Gao, E.; Liu, C.; Zhu, M.; Lin, H.; Wu, Q.; Liu, L. Current Development of Pd(II) Complexes as Potential Antitumor Agents. *Anticancer. Agents Med. Chem.* **2009**, *9*, 356–368, doi:10.2174/1871520610909030356.

111. Czarnomysy, R.; Radomska, D.; Szewczyk, O.K.; Roszczenko, P.; Bielawski, K. Platinum and Palladium Complexes as Promising Sources for Antitumor Treatments. *Int. J. Mol. Sci.* **2021**, *22*, 8271, doi:10.3390/IJMS22158271.
112. Caires, A.C.F. Recent Advances Involving Palladium (II) Complexes for the Cancer Therapy. *Anticancer. Agents Med. Chem.* **2007**, *7*, 484–491, doi:10.2174/187152007781668661.
113. Carneiro, T.J.; Martins, A.S.; Marques, M.P.M.; Gil, A.M. Metabolic Aspects of Palladium(II) Potential Anti-Cancer Drugs. *Front. Oncol.* **2020**, *10*, 590970, doi:10.3389/FONC.2020.590970.
114. Alam, M.N.; Huq, F. Comprehensive Review on Tumour Active Palladium Compounds and Structure–Activity Relationships. *Coord. Chem. Rev.* **2016**, *316*, 36–67, doi:10.1016/J.CCR.2016.02.001.
115. Vojtek, M.; Marques, M.P.M.; Ferreira, I.M.P.L.V.O.; Mota-Filipe, H.; Diniz, C. Anticancer Activity of Palladium-Based Complexes against Triple-Negative Breast Cancer. *Drug Discov. Today* **2019**, *24*, 1044–1058, doi:10.1016/J.DRUDIS.2019.02.012.
116. Espino, J.; Fernández-Delgado, E.; Estirado, S.; de la Cruz-Martinez, F.; Villa-Caballar, S.; Viñuelas-Zahinos, E.; Luna-Giles, F.; Pariente, J.A.J.A. Synthesis and Structure of a New Thiazoline-Based Palladium(II) Complex That Promotes Cytotoxicity and Apoptosis of Human Promyelocytic Leukemia HL-60 Cells. *Sci. Rep.* **2020**, *10*, 16745, doi:10.1038/s41598-020-73488-0.
117. Kapdi, A.R.; Fairlamb, I.J.S. Anti-Cancer Palladium Complexes: A Focus on PdX₂L₂, Palladacycles and Related Complexes. *Chem. Soc. Rev.* **2014**, *43*, 4751–4777, doi:10.1039/C4CS00063C.
118. Kimani, S.; Chakraborty, S.; Irene, I.; de la Mare, J.; Edkins, A.; du Toit, A.; Loos, B.; Blanckenberg, A.; Van Niekerk, A.; Costa-Lotufo, L. V.; et al. The Palladacycle, BTC₂, Exhibits Anti-Breast Cancer and Breast Cancer Stem Cell Activity. *Biochem. Pharmacol.* **2021**, *190*, 114598, doi:10.1016/J.BCP.2021.114598.
119. Azzouzi, A.R.; Barret, E.; Bennet, J.; Moore, C.; Taneja, S.; Muir, G.; Villers, A.; Coleman, J.; Allen, C.; Scherz, A.; et al. TOOKAD® Soluble Focal Therapy: Pooled Analysis of Three Phase II Studies Assessing the Minimally Invasive Ablation of Localized Prostate Cancer. *World J. Urol.* **2015**, *33*, 945–953, doi:10.1007/S00345-015-1505-8.

120. Noweski, A.; Roosen, A.; Lebdai, S.; Barret, E.; Emberton, M.; Benzaghrou, F.; Apfelbeck, M.; Gaillac, B.; Gratzke, C.; Stief, C.; et al. Medium-Term Follow-up of Vascular-Targeted Photodynamic Therapy of Localized Prostate Cancer Using TOOKAD Soluble WST-11 (Phase II Trials). *Eur. Urol. Focus* **2019**, *5*, 1022–1028, doi:10.1016/J.EUF.2018.04.003.
121. Murray, K.S.; Winter, A.G.; Corradi, R.B.; LaRosa, S.; Jebiwott, S.; Somma, A.; Takaki, H.; Srimathveeravalli, G.; Lephherd, M.; Monette, S.; et al. Treatment Effects of WST11 Vascular Targeted Photodynamic Therapy for Urothelial Cell Carcinoma in Swine. *J. Urol.* **2016**, *196*, 236–243, doi:10.1016/J.JURO.2016.01.107.
122. Chiang, L.; Jones, M.R.; Ferreira, C.L.; Storr, T. Multifunctional Ligands in Medicinal Inorganic Chemistry- Current Trends and Future Directions. *Curr. Top. Med. Chem.* **2012**, *12*, 122–144, doi:10.2174/156802612799078973.
123. Klein, A.V.; Hambley, T.W. *Platinum-Based Anticancer Agents*; 2014; Vol. 9781118488; ISBN 9781118697191.
124. Dua, R.; Shrivastava, S.; Sonwane, S.K.; Srivastava, S.K. Pharmacological Significance of Synthetic Heterocycles Scaffold: A Review. *Adv. Biol. Res.* **2011**, *5*, 120–144.
125. Jampilek, J. Heterocycles in Medicinal Chemistry. *Molecules* **2019**, *24*, 3839, doi:10.3390/MOLECULES24213839.
126. Mahapatra, D.K.; Bharti, S.K.; Asati, V.; Singh, S.K. Perspectives of Medicinally Privileged Chalcone Based Metal Coordination Compounds for Biomedical Applications. *Eur. J. Med. Chem.* **2019**, *174*, 142–158, doi:10.1016/J.EJMECH.2019.04.032.
127. Sharma, P.K.; Amin, A.; Kumar, M. A Review: Medicinally Important Nitrogen Sulphur Containing Heterocycles. *Open Med. Chem. J.* **2020**, *14*, 49–64, doi:10.2174/1874104502014010049.
128. Kumar, A.; Singh, A.K.; Singh, H.; Vijayan, V.; Kumar, D.; Naik, J.; Thareja, S.; Yadav, J.P.; Pathak, P.; Grishina, M.; et al. Nitrogen Containing Heterocycles as Anticancer Agents: A Medicinal Chemistry Perspective. *Pharmaceuticals* **2023**, *16*, 299, doi:10.3390/PH16020299.
129. Faria, J.V.; Vegi, P.F.; Miguita, A.G.C.; dos Santos, M.S.; Boechat, N.; Bernardino, A.M.R. Recently Reported Biological Activities of Pyrazole Compounds. *Bioorg. Med. Chem.* **2017**, *25*, 5891–5903,

- doi:10.1016/J.BMC.2017.09.035.
130. Keter, F.K.; Darkwa, J. Perspective: The Potential of Pyrazole-Based Compounds in Medicine. *BioMetals* **2011**, *25*, 9–21, doi:10.1007/S10534-011-9496-4.
131. Han, F.S.; Osajima, H.; Cheung, M.; Tokuyama, H.; Fukuyama, T. Novel Structural Motifs Consisting of Chiral Thiazolines: Synthesis, Molecular Recognition, and Anticancer Activity. *Chemistry* **2007**, *13*, 3026–3038, doi:10.1002/CHEM.200601446.
132. Nagendra Prasad, T.; Eeda, K.R.; Gudise, V.B.; Basha, S.F.; Anwar, S. Design, Synthesis and Biological Evaluation of Substituted 2-Amino-1,3-Thiazine Derivatives as Antituberculosis and Anti-Cancer Agents. *Synth. Commun.* **2019**, *49*, 1277–1285, doi:10.1080/00397911.2019.1597125.
133. Ferreira, M.; Assunção, L.S.; Filippin-Monteiro, F.B.; Creczynski-Pasa, T.B.; Sá, M.M. Synthesis of 1,3-Thiazine-2,4-Diones with Potential Anticancer Activity. *Eur. J. Med. Chem.* **2013**, *70*, 411–418, doi:10.1016/J.EJMECH.2013.10.017.
134. Goodman & Gilman's: The Pharmacological Basis of Therapeutics, 13e | AccessMedicine | McGraw Hill Medical Available online: <https://accessmedicine.mhmedical.com/book.aspx?bookID=2189> (accessed on 24 April 2023).
135. Yamamoto, H.; Eikyu, Y.; Okuda, S.; Kawabata, K.; Takasugi, H.; Tanaka, H.; Matsumoto, S.; Matsumoto, Y.; Tawara, S. Orally Active Cephalosporins. Part 4: Synthesis, Structure-Activity Relationships and Oral Absorption of Novel 3-(4-Pyrazolylmethylthio)Cephalosporins with Various C-7 Side Chains. *Bioorganic Med. Chem.* **2002**, *10*, 1535–1545, doi:10.1016/S0968-0896(01)00416-3.
136. Bekhit, A.A.; Abdel-Aziem, T. Design, Synthesis and Biological Evaluation of Some Pyrazole Derivatives as Anti-Inflammatory-Antimicrobial Agents. *Bioorganic Med. Chem.* **2004**, *12*, 1935–1945, doi:10.1016/j.bmc.2004.01.037.
137. Bulman, R.A. *Structural Bonding*; 1987; Vol. 67;.
138. Ragavan, R.V.; Vijayakumar, V.; Suchetha Kumari, N. Synthesis and Antimicrobial Activities of Novel 1,5-Diaryl Pyrazoles. *Eur. J. Med. Chem.* **2010**, *45*, 1173, doi:10.1016/j.ejmech.2009.12.042.
139. Palomer, A.; Cabré, F.; Pascual, J.; Campos, J.; Trujillo, M.A.; Entrena, A.; Gallo, M.A.; García, L.; Mauleón, D.; Espinosa, A. Identification of Novel Cyclooxygenase-2 Selective Inhibitors Using Pharmacophore Models. *J. Med. Chem.* **2002**, *45*, 1402–1411, doi:10.1021/JM010458R.

140. Windholz, M. *The Merck Index*; Merck & Co., Ed.; 9^a.; Rahway, New Jersey., 1976;
141. Marchetti, F.; Pettinari, C.; Pettinari, R. Acylpyrazolone Ligands: Synthesis, Structures, Metal Coordination Chemistry and Applications. *Coord. Chem. Rev.* **2005**, *249*, 2909–2945, doi:10.1016/J.CCR.2005.03.013.
142. Casas, J.S.; Castellano, E.E.; Ellena, J.; García-Tasende, M.S.; Pérez-Parallé, M.L.; Sánchez, A.; Sánchez-González, Á.; Sordo, J.; Touceda, Á. New Pd(II) and Pt(II) Complexes with N,S-Chelated Pyrazolonate Ligands: Molecular and Supramolecular Structure and Preliminary Study of Their in Vitro Antitumoral Activity. *J. Inorg. Biochem.* **2008**, *102*, 33–45, doi:10.1016/J.JINORGBIO.2007.06.032.
143. Shaw, A.Y.; Liao, H.H.; Lu, P.J.; Yang, C.N.; Lee, C.H.; Chen, J.Y.; Xu, Z.; Flynn, G. 3,5-Diaryl-1H-Pyrazole as a Molecular Scaffold for the Synthesis of Apoptosis-Inducing Agents. *Bioorg. Med. Chem.* **2010**, *18*, 3270–3278, doi:10.1016/J.BMC.2010.03.016.
144. Lv, P.C.; Li, H.Q.; Sun, J.; Zhou, Y.; Zhu, H.L. Synthesis and Biological Evaluation of Pyrazole Derivatives Containing Thiourea Skeleton as Anticancer Agents. *Bioorg. Med. Chem.* **2010**, *18*, 4606–4614, doi:10.1016/J.BMC.2010.05.034.
145. Ciesielska, E.; Szulawska, A.; Studzian, K.; Ochocki, J.; Malinowska, K.; Kik, K.; Szmigiero, L. Comparative Studies on the Mechanism of Cytotoxic Action of Novel Platinum II Complexes with Pyrazole Ligands. *J. Inorg. Biochem.* **2006**, *100*, 1579–1585, doi:10.1016/J.JINORGBIO.2006.05.001.
146. Quirante, J.; Ruiz, D.; Gonzalez, A.; López, C.; Cascante, M.; Cortés, R.; Messeguer, R.; Calvis, C.; Baldomà, L.; Pascual, A.; et al. Platinum(II) and Palladium(II) Complexes with (N,N') and (C,N,N')- Ligands Derived from Pyrazole as Anticancer and Antimalarial Agents: Synthesis, Characterization and in Vitro Activities. *J. Inorg. Biochem.* **2011**, *105*, 1720–1728, doi:10.1016/J.JINORGBIO.2011.09.021.
147. Kasparkova, J.; Kosthunova, H.; Novohradsky, V.; Logvinov, A.A.; Temnov, V. V.; Borisova, N.E.; Podrugina, T.A.; Markova, L.; Starha, P.; Nazarov, A.A.; et al. Novel Cis-Pt(II) Complexes with Alkylpyrazole Ligands: Synthesis, Characterization, and Unusual Mode of Anticancer Action. *Bioinorg. Chem. Appl.* **2022**, *2022*, 1717200, doi:10.1155/2022/1717200.

148. Lunagariya, M. V.; Thakor, K.P.; Varma, R.R.; Waghela, B.N.; Pathak, C.; Patel, M.N. Synthesis, Characterization and Biological Application of 5-Quinoline 1,3,5-Trisubstituted Pyrazole Based Platinum(II) Complexes. *Medchemcomm* **2017**, *9*, 282–298, doi:10.1039/C7MD00472A.
149. Metzger, J. *Comprehensive Heterocyclic Chemistry*; Pergamon Press, Ed.; K.T. Potts, Ed.; Oxford, 1984; Vol. 4;.
150. Guiliano, M.; Mille, G.; Avignon, T.; Chouteau, J. Transfert Du Champ de Forces de La Thiazolidine: Analyse Vibrationnelle et Conformationnelle de Monomethyl Thiazolidines. *J. Raman Spectrosc.* **1978**, *7*, 214, doi:10.1016/0022-2860(78)80081-7.
151. Wipf, P.; Reeves, J.; Day, B. Chemistry and Biology of Curacin A. *Curr. Pharm. Des.* **2005**, *10*, 1417–1437, doi:10.2174/1381612043384853.
152. Brugarolas, A.; Gosálvez, M. Treatment of Cancer by an Inducer of Reverse Transformation. *Lancet* **1980**, *1*, 68–70, doi:10.1016/S0140-6736(80)90494-8.
153. Brugarolas, A.; Gosálvez, M. Preliminary Clinical Results with Norgamem (Thioprolone) and Revercan (2-Amino-2-Thiazoline): The First Inducers of Reverse Transformation. *Recent Results Cancer Res.* **1982**, *80*, 346–350, doi:10.1007/978-3-642-81685-7_56/COVER.
154. Dehand, J.; Jordanov, J.; Beck, J.P. Anti-Tumour Activity of Heavy Transition Metal Complexes against Hepatoma Cells. *Chem. Biol. Interact.* **1975**, *11*, 605–609, doi:10.1016/0009-2797(75)90035-6.
155. Chaviara, A.T.; Christidis, P.C.; Papageorgiou, A.; Chrysogelou, E.; Hadjipavlou-Litina, D.J.; Bolos, C.A. In Vivo Anticancer, Anti-Inflammatory, and Toxicity Studies of Mixed-Ligand Cu(II) Complexes of Dien and Its Schiff Bases with Heterocyclic Aldehydes and 2-Amino-2-Thiazoline. Crystal Structure of [Cu(Dien)(Br)(2a-2tzn)](Br)(H₂O). *J. Inorg. Biochem.* **2005**, *99*, 2102–2109, doi:10.1016/J.JINORGBIO.2005.07.011.
156. Bolos, C.A.; Papazisis, K.T.; Kortsaris, A.H.; Voyatzi, S.; Zambouli, D.; Kyriakidis, D.A. Antiproliferative Activity of Mixed-Ligand Dien-Cu(II) Complexes with Thiazole, Thiazoline and Imidazole Derivatives. *J. Inorg. Biochem.* **2002**, *88*, 25–36, doi:10.1016/S0162-0134(01)00344-0.
157. Salvador-Gil, D.; Herrera, R.P.; Gimeno, M.C. Catalysis-Free Synthesis of Thiazolidine–Thiourea Ligands for Metal Coordination (Au and Ag) and Preliminary Cytotoxic Studies. *Dalt. Trans.* **2023**, *52*, 7797–7808,

- doi:10.1039/D3DT00079F.
158. Fernández-Delgado, E.; de la Cruz-Martínez, F.; Galán, C.; Franco, L.; Espino, J.; Viñuelas-Zahinos, E.; Luna-Giles, F.; Bejarano, I. Pt(II) and Pd(II) Complexes with a Thiazoline Derivative Ligand: Synthesis, Structural Characterization, Antiproliferative Activity and Evaluation of pro-Apoptotic Ability in Tumor Cell Lines HT-29 and U-937. *J. Inorg. Biochem.* **2020**, *202*, 110870, doi:10.1016/j.jinorgbio.2019.110870.
159. Sainsbury, M. *Comprehensive Heterocyclic Chemistry*; Katritzky, A.R., Rees, C.W., Eds.; Pergamon Press: Oxford, 1984; Vol. 3.
160. Orlova, M.A.; Trofimova, T.P.; Filimonova, M.V.; Proshin, A.N.; Zaitsev, D. Effect of the Thiazine and Thiourea Derivatives as NO-Synthase Effectors on the Survival of Leukemic Cells. *Russ. Chem. Bull.* **2013**, *62*, 1111–1114, doi:10.1007/s11172-013-0150-x.
161. Jeleń, M.; Pluta, K.; Suwińska, K.; Morak-Młodawska, B.; Latocha, M.; Shkurenko, A. Quinonaphthothiazines, Syntheses, Structures and Anticancer Activities. *J. Mol. Struct.* **2015**, *1099*, 10–15, doi:10.1016/J.MOLSTRUC.2015.06.046.
162. Jeleń, M.; Pluta, K.; Latocha, M.; Morak-Młodawska, B.; Suwińska, K.; Kuśmierz, D. Evaluation of Angularly Condensed Diquinothiazines as Potential Anticancer Agents. *Bioorg. Chem.* **2019**, *87*, 810–820, doi:10.1016/J.BIOORG.2019.04.005.
163. Pomarnacka, E.; Gdaniec, M. Synthesis and Anticancer Activity of 2-Amino-8-Chloro-5,5-Dioxo[1,2,4]Triazolo[2,3-b][1,4,2]Benzodithiazine Derivatives. *Bioorganic Med. Chem.* **2003**, *11*, 1259–1267, doi:10.1016/S0968-0896(02)00638-7.
164. Pomarnacka, E.; Kornicka, A.; Kuchnio, A.; Heinrichs, M.; Grünert, R.; Gdaniec, M.; Bednarski, P.J. Synthesis, Cytotoxicity Testing, and Structure-Activity Relationships of Novel 6-Chloro-7-(4-Phenylimino-4H-3,1-Benzoxazin-2-Yl)-3-(Substituted)-1,4,2-Benzodithiazine 1,1-Dioxides. *Arch. Pharm.* **2011**, *344*, 431–441, doi:10.1002/ARDP.201000183.
165. Niewiadomy, A.; Matysiak, J.; Karpińska, M.M. Synthesis and Anticancer Activity of New 2-Aryl-4h-3,1-Benzothiazines. *Arch. Pharm.* **2011**, *344*, 224–230, doi:10.1002/ARDP.201000228.
166. Zięba, A.; Latocha, M.; Sochanik, A. Synthesis and in Vitro Antiproliferative Activity of Novel 12(H)-Quino[3,4- b][1,4]Benzothiazine Derivatives. *Med.*

- Chem. Res.* **2013**, *22*, 4158–4163, doi:10.1007/S00044-012-0384-4.
167. Jeleń, M.; Pluta, K.; Zimecki, M.; Morak-Młodawska, B.; Artym, J.; Kocięba, M.; Kochanowska, I. Synthesis and Biological Evaluation of Novel Propargylquinobenzothiazines and Their Derivatives as Potential Antiproliferative, Anti-Inflammatory, and Anticancer Agents. *J. Enzyme Inhib. Med. Chem.* **2016**, *31*, 83–88, doi:10.1080/14756366.2016.1205046.
168. Zieba, A.; Latocha, M.; Sochanik, A.; Nycz, A.; Kuśmierz, D. Synthesis and In Vitro Antiproliferative Activity of Novel Phenyl Ring-Substituted 5-Alkyl-12(H)-Quino[3,4-b][1,4]Benzothiazine Derivatives. *Molecules* **2016**, *21*, 1455, doi:10.3390/MOLECULES21111455.
169. Rai, A.; Singh, A.K.; Raj, V.; Saha, S. 1,4-Benzothiazines-A Biologically Attractive Scaffold. *Mini Rev. Med. Chem.* **2018**, *18*, 42–57, doi:10.2174/1389557517666170529075556.
170. Morak-Młodawska, B.; Pluta, K.; Latocha, M.; Suwińska, K.; Jeleń, M.; Kuśmierz, D. 3,6-Diazaphenothiazines as Potential Lead Molecules - Synthesis, Characterization and Anticancer Activity. *J. Enzyme Inhib. Med. Chem.* **2016**, *31*, 1512–1519, doi:10.3109/14756366.2016.1151014.
171. Morak-Młodawska, B.; Pluta, K.; Latocha, M.; Jeleń, M. Synthesis, Spectroscopic Characterization, and Anticancer Activity of New 10-Substituted 1,6-Diazaphenothiazines. *Med. Chem. Res.* **2016**, *25*, 2425–2433, doi:10.1007/S00044-016-1646-3.
172. Pluta, K.; Jeleń, M.; Morak-Młodawska, B.; Zimecki, M.; Artym, J.; Kocięba, M.; Zaczyńska, E. Azaphenothiazines - Promising Phenothiazine Derivatives. An Insight into Nomenclature, Synthesis, Structure Elucidation and Biological Properties. *Eur. J. Med. Chem.* **2017**, *138*, 774–806, doi:10.1016/J.EJMECH.2017.07.009.
173. Morak-Młodawska, B.; Pluta, K.; Latocha, M.; Jeleń, M.; Kuśmierz, D.; Suwińska, K.; Shkurenko, A.; Czuba, Z.; Jurzak, M. 10 H-1,9-Diazaphenothiazine and Its 10-Derivatives: Synthesis, Characterisation and Biological Evaluation as Potential Anticancer Agents. *J. Enzyme Inhib. Med. Chem.* **2019**, *34*, 1298–1306, doi:10.1080/14756366.2019.1639695.
174. Morak-Młodawska, B.; Jeleń, M.; Pluta, K. Phenothiazines Modified with the Pyridine Ring as Promising Anticancer Agents. *Life* **2021**, *11*, 1–18, doi:10.3390/LIFE11030206.

175. Gutiérrez-Tarriño, S.; Espino, J.; Luna-Giles, F.; Rodríguez, A.B.; Pariente, J.A.; Viñuelas-Zahinos, E.; Crisponi, G.; Dominguez-Martin, A. Synthesis, Characterization and Antiproliferative Evaluation of Pt(II) and Pd(II) Complexes with a Thiazine-Pyridine Derivative Ligand. *Pharmaceuticals* **2021**, *14*, 395, doi:10.3390/ph14050395.
176. Bernalte-García, A.; Lozano-Vila, A.M.; Luna-Giles, F.; Pedrero-Marín, R. Structural Characterization of a Thiazoline-Pyrazole Ligand and Its Complexes with Cobalt(II) and Copper(II). *Polyhedron* **2006**, *25*, 1399–1407, doi:10.1016/j.poly.2005.09.028.
177. Rosario Pedrero Marín Tesis Doctoral: Compuestos de Coordinación Derivados de Pirazol, 3,5-Dimetilpirazol y 2-Tiazolina e Iones de Metales Del Bloque D, Universidad de Extremadura: Badajoz, **2010**.
178. Torres García, P. Tesis Doctoral: Química de Coordinación de Ligandos Derivados de 1,3-Tiazina, Pirazol y Pirazol-3,5-Disustituidos. Consideraciones Estéricas., Universidad de Extremadura: Badajoz, **2010**.
179. Torres-García, P.; Pedrero-Marín, R.; Luna-Giles, F.; Huertas-Sánchez, A.V. V.; Viñuelas-Zahinos, E. Influence of Steric Strain of S,N-Heterocycles Derivative Ligands on the Coordination Geometry in Cadmium(II) Nitrate Complexes. *Polyhedron* **2012**, *31*, 307–318, doi:10.1016/j.poly.2011.09.033.
180. Torres-García, P.; Viñuelas-Zahinos, E.; Luna-Gilés, F.; Bernalte-García, A. Effects of the Substituents of Pyrazole / Thiazine Ligands on Nuclearity of Cu(II) Nitrate Complexes. *J. Coord. Chem.* **2012**, 37–41, doi:10.1080/00958972.2012.718764.
181. Pedrero-Marín, R.; Sánchez-Huertas, A. V.; Luna-Giles, F.; De La Cruz-Martínez, F.; Viñuelas-Zahinos, E. Substituent's Size in Pyrazole Derivative Ligands as Determining Factor on Nuclearity in Cu(II) Complexes. *Polyhedron* **2014**, *80*, 265–271, doi:10.1016/j.poly.2014.05.029.
182. Huertas-Sánchez, A. V.; Luna-Giles, F.; Viñuelas-Zahinos, E.; Barros-García, F.J.; Bernalte-García, A. Copper(II) Halide Coordination Complexes with 2-(3,5-Diphenyl-1-Pyrazolyl)-2-Thiazoline (DPhPyTn): Synthesis, Characterization and Crystal Structures. *Polyhedron* **2015**, *102*, 394–400, doi:10.1016/j.poly.2015.10.013.
183. Torres-García, P.; Luna-Giles, F.; Bernalte-García, Á.; Platas-Iglesias, C.; Esteban-Gómez, D.; Viñuelas-Zahinos, E. Effects of the Substituents of

- Pyrazole/Thiazine Ligands on the Magnetic Properties of Chloro-Bridged Cu(II) Complexes. *New J. Chem.* **2017**, *41*, 8818–8827, doi:10.1039/C7NJ01581J.
184. Torres-García, P.; Viñuelas-Zahínos, E.; Luna-Giles, F.; Espino, J.; Barros-García, F.J. Zinc(II) Complexes with Novel 1,3-Thiazine/Pyrazole Derivative Ligands: Synthesis, Structural Characterization and Effect of Coordination on the Phagocytic Activity of Human Neutrophils. *Polyhedron* **2011**, *30*, 2627–2636, doi:10.1016/j.poly.2011.07.014.
185. Torres-García, P.; Pedrero-Marín, R.; Luna-Giles, F.; Viñuelas-Zahínos, E.; Barros-García, F.J. Synthesis and Characterization of New Ni(II) Complexes with S,N-Heterocycle Ligands: Influence of the Steric Strain of Ligands on Coordination. *J. Coord. Chem.* **2011**, *64*, 3887–3899, doi:10.1080/00958972.2011.632414.
186. De la Cruz Martínez, F. Trabajo Fin de Máster: “Nuevos Compuestos de Coordinación Basados En Quimioterapéuticos de Pt(II),” Universidad de Extremadura, **2016**.
187. Khan, I.; Saeed, K.; Khan, I. Nanoparticles: Properties, Applications and Toxicities. *Arab. J. Chem.* **2019**, *12*, 908–931, doi:10.1016/J.ARABJC.2017.05.011.
188. Najahi-Missaoui, W.; Arnold, R.D.; Cummings, B.S. Safe Nanoparticles: Are We There Yet? *Int. J. Mol. Sci.* **2020**, *22*, 1–22, doi:10.3390/IJMS22010385.
189. Mitchell, M.J.; Billingsley, M.M.; Haley, R.M.; Wechsler, M.E.; Peppas, N.A.; Langer, R. Engineering Precision Nanoparticles for Drug Delivery. *Nat. Rev. Drug Discov.* **2020**, *20*, 101–124, doi:10.1038/s41573-020-0090-8.
190. Gavas, S.; Quazi, S.; Karpiński, T.M. Nanoparticles for Cancer Therapy: Current Progress and Challenges. *Nanoscale Res. Lett.* **2021**, *16*, 1–21, doi:10.1186/S11671-021-03628-6.
191. Fenton, O.S.; Olafson, K.N.; Pillai, P.S.; Mitchell, M.J.; Langer, R.; Fenton, O.S.; Olafson, K.N.; Pillai, P.S.; Langer, R.; Mitchell, M.J. Advances in Biomaterials for Drug Delivery. *Adv. Mater.* **2018**, *30*, 1705328, doi:10.1002/ADMA.201705328.
192. Fonseca-Santos, B.; Gremião, M.P.D.; Chorilli, M. Nanotechnology-Based Drug Delivery Systems for the Treatment of Alzheimer’s Disease. *Int. J. Nanomedicine* **2015**, *10*, 4981, doi:10.2147/IJN.S87148.
193. Alyautdin, R.; Khalin, I.; Nafeeza, M.I.; Haron, M.H.; Kuznetsov, D. Nanoscale

- Drug Delivery Systems and the Blood–Brain Barrier. *Int. J. Nanomedicine* **2014**, *9*, 795, doi:10.2147/IJN.S52236.
194. Berraondo, P.; Martini, P.G.V.; Avila, M.A.; Fontanellas, A. Messenger RNA Therapy for Rare Genetic Metabolic Diseases. *Gut* **2019**, *68*, 1323–1330, doi:10.1136/GUTJNL-2019-318269.
195. Jose, S.; Cinu, T.A.; Sebastian, R.; Shoja, M.H.; Aleykutty, N.A.; Durazzo, A.; Lucarini, M.; Santini, A.; Souto, E.B. Transferrin-Conjugated Docetaxel–PLGA Nanoparticles for Tumor Targeting: Influence on MCF-7 Cell Cycle. *Polymers (Basel)*. **2019**, *11*, 1905, doi:10.3390/POLYM11111905.
196. Liu, X.; Li, C.; Lv, J.; Huang, F.; An, Y.; Shi, L.; Ma, R. Glucose and H₂O₂ Dual-Responsive Polymeric Micelles for the Self-Regulated Release of Insulin. *ACS Appl. Bio Mater.* **2020**, *3*, 1598–1606, doi:10.1021/acsabm.9b01185.
197. Zelmer, C.; Zweifel, L.P.; Kapinos, L.E.; Craciun, I.; Güven, Z.P.; Palivan, C.G.; Lim, R.Y.H. Organelle-Specific Targeting of Polymersomes into the Cell Nucleus. *Proc. Natl. Acad. Sci. U. S. A.* **2020**, *117*, 2770–2778, doi:10.1073/pnas.1916395117.
198. Lee, S.W.; Kim, Y.M.; Cho, C.H.; Kim, Y.T.; Kim, S.M.; Hur, S.Y.; Kim, J.H.; Kim, B.G.; Kim, S.C.; Ryu, H.S.; et al. An Open-Label, Randomized, Parallel, Phase II Trial to Evaluate the Efficacy and Safety of a Cremophor-Free Polymeric Micelle Formulation of Paclitaxel as First-Line Treatment for Ovarian Cancer: A Korean Gynecologic Oncology Group Study (KGOG-3021). *Cancer Res. Treat.* **2018**, *50*, 195–203, doi:10.4143/CRT.2016.376.
199. Mendes, L.P.; Pan, J.; Torchilin, V.P. Dendrimers as Nanocarriers for Nucleic Acid and Drug Delivery in Cancer Therapy. *Molecules* **2017**, *22*, 1401, doi:10.3390/MOLECULES22091401.
200. Yang, W.; Liang, H.; Ma, S.; Wang, D.; Huang, J. Gold Nanoparticle Based Photothermal Therapy: Development and Application for Effective Cancer Treatment. *Sustain. Mater. Technol.* **2019**, *22*, e00109, doi:10.1016/J.SUSMAT.2019.E00109.
201. Bobo, D.; Robinson, K.J.; Islam, J.; Thurecht, K.J.; Corrie, S.R. Nanoparticle-Based Medicines: A Review of FDA-Approved Materials and Clinical Trials to Date. *Pharm. Res.* **2016**, *33*, 2373–2387, doi:10.1007/S11095-016-1958-5.
202. Xu, C.; Nam, J.; Hong, H.; Xu, Y.; Moon, J.J. Positron Emission Tomography-Guided Photodynamic Therapy with Biodegradable Mesoporous Silica

- Nanoparticles for Personalized Cancer Immunotherapy. *ACS Nano* **2019**, *13*, 12148–12161, doi:10.1021/ACSNANO.9B06691.
203. Wagner, A.M.; Knipe, J.M.; Orive, G.; Peppas, N.A. Quantum Dots in Biomedical Applications. *Acta Biomater.* **2019**, *94*, 44–63, doi:10.1016/J.ACTBIO.2019.05.022.
204. Yadav, A.; Singh, S.; Sohi, H.; Dang, S. Advances in Delivery of Chemotherapeutic Agents for Cancer Treatment. *AAPS PharmSciTech* **2022**, *23*, 1–14, doi:10.1208/S12249-021-02174-9/TABLES/5.
205. Rocha, M.; Chaves, N.; Bão, S.; Rocha, M.; Chaves, N.; Bão, S. Nanobiotechnology for Breast Cancer Treatment. *Breast Cancer - From Biol. to Med.* **2017**, doi:10.5772/66989.
206. Yan, L.; Shen, J.; Wang, J.; Yang, X.; Dong, S.; Lu, S. Nanoparticle-Based Drug Delivery System: A Patient-Friendly Chemotherapy for Oncology. *Dose-Response* **2020**, *18*, 1559325820936161, doi:10.1177/1559325820936161.
207. Janjua, T.I.; Cao, Y.; Yu, C.; Popat, A. Clinical Translation of Silica Nanoparticles. *Nat. Rev. Mater.* **2021**, *6*, 1072–1074, doi:10.1038/s41578-021-00385-x.
208. Farjadian, F.; Roointan, A.; Mohammadi-Samani, S.; Hosseini, M. Mesoporous Silica Nanoparticles: Synthesis, Pharmaceutical Applications, Biodistribution, and Biosafety Assessment. *Chem. Eng. J.* **2019**, *359*, 684–705, doi:10.1016/J.CEJ.2018.11.156.
209. Wang, Y.; Zhao, Q.; Han, N.; Bai, L.; Li, J.; Liu, J.; Che, E.; Hu, L.; Zhang, Q.; Jiang, T.; et al. Mesoporous Silica Nanoparticles in Drug Delivery and Biomedical Applications. *Nanomedicine Nanotechnology, Biol. Med.* **2015**, *11*, 313–327, doi:10.1016/j.nano.2014.09.014.
210. Lee, N.-K.; Park, S.S.; Ha, C.-S. PH-Sensitive Drug Delivery System Based on Mesoporous Silica Modified with Poly-L-Lysine (PLL) as a Gatekeeper. *J. Nanosci. Nanotechnol.* **2020**, *20*, 6925–6934, doi:10.1166/JNN.2020.18821.
211. Cai, D.; Han, C.; Liu, C.; Ma, X.; Qian, J.; Zhou, J.; Li, Y.; Sun, Y.; Zhang, C.; Zhu, W. Chitosan-Capped Enzyme-Responsive Hollow Mesoporous Silica Nanoplatforams for Colon-Specific Drug Delivery. *Nanoscale Res. Lett.* **2020**, *15*, 123, doi:10.1186/S11671-020-03351-8.
212. Wagner, V.; Dullaart, A.; Bock, A.K.; Zweck, A. The Emerging Nanomedicine Landscape. *Nat. Biotechnol.* *2006* *2410* **2006**, *24*, 1211–1217, doi:10.1038/nbt1006-1211.

213. Kundu, M.; Chatterjee, S.; Ghosh, N.; Manna, P.; Das, J.; Sil, P.C. Tumor Targeted Delivery of Umbelliferone via a Smart Mesoporous Silica Nanoparticles Controlled-Release Drug Delivery System for Increased Anticancer Efficiency. *Mater. Sci. Eng. C. Mater. Biol. Appl.* **2020**, *116*, 111239, doi:10.1016/J.MSEC.2020.111239.
214. Lu, J.; Liong, M.; Zink, J.I.; Tamanoi, F. Mesoporous Silica Nanoparticles as a Delivery System for Hydrophobic Anticancer Drugs. *Small* **2007**, *3*, 1341–1346, doi:10.1002/SMLL.200700005.
215. Koochi Moftakhari Esfahani, M.; Alavi, S.E.; Cabot, P.J.; Islam, N.; Izake, E.L. Application of Mesoporous Silica Nanoparticles in Cancer Therapy and Delivery of Repurposed Anthelmintics for Cancer Therapy. *Pharmaceutics* **2022**, *14*, 1579, doi:10.3390/PHARMACEUTICS14081579.
216. Zhang, Y.; Wang, J.; Bai, X.; Jiang, T.; Zhang, Q.; Wang, S. Mesoporous Silica Nanoparticles for Increasing the Oral Bioavailability and Permeation of Poorly Water Soluble Drugs. *Mol. Pharm.* **2012**, *9*, 505–513, doi:10.1021/mp200287c.
217. Sarkar, A.; Ghosh, S.; Chowdhury, S.; Pandey, B.; Sil, P.C. Targeted Delivery of Quercetin Loaded Mesoporous Silica Nanoparticles to the Breast Cancer Cells. *Biochim. Biophys. Acta* **2016**, *1860*, 2065–2075, doi:10.1016/J.BBAGEN.2016.07.001.
218. He, Y.; Liang, S.; Long, M.; Xu, H. Mesoporous Silica Nanoparticles as Potential Carriers for Enhanced Drug Solubility of Paclitaxel. *Mater. Sci. Eng. C. Mater. Biol. Appl.* **2017**, *78*, 12–17, doi:10.1016/J.MSEC.2017.04.049.
219. Jia, L.; Shen, J.; Li, Z.; Zhang, D.; Zhang, Q.; Liu, G.; Zheng, D.; Tian, X. In Vitro and in Vivo Evaluation of Paclitaxel-Loaded Mesoporous Silica Nanoparticles with Three Pore Sizes. *Int. J. Pharm.* **2013**, *445*, 12–19, doi:10.1016/J.IJPHARM.2013.01.058.
220. Meka, A.K.; Jenkins, L.J.; Dávalos-Salas, M.; Pujara, N.; Wong, K.Y.; Kumeria, T.; Mariadason, J.M.; Papat, A. Enhanced Solubility, Permeability and Anticancer Activity of Vorinostat Using Tailored Mesoporous Silica Nanoparticles. *Pharmaceutics* **2018**, *10*, 283, doi:10.3390/PHARMACEUTICS10040283.
221. He, H.; Xiao, H.; Kuang, H.; Xie, Z.; Chen, X.; Jing, X.; Huang, Y. Synthesis of Mesoporous Silica Nanoparticle–Oxaliplatin Conjugates for Improved Anticancer Drug Delivery. *Colloids Surfaces B Biointerfaces* **2014**, *117*, 75–81, doi:10.1016/J.COLSURFB.2014.02.014.

222. Li, T.; Chen, X.; Liu, Y.; Fan, L.; Lin, L.; Xu, Y.; Chen, S.; Shao, J. PH-Sensitive Mesoporous Silica Nanoparticles Anticancer Prodrugs for Sustained Release of Ursolic Acid and the Enhanced Anti-Cancer Efficacy for Hepatocellular Carcinoma. *Cancer. Eur. J. Pharm. Sci.* **2017**, *96*, 456–463, doi:10.1016/J.EJPS.2016.10.019.
223. Alvarez-Berríos, M.P.; Vivero-Escoto, J.L. In Vitro Evaluation of Folic Acid-Conjugated Redox-Responsive Mesoporous Silica Nanoparticles for the Delivery of Cisplatin. *Int. J. Nanomedicine* **2016**, *11*, 6251–6265, doi:10.2147/IJN.S118196.
224. Marinheiro, D.; Ferreira, B.J.M.L.; Oskoei, P.; Oliveira, H.; Daniel-da-silva, A.L. Encapsulation and Enhanced Release of Resveratrol from Mesoporous Silica Nanoparticles for Melanoma Therapy. *Mater.* **2021**, *14*, 1–18, doi:10.3390/MA14061382.
225. Lin, M.; Yao, W.; Xiao, Y.; Dong, Z.; Huang, W.; Zhang, F.; Zhou, X.; Liang, M. Resveratrol-Modified Mesoporous Silica Nanoparticle for Tumor-Targeted Therapy of Gastric Cancer. *Bioengineered* **2021**, *12*, 6343–6353, doi:10.1080/21655979.2021.1971507.
226. Li, H.; Yu, H.; Zhu, C.; Hu, J.; Du, M.; Zhang, F.; Yang, D. Cisplatin and Doxorubicin Dual-Loaded Mesoporous Silica Nanoparticles for Controlled Drug Delivery. *RSC Adv.* **2016**, *6*, 94160–94169, doi:10.1039/c6ra17213j.
227. Fröhlich, E. The Role of Surface Charge in Cellular Uptake and Cytotoxicity of Medical Nanoparticles. *Int. J. Nanomedicine* **2012**, *7*, 5577–5591, doi:10.2147/IJN.S36111.
228. Sahay, G.; Alakhova, D.Y.; Kabanov, A. V. Endocytosis of Nanomedicines. *J. Control. Release* **2010**, *145*, 182–195, doi:10.1016/J.JCONREL.2010.01.036.
229. Rastegari, E.; Hsiao, Y.-J.; Lai, W.-Y.; Lai, Y.-H.; Yang, T.-C.; Chen, S.-J.; Huang, P.-I.; Chiou, S.-H.; Mou, C.-Y.; Chien, Y.; et al. An Update on Mesoporous Silica Nanoparticle Applications in Nanomedicine. *Pharmaceutics* **2021**, *13*, 1067, doi:10.3390/PHARMACEUTICS13071067.
230. Yamada, H.; Urata, C.; Aoyama, Y.; Osada, S.; Yamauchi, Y.; Kuroda, K. Preparation of Colloidal Mesoporous Silica Nanoparticles with Different Diameters and Their Unique Degradation Behavior in Static Aqueous Systems. *Chem. Mater.* **2012**, *24*, 1462–1471, doi:10.1021/CM3001688/SUPPL_FILE/CM3001688_SI_001.PDF.

231. Jurkić, L.M.; Ceganec, I.; Pavelić, S.K.; Pavelić, K. Biological and Therapeutic Effects of Ortho-Silicic Acid and Some Ortho-Silicic Acid-Releasing Compounds: New Perspectives for Therapy. *Nutr. Metab.* **2013**, *10*, 1–12, doi:10.1186/1743-7075-10-2/FIGURES/6.
232. Cauda, V.; Schlossbauer, A.; Bein, T. Bio-Degradation Study of Colloidal Mesoporous Silica Nanoparticles: Effect of Surface Functionalization with Organo-Silanes and Poly(Ethylene Glycol). *Microporous Mesoporous Mater.* **2010**, *132*, 60–71, doi:10.1016/J.MICROMESO.2009.11.015.
233. He, Q.; Zhang, Z.; Gao, F.; Li, Y.; Shi, J. In Vivo Biodistribution and Urinary Excretion of Mesoporous Silica Nanoparticles: Effects of Particle Size and PEGylation. *Small* **2011**, *7*, 271–280, doi:10.1002/SMLL.201001459.
234. Kempen, P.J.; Greasley, S.; Parker, K.A.; Campbell, J.L.; Chang, H.Y.; Jones, J.R.; Sinclair, R.; Gambhir, S.S.; Jokerst, J. V. Theranostic Mesoporous Silica Nanoparticles Biodegrade after Pro-Survival Drug Delivery and Ultrasound/Magnetic Resonance Imaging of Stem Cells. *Theranostics* **2015**, *5*, 631, doi:10.7150/THNO.11389.
235. Choi, Y.; Lee, J.E.; Lee, J.H.; Jeong, J.H.; Kim, J. A Biodegradation Study of SBA-15 Microparticles in Simulated Body Fluid and in Vivo. *Langmuir* **2015**, *31*, 6457–6462, doi:10.1021/acs.langmuir.5b01316.
236. Souris, J.S.; Lee, C.H.; Cheng, S.H.; Chen, C.T.; Yang, C.S.; Ho, J. an A.; Mou, C.Y.; Lo, L.W. Surface Charge-Mediated Rapid Hepatobiliary Excretion of Mesoporous Silica Nanoparticles. *Biomaterials* **2010**, *31*, 5564–5574, doi:10.1016/J.BIOMATERIALS.2010.03.048.
237. Rosenholm, J.M.; Mamaeva, V.; Sahlgren, C.; Lindén, M. Nanoparticles in Targeted Cancer Therapy: Mesoporous Silica Nanoparticles Entering Preclinical Development Stage. *Nanomedicine* **2011**, *7*, 111–120, doi:10.2217/NNM.11.166.
238. Diab, R.; Canilho, N.; Pavel, I.A.; Haffner, F.B.; Girardon, M.; Pasc, A. Silica-Based Systems for Oral Delivery of Drugs, Macromolecules and Cells. *Adv. Colloid Interface Sci.* **2017**, *249*, 346–362, doi:10.1016/J.CIS.2017.04.005.
239. Shi, Y.; Miller, M.L.; Di Pasqua, A.J. Biocompatibility of Mesoporous Silica Nanoparticles? *Comments Inorg. Chem.* **2015**, *36*, 61–80, doi:10.1080/02603594.2015.1088439.
240. Sergent, J.A.; Paget, V.; Chevillard, S. Toxicity and Genotoxicity of Nano-SiO₂ on Human Epithelial Intestinal HT-29 Cell Line. *Ann. Occup. Hyg.* **2012**, *56*, 622–

- 630, doi:10.1093/ANNHYG/MES005.
241. Lu, J.; Liong, M.; Li, Z.; Zink, J.I.; Tamanoi, F. Biocompatibility, Biodistribution, and Drug-Delivery Efficiency of Mesoporous Silica Nanoparticles for Cancer Therapy in Animals. *Small* **2010**, *6*, 1794–1805, doi:10.1002/SMLL.201000538.
242. Tarn, D.; Ashley, C.E.; Xue, M.; Carnes, E.C.; Zink, J.I.; Brinker, C.J. Mesoporous Silica Nanoparticle Nanocarriers: Biofunctionality and Biocompatibility. *Acc. Chem. Res.* **2013**, *46*, 792–801, doi:10.1021/ar3000986.
243. Wisher, D. Martindale: The Complete Drug Reference. 37th Ed. *J. Med. Libr. Assoc.* **2012**, *100*, 75, doi:10.3163/1536-5050.100.1.018.
244. Price, J.H.; Williamson, A.N.; Schramm, R.F.; Wayland, B.B. Palladium(II) and Platinum(II) Alkyl Sulfoxide Complexes. Examples of Sulfur-Bonded, Mixed Sulfur- and Oxygen-Bonded, and Totally Oxygen-Bonded Complexes. *Inorg. Chem.* **1972**, *11*, 1280–1284, doi:10.1021/ic50112a025.
245. Bruker, A.X.S.I. SADABS, Madison, WI, **2012**.
246. Sheldrick, M. SHELXS-14, Program for Crystal Structures Solution, University of Göttingen, **2014**.
247. Sheldrick, G.M. Crystal Structure Refinement with SHELXL. *Acta Crystallogr. Sect. C* **2015**, *71*, 3–8, doi:10.1107/S2053229614024218.
248. Farrugia, L.J. WinGX and ORTEP for Windows: An Update. *J. Appl. Crystallogr.* **2012**, *45*, 849–854, doi:10.1107/S0021889812029111.
249. Macrae C.F.; Bruno I.J.; Chisholm J.A.; Edgington P.R.; McCabe P.; Pidcock E.; Rodríguez-Monje L.; Taylor R.; Van de Streek J.; P.A. Wood P.A. Mercury. *J. Appl. Crystallogr.* **2008**, *41*, 466–470, doi:doi.org/10.1107/S0021889807067908.
250. Cason C. POV-Ray for Windows, Versión 3.5.Icl.Win32, 1991-2002 Persistence of Vision Team.
251. Espino, J.; Rodríguez, A.B.; Pariente, J.A. The Inhibition of TNF- α -Induced Leucocyte Apoptosis by Melatonin Involves Membrane Receptor MT1/MT2 Interaction. *J. Pineal Res.* **2013**, *54*, 442–452, doi:10.1111/jpi.12042.
252. Bruno, I.J.; Cole, J.C.; Edgington, P.R.; Kessler, M.; Macrae, C.F.; McCabe, P.; Pearson, J.; Taylor, R. New Software for Searching the Cambridge Structural Database and Visualizing Crystal Structures. *Acta Crystallogr. Sect. B Struct. Sci.* **2002**, *58*, 389–397, doi:10.1107/S0108768102003324.
253. Ocansey, E.; Darkwa, J.; Makhubela, B.C.E. Bis(Pyrazolyl)Palladium(II) Complexes as Catalysts for Mizoroki–Heck Cross-Coupling Reactions.

- Polyhedron* **2019**, *166*, 52–59, doi:10.1016/j.poly.2019.03.030.
254. Zulu, S.; Alam, M.; Ojwach, S.O.; Akerman, M.P.; Stephen Ojwach, C.O.; Address, P. Structural and Theoretical Studies of the Methoxycarbonylation of Higher Olefins Catalysed by (Pyrazolyl-Ethyl)Pyridine Palladium (II) Complexes. *Appl Organometal Chem.* **2019**, *33*, e5175, doi:10.1002/aoc.5175.
255. Malešević, N.; Srdić, T.; Radulović, S.; Sladić, D.; Radulović, V.; Brčeski, I.; Anđelković, K. Synthesis and Characterization of a Novel Pd(II) Complex with the Condensation Product of 2-(Diphenylphosphino)Benzaldehyde and Ethyl Hydrazinoacetate. Cytotoxic Activity of the Synthesized Complex and Related Pd(II) and Pt(II) Complexes. *J. Inorg. Biochem.* **2006**, *100*, 1811–1818, doi:10.1016/J.JINORGBIO.2006.07.002.
256. Gligorijević, N.; Todorović, T.; Radulović, S.; Sladić, D.; Filipović, N.; Godevac, D.; Jeremić, D.; Anđelković, K. Synthesis and Characterization of New Pt(II) and Pd(II) Complexes with 2-Quinolinecarboxaldehyde Selenosemicarbazone: Cytotoxic Activity Evaluation of Cd(II), Zn(II), Ni(II), Pt(II) and Pd(II) Complexes with Heteroaromatic Selenosemicarbazones. *Eur. J. Med. Chem.* **2009**, *44*, 1623–1629, doi:10.1016/J.EJMECH.2008.07.033.
257. Mašković, J.M.; Hatzidimitriou, A.; Damjanović, A.; Stanojković, T.P.; Trifunović, S.R.; Geronikaki, A.A.; Papagiannopoulou, D. MedChemComm Synthesis, Characterization and Biological Evaluation of Pd(II), Cu(II), Re(I) and ^{99m}Tc(I) Thiazole-Based Complexes. *Cite this Med. Chem. Commun* **2018**, *9*, 831, doi:10.1039/c8md00067k.
258. Omondi, R.O.; Bellam, R.; Ojwach, S.O.; Jaganyi, D.; Fatokun, A.A. Palladium(II) Complexes of Tridentate Bis(Benzazole) Ligands: Structural, Substitution Kinetics, DNA Interactions and Cytotoxicity Studies. *J. Inorg. Biochem.* **2020**, *210*, 111156, doi:10.1016/J.JINORGBIO.2020.111156.
259. Zafar, M.N.; Butt, A.M.; Chaudhry, G. e. S.; Perveen, F.; Nazar, M.F.; Masood, S.; Dalebrook, A.F.; Mughal, E.U.; Sumrra, S.H.; Sung, Y.Y.; et al. Pd(II) Complexes with Chelating N-(1-Alkylpyridin-4(1H)-Ylidene)Amide (PYA) Ligands: Synthesis, Characterization and Evaluation of Anticancer Activity. *J. Inorg. Biochem.* **2021**, *224*, 111590, doi:10.1016/J.JINORGBIO.2021.111590.
260. He, Y.; Luo, L.; Liang, S.; Long, M.; Xu, H. Amino-Functionalized Mesoporous Silica Nanoparticles as Efficient Carriers for Anticancer Drug Delivery. *J. Biomater. Appl.* **2017**, *32*, 524–532, doi:10.1177/0885328217724638.

261. Gou, K.; Wang, Y.; Guo, X.; Wang, Y.; Bian, Y.; Zhao, H.; Guo, Y.; Pang, Y.; Xie, L.; Li, S.; et al. Carboxyl-Functionalized Mesoporous Silica Nanoparticles for the Controlled Delivery of Poorly Water-Soluble Non-Steroidal Anti-Inflammatory Drugs. *Acta Biomater.* **2021**, *134*, 576–592, doi:10.1016/J.ACTBIO.2021.07.023.
262. Braun, K.; Stürzel, C.M.; Biskupek, J.; Kaiser, U.; Kirchhoff, F.; Lindén, M. Comparison of Different Cytotoxicity Assays for in Vitro Evaluation of Mesoporous Silica Nanoparticles. *Toxicol. Vitro.* **2018**, *52*, 214–221, doi:10.1016/j.tiv.2018.06.019.
263. Fisichella, M.; Dabboue, H.; Bhattacharyya, S.; Saboungi, M.L.; Salvetat, J.P.; Hevor, T.; Guerin, M. Mesoporous Silica Nanoparticles Enhance MTT Formazan Exocytosis in HeLa Cells and Astrocytes. *Toxicol. In Vitro* **2009**, *23*, 697–703, doi:10.1016/J.TIV.2009.02.007.
264. Side Effects of Cancer Treatment - NCI Available online: <https://www.cancer.gov/about-cancer/treatment/side-effects> (accessed on 10 July 2023).
265. Carland, M.; Grannas, M.J.; Cairns, M.J.; Roknic, V.J.; Denny, W.A.; McFadyen, W.D.; Murray, V. Substituted 9-Aminoacridine-4-Carboxamides Tethered to Platinum(II)Diamine Complexes: Chemistry, Cytotoxicity and DNA Sequence Selectivity. *J. Inorg. Biochem.* **2010**, *104*, 815–819, doi:10.1016/J.JINORGBIO.2010.03.011.
266. Segapelo, T. V.; Guzei, I.A.; Spencer, L.C.; Van Zyl, W.E.; Darkwa, J. (Pyrazolylmethyl)Pyridine Platinum(II) and Gold(III) Complexes: Synthesis, Structures and Evaluation as Anticancer Agents. *Inorganica Chim. Acta* **2009**, *362*, 3314–3324, doi:10.1016/J.ICA.2009.02.046.
267. Eren, G.; Yilmaz, S.; Gumus, F. In Vitro Cytotoxic Activities of Platinum(II) Complex with 1-Methyl-2-(3'-Hydroxypropyl)Benzimidazole and 2-(3'-Hydroxypropyl)Benzimidazolium Hexa- and Tetrachloroplatinate Salts. *Lett. Drug Des. Discov.* **2017**, *15*, 65–69, doi:10.2174/1570180814666171012163325.
268. Xu, G.; Yan, Z.; Wang, N.; Liu, Z. Synthesis and Cytotoxicity of Cis-Dichloroplatinum (II) Complexes of (1S,3S)-1,2,3,4-Tetrahydroisoquinolines. *Eur. J. Med. Chem.* **2011**, *46*, 356–363, doi:10.1016/J.EJMECH.2010.11.025.
269. Württenberger, I.; Angermaier, B.; Kircher, B.; Gust, R. Synthesis and in Vitro Pharmacological Behavior of Platinum(II) Complexes Containing 1,2-Diamino-1-

- (4-Fluorophenyl)-2-Alkanol Ligands. *J. Med. Chem.* **2013**, *56*, 7951–7964, doi:https://doi.org/10.1021/jm400967z.
270. Moradell, S.; Lorenzo, J.; Rovira, A.; Robillard, M.S.; Avilés, F.X.; Moreno, V.; De Llorens, R.; Martínez, M.A.; Reedijk, J.; Llobet, A. Platinum Complexes of Diaminocarboxylic Acids and Their Ethyl Ester Derivatives: The Effect of the Chelate Ring Size on Antitumor Activity and Interactions with GMP and DNA. *J. Inorg. Biochem.* **2003**, *96*, 493–502, doi:10.1016/S0162-0134(03)00252-6.
271. Moradell, S.; Lorenzo, J.; Rovira, A.; Van Zutphen, S.; Avilés, F.X.; Moreno, V.; De Llorens, R.; Martínez, M.A.; Reedijk, J.; Llobet, A. Water-Soluble Platinum(II) Complexes of Diamine Chelating Ligands Bearing Amino-Acid Type Substituents: The Effect of the Linked Amino Acid and the Diamine Chelate Ring Size on Antitumor Activity, and Interactions with 5'-GMP and DNA. *J. Inorg. Biochem.* **2004**, *98*, 1933–1946, doi:10.1016/J.JINORGBIO.2004.08.011.
272. Keter, F.K.; Kanyanda, S.; Lyantagaye, S.S.L.; Darkwa, J.; Rees, D.J.G.; Meyer, M. In Vitro Evaluation of Dichloro-Bis(Pyrazole)Palladium(II) and Dichloro-Bis(Pyrazole)Platinum(II) Complexes as Anticancer Agents. *Cancer Chemother. Pharmacol.* **2008**, *63*, 127–138, doi:10.1007/S00280-008-0721-Y/FIGURES/6.
273. Pérez-Arnaiz, C.; Leal, J.; Busto, N.; Carrión, M.C.; Rubio, A.R.; Ortiz, I.; Barone, G.; Díaz De Greñu, B.; Santolaya, J.; Leal, J.M.; et al. Role of Seroalbumin in the Cytotoxicity of Cis-Dichloro Pt(II) Complexes with (N[^]N)-Donor Ligands Bearing Functionalized Tails. *Inorg. Chem.* **2018**, *57*, 6124–6134, doi:doi.org/10.1021/acs.inorgchem.8b00713.
274. Marzano, C.; Sbovata, S.M.; Gandin, V.; Michelin, R.A.; Venzo, A.; Bertani, R.; Seraglia, R. Cytotoxicity of Cis-Platinum(II) Cycloaliphatic Amidine Complexes: Ring Size and Solvent Effects on the Biological Activity. *J. Inorg. Biochem.* **2009**, *103*, 1113–1119, doi:10.1016/J.JINORGBIO.2009.05.009.
275. Kuo, C.Y.; Wu, M.J.; Lin, C.C. Synthesis and Antitumor Activity of Cis-Dichloridoplatinum(II) Complexes of 1,1'-Biisoquinolines. *Eur. J. Med. Chem.* **2010**, *45*, 55–62, doi:10.1016/J.EJMECH.2009.09.023.
276. D'errico, S.; Falanga, A.P.; Capasso, D.; Gaetano, S. Di; Marzano, M.; Terracciano, M.; Roviello, G.N.; Piccialli, G.; Oliviero, G.; Borbone, N. Probing the DNA Reactivity and the Anticancer Properties of a Novel Tubercidin-Pt(II) Complex. *Pharm.* **2020**, *Vol. 12*, *Page 627* **2020**, *12*, 627, doi:10.3390/PHARMACEUTICS12070627.

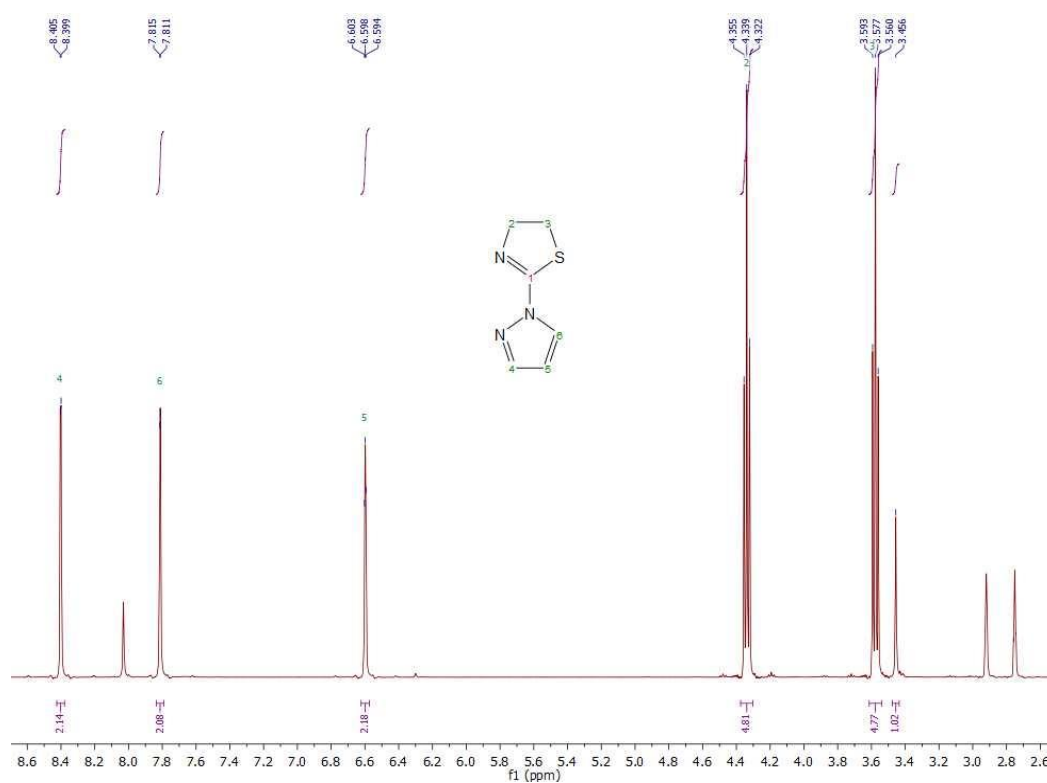
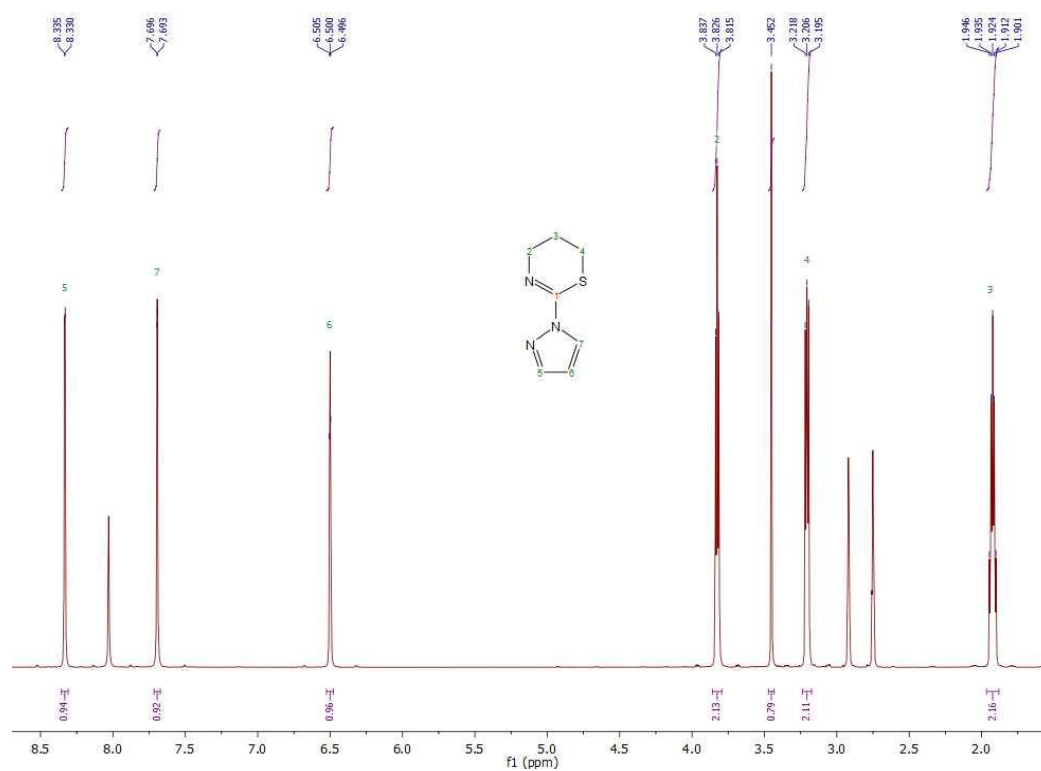
277. Buyukliev, R.T.; Cherneva, E.D.; Konstantinov, S.M.; Bakalova, A.G. Spectroscopic Investigation, DFT Calculations and Cytotoxic Activity of a 1-Amino-1,3-Dihydrospiro[Imidazoline-4,2-Indene]-2,5-Dione and Its Platinum and Palladium Complexes. *Arkivoc* **2017**, *2016*, 235–246, doi:10.24820/ARK.5550190.P009.939.
278. Paisano de Laverá, M.L. Trabajo Fin de Grado: Síntesis, Caracterización y Actividad Citotóxica de Complejos de Platino(II) y Paladio(II), **2022**.
279. Márquez Sánchez, M. Trabajo Fin de Grado: Complejos de Paladio y Platino Con Un Ligando Que Contiene Anillos de Tiazina, **2022**.
280. Fernández-Delgado, E.; de la Cruz-Martínez, F.; Galán, C.; Franco, L.; Espino, J.; Viñuelas-Zahinos, E.; Luna-Giles, F.; Bejarano, I. Pt(II) and Pd(II) Complexes with a Thiazoline Derivative Ligand: Synthesis, Structural Characterization, Antiproliferative Activity and Evaluation of pro-Apoptotic Ability in Tumor Cell Lines HT-29 and U-937. *J. Inorg. Biochem.* **2020**, *202*, 110870, doi:10.1016/j.jinorgbio.2019.110870.
281. Mbugua, S.N.; Sibuyi, N.R.S.; Njenga, L.W.; Odhiambo, R.A.; Wandiga, S.O.; Meyer, M.; Lalancette, R.A.; Onani, M.O. New Palladium(II) and Platinum(II) Complexes Based on Pyrrole Schiff Bases: Synthesis, Characterization, X-Ray Structure, and Anticancer Activity. *ACS Omega* **2020**, *5*, 14942–14954, doi:doi.org/10.1021/acsomega.0c00360.
282. Zalevskaya, O.A.; Gur'eva, Y.A.; Kutchin, A. V.; Aleksandrova, Y.R.; Yandulova, E.Y.; Nikolaeva, N.S.; Neganova, M.E. Palladium Complexes with Terpene Derivatives of Ethylenediamine and Benzylamine: Synthesis and Study of Antitumor Properties. *Inorganica Chim. Acta* **2021**, *527*, 120593, doi:10.1016/J.ICA.2021.120593.
283. Molaei, H.; Moghadam, M.; Mirkhani, V.; Tangestaninejad, S.; Mohammadpoor-Baltork, I.; Kajani, A.A.; Kia, R. Synthesis of Chiral Palladium Oxazolidine and Imine Complexes: Investigation the Oxazolidine-Imine Conversion by DFT Method. *Polyhedron* **2019**, *160*, 130–138, doi:10.1016/J.POLY.2018.11.037.
284. Czarnomysy, R.; Surazyński, A.; Muszynska, A.; Gornowicz, A.; Bielawska, A.; Bielawski, K. A Novel Series of Pyrazole-Platinum(II) Complexes as Potential Anti-Cancer Agents That Induce Cell Cycle Arrest and Apoptosis in Breast Cancer Cells. *J. Enzyme Inhib. Med. Chem.* **2018**, *33*, 1006–1023, doi:10.1080/14756366.2018.1471687.

285. Querino, A.L. de A.; Enes, K.B.; Chaves, O.A.; Dittz, D.; Couri, M.R.C.; Diniz, R.; Silva, H. Modified Pyrazole Platinum(II) Complex Can Circumvent Albumin and Glutathione: Synthesis, Structure and Cytotoxic Activity. *Bioorg. Chem.* **2020**, *100*, 103936, doi:10.1016/j.bioorg.2020.103936.
286. Basolo, F.; Gray, H.B.; Pearson Yol, R.G.; Herwig, W.; Zeiss, H.; Fred Basolo, B.; Pearson, R.G.; Basolo, F.; Pearson, R.G.; Zvyagintsev, O.K.; et al. Mechanisms of Inorganic Reactions. *J. Inorg. Nucl. Chem.* **1958**, *23*, 1649.
287. Marques, M.P.M. Platinum and Palladium Polyamine Complexes as Anticancer Agents: The Structural Factor. *ISRN Spectrosc.* **2013**, *2013*, 1–29, doi:10.1155/2013/287353.
288. Al-Khayal, K.; Vaali-Mohammed, M.A.; Elwatidy, M.; Bin Traiki, T.; Al-Obeed, O.; Azam, M.; Khan, Z.; Abdulla, M.; Ahmad, R. A Novel Coordination Complex of Platinum (PT) Induces Cell Death in Colorectal Cancer by Altering Redox Balance and Modulating MAPK Pathway. *BMC Cancer* **2020**, *20*, 685, doi:10.1186/s12885-020-07165-w.
289. Wang, F.Y.; Huang, K. Bin; Feng, H.W.; Chen, Z.F.; Liu, Y.N.; Liang, H. New Platinum(II) Agent Induces Bimodal Death of Apoptosis and Autophagy against A549 Cancer Cell. *Free Radic. Biol. Med.* **2018**, *129*, 418–429, doi:10.1016/j.freeradbiomed.2018.09.040.
290. Wang, F.Y.; Tang, X.M.; Wang, X.; Huang, K. Bin; Feng, H.W.; Chen, Z.F.; Liu, Y.N.; Liang, H. Mitochondria-Targeted Platinum(II) Complexes Induce Apoptosis-Dependent Autophagic Cell Death Mediated by ER-Stress in A549 Cancer Cells. *Eur. J. Med. Chem.* **2018**, *155*, 639–650, doi:10.1016/j.ejmech.2018.06.018.
291. Erxleben, A. Mitochondria-Targeting Anticancer Metal Complexes. *Curr. Med. Chem.* **2019**, *26*, 694–728, doi:10.2174/0929867325666180307112029.
292. Zhang, C.; Xie, H.; Zhang, Z.; Wen, B.; Cao, H.; Bai, Y.; Che, Q.; Guo, J.; Su, Z. Applications and Biocompatibility of Mesoporous Silica Nanocarriers in the Field of Medicine. *Front. Pharmacol.* **2022**, *13*, 829796, doi:10.3389/FPHAR.2022.829796/BIBTEX.
293. Li, Z.; Zhang, Y.; Feng, N. Mesoporous Silica Nanoparticles: Synthesis, Classification, Drug Loading, Pharmacokinetics, Biocompatibility, and Application in Drug Delivery. *Expert Opin. Drug Deliv.* **2019**, *16*, 219–237, doi:10.1080/17425247.2019.1575806.

294. Trzeciak, K.; Chotera-ouda, A.; Bak-sypien, I.I.; Potrzebowski, M.J. Mesoporous Silica Particles as Drug Delivery Systems—The State of the Art in Loading Methods and the Recent Progress in Analytical Techniques for Monitoring These Processes. *Pharmaceutics* **2021**, *13*, 950, doi:10.3390/pharmaceutics13070950.
295. Tao, Z.; Toms, B.; Goodisman, J.; Asefa, T. Mesoporous Silica Microparticles Enhance the Cytotoxicity of Anticancer Platinum Drugs. **2023**, *4*, 56, doi:10.1021/nn9015345.
296. Lin, C.H.; Cheng, S.H.; Liao, W.N.; Wei, P.R.; Sung, P.J.; Weng, C.F.; Lee, C.H. Mesoporous Silica Nanoparticles for the Improved Anticancer Efficacy of Cis-Platin. *Int. J. Pharm.* **2012**, *429*, 138–147, doi:10.1016/J.IJPHARM.2012.03.026.
297. Mishra, A.K.; Pandey, H.; Agarwal, V.; Ramteke, P.W.; Pandey, A.C. Nanoengineered Mesoporous Silica Nanoparticles for Smart Delivery of Doxorubicin. *J. Nanoparticle Res.* **2014**, *16*, 1–10, doi:10.1007/S11051-014-2515-Y/FIGURES/12.
298. Gu, J.; Liu, J.; Li, Y.; Zhao, W.; Shi, J. One-Pot Synthesis of Mesoporous Silica Nanocarriers with Tunable Particle Sizes and Pendent Carboxylic Groups for Cisplatin Delivery. *Langmuir* **2013**, *29*, 403–410, doi:10.1021/la3036264.
299. Ren, B.; Chen, D.F.; Zhao, X.J.; Li, L.S.; Zhao, M.X. Evaluating Biological Activity of Folic Acid-Modified and 10-Hydroxycamptothecin-Loaded Mesoporous Silica Nanoparticles. *Mater. Chem. Phys.* **2022**, *292*, 126756, doi:10.1016/J.MATCHEMPHYS.2022.126756.
300. Cheralayikkal, S.; Manoj, K.; Safna Hussan, K. Formulation and Evaluation of a Smart Drug Delivery System of 5-Fluorouracil for PH-Sensitive Chemotherapy. *Heliyon* **2022**, *8*, e09926, doi:10.1016/j.heliyon.2022.e09926.
301. Racles, C.; Zaltariov, M.F.; Peptanariu, D.; Vasiliu, T.; Cazacu, M. Functionalized Mesoporous Silica as Doxorubicin Carriers and Cytotoxicity Boosters. *Nanomaterials* **2022**, *12*, 1823, doi:10.3390/NANO12111823.
302. Al-Nadaf, A.H.; Dahabiyeh, L.A.; Jawarneh, S.; Bardaweel, S.; Mahmoud, N.N. Folic Acid-Hydrophilic Polymer Coated Mesoporous Silica Nanoparticles Target Doxorubicin Delivery. *Pharm. Dev. Technol.* **2021**, *26*, 582–591, doi:10.1080/10837450.2021.1904258.

8. APPENDIX

8. APPENDIX

Figure A1. ^1H NMR spectrum of PzTn in DMF-d_7 .Figure A2. ^1H NMR spectrum of PzTz in DMF-d_7 .

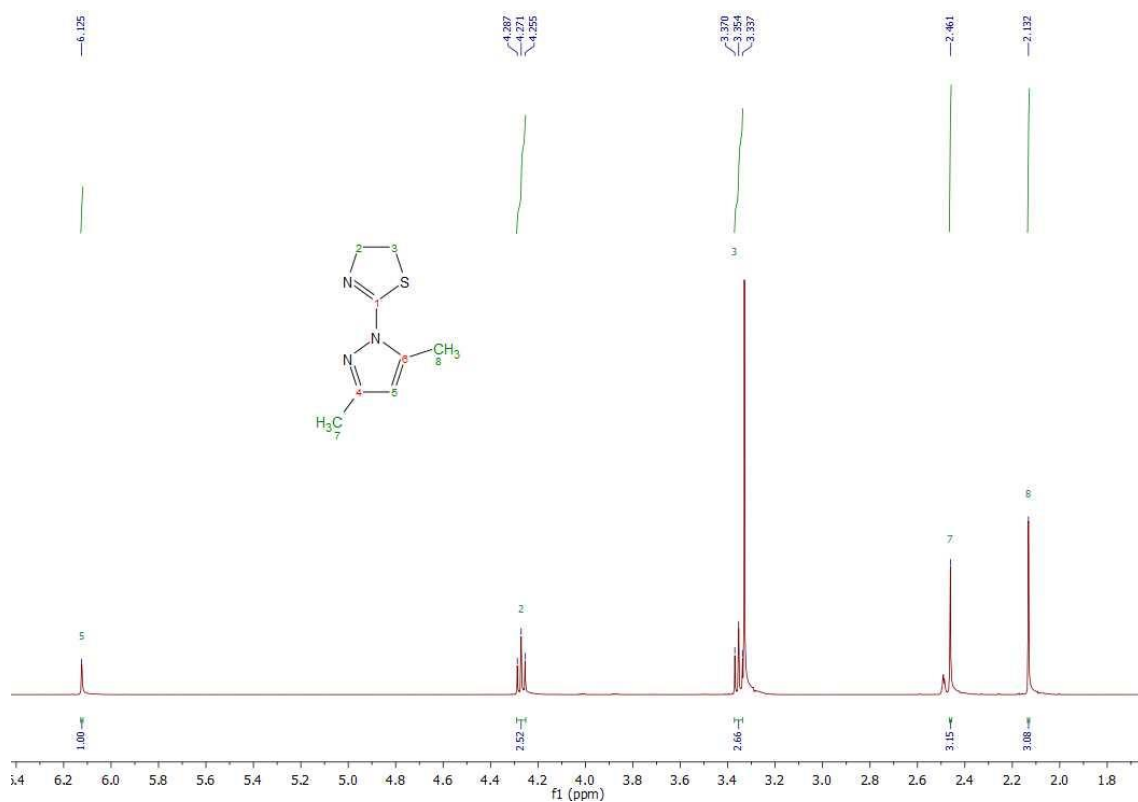


Figure A3. ^1H NMR spectrum of DMPzTn in DMSO- d_6 .

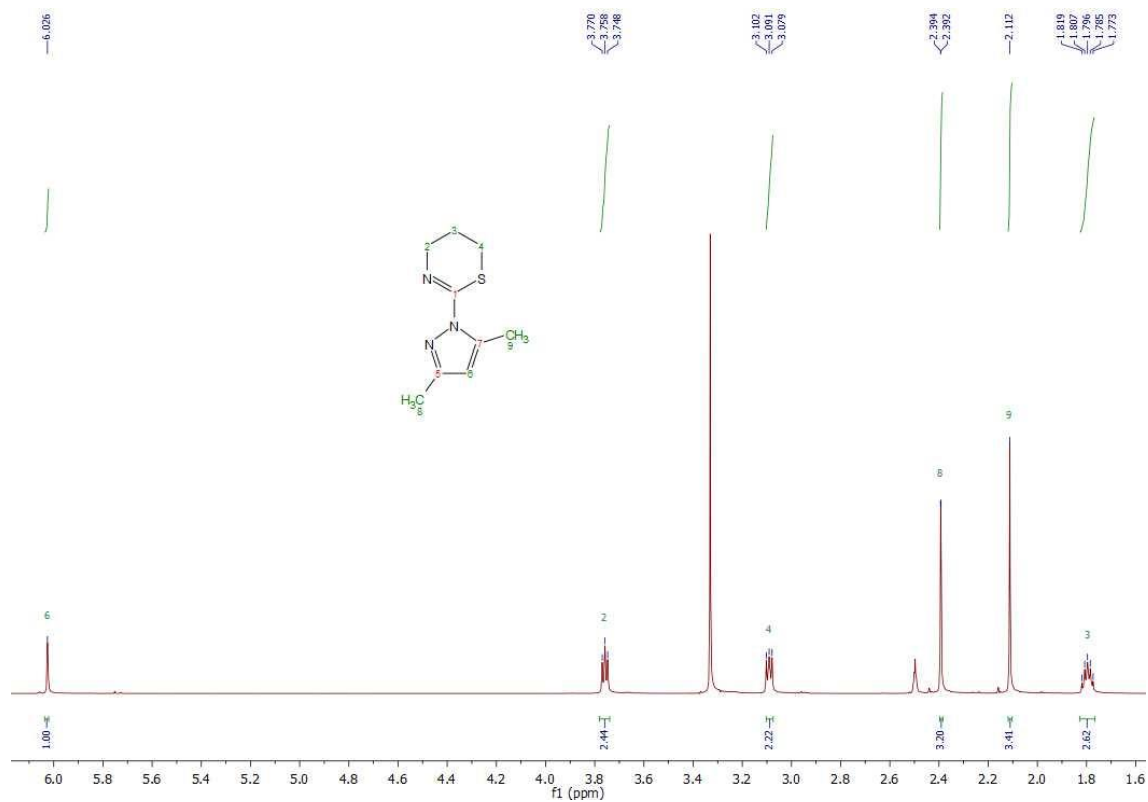


Figure A4. ^1H NMR spectrum of DMPzTz in DMSO- d_6 .

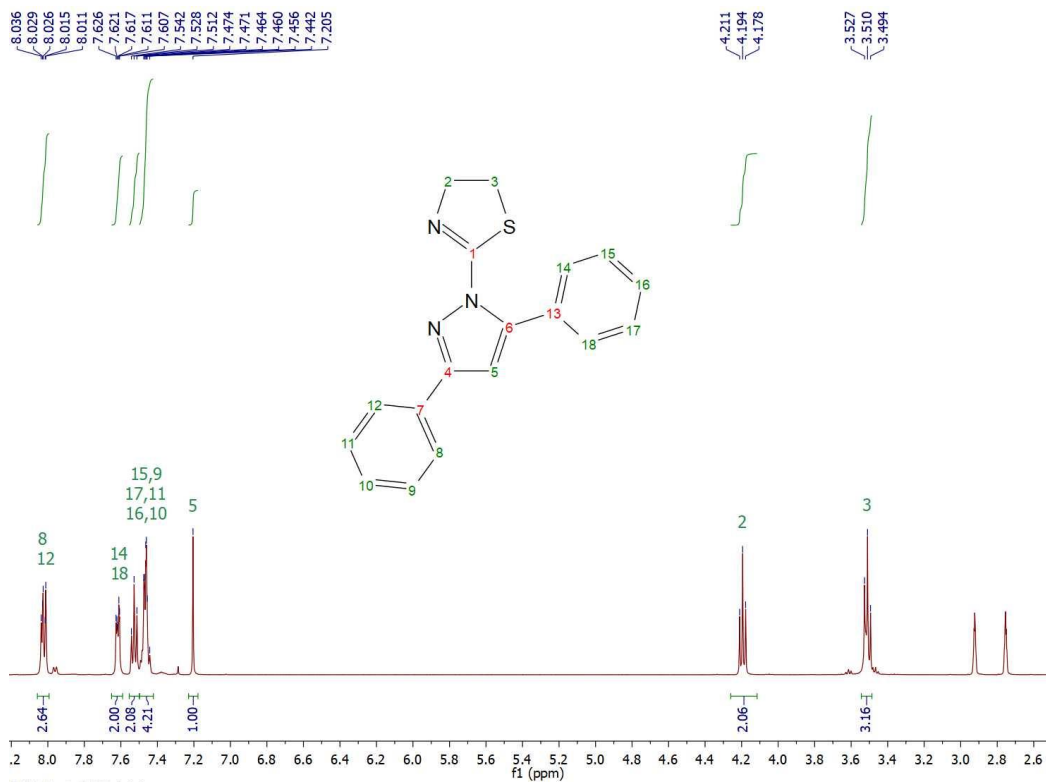


Figure A5. ¹H NMR spectrum of DPhPzTn in DMF-d₇.

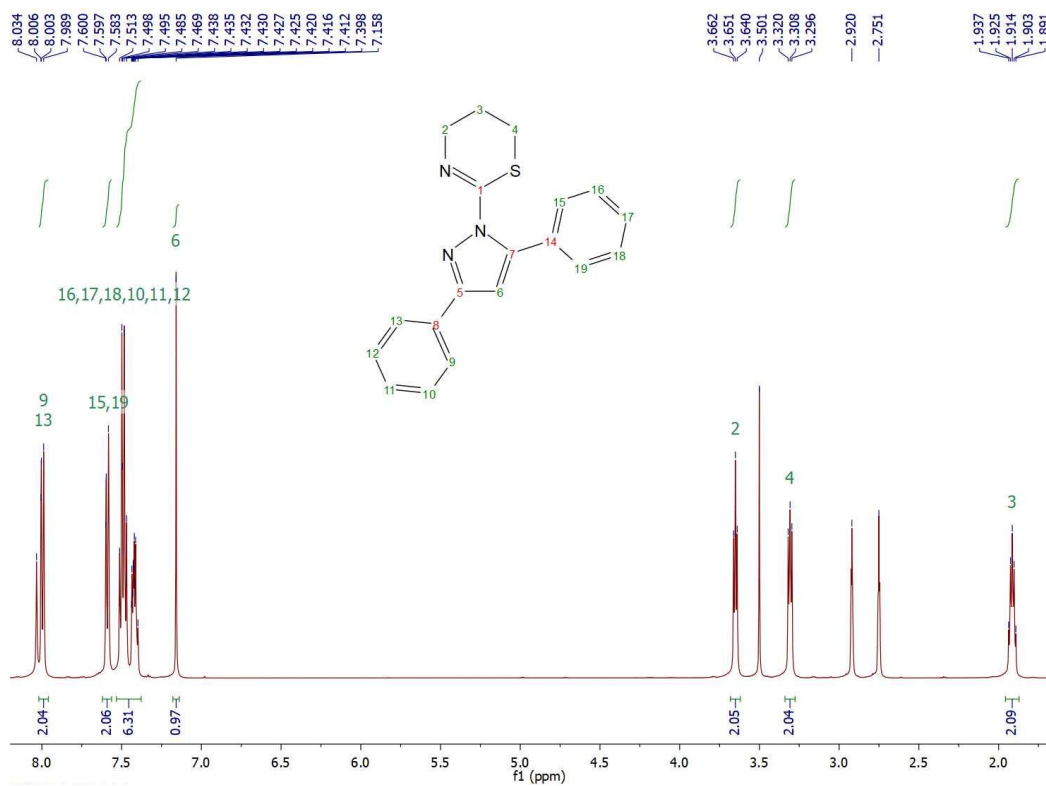


Figure A6. ¹H NMR spectrum of DPhPzTz in DMF-d₇.

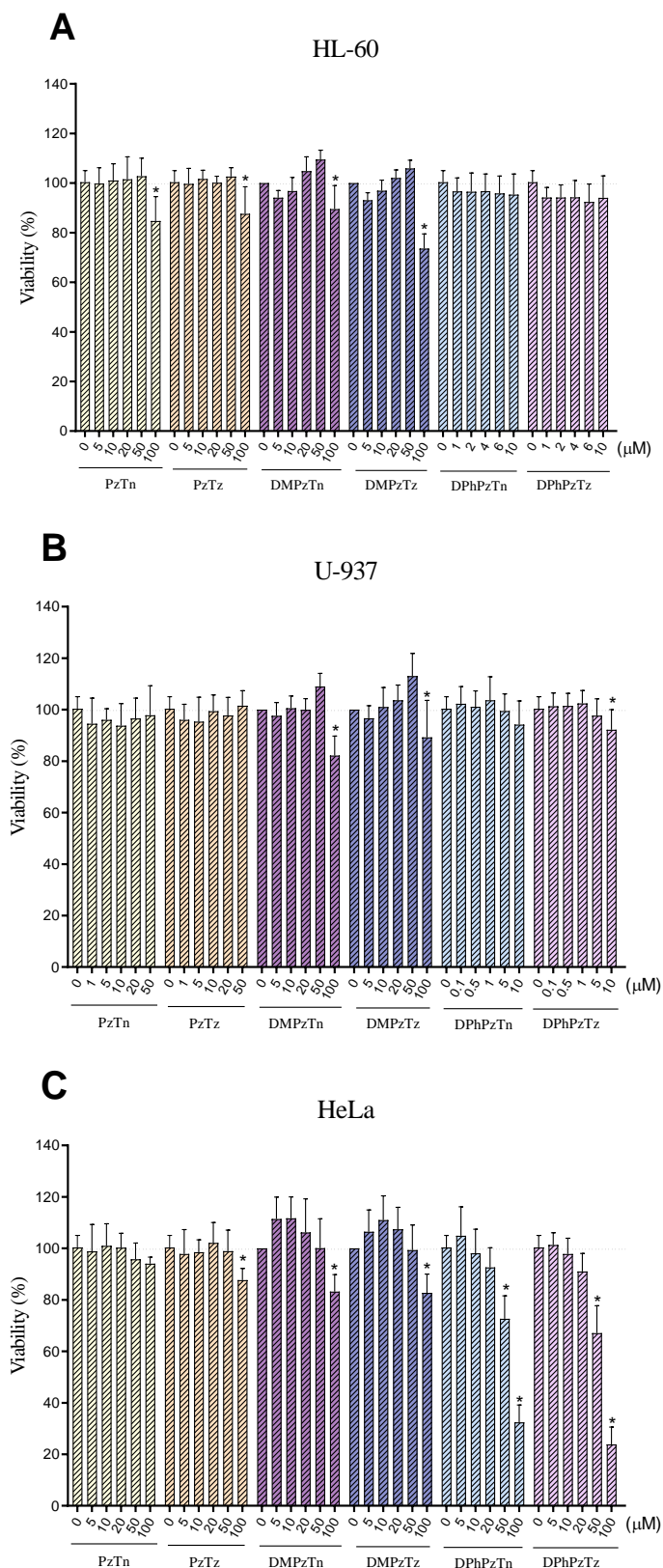


Figure A7. Cytotoxic effect of ligands. Promyelocytic leukemia HL-60 (A), histiocytic lymphoma U-937 (B) and epithelial cervix carcinoma HeLa (C) cell lines were challenged with concentrations from 0-100 μM of the six ligands, namely PzTn, PzTn, DMPzTn, DMPzTz, DPhPzTn and DPhPzTz, or the vehicle (DMF or DMSO) for 24 h. Values are presented as means \pm S.D. ($n = 6$) and depicted as percentage over untreated samples. * $P < 0.05$ vs. control (0 μM) (Dunnett's test).

Table A1. IR spectral assignments (cm⁻¹) for PzTn, DMPzTn and DPhPzTn.

	<i>PzTn</i>	<i>DMPzTn</i>	<i>DPhPzTn</i>
$W_1[\nu(C=N)]$	1641	1635	1639
<i>Pyrazole ring vibrations</i>	1514	1574	1560
	1382	1410	1408
	1350	1387	1319
	991	970	1000

Table A2. IR spectral assignments (cm⁻¹) for PzTz, DMPzTz and DPhPzTz.

	<i>PzTz</i>	<i>DMPzTz</i>	<i>DPhPzTz</i>
$\Psi_1[\nu(C=N)]$	1635	1639	1639
<i>Pyrazole ring vibrations</i>	1510	1566	1548
	1419	1411	1406
	1386	1375	
	1327	1315	1303
	995	981	998

Table A3. Cytotoxic effect of PzTn, PzTz, DMPzTn, DMPzTz, DPhPzTn and DPhPzTz towards selected tumor cell lines.

	<i>HeLa</i>	<i>HL-60</i>	<i>U-937</i>
<i>PzTn</i>	133.60 ± 22.56	> 150	> 150
<i>PzTz</i>	> 150	> 150	> 150
<i>DMPzTn</i>	> 500	> 500	> 500
<i>DMPzTz</i>	> 500	> 500	> 500
<i>DPhPzTn</i>	95.62 ± 7.73	> 150	> 150
<i>DPhPzTz</i>	78.71 ± 6.41	> 150	> 150

Table A4. *Cis*-complexes in the literature with a Cl₂N₂ coordination environment around Pt(II) and Pd(II) tested in HeLa cell line, including IC₅₀ (μM) and treatment incubation time.

HeLa				
	Compound	IC ₅₀ (μM)	Incubation time (h)	Reference
	[PtCl ₂ (PzTn)]	140.20 ± 24.31	24	This PhD thesis
	[PtCl ₂ (PzTz)]	142.20 ± 14.26	24	
	[PtCl ₂ (DMPzTn)]	119.8 ± 8.38	24	
	[PtCl ₂ (DMPzTz)]	144.7 ± 14.25	24	
	[PtCl ₂ (DPhPzTn)]	12.15 ± 0.89	24	
	[PtCl ₂ (DPhPzTz)]	14.09 ± 1.17	24	
1	[PtCl ₂ (L1)] L1: 9-amino- <i>N</i> -[2-[(2-aminoethyl)amino]ethyl]acridine-4-carboxamide	0.4*	48	[265]
2	[PtCl ₂ (L2)] L2: 9-amino- <i>N</i> -[2-[(2-aminoethyl)amino]ethyl]-7-methoxyacridine-4-carboxamide	10*	48	
3	[PtCl ₂ (L3)] L3: 9-amino- <i>N</i> -[2-[(2-aminoethyl)amino]ethyl]-7-fluoroacridine-4-carboxamide	1.3*	48	
4	[PtCl ₂ (L4)] L4: <i>N</i> -[2-[(2-aminoethyl)amino]ethyl]-9-[(2-hydroxyethyl)amino]acridine-4-carboxamide	1.1*	48	
5	[PtCl ₂ (L5)] L5: 2-(3,5-dimethylpyrazol-1-ylmethyl)pyridine	> 50	7 days	
6	[PtCl ₂ (L6)] L6: 2-(3,5-diphenylpyrazol-1-ylmethyl)pyridine	3.849	7 days	
7	[PtCl ₂ (L7)] L7: 2-(3,5-di- <i>tert</i> -butylpyrazol-1-ylmethyl)pyridine	> 25	7 days	
8	[PtCl ₂ (L8)] L8: 2-(3- <i>p</i> -tolylpyrazol-1-ylmethyl)pyridine	8.920	7 days	
9	[PtCl ₂ (L9)]·3½H ₂ O L9: bis(1-methyl-2-(3'-hydroxypropyl)benzimidazole)	< 2.5	72	[267]
10	[PtCl ₂ (L10)] L10: <i>N</i> -[(1 <i>S</i> ,3 <i>S</i>)-6,7-Dimethoxy-1-phenyl-1,2,3,4-tetrahydro-3-isoquinolinyl]methyl- <i>N</i> -phenylamine	8.92 ± 0.77	96	[268]
11	[PtCl ₂ (L11)] L11: <i>N</i> -[(1 <i>S</i> ,3 <i>S</i>)-6,7-Dimethoxy-1-phenyl-1,2,3,4-tetrahydro-3-isoquinolinyl]methyl- <i>N</i> -(4-methoxyphenyl)amine	6.43 ± 0.77	96	
12	[PtCl ₂ (L12)] L12: <i>N</i> -(4-Chlorophenyl)- <i>N</i> -[(1 <i>S</i> ,3 <i>S</i>)-6,7-dimethoxy-1-(4-methoxyphenyl)-1,2,3,4-tetrahydro-3-isoquinolinyl]methylamine	3.01 ± 0.57	96	
13	[PtCl ₂ (L13)] L13: Methyl 4-([(1 <i>S</i> ,3 <i>S</i>)-6,7-dimethoxy-1-(4-methoxyphenyl)-1,2,3,4-tetrahydro-3-isoquinolinyl]methylamino)benzoate	2.92 ± 0.78	96	
14	[PtCl ₂ (L14)] L14: <i>N</i> -[(1 <i>S</i> ,3 <i>S</i>)-1-(4-Chlorophenyl)-6,7-dimethoxy-1,2,3,4-tetrahydro-3-isoquinolinyl]methyl- <i>N</i> -(4-methylphenyl)amine	2.23 ± 0.33	96	
15	[PtCl ₂ (L15)] L15: <i>N</i> -[(1 <i>S</i> ,3 <i>S</i>)-1-(4-Chlorophenyl)-6,7-dimethoxy-1,2,3,4-tetrahydro-3-isoquinolinyl]methyl- <i>N</i> -[4-(trifluoromethyl)phenyl]amine	0.91 ± 0.47	96	

16	[PtCl ₂ (dap)]·H ₂ O dap: 1-(carboxylic acid)-1,2-diaminoethane	340	24	[270]
		220	48	
		165	72	
17	[PtCl ₂ (dab)]·1/4 HCl dab: 1-(carboxylic acid)-1,3-diaminopropane	330	24	
		230	48	
		215	72	
18	[PtCl ₂ (dap-phe)] dap-phe: 2-(1,2-diaminoethylcarboxiamide)-3-phenylpropionic	> 500	24	[271]
		> 500	48	
		> 500	72	
19	[PtCl ₂ (dab-phe)] dab-phe: 2-(1,3-diaminopropylcarboxiamide)-3-phenylpropionic acid	> 500	24	
		> 500	48	
		> 500	72	
20	[PtCl ₂ (dap-ala)] dap-ala: 2-(1,2-diaminoethylcarboxiamide)propionic acid	415	24	
		310	48	
		160	72	
21	[PtCl ₂ (dab-ala)] dab-ala: 2-(1,3-diaminopropylcarboxiamide)propionic acid	220	24	
		190	48	
		60	72	
22	[PtCl ₂ (L16)] L16: bis(pyrazole)	20 ± 0.01 [#]	24	[272]
23	[PtCl ₂ (L17)] L17: bis(3,5-dimethylpyrazole)	200 ± 0.1 [#]	24	
24	[PtCl ₂ (pbiCN)] pbiCN: 1-(Cyanoethyl)-2-(2-pyridyl)benzimidazole	15.4 ± 0.9	72	[273]
25	[PtCl ₂ (pbiSO ₃)] pbiSO ₃ : 3-(2-(2-pyridyl)-benzimidazol-1-yl)propane-1-sulfonate)	> 100	72	
26	[PtCl ₂ (bpyam)] bpyam: 4,4'-bis(N-(4-pentyl)diethylamine)carbamoyl)-2,2'-bipyridine	> 100	72	
27	[PtCl ₂ (bpyst)] bpyst: 4,4'-bis(α-styrene)-2,2'-bipyridine	33 ± 2	72	
28	[PtCl ₂ (L18)] L18: Z-NHC(NHcyclopropyl)Me ₂	> 100	48	[274]
29	[PtCl ₂ (L19)] L19: (Z-NHC(NHcyclopentyl)Me ₂	> 100	48	
30	[PtCl ₂ (L20)] L20: (Z-NHC(NHcyclohexyl)Me ₂	87.89 ± 2.22	48	
31	[PtCl ₂ (L21)] L21: 6,6',7,7'-tetramethoxy-3,3',4,4'-tetrahydro-1,1'-biisoquinoline	> 50	72	[275]
32	[PtCl ₂ (L22)] L22: Rac-6,6',7,7'-tetramethoxy-1,1', 2,2',3,3',4,4'-octahydro-1,1'-biisoquinoline	> 50	72	
33	[PtCl ₂ (L23)] L23: Meso-6,6',7,7'-tetramethoxy-1,1',2,2',3,3',4,4'-octahydro-1,1'-biiso quinoline	> 50	72	
34	[PtCl ₂ (L24)] L24: (1S, 1S')-6,6',7,7'-tetramethoxy -1,1',2,2',3,3',4,4'-octahydro-1,1'-biiso quinoline	29.94 ± 1.07	72	
35	[PtCl ₂ (L25)] L25: (1R, 1R')-6,6',7,7'-tetramethoxy -1,1',2,2',3,3',4,4'-octahydro-1,1'-biiso quinoline	21.95 ± 0.32	72	
36	[PtCl ₂ (L26)] L26: Rac-6,6',7,7'-tetrahydroxy-1,1', 2,2',3,3',4,4'-octahydro-1,1'-biisoquinoline	> 50	72	
37	[PtCl ₂ (L27)] L27: Meso-6,6',7,7'-tetrahydroxy-1, 1',2,2',3,3',4,4'-octahydro-1,1'-biisoquinoline	23.67 ± 0.84	72	

38	[PtCl ₂ (L28)] L28: 6-(4-(3-(2-aminoethylamino)propylamino)-7-deazapurine-β-D-ribose)	55.1 ± 14.6	72	[276]	
39	[PtCl ₂ (TdTz)] TdTz: 2-(3,4-dichlorophenyl)imino-N-(4H-5,6-dihydro-1,3-thiazin-2-yl)thiazolidine)	14.9 ± 1.2	24	[278]	
40	[PtCl ₂ (PyTz)]·C ₂ H ₆ O PyTz: 2-(2-pyridyl)iminotetrahydro-1,3-thiazine	63.38 ± 5.63	24	[175]	
41	[PtCl ₂ (TzTz)] TzTz: 2-(3,4-dichlorophenyl)imino-N-(4H-5,6-dihydro-1,3-thiazine-2-yl)tetrahydro-1,3-thiazine	9.8 ± 0.9	24	[279]	
	[PdCl ₂ (PzTn)]	67.55 ± 7.27	24	This PhD thesis	
		58.22 ± 9.66	48		
		44.17 ± 6.33	72		
	[PdCl ₂ (PzTz)]	77.75 ± 9.68	24		
		66.01 ± 11.43	48		
		46.59 ± 6.55	72		
	[PdCl ₂ (DMPzTn)]	> 150	24		
		> 150	48		
		> 150	72		
	[PdCl ₂ (DMPzTz)]	> 150	24		
		> 150	48		
		> 150	72		
	[PdCl ₂ (DPhPzTn)]	62.74 ± 6.45	24		
		34.85 ± 4.00	48		
		23.28 ± 2.44	72		
	[PdCl ₂ (DPhPzTz)]	57.83 ± 6.45	24		
		32.09 ± 4.23	48		
		27.98 ± 3.33	72		
42	[PdCl ₂ (L16)] L16: bis(pyrazole)	10 ± 0.1 [#]	24	[272]	
43	[PdCl ₂ (L17)] L17: bis(3,5-dimethylpyrazole)	350 ± 0.01 [#]	24		
44	[PdCl ₂ (L29)] L29: (pyrrolylmethylidene) (Pyridyl-2-yl-methyl) Amine <i>N,N</i>	45.5 ± 0.167	24	[281]	
45	[PdCl ₂ (L30)] L30: N ¹ ,N ¹ -dimethyl-N ² -[(1R,2S,3R,4S)-2-oxy-1,7,7-trimethylbicyclo[2.2.1]heptan-3-yl] ethane-1,2-diamine-N ¹ ,N ²	≥ 100	24	[282]	
46	[PdCl ₂ (L31)] L31: (Z)-N ¹ ,N ¹ -dimethyl-N ² -[(1R,4S)-2-oxo-1,7,7-trimethylbicyclo[2.2.1]heptane-3-ylidene]ethane-1,2-diamine - N ¹ ,N ²	≥ 100	24		
47	[PdCl ₂ (L32)] L32: (1R,2R,5R)-3-(Benzylimino)-2,6,6-Trimethylbicyclo [3.1.1]Heptane-2-ol <i>N,N</i>	4.28 ± 0.09	24		
48	[PdCl ₂ (L33)] L33: (1S,2S,3S,5S)-3-(Benzylamino)-2,6,6- Trimethylbicyclo [3.1.1]Heptane-2-ol- <i>N,N</i>	28.44 ± 0.18	24		
49	[PdCl ₂ (L34)] L34: (1R,2R,5R,3E)-3-{[2-(amino)ethyl]imino}-2,6,6-trimethylbicyclo[3.1.1]- heptan-2-ol-κ ₂ N	≥ 100	24		
50	[PdCl ₂ (L35)] L35: (N-(2E,1S,4S)-1,7,7-Trimethylbicyclo[2.2.1]- hept-2-ylidene)ethane-1,2-diamine-N ¹ ,N ²	≥ 100	24		
51	[PdCl ₂ (L36)] L36: (1R,2R,5R,3E)-3-{[2-(dimethylamino)ethyl]imino}-2,6,6-trimethylbicyclo[3.1.1]- heptan-2-ol-κ ₂ N	≥ 100	24		
52	[PdCl ₂ (L37)] L37: (S,E)-2-(pyridine-2-ylmethyleneamino)propan-1-ol	50	48		[283]

53	[PdCl ₂ (L38)] L38: @-2-(4,4-dimethyloxazolidin-2-yl)pyridine	> 100	48	
54	[PdCl ₂ (L _{Bn})] L _{BN} : <i>N,N'</i> -bis(1-benzylpyridylidene)oxalamide	30.8 ± 1.9	72	[259]
55	[PdCl ₂ (L _{Me})] L _{Me} : <i>N,N'</i> -bis(1-methylpyridylidene)oxalamide	75.1 ± 1.0	72	
56	[PdCl ₂ (TdTz)] TdTz: 2-(3,4-dichlorophenyl)imino-N-(4H-5,6-dihydro-1,3-thiazin-2-yl)thiazolidine	44.8 ± 3.8	24	[278]
57	[PdCl ₂ (PyTz)]·C ₂ H ₆ O PyTz: 2-(2-pyridyl)iminotetrahydro-1,3-thiazine	78.62 ± 8.21	24	[175]
58	[PdCl ₂ (TzTz)] TzTz: 2-(3,4-dichlorophenyl)imino-N-(4H-5,6-dihydro-1,3-thiazine-2-yl)tetrahydro-1,3-thiazine	55.76 ± 2.6	24	[279]

* Amylar blue assay, # Neutral red assay

Table A5. *Cis*-complexes in the literature with a Cl₂N₂ coordination environment around Pt(II) and Pd(II) tested in HL-60 cell line, including IC₅₀ (μM) and treatment incubation time.

HL-60				
	Compound	IC ₅₀ (μM)	Incubation time (h)	Reference
	[PtCl ₂ (PzTn)]	15.02 ± 1.41	24	This PhD thesis
	[PtCl ₂ (PzTz)]	23.93 ± 2.49	24	
	[PtCl ₂ (DMPzTn)]	42.83 ± 1.75	24	
	[PtCl ₂ (DMPzTz)]	62.32 ± 1.87	24	
	[PtCl ₂ (DPhPzTn)]	6.05 ± 0.47	24	
	[PtCl ₂ (DPhPzTz)]	5.79 ± 0.45	24	
1	[PtCl ₂ (dap)]·H ₂ O dap: 1-(carboxylic acid)-1,2-diaminoethane	265	24	[270]
		220	48	
		160	72	
2	[PtCl ₂ (dab)]·1/4 HCl dab: 1-(carboxylic acid)-1,3-diaminopropane	150	24	
		113	48	
		95	72	
3	[PtCl ₂ (dap-phe)] dap-phe: 2-(1,2-diaminoethylcarboxiamide)-3-phenylpropionic acid	448	24	[271]
		420	48	
		340	72	
4	[PtCl ₂ (dab-phe)] dab-phe: 2-(1,3-diaminopropylcarboxiamide)-3-phenylpropionic acid	470	24	
		340	48	
		330	72	
5	[PtCl ₂ (dap-ala)] dap-ala: 2-(1,2-diaminoethylcarboxiamide)propionic acid	240	24	
		98	48	
		90	72	
6	[PtCl ₂ (dab-ala)] dab-ala: 2-(1,3-diaminopropylcarboxiamide)propionic acid	245	24	
		195	48	
		130	72	
7	[PtCl ₂ (L39)] L39: 1-Amino-1,3-dihydrospiro[imidazoline-4,2-indene]-2,5-dione	165.2	72	[277]
8	[PtCl ₂ (PyTz)]·C ₂ H ₆ O PyTz: 2-(2-pyridyl)iminotetrahydro-1,3-thiazine	39.25 ± 3.86	24	[175]

	[PdCl ₂ (PzTn)]	71.81 ± 9.09	24	This PhD thesis
	[PdCl ₂ (PzTz)]	54.50 ± 6.68	24	
	[PdCl ₂ (DMPzTn)]	> 150	24	
	[PdCl ₂ (DMPzTz)]	> 150	24	
	[PdCl ₂ (DPhPzTn)]	58.83 ± 4.94	24	
	[PdCl ₂ (DPhPzTz)]	46.39 ± 3.99	24	
9	[PdCl ₂ (L40)] L40: 1-Amino-1,3-dihydrospiro[imidazoline-4,2-indene]-2,5-dione	> 200	72	[277]
10	[PdCl ₂ (PyTz)]·C ₂ H ₆ O PyTz: 2-(2-pyridyl)iminotetrahydro-1,3-thiazine	115.20 ± 17.01	24	[175]

Table A6. *Cis*-complexes in the literature with a Cl₂N₂ coordination environment around Pt(II) and Pd(II) tested in U-937 cell line, including IC₅₀ (μM) and treatment incubation time.

U-937				
	Compound	IC ₅₀ (μM)	Incubation time (h)	Reference
	[PtCl ₂ (PzTn)]	6.48 ± 0.54	24	This PhD thesis
	[PtCl ₂ (PzTz)]	8.09 ± 0.81	24	
	[PtCl ₂ (DMPzTn)]	32.59 ± 0.83	24	
	[PtCl ₂ (DMPzTz)]	43.04 ± 1.17	24	
	[PtCl ₂ (DPhPzTn)]	3.23 ± 1.36	24	
	[PtCl ₂ (DPhPzTz)]	2.75 ± 0.34	24	
1	[PtCl ₂ (t-L41)] L41: <i>threo</i> -2,3-Diamino-3-(4-fluorophenyl)propane	0.33 ± 1.20	72	[269]
2	[PtCl ₂ (e-L41)] L41: <i>erythro</i> -2,3-Diamino-3-(4-fluorophenyl)propane	2.17 ± 1.11	72	
3	[PtCl ₂ (rac-L42)] L42: 1,2-diamino-1,2-bis(4-fluorophenyl)ethane	0.37 ± 1.19	72	
4	[PtCl ₂ (meso-L42)] L42: 1,2-diamino-1,2-bis(4-fluorophenyl)ethane	1.17 ± 1.12	72	
5	[PtCl ₂ (t-L43)] L43: <i>threo</i> -2,3-Diamino-3-(4-fluorophenyl)propan-1-ol	0.37 ± 1.20	72	
6	[PtCl ₂ (e-L43)] L43: <i>erythro</i> -2,3-Diamino-3-(4-fluorophenyl)propan-1-ol	1.16 ± 1.14	72	
7	[PtCl ₂ (L44)] L44: 2,3-Diamino-3-(4-fluorophenyl)ethane	0.58 ± 1.16	72	
8	[PtCl ₂ (t-L45)] L45: <i>threo</i> -3,4-Diamino-4-(4-fluorophenyl)butan-1-ol	0.63 ± 1.16	72	
9	[PtCl ₂ (e-L45)] L45: <i>erythro</i> -3,4-Diamino-4-(4-fluorophenyl)butan-1-ol	2.98 ± 1.15	72	
10	[PtCl ₂ (PyTz)]·C ₂ H ₆ O PyTz: 2-(2-pyridyl)iminotetrahydro-1,3-thiazine	26.36 ± 2.56	24	
11	[PtCl ₂ (TdTn)] TdTn: 2-(2-pyridyl)iminotetrahydro-1,3-thiazine	~ 10	24	[280]
	[PdCl ₂ (PzTn)]	70.95 ± 8.73	24	This PhD thesis
	[PdCl ₂ (PzTz)]	70.21 ± 7.67	24	
	[PdCl ₂ (DMPzTn)]	> 150	24	
	[PdCl ₂ (DMPzTz)]	> 150	24	
	[PdCl ₂ (DPhPzTn)]	53.43 ± 4.91	24	
	[PdCl ₂ (DPhPzTz)]	50.35 ± 4.82	24	
12	[PdCl ₂ (PyTz)]·C ₂ H ₆ O PyTz: 2-(2-pyridyl)iminotetrahydro-1,3-thiazine	90.96 ± 17.66	24	[175]
13	[PdCl ₂ (TdTn)] TdTn: 2-(2-pyridyl)iminotetrahydro-1,3-thiazine	~ 5	24	[280]

